UNIVERSITY OF SOUTHAMPTON

IN SILICO SIMULATION OF LONG TERM CEMENT MANTLE FAILURE IN TOTAL HIP REPLACEMENT

Jonathan R T Jeffers

A thesis submitted in partial fulfilment of the requirements for the degree of

Doctor of Philosophy

SCHOOL OF ENGINEERING SCIENCES

BIOENGINEERING SCIENCES RESEARCH GROUP

January 2005

UNIVERSITY OF SOUTHAMPTON

ABSTRACT

SCHOOL OF ENGINEERING SCIENCES
BIOENGINEERING SCIENCES RESEARCH GROUP

Doctor of Philosophy

In silico simulation of long term cement mantle failure in total hip replacement

by Jonathan R T Jeffers

Hip replacement has become a successful treatment for severe arthritis, and this success has led to a high number of replacement procedures being performed every year. There are also a large number of replacement designs currently available, and more are introduced every year. New designs are not always a success and there have been instances of poor prosthesis designs being withdrawn from the market. For this reason, along with the increased demands placed on the replacement by younger patients, novel preclinical testing methods are necessary to prevent inferior designs reaching clinical trials and thereby accelerate the development process.

Prosthesis loosening is recognised as the most common cause of hip replacement failure. Prostheses can be fixed in the bone with bone cement, and clinical studies have identified cement fatigue failure as a common cause of prosthesis loosening. This thesis describes the generation of a computational simulation of the cement fatigue process. Experimental tests are performed to generate S-N and creep data for a particular brand of bone cement under uniaxial tensile fatigue loading. These data are then used to simulate fatigue and creep in finite element analyses. Porosity and residual stress have been shown to influence bone cement fatigue, these parameters are also simulated in the finite element models. The number of pores in each finite element model is generated using experimental data and Monte Carlo simulation. An initial stress field is created to represent residual stress such that the stress distribution and magnitude are similar to experimental observations. The first computational analysis performed is for uniaxial tensile and 4-point bend fatigue, and compared to experimental tests. Subsequently, experimental specimens and finite element models of a simplified implanted femur model are generated. The computational simulation is performed for this structure, and compared to the experimental results. The computational simulation is then performed on an implanted femur geometry, and the results compared to clinical observations of cement mantle fatigue failure. Correlations can be drawn with clinical observations. The computational analysis also allows the simulated parameters active during fatigue loading to be switched off, allowing the influence of each to be isolated. This identifies cement porosity as having the greatest negative influence on cement fatigue, followed by residual stress. Creep is shown to have a positive effect on the cement mantle fatigue failure, by dissipating peak stresses in the material.

The uniaxial fatigue experimental testing also incorporates the acoustic emission technique to monitor cement damage. The condition monitoring capabilities of this technique in relation to bone cement are demonstrated, specifically the ability to detect and locate damage, and to predict whether or not specimen failure is imminent.

TABLE OF CONTENTS

TABLE OF FIGURES

TABLE OF TABLES

ACKNOWLEDGEMENTS

There are many souls out there that have, in one way or another, directly or indirectly, helped in the writing of this thesis. I really should trace my family tree back a few levels, and thank each of my ancestors for not getting killed in a freak accident and thus negating my existence. But I'm not going to. I think few people who read this want to know the details of my ancestry.

Yet I will go back one generation and thank Mum and Dad, who really have helped overall in the greatest way. For decent schooling, the countless trips in the early, unfriendly, cold mornings to the DART station, and of course all the runs to the airport. Graveyard shifts and all, no bother. Whatever the weather! Thanks, you know I couldn't operate the same without ye. Also the rest of the clan, Sandra, Nicholas and of course the dog. And all the relations, you've all played a part. See you at Christmas.

Thanks to all my associates, back in Ireland and here in Southampton. For all the craic when we're together, whether at home, in Dublin or Southampton, or indeed anywhere else in the world.

Now, there are a number of people that have directly aided this project. Firstly thanks to my supervisors, Mark and Martin. Mark, for your guidance over the course of the project, having faith in my abilities and putting up with a researcher with a penchant for jumping out of windows. Martin, for your supervision and especially aiding the experimental side of things. Also for Browne tours, next trip Wicklow! Thanks to Anne for all her input from showing me how to use the test machine to correcting papers for journal publication. And for the French lessons. Thanks to Eric for all the help getting things done in the labs. Thanks to Andrew for the finite element models, to Chris for sharing his acoustic emission expertise, to Adam and Andy for the amateur orthopaedics, to Antonio and Ana for help with licensing and finite element problems, to Polly for making all those tensile test specimens and to everyone else in the group for putting up with me in a grump on a Monday morning. Finally thanks to Lucy for her ambulance driving. It was a *very* high fence.

Go raibh míle maith agaibh go léir.

CHAPTER 1

INTRODUCTION

The first known case of arthritis was discovered in a somewhat unlikely place – a cave in the south of France. The year was 1908, and French palaeontologist Marcellin Boule (1861-1942) was excavating the bones of the *old man of La Chapelle-aux-Saints*. The 'old man' was a Neanderthal who lived about 50,000 years ago, and is thought to have died some time in his 40's. Perhaps the most remarkable thing about the old man was that he suffered from severe osteoarthritis, a deformed hip, a crushed toe, a broken rib and a damaged patella (Stringer and Gamble, 1993).

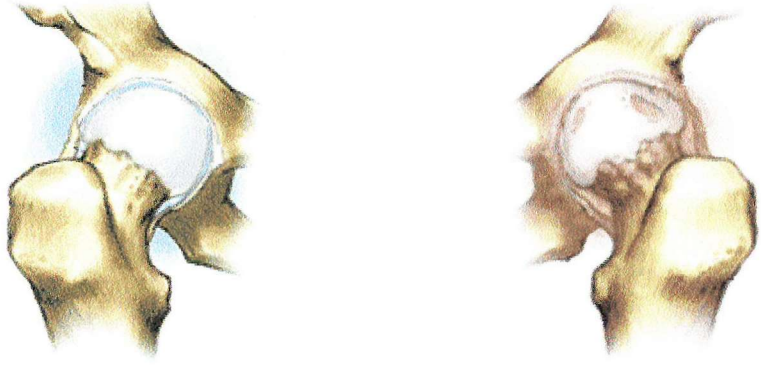

Figure 1.1: Healthy (left) and arthritic (right) hip[1].

We are better equipped today to treat ailments like those suffered by the old man, specifically the osteoarthritis. We now know that the articulating surfaces in joints are lined with cartilage and that joints are surrounded by a membrane called the synovium. We know that fluid within the synovium, synovial fluid, provides lubrication for the cartilage. We also know what happens when a joint develops osteoarthritis (see Figure

[1] The Center for Orthopaedics, http://www.centerorthopedic.com/arthritis.html

1.1). The cartilage roughens and begins to thin, the underlying bone thickens, and bony spurs or osteophytes may grow. The synovium may become swollen and generate more synovial fluid, effectively swelling the joint. These responses are the joint's attempt to repair itself, and can be successful, especially in small finger joints. However, sometimes the repair cannot compensate for the damage, and in severe cases, the cartilage can become so thin that the underlying bone is exposed. We know osteoarthritis is uncommon before the age of 40 and, for most joints, is more common in women. We have also noticed that being overweight can increase the likelihood of developing osteoarthritis, as can injuring a joint earlier in life. What we do not know is the cause of osteoarthritis, and while this remains the case we cannot develop a cure[1].

Currently in the UK there are about 8 million people suffering from osteoarthritis, and some 1 million have sought treatment. Of the other 7 million, many do not even realise they have osteoarthritis, even when there is radiographic evidence of the disease[1]. Although there is no cure for osteoarthritis, the condition can certainly be treated. For severe arthritis, this can involve a steroid injection into the joint for near instant pain relief, or a course of hyaluronan (similar to synovial fluid) injections over a 3-5 week period. For the most severe cases, surgery is necessary to restore function and reduce pain. This is usually achieved by replacing one or both articulating surfaces, or the insertion of a layer of material to separate them. Such procedures require extensive knowledge of engineering and biology to firstly design the prosthetic components and then implant them in the body. The first bridge between these sciences was built in the 17th century, when biomechanics came into being (Thurston, 1999).

A fundamental concept of biomechanics is that the human body is considered as a machine. That is not to say that we humans are ourselves machines, but we can leave any discussions regarding the mind and soul to the philosophers. The 'father of biomechanics', as he became known, was Giovanni Borelli (1608-1679) an Italian scientist whose *De Motu Animalium (On the Movement of Animals)* was published in 1680 (Thurston, 1999). This seminal work described the human body in terms of applied loads and levers and became, one could argue, the first biomechanics textbook (Figure

[1] Osteoarthritis, an information booklet. The Arthritis Research Campaign, http://www.arc.org.uk/about_arth/booklets/6025/6025.htm

1.2). Today, over three centuries later, the study of biomechanics is by no means complete. Taking the lower extremity as an example, the introduction of photography, force plates and telemeterised hip prostheses have given us knowledge of the kinematics, ground reaction and hip contact forces experienced during gait. However, forces in the muscles associated with gait remain elusive quantities – this is discussed in greater detail in Chapter 2. Despite our incomplete knowledge of biomechanics, joint arthroplasty (surgical repair of the joint), and specifically hip arthroplasty, is now commonplace and has become one of the most successful and cost-effective procedures in contemporary surgery.

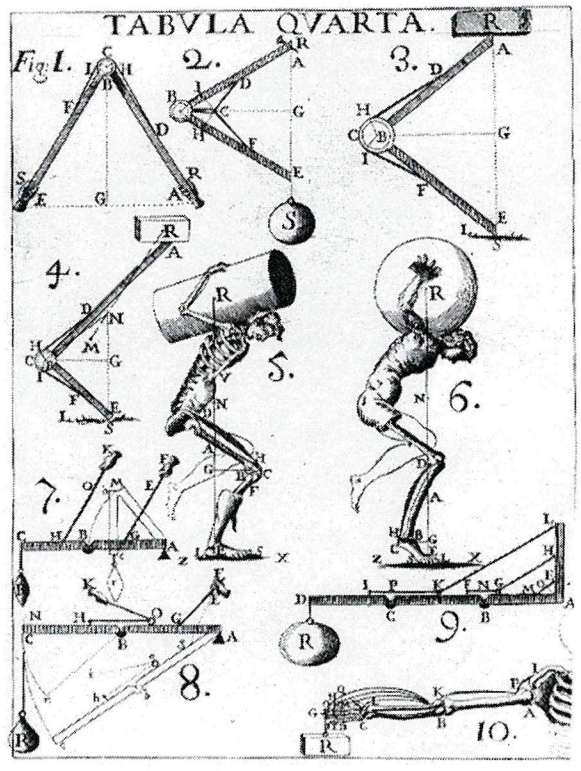

Figure 1.2: Plate from *De Motu Animalium (On the movement of animals)*, Giovanni Borelli, 1680[1].

Interposition arthroplasty was one of the earliest recorded surgical treatments of arthritis (Kingston and Walsh, 2001). This aimed to separate arthritic joint surfaces with a layer of material, and dates back to 1860 when French surgeon Aristide Verneuil (1823–1895) performed the procedure on the knee joint using joint capsule tissue as the interpositional

[1] http://www.princeton.edu/~his291/Borelli.html

material. Other materials were subsequently tried – skin, gold foil, rubber, celluloid, and even tanned pig bladder. These early biomaterials limited the success of the procedure, but it remained the most common treatment for hip arthritis well into the 20th century. In 1932, the Norwegian born American physician Marius Smith-Petersen (1886-1953) started using glass moulds between the femoral head and acetabulum. Although these sometimes broke, Smith-Petersen was undeterred and in 1936, on the advice of his dentist, began to use Vitallium (a cobalt chromium alloy) moulds to separate the joint surfaces. Clinical results with the Vitallium moulds were (relatively) good, leading to the implantation of almost 500. A remarkable case involving one of these prostheses was that of a patient who received treatment in 1948 and was lost to follow-up. 46 years later, she had total hip replacement of the opposite hip, and was still pleased with the function of the Smith-Peterson arthroplasty (see Figure 1.3). She declined revision to a total hip arthroplasty (Radcliffe and Geary, 1997).

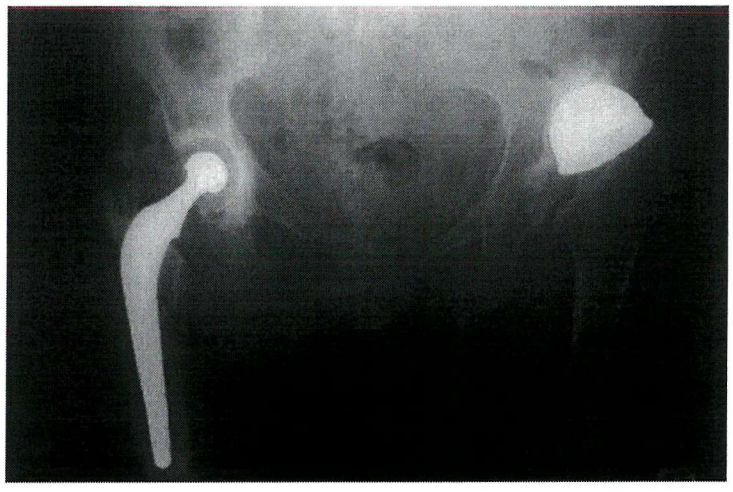

Figure 1.3: Radiograph of Charnley low friction arthroplasty (left) and Smith-Petersen Vitallium mould arthroplasty (right). The Smith-Petersen mould was functional 46 years post-operatively (Radcliffe and Geary, 1997).

Hip replacement is now the most common surgical treatment of arthritis. This involves resection of the femoral head and replacing it with a ball fixed to/in the femur. Ivory was the first material used to replace the femoral head; this procedure was performed by the German Professor Themistokles Gluck (1853-1942) in 1890. It was not a success, and led surgeons to continue with interposition arthroplasty (Klenerman, 2002). In 1943,

French brothers Robert (1909-1980) and Jean (1905-1995) Judet developed a short-stemmed polymethylmethacrylate prosthesis reinforced with a cobalt chrome rod (Figure 1.4). The stem of this prosthesis was inserted in the axis of the femoral neck (see Figure 1.4), and weight bearing tended to shear the head off at the stem. However, cases of extraordinary survival rates have been reported for the Judet prostheses – up to forty and even fifty years (Hettfleisch and Wissenbach, 1994; Kamangu and Burette, 2002).

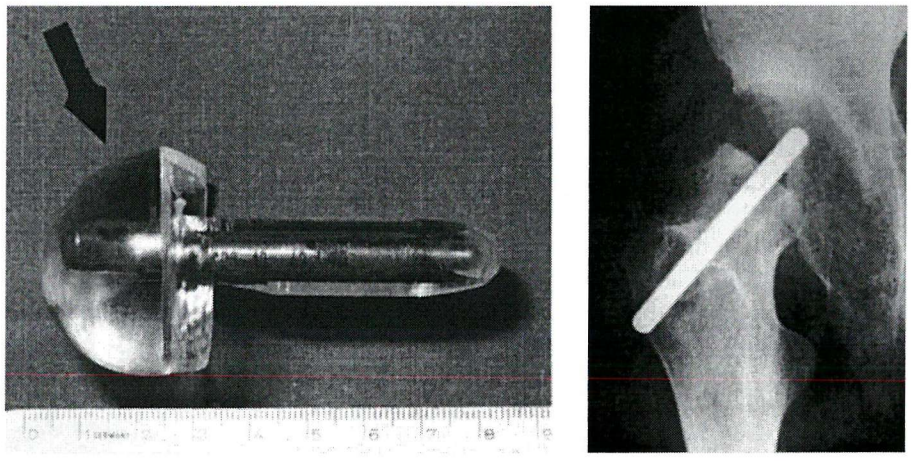

Figure 1.4: Judet prosthesis replaced 40 years post operatively. Arrow points to worn surface (Hettfleisch and Wissenbach, 1994). Radiograph shows prosthesis immediately post operatively.

In the early 1950's, and unimpressed with the design of the Judet prosthesis, Austin Moore (1899-1963) of South Carolina and Frederick Thompson (1907-1983) of New York developed prostheses with longer stems that fitted into the medullary canal of the femur (Figure 1.5). Both these stems had an offset and angled head to best recreate the physiological geometry. This design was an improvement over the Judet prosthesis, as loads were transferred to the shaft of the femur. The Moore and Thompson prosthesis designs remain relatively unchanged and are still in use today for hip fractures in elderly patients (Klenerman, 2002).

Oddly enough, it was a squeaking Judet prosthesis that led to arguably the biggest revolution in hip arthroplasty and the high survival rates enjoyed today. The squeaky Judet led Professor Sir John Charnley (1911-1982) to think about joint friction and wear (Kingston and Walsh, 2001). Charnley proposed a low-friction arthroplasty, with a

reduced diameter head on the femoral component (Figure 1.5) articulating against a plastic liner fitted in the acetabulum. Dennis Smith, an English dental materials scientist introduced Charnley to self-curing polymethylmethacrylate (PMMA) as a means to fix the components in the bone[1]. Charnley initially tried using polytetrafluorethylene (PTFE or Teflon) as the plastic acetabular lining, and although this had good wear resistance properties, wear debris caused adverse tissue reactions that eventually led to loosening. It was Charnley's technician, Harry Craven that considered using ultra high molecular weight polyethylene (UHMWPE) as a substitute to PTFE. Craven knew of this material being used for gears in a weaving factory in Lancashire, England[1]. The combination of a metal stem with a small head and a UHMWPE acetabular cup, both fixed in the bone with bone cement, revolutionised the world of hip arthroplasty, yielding high success rates still regarded today as the gold standard. Recent follow up studies report "remarkable durability" of the cemented Charnley total hip replacements, with up to 88% of replacements still functioning satisfactorily at a minimum of 30 years (Callaghan *et al.*, 2004; Wroblewski *et al.*, 2001).

Figure 1.5: Thompson (Stryker Orthopaedics, left), Moore (Stryker Orthopaedics, centre) and Charnley (DePuy Orthopaedics, right) prostheses. Note smaller diameter head on the Charnley.

The success Charnley brought to total hip replacement has made it an extremely popular procedure; worldwide the number of hips replaced is thought to number 1 million annually (Herberts and Malchau, 2000). Making a very simple prediction by assuming

[1] Improving musculoskeletal care in America, information on the impact and treatment of musculoskeletal conditions. American Academy of Orthopaedic Surgeons, http://www3.aaos.org/research/imca/OAhipContents/OAHip_replace.pdf

similar survival rates 30 years from now to those reported above (88%), over 120,000 revision procedures may be necessary in thirty years time. This is a considerable number that impressive survival percentages tend to mask, and prevents surgeons from performing 120,000 primary procedures. Revision is distressing for the patients involved, and the survival rate is far inferior to primary surgery (Robinson *et al.*, 1999). The monetary cost of surgery is also significant – a recent report places the cost of primary surgery at around €8,000 (O'Shea *et al.*, 2002). Assuming a similar cost for revision surgery, revision procedures could cost up to €1 billion worldwide in thirty years time.

The success rate of total hip replacement means it is being performed on younger (and therefore generally more active) patients. The increased activity of such patients places greater demands on the reconstruction, and is likely to decrease survival rates. Charnley himself was aware of this, and warned that for younger patients the surgeon should guard against allowing the patients subjective symptoms to influence their judgement, advising surgeons to *"turn deaf ears to exaggerated adjectives used to describe the intolerable quality of the pain"* (Charnley, 1979).

Orthopaedic research has not been stagnant since Charnley introduced the low friction arthroplasty, and there are now several different types of hip replacement available to the surgeon. In the early 1980's, cementless prostheses were introduced. Instead of being fixed with bone cement, these prostheses had porous coatings that promoted bone growth into the prosthesis (Figure 1.6), therefore relying on good quality bone for adequate ingrowth and precise reaming of the femoral canal to ensure a tight fit for the stem. Cementless arthroplasty has become more popular than cemented in the United States, but this has yet to happen in Europe where it is generally reserved for young patients to simplify any revision surgery that may become necessary (Herberts and Malchau, 2000).

Resurfacing arthroplasty is another relatively new surgical option, requiring less bone removal than the Charnley prosthesis. The femoral prosthesis looks like a combination of the Smith-Peterson and Judet prostheses (Figure 1.7), and articulates against a metallic acetabular component. Resurfacing preserves the femoral head and neck, and transfers stress to the femoral shaft in a more natural way than the cemented or cementless stems discussed previously. Because the diameter of the femoral component is large compared to the Charnley low friction prosthesis (Figure 1.4), the friction between articulating

surfaces must be kept to a minimum. Great efforts are put into manufacturing techniques that minimise variation of sphericity, surface finish, clearance and metallurgy – factors that can exacerbate the wear rate. Resurfacing survival rates are good, but available only in the short term (Treacy *et al.*, 2005).

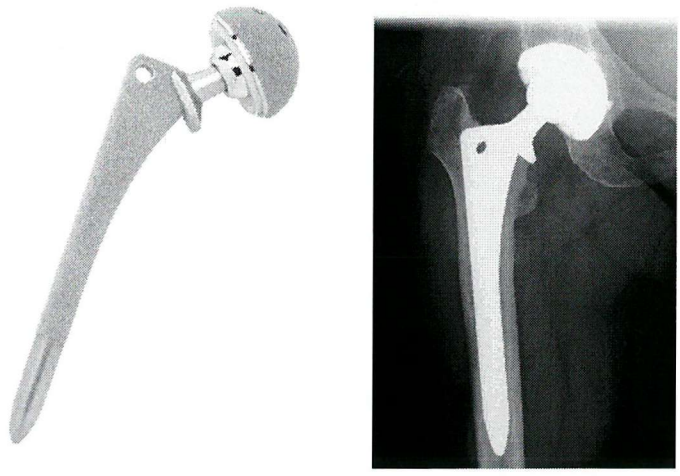

Figure 1.6: Cementless prosthesis (DePuy AML), and radiograph of cementless total hip arthroplasty.

Development of alternative arthroplasty procedures has not stopped the development of cemented total hip arthroplasty. Perhaps the greatest improvement since its inception has been in the cementing technique. This includes efforts to reduce the likelihood of air entrapment during cement mixing (creating pores), and better preparation of the femoral cavity to increase bone/cement interdigitation. The latest generation of cementing technique includes brushing, irrigation and drying of the femoral canal, mixing the cement under a vacuum, cement injection into the femoral canal using a delivery gun and using centralisers to ensure optimal positioning of the prosthesis (Haydon *et al.* 2004). The development of cemented prostheses has not been stagnant either – a major development was the introduction of the Exeter prosthesis in 1970, which had a polished double tapered stem designed to press the cement into the trabecular bone of the femoral canal during insertion of the stem (Figure 1.8). This design in polished form (a matte finish was tried and soon abandoned due to increased instances of loosening) was, and indeed still is, a success with 100% survivorship reported at 8-12 years follow-up (Williams *et al.*, 2002). The Exeter prosthesis deals with load transfer in a different way to the Charnley prosthesis, as the tapered stem, polished surface finish and absence of a

collar suggest. The Charnley is a shape-closed design, i.e. it relies on the prosthesis shape (the collar and cobra-like flanges) to minimise the stresses in the cement. The Exeter on the other hand is a force-closed design, i.e. it subsides within the cement mantle and wedges tighter to achieve stability.

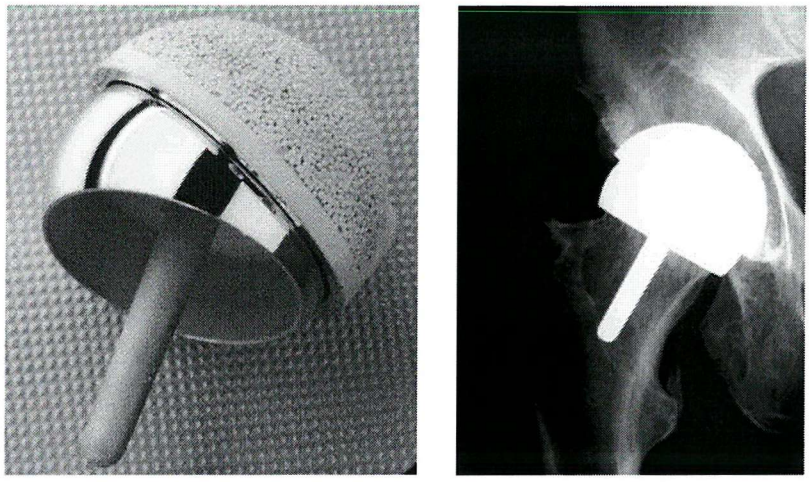

Figure 1.7: Femoral resurfacing components (manufactured by Finsbury Orthopaedics). Femoral head is hollow and requires minimal bone removal.

The Charnley and Exeter prostheses are examples of successful innovation in total hip replacement, and remain the most popular brands in use today in the UK (Gregg *et al.*, 2004). In addition to these two brands, there are 79 other prosthesis brands in use in the UK alone, made by 23 different manufacturers, and mostly introduced since the Charnley and Exeter designs (Gregg *et al.*, 2004). These have not always been successful devices – for example the Capital prosthesis, introduced to the market by the 3M Corporation in 1991. High early loosening rates were reported (26% at 26 months (Massoud *et al.*, 1997)), leading to its withdrawal from clinical use in 1998. Newly introduced prostheses should ideally perform better than the existing standard, but at least not perform *worse* than the existing standard (in this case the Charnley/Exeter). However, as demonstrated with the 3M Capital hip, this is not always the case, suggesting that manufacturers are under pressure to introduce new prosthesis designs to clinical trials without adequate preclinical testing.

One of the problems with orthopaedic research is that only long-term follow up studies can say definitively that a design modification, or change of materials for example, is a success. However, the latest preclinical testing methods do attempt to simulate the long term *in vivo* (in the body) failure mechanisms, and can be performed *in vitro* (outside the body) or *in silico* (by computer simulation). Of course such methods cannot simulate *exactly* the *in vivo* conditions, for example the biological response to either wear debris or a change in bone architecture due to the stress change when the prosthesis is introduced. However, as long as the limitations of these preclinical tests are considered when interpreting the results, they can be used to prevent inferior designs reaching clinical trials. This in turn may accelerate the development process, which would be advantageous when considering the number of candidates put forward for hip replacement, and the increased demands made of the reconstructed hip.

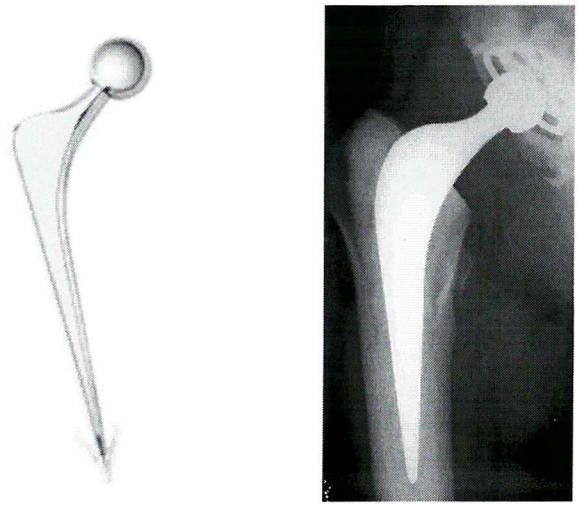

Figure 1.8: Exeter double tapered cemented prosthesis (Stryker Orthopaedics).

This thesis describes the development of existing *in silico* methods to simulate the long term failure of the cement mantle in total hip replacement – a failure mechanism that has been identified as one of the most common causes of implant loosening. The *in silico* method is developed and first applied to simple uniaxial tensile and 4-point bend fatigue models, with results compared to experimental tests. The method is then applied to a quasi-3D *in vitro* model of the implanted femur, and results again compared to experimental tests. Finally, the analysis is applied to a physiological model of the implanted femur, and results compared to failure modes observed clinically. The goal,

therefore, of the thesis is to present a method that can be used by the device manufacturers to prevent future prostheses, that may cause early cement mantle failure, reaching clinical trials. However, as with all preclinical testing, caution must be exercised in extrapolating the results to the *in vivo* situation.

1.1 References

Callaghan, J.J., Templeton, J.E., Liu, S.S., Pedersen, D.R., Goetz, D.D., Sullivan, P.M. and Johnson, R.C., 2004. Results of Charnley total hip arthroplasty at a minimum of thirty years. Journal of Bone and Joint Surgery-American Volume, 86(4): 690-695.

Charnley, J., 1979. Low friction arthroplasty of the hip, theory and practice. Springer-Verlag, Berlin.

Gregg, P.J., Porter, M., Wilton, T., Thompson, C., Crosbie, A., Borroff, M., Timperly, J., Howard, P., Van der Meulen, J.H.P. and Davies, F., 2004. National joint registry for England and Wales. The National Joint Registry Centre, www.njrcentre.org.uk.

Haydon, C.M., Mehin, R., Burnett, S., Rorabeck, C.H., Bourne, R.B., McCalden, R.W. and MacDonald, S.J., 2004. Revision total hip arthroplasty with use of a cemented femoral component - Results at a mean of ten years. Journal of Bone and Joint Surgery-American Volume, 86A(6): 1179-1185.

Hettfleisch, J. and Wissenbach, R., 1994. Forty-year survival of a Judet prosthesis: A case report. Journal of Bone and Joint Surgery-British Volume, 76(4): 671-672.

Herberts, P. and Malchau, H., 2000. Prognosis of Total Hip Replacement. http://www.jru.orthop.gu.se.

Kamangu, M. and Burette, J.L., 2002. Fifty year survival of a Judet acrylic prosthesis. Acta Orthopaedica Belgica, 68(4): 408.

Kingston, R. and Walsh, M.G., 2001. The evolution of hip replacement surgery. The Irish Medical Journal, 94(1) Editorial.

Klenerman, L., 2002. The evolution of orthopaedic surgery. The Royal Society of Medicine Press Ltd, London.

Massoud, S.N., Hunter, J.B., Holdsworth, B.J., Wallace, W.A. and Juliusson, R., 1997. Early femoral loosening in one design of cemented hip replacement. Journal of Bone and Joint Surgery-British Volume, 79B(4): 603-608.

O'Shea, K., Bale, E. and Murray, P., 2002. Cost analysis of primary total hip replacement. The Irish Medical Journal, 95(6): 177-180.

Radcliffe, S.N. and Geary, N.P.J., 1997. 46-year survival of a Smith-Petersen mould arthroplasty. Journal of Arthroplasty, 12(5): 584-585.

Robinson, A., Palmer, C. and Villar, R., 1999. Is revision as good as primary hip replacement? Journal of Bone and Joint Surgery-British Volume, 81(1): 42-45.

Stringer, C. and Gamble, C., 1993. In search of the Neanderthals: solving the puzzle of human origins. Thames & Hudson, London.

Thurston, A.J., 1999. Giovanni Borelli and the study of human movement: an historical review. Australian and New Zealand Journal of Surgery, 69: 276-288.

Treacy, R.B.C., McBryde, C.W. and Pynsent, P.B., 2005. Birmingham hip resurfacing arthroplasty - A minimum follow-up of five years. Journal of Bone And Joint Surgery-British Volume, 87B(2): 167-170.

Williams, H.D.W., Browne, G., Gie, G.A., Ling, R.S.M., Timperley, A.J. and Wendover, N.A., 2002. The Exeter universal cemented femoral component at 8 to 12 years. Journal of Bone and Joint Surgery-British Volume, 84(3): 324-334.

Wroblewski, B.M., Siney, P.D. and Fleming, P.A., 2001. Charnley low-frictional torque arthroplasty in patients under the age of 51 years - follow up to 33 years. Journal of Bone and Joint Surgery-British Volume, 84(4): 540-543.

CHAPTER 2

LITERATURE REVIEW

The literature review is divided into three sections:

(2.1) *Biomechanics of the hip* covers literature regarding the anatomy of the hip and the loading/forces experienced during various activities.

(2.2) *Loosening of the femoral component in total hip replacement* includes studies that have investigated loosening (or failure) scenarios *in vivo*, *in vitro* and *in silico*.

(2.3) *Bone cement in orthopaedic surgery* deals with the mechanical properties of bone cement that have been related to its long-term performance.

A final section (2.4) describes briefly the aims of this thesis, and how they relate to the existing literature.

2.1 Biomechanics of the hip

2.1.1 Anatomy of the hip

The hip is one of the largest and most stable of the joints in the human body. It has a large range of motion, which allows normal movement in the performance of daily activities. The primary stability is provided by the ball and socket configuration and is enhanced by ligaments and the surrounding musculature. The bony structure of the hip, joint capsule and reinforcing ligaments are shown in Figure 2.1. The Young's modulus for the cancellous bone is in the region of 0.1 – 2GPa, and approximately 17GPa for the surrounding cortical bone (Reilley *et al.*, 1974).

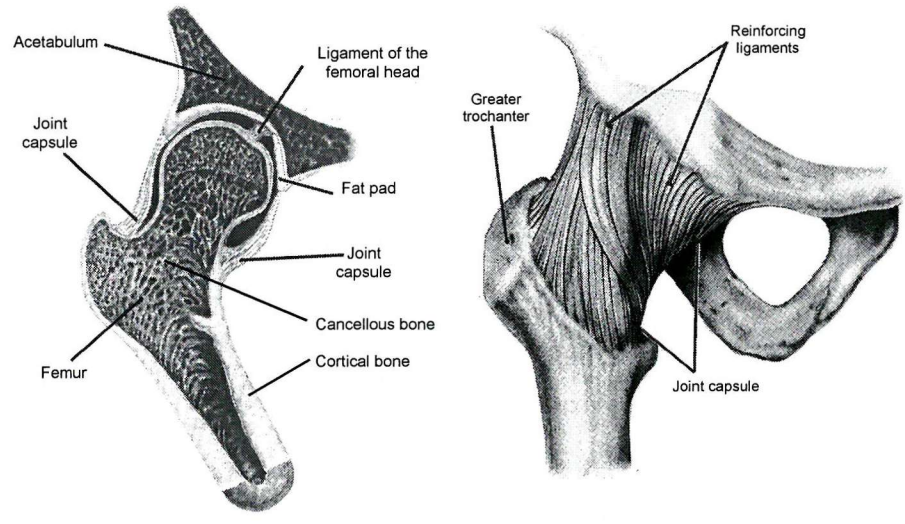

Figure 2.1: Bony structure of the hip and the joint capsule (Martini and Bartholomew, 2000).

Figure 2.2 illustrates the directions of motion of the lower extremity. Medial and lateral directions are towards and away from the midline of the body respectively, anterior and posterior are towards the front and back of the body respectively and proximal and distal are towards and away from the point of limb attachment to the body respectively. Abduction is the action of raising the thigh to the side of the body from the stance position; adduction returns it to the stance position. The muscles active during abduction are the gluteus medius and minimus (Figure 2.3a) and the tensor fasciae latae (Figure 2.4a). Muscles required to perform adduction include the adductor magnus, the adductor brevis, the adductor longus, the pectineus and the

gracilis (Figure 2.3b). When an athlete suffers a pulled groin, one of these muscles has been injured (Martini and Bartholomew, 2000).

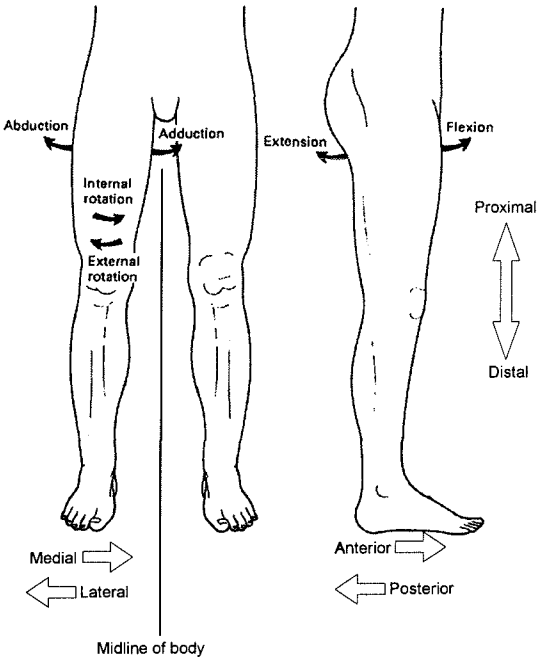

Figure 2.2: Classification of movement of the lower limb (Martini and Bartholomew, 2000).

From the stance position, flexion at the hip raises the thigh in front of the body. Extension returns the thigh to the stance position (see Figure 2.2). The largest hip flexor is the iliopsoas muscle (Figure 2.3b). This is really two muscles, the psoas major and the iliacus, which both connect to the femur at the greater trochanter. The tensor fasciae latae, rectus femoris and the sartorius (see Figure 2.4a) are also active during flexion. Thigh extension requires activity from the gluteus maximus (Figure 2.3a) and the hamstrings (the hamstrings is made up of three muscles – the biceps femoris, the semimembranosus and the semitendinosus, shown in Figure 2.4b).

Internal and external rotation of the thigh is shown in Figure 2.2. The gluteus medius, adductor longus, pectineus and hamstring muscles (Figures 2.3a, 2.3b & 2.4b) are active during internal rotation. For external rotation, the gluteus maximus and sartorius are required (Figure 2.3). The muscles active for the described movements are summarised in Table 2.1. The range of motion for each movement is summarised in Table 2.2. A greater angle of abduction can be achieved than adduction (30° versus 25°), and the largest motion is flexion (140°). More external rotation is possible (90°)

than internal rotation (70°), but these values are only a rough guide, different people will exhibit different ranges of motions.

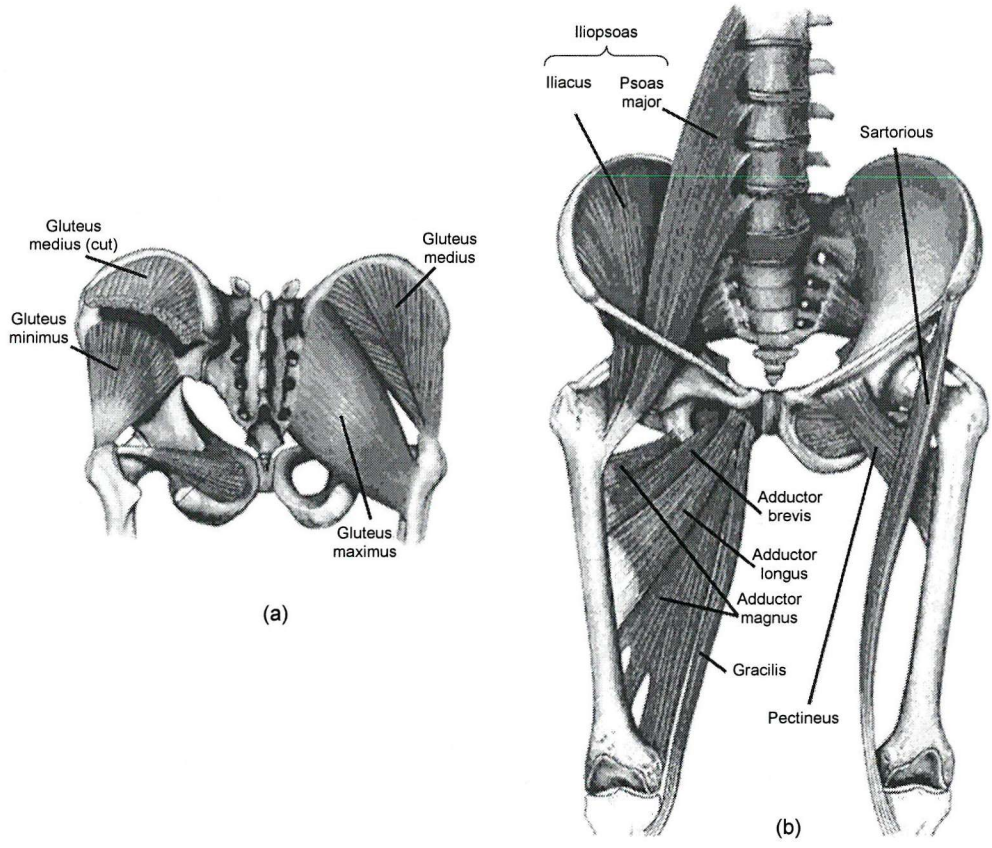

Figure 2.3: Anterior and posterior view of the pelvis showing (a) the gluteal muscle group and (b) the iliopsoas muscles and the adductor group (Martini and Bartholomew, 2000).

Action	Muscles active
Abduction	Gluteus medius/minimus, tensor fasciae latae
Adduction	Adductor magnus, adductor brevis, adductor longus, pectineus, gracilis
Flexion	Iliopsoas, tensor fasciae latae, rectus femoris, sartorius
Extension	Gluteus maximus, biceps femoris, semimembranosus, semitendinosus
Internal rotation	Gluteus medius, adductor longus, pectineus, semimembranosus, semitendinosus
External rotation	Gluteus maximus, sartorius

Table 2.1: Movements possible at the hip joint and muscles active during those movements (Martini and Bartholomew, 2000).

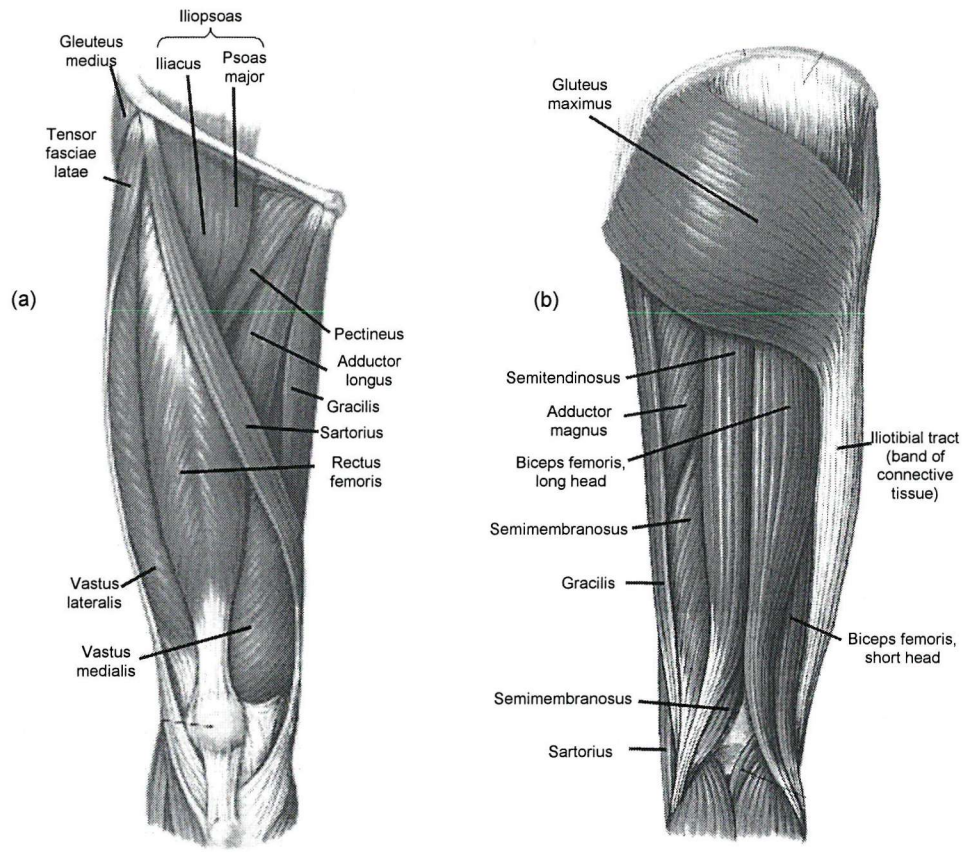

Figure 2.4: (a) Anterior and (b) posterior view of the thigh showing (a) the leg extensors, and (b) the leg flexors (Martini and Bartholomew, 2000).

Range of Motion	Angle
Abduction	30°
Adduction	25°
Flexion	140°
Extension	15°
Internal rotation	70°
External rotation	90°

Table 2.2: Range of motion of the hip joint (Martini and Bartholomew, 2000).

2.1.2 *Hip contact force*

The force experienced at the hip, or hip contact force, varies through the gait cycle. The gait cycle is summarised in Figure 2.5a, beginning with heel contact at the start of the right foot stance phase. The right foot is then in flat contact with the ground before the heel rises. The toe lifts off the ground after the heel and marks the end of the stance and beginning of the right swing phase. During the right swing phase, the left leg wholly supports the body. The swing phase ends with heel contact, and the cycle repeats itself. The same cycle applies to the left leg, with a difference in time as shown in Figure 2.5b.

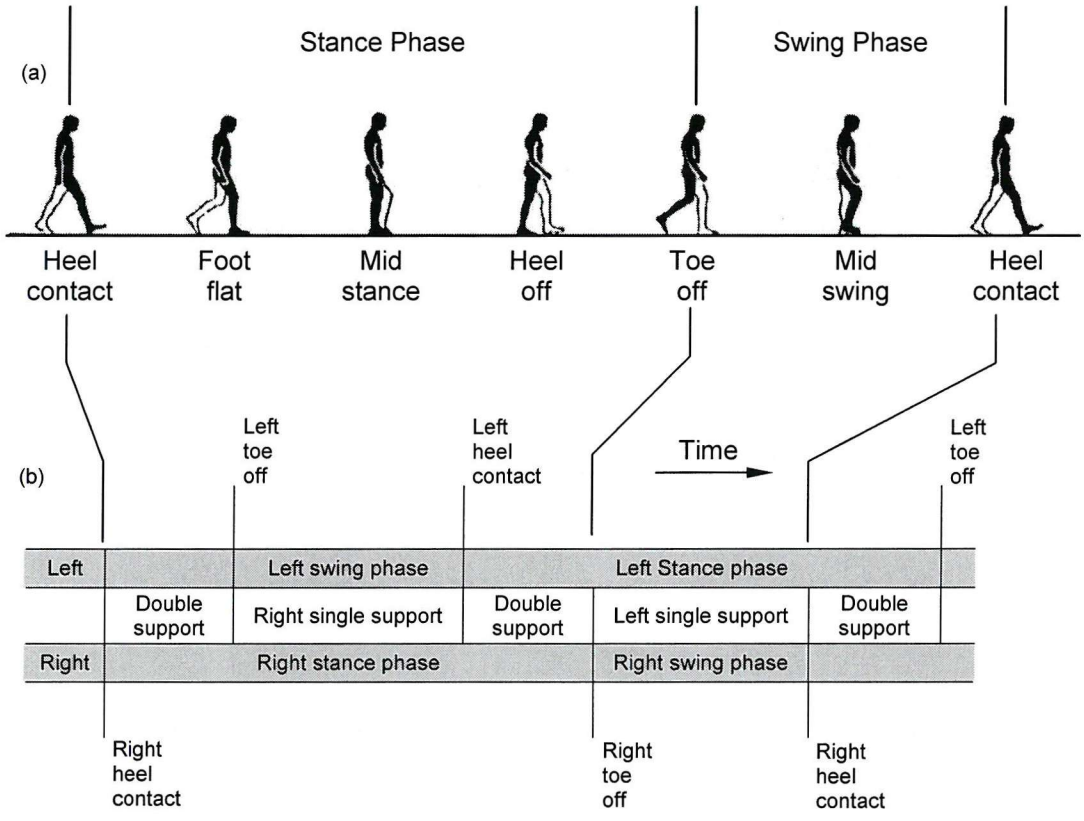

Figure 2.5: (a) The gait cycle and (b) timing of the gait cycle (Inman *et al.*, 1981).

The hip contact force through the gait cycle has been measured directly using instrumented hip prostheses (see Figure 2.6 for an example). Davy *et al.* (1988) implanted such a telemeterised total hip prosthesis in one patient, and recorded force data 31 days later. The force during the gait cycle followed a similar pattern to that in Figure 2.7, but with a peak hip contact force of between 260 and 280% bodyweight

(%BW). During stair climbing, the peak force was 260%BW. The torque on the implant was observed to increase notably during stair climbing. Taylor *et al.* (1997) implanted an instrumented proximal femoral endoprosthesis to record axial forces in the proximal shaft and at the distal end of the prosthesis in two patients. One week after implantation, the force in the proximal shaft of the prosthesis for normal gait was approximately 53%BW. After 23 months, gait forces were recorded again and had increased to a peak magnitude of 277%BW. A similar increase was noted for stair climbing loading, with a peak magnitude of 320%BW after 23 months. Bergmann *et al.* (1993) implanted instrumented hip prostheses in two patients, and measured force data during walking and running. Peak hip contact forces during walking were between 280 (walking at 1 km/hr) and 480 (walking at 5 km/hr) %BW. The peak torsional moments about the axis of the stem for walking were between 1.3 (at 1 km/hr) and 4.4%BWm (at 5 km/hr). Jogging raised the peak hip contact force to about 550%BW and the torsional moment to 5.3%BWm. During the course of this study, one patient stumbled while force data was being recorded, and a hip contact force of 870%BW was recorded, with a torsional moment of 5.4%BWm.

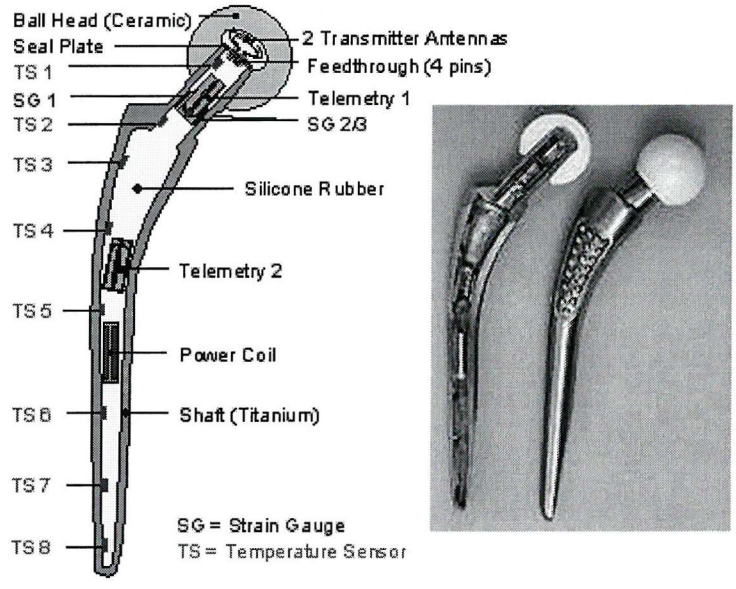

Figure 2.6: Instrumented hip prosthesis of Bergmann (2001).

In a further study, Bergmann *et al.* (1995) measured the hip contact forces for two patients during stair climbing. For one patient the peak hip contact force was about

350%BW, with a torsional moment of approximately 3.7%BWm. The other patient in this study generated a peak hip contact force of 550%BW and torsional moment of 5.7%BWm. The difference in these results led the authors to conclude that it might be possible to train patients to climb stairs in a manner that generates minimal hip contact forces and torsional moments. Bergmann *et al.* (2001) investigated the hip loading during activities other than gait or stair climbing, for example standing up, sitting down, 2-1-2 stance (two leg stance, followed by one leg stance and returning to two leg stance) and knee bend. These activities produced lower forces than those experienced during walking or stair climbing. The hip contact force and torsional moments for all the mentioned activities are summarised in Table 2.3.

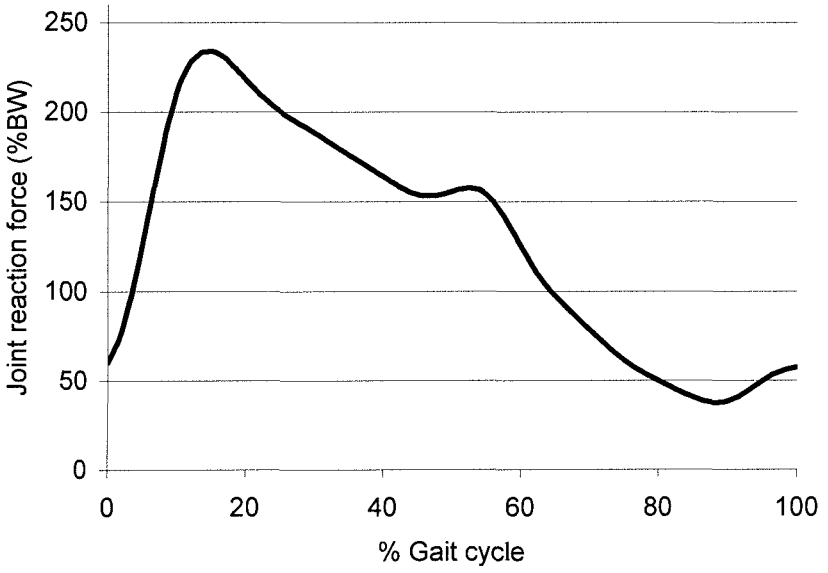

Figure 2.7: Typical joint reaction force diagram for the hip for normal gait. BW=bodyweight (Bergmann, 2001).

The hip contact force and torsional moment experienced by the implanted femur are critical in terms of the survival of the reconstruction. Identifying the activities that generate elevated forces/moments in the hip allows the patient to avoid or minimise these activities. Walking upstairs generates hip contact forces and torsional moments greater than level walking, but of a similar magnitude to walking quickly or jogging. This suggests stair climbing is not an extreme activity for a patient with an implanted

femur and that stumbling and other accidental movements, like missing the last stair or the pavement curb are more dangerous.

Activity	JRF (%BW)	Torsional moment (%BWm)	Reference
Walking	260-280	–	(Davy *et al.*, 1988)
	53*-277	–	(Taylor *et al.*, 1997)
	280-480†	1.3-4.4†	(Bergmann *et al.*, 1993)
	211-285	1.2-1.9	(Bergmann *et al.*, 2001)
Jogging	550	5.3	(Bergmann *et al.*, 1993)
Stumbling	870	5.4	(Bergmann *et al.*, 1993)
Stair climbing	260	–	(Davy *et al.*, 1988)
	61*-320	–	(Taylor *et al.*, 1997)
	350-550‡	3.7-5.7‡	(Bergmann *et al.*, 1995)
	227-314	1.8-3.0	(Bergmann *et al.*, 2001)
Standing up	181-220	0.8-1.2	(Bergmann *et al.*, 2001)
Sitting down	149-176	0.4-0.91	
2-1-2 stance	223-253	0.96-1.64	
Knee bend	117-177	0.58-0.83	

Table 2.3: Joint reaction force and torsional moments for routine activities. *Measurements taken one month post operatively. †Upper value for fast walking at 5 km/hr. ‡Upper value measured in one patient only and considered abnormally high (see text).

2.1.3 Calculated hip contact and muscle force

Current knowledge of muscle forces in the human body is limited. Non-invasive measurement of *in vivo* muscle forces has yet to be achieved and ethical considerations discourage the use of invasive methods to quantify these forces. The method that is currently practiced to estimate the complex distribution of *in vivo* muscle forces is mathematical optimisation algorithms. These require the assumption that the body selects muscles for a given activity according to some criterion, for example minimisation of muscle force, or maximum endurance of musculoskeletal function.

Crowninshield and Brand (1981) used the maximum endurance of musculoskeletal function criterion to calculate the muscle force in 47 muscles of the lower extremity. A relationship between a muscle's contractile force and the maximum time for which the contraction could be held was derived. By maximising the endurance of the muscles across the hip, knee and ankle joints, the forces in the muscles could be calculated, allowing the hip contact force to be predicted. The active muscles according to the optimisation method were compared to electromyographic data for the complete gait cycle, and 'substantial agreement' was observed. The predicted hip contact force for the gait cycle followed a similar double-peak pattern to Figure 2.7, with a maximum force of about 3.3kN (or 440%BW). This was higher than that measured with instrumented prostheses (see Table 2.3).

Glitsch and Baumann (1997) performed a study to investigate the influence of modelling the joints of the lower extremity as either hinged or spherical joints. Gait data and muscle optimisation techniques were used to calculate muscle forces and hip contact forces for normal gait and jogging. Depending on the means of joint modelling (hinged vs. spherical) the peak hip contact force was between 200 and 650%BW for walking, and 500 and 1700%BW for jogging. The active muscles according to the optimisation method were compared to electromyographic data gathered during the gait analysis, and were in good agreement. As with the study by Crowninshield and Brand (1981), the hip contact forces for both walking and running were higher than those measured with instrumented prostheses (see Table 2.3).

Brand *et al.* (1994) performed a similar muscle force optimisation study, but was able to compare the predicted hip contact force to that measured *in vivo* with an instrumented hip implant (for the same patient). The optimisation method yielded calculated values reasonably similar to measured values, with peak resultant forces in the range of 250 to 350%BW during level walking. The force varied through the gait cycle in a similar manner to Figure 2.7. In this study, the hip contact forces were measured 58 days post operatively, but the gait analysis was performed 90 days post operatively, so a cycle-to-cycle comparison of measured and calculated hip contact forces was not possible.

Pedersen *et al.* (1997) further developed the optimisation method of Brand *et al.* (1994), and predicted not only the magnitude of the hip contact force but also the direction of this force. The peak force was similar to previous studies – 310%BW, and while loads on the femoral head had a fairly constant direction, the loading direction on the acetabulum varied considerably. The authors proposed that it might be reasonable to only consider two or three major muscles when analysing the proximal femur, but studies of the acetabulum should have a more comprehensive muscle loading.

A further optimisation study was conducted by Heller *et al.* (2001), and arguably provides the most comprehensive analysis of the muscle forces at the hip as four patients were included, each with an instrumented hip prosthesis. Gait analysis was performed, and the minimisation of muscle force optimisation criterion employed to calculate muscle forces for walking and stair climbing. Figure 2.8 shows a graphical representation of the measured and calculated values for hip contact force gained in one patient. The muscle forces at the time of peak hip contact force are summarised in Table 2.4.

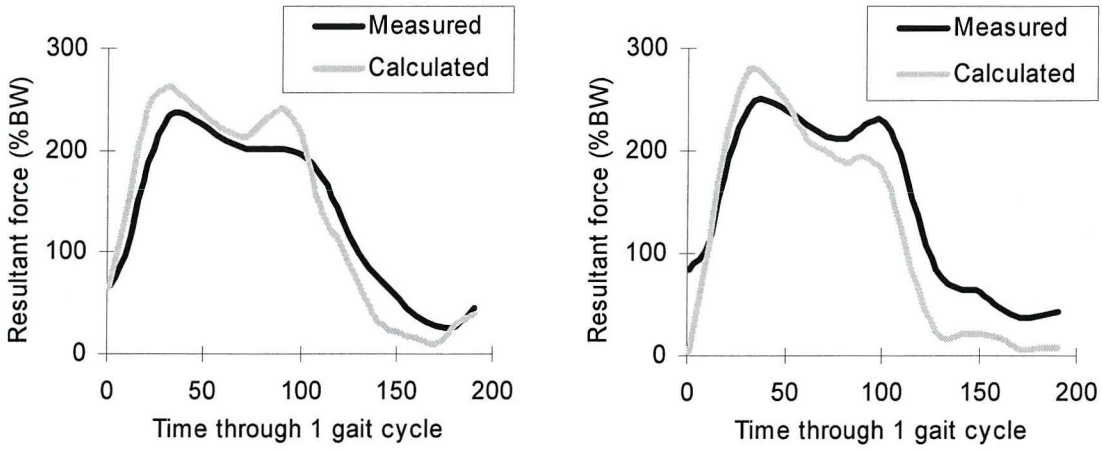

Figure 2.8: Resultant hip joint reaction force over (a) one gait cycle and (b) one stair climbing cycle as calculated and measured by Heller *et al.* (2001).

Muscle	Force (%BW)	
	Normal gait	Stairs up
Abductor	104.2	113.8
Adductor	0.0	0.0
Iliotibial tract, proximal	0.0	16.8
Iliotibial tract, distal	0.0	16.8
Biceps femoris long head, segment 1	4.1	0.0
Biceps femoris long head, segment 2	4.1	0.0
Semimembranosus, segment 1	60.0	0.0
Semimembranosus, segment 2	60.0	0.0
Semitendinosus, segment 1	0.0	85.3
Semitendinosus, segment 2	0.0	85.3
Tensor fascia lata, proximal part	19.0	6.5
Tensor fascia lata, distal part	19.0	6.5
Vastus lateralis	94.8	137.0
Vastus medialis	0.0	270.1

Table 2.4: Forces in the muscles of the hip joint calculated by Heller *et al.* (2001).

2.1.4 *The influence of muscle forces in the proximal femur – experimental studies*

One major mechanical function of muscles is to provide static and dynamic stability of the musculoskeletal system by balancing external moments not only at joints but also along limbs. Pauwels (1980) proposed that bending moments are transmitted along limbs by a combination of tensile forces in the muscles and compressive forces in the bones. Since the lever arm available to external loads can be much greater than those of the muscles, the force in the muscles can be greater than the external load. As a result, the force transmitted through the bones will be even larger. Several studies have investigated the influence of muscle force on the proximal femur (intact and implanted), using *in vivo*, *in vitro* and numerical approaches.

An *in vivo* study by Lu *et al.* (1997) recorded axial force from two patients with instrumented massive proximal femoral endoprostheses. By subjecting the patients to exercises of the hip flexors, extensors, gluteal muscles (abductors) and adductors, the lever arms available to external loads could be varied. Kinematic, force plate and electromyographic data was recorded for the exercises, and the ratio of the telemerised axial force to the external force calculated. This ratio ranged from 1.3 for double leg stance to 29.8 when the abductors were exercised, suggesting that the abductor muscles were increasing the compressive axial force on the femur. This in turn implied that the moments transmitted by bones were much smaller than limb moments.

In vitro studies of muscle force activity at the proximal femur have also been undertaken. Cristofolini *et al.* (1995), using an embalmed human femur, simulated proximal loading during early stance phase in gait. Ten thigh muscles were simulated with nylon straps: 3x abductors, 3x vasti, rectus femoris, adductor longus, adductor magnus and the biceps femoris. The muscle forces applied were taken from two previous optimisation studies (Crowninshield *et al.*, 1978; Patriarco *et al.*, 1981). Femoral strains were recorded with hip contact force alone, and compared to those recorded with each of the muscles listed above. The abductors had the greatest influence on the strains in the femur – including them elevated the strains on the medial and lateral aspects by a factor of two with respect to the hip contact force only loadcase. The increase in strains corresponded to bending in the mediolateral plane.

The second most significant muscle was the rectus femoris, which also generated bending in the mediolateral plane. However the increase in strains were only 10 to 50% of those generated by the abductors.

Simoes *et al.* (2000) considered that there is little medial deflection of the loaded femoral head during one-legged stance, and proposed that a horizontally constrained femoral head may be a reasonable simplification. Abductors, iliopsoas muscles and the vastus lateralis were applied to an *in vitro* synthetic composite femur. Muscle forces were taken from optimisation studies in the literature. The strains produced by the hip contact force were greater than those gained with an unconstrained femoral head (measured by Cristofolini *et al.* (1995), previous paragraph). The abductors served to reduce the strains in the femur, but only because the horizontal component of the force was removed by the constrained femoral head. The constrained femoral head also minimised femoral bending, and increased the horizontal component of the hip contact force. In this study, the iliopsoas and vastus lateralis had the effect of creating a predominantly compressive strain distribution in the femur.

In a study to develop an *in vitro* preclinical testing procedure, Britton *et al.* (2003) tested implanted synthetic composite femurs, and investigated the effect of including abductors, vastus lateralis and tensor fasciae latae. Ten implanted femur models were tested, five with muscle loading and five without. Fatigue testing was performed and the migration of the implants monitored with linear variable displacement transducers (LVDTs). The implant migration rates for both sets of femoral components were comparable to clinical data, but a lower mean migration and less experimental scatter was observed for the specimens with muscle loading, suggesting the action of the muscles stabilised the implanted construct. The authors recommended that further *in vitro* tests include the action of muscle forces to provide increased confidence in the results obtained.

2.1.5 *The influence of muscle forces in the proximal femur – computational studies*

Finite element studies allow the stress throughout the femur to be analysed, and can therefore provide useful information regarding the muscle loading of the femur. Lengsfeld *et al.* (1996) simulated the hip contact force and iliotibial tract in a finite element model of the intact proximal femur and found the femoral strains were sensitive to the iliotibial tract force. The iliotibial tract was modelled as a tension band running from the greater trochanter (see Figure 2.9a). Taylor *et al.* (1996) performed a combined finite element/radiological study to investigate the primary mode of loading of the intact femur. Radiological assessment of two subjects revealed minimal bending of the femur during one-legged stance, suggesting the femur was primarily loaded in compression. In a finite element model of the intact femur, the hip contact force, abductors, iliotibial tract and iliopsoas were simulated, and it was found that including the muscle forces reduced bending in the femur, but did not eliminate it completely. The cross-section of the diaphyseal region of the femur is approximately circular, indicating the *in vivo* loadcase is more likely to be compressive. The iliotibial tract was modelled in the same manner as Lengsfeld *et al.* (1996), shown in Figure 2.9a.

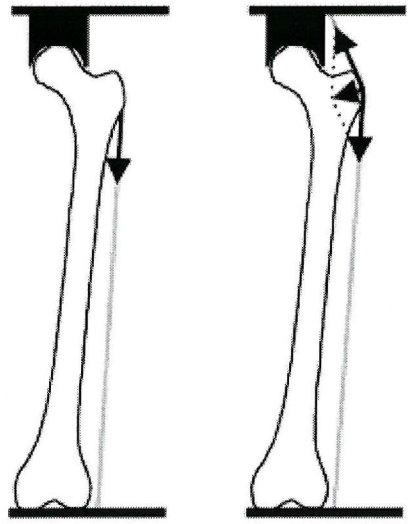

Figure 2.9: Two different ways of modelling the iliotibial tract: (a) as a tension band running from the greater trochanter and (b) as a tension band running from the pelvis to the tibia, wrapped around the greater trochanter (Stolk *et al.*, 2001).

Another finite element study was presented by Duda *et al.* (1998), and used muscle attachment data and muscle force magnitudes and orientations from the literature. The stresses and strains in the femur were compared for several stages during the gait cycle. When all muscles were included with the hip contact force, the femoral strains were considered similar to *in vivo* recordings. Simplifying the muscular loading to include just the abductors and iliotibial tract increased femoral strains by up to 26%. This difference was reduced to 5% by including the adductors, suggesting that a reasonable representation of the forces in the femur can be obtained by including hip contact force, abductors, iliotibial tract and adductors. In this study, the iliotibial tract was modelled as a tension band running from the pelvis to the tibia, wrapped around the greater trochanter (2.9b).

The finite element studies discussed thus far used a model of the intact femur. A finite element model of an implanted femur was generated by Stolk *et al.* (2001), and hip contact forces applied for several stages during level gait. Firstly, the hip contact was applied with no muscular loading, followed by inclusion of the abductors, then the iliotibial tract and finally addition of the adductor and vastus groups. The abductors had the most pronounced effect on the stress distribution in the implanted construct, compared with the other muscles. The iliotibial tract was modelled in the same manner as Duda *et al.* (1998) (see Figure 2.9b).

The only common theme in the studies discussed in this and the previous section is that the abductor muscles have the greatest influence of all the muscular forces in both the intact and implanted proximal femur. After that the findings are subjective – Cristofolini *et al.* (1995) found the rectus femoris to be the next most significant, Simoes *et al.* (2000) consider the iliopsoas and vastus lateralis important and Britton *et al.* (2003) regarded the vastus lateralis and tensor fasciae latae as important. Finite element studies also agree that the abductor muscles have the greatest influence on the stresses in the intact and implanted femur. Lengsfeld *et al.* (1996), Taylor *et al.* (1996) and Duda *et al.* (1998) all found the iliotibial tract to have an influence of the stress/strain distribution in the intact femur, but Stolk *et al.* (2001) found it to have a negligible influence on the stresses/strains in the implanted femur. More recent studies of the proximal femur, for example the *in vivo* study by Britton *et al.* (2003) and the computational simulation of cement mantle damage by Stolk (2003) used the

simplified muscle force loading presented by Heller *et al.* (2001), which appeared as part of a CD-ROM attachment to the Journal of Biomechanics (Bergmann, 2001) (discussed earlier, see Table 2.4). This included the abductors, tensor fascia latae and the vastus lateralis.

This CD-ROM attachment included the joint reaction force data of Bergmann (2001) (discussed in Section 2.1.2) and muscle force data of Heller *et al.* (2001), and therefore represents the most comprehensive study of hip contact and muscular force to date. The CD-ROM format also allowed a large amount of data to be presented – hip contact and muscular forces data were presented at many stages through the gait cycle.

2.2 Failure of the femoral component in hip replacement

2.2.1 Failure scenarios

A total hip replacement should ideally remain functional for the lifetime of the patient, but unfortunately this is not always the case. A hip replacement is considered to have failed when it causes the patient pain and/or loss of function, and requires a revision operation to relieve that pain. Hip register studies are a valuable source of information regarding likely causes of hip replacement failure. Sweden was the first European country to have a national hip register (1979) (Herberts *et al.*, 2002), followed by Finland (1980) (Puolakka *et al.*, 2001), Norway (1987) (Havelin *et al.*, 2000) and Denmark (1995) (Lucht, 2000). Despite the success of the Scandinavian national registers, other European countries have been slow to follow – in the UK for example, the first regional hip study did not appear until 1999 (Fender *et al.*, 1999). According to the register studies, aseptic loosening is the major failure mechanism, and accounts for 60% to 75% of revision operations (Havelin *et al.*, 2000; Herberts *et al.*, 2002; Lucht, 2000; Puolakka *et al.*, 2001). Other less common causes of failure include infection (7%), dislocation (5%) and implant fracture (2%) (Herberts *et al.*, 2002). The register studies also provide useful data on the performance of different implant designs or bone cements. Aseptic loosening, as the primary cause of implant failure is now examined in more detail.

Implant failure by aseptic loosening should be considered a process, rather than an event. Defects in the cement mantle, implant migration and radiolucent lines have all been associated with loosening, and can be monitored *in vivo* by radiographic assessment. The criteria introduced by Harris *et al.* (1982) have become a popular means to quantify implant loosening in radiographic studies (see Table 2.5), but a loose implant does not necessarily mean a failed implant. Figure 2.10 shows a radiograph of a replacement 10 years post operatively, with signs of definite loosening according to Table 2.5 (Stauffer, 1982). There is a 5mm radiolucency at the superolateral aspect of the stem, a crack in the cement mantle near the tip of the stem and an implant migration of 7mm. Despite the signs of loosening, the patient was quite comfortable and not experiencing any pain.

Definite loosening	Stem migration (medial collar to calcar; if no collar, then tip of prosthesis to calcar); stem/cement mantle fracture
Probable loosening	Continuous radiolucent line surrounding entire cement mantle on any view
Possible loosening	Radiolucent zone involving 50%-99% of cement-bone interface on any view and radiolucency not present immediately postoperatively
Stable	None of above criteria met

Table 2.5: Classification of radiographic loosening according to Harris *et al.* (1982).

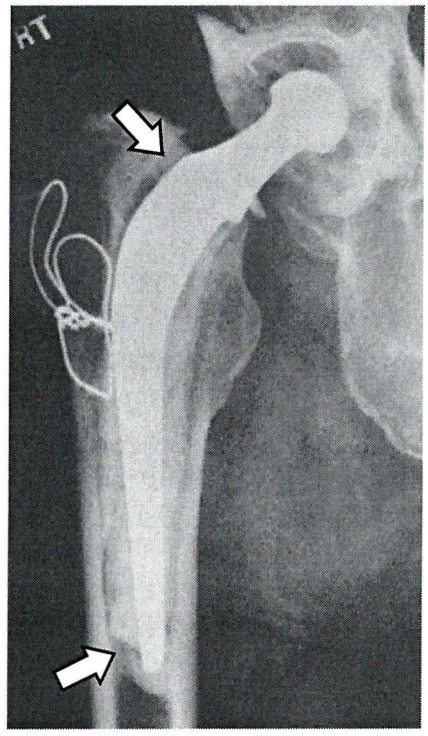

Figure 2.10: Radiograph of femoral component with signs of definite loosening. There is a 5mm radiolucency at the superolateral aspect of the stem (top arrow) and a cement mantle fracture at the stem tip (bottom arrow). Patient was asymptomatic at this time (Stauffer, 1982).

Concerns have been raised over the reliability of using radiographs to assess loosening. Reading *et al.* (1999) performed simulated hip arthroplasties on six pairs of cadaveric femurs and took radiographic images of the specimens. Specimens were then sectioned into 7mm slices, and assessed with high-resolution faxitron radiographs. Defects in the cement were observed up to 100 times more frequently in

the sectioned specimens, and the standard radiographs failed to show the presence of even "potentially serious defects in the cement mantle".

Because the *in vivo* loosening process is difficult to observe, most information regarding the mechanism of implant loosening is gained at time of revision or posthumously. These studies, along with the radiographic studies, have led to the proposal of several loosening mechanisms – particulate reaction, stress shielding, surgical trauma and damage accumulation in the cement mantle (Huiskes, 1993). These are discussed briefly below, but damage accumulation, being the focus of this thesis, is discussed fully in the following section.

The particulate reaction scenario is a wear related failure scenario. Wear particles are generated in the joint capsule, due to the articulation of the femoral head against the acetabular cup. These particles are capable of causing bone resorption (or osteolysis, dissolving of the bone matrix) (Athanasou *et al.*, 1992), and have been implicated in the particulate reaction failure scenario for the femoral stem (Schmalzreid *et al.*, 1992). Areas of resorbed bone (lysis) at the bone/cement interface were observed by Anthony *et al.* (1990), and could be related to a local defect in the cement mantle. Schmalzreid *et al.* (1992) suggested that wear particles travel from the joint capsule along a debonded stem/cement interface and through the defect in the cement to the bone/cement interface. The bone resorption usually coincides with fibrous tissue growth at the interface, which may be visible radiologically as a radiolucent zone.

Julius Wolff (1892) proposed that mechanical stress was responsible for determining the architecture of bone, i.e. bone is deposited in sites subject to an increase in stress and resorbed from sites subject to a decrease in stress. This became known as Wolff's law, and is the basis of the hypothesised stress shielding loosening mechanism. When a prosthesis is implanted in the femur, parts of the femur become under-stressed when compared to the intact femur, and resorption can occur according to Wolff's law. The resorption of bone has been observed on radiographs (although bone-mass reductions of up to 30 % may occur before they become visible), but failures were rarely reported (Karachalios *et al.*, 2004). Whether stress shielding is a failure mechanism or not, the loss of precious bone stock is of concern should a revision operation be necessary (Huiskes, 1993).

Trauma during surgery may result in bone death, resulting in poor initial stability for the implant, and thereby reducing the life of the replacement. Polymerisation of the bone cement and the associated exotherm has also been hypothesised as a cause of bone death during surgery. Bone cement is well tolerated by the body, but the monomer component (methylmethacrylate, MMA) can cause bone cell death at the bone/cement interface (Gough and Downes, 2001). It is possible to reduce the amount of residual monomer by increasing the polymerisation temperature, but high temperatures can also lead to bone death if the exposure time is long enough (Nzihou *et al.*, 1999).

The damage accumulation hypothesis is that pores and microcracks exist in the cement mantle of the implanted femur, even before loading commences (discussed in Section 2.3, page 59). When subject to a fatigue load, for example during normal gait, stress concentrations caused by pores may serve to initiate more microcracks. These cracks, and those that were previously present, may grow and coalesce under the fatigue loading, and eventually form critical defects, which serve to loosen the prosthesis. This process of damage accumulation also includes debonding at the interfaces (stem/cement and bone/cement), as well as failure of the supporting bone. There exists a large volume of literature investigating the role of cement mantle fracture in femoral component loosening, which can be divided into three categories: clinical studies that monitor *in vivo* conditions, *in vitro/silico* studies that consider initial conditions and *in vitro/silico* studies that consider the construct subject to fatigue loading.

2.2.2 *Cement mantle failure: in vivo studies*

Follow up studies have investigated the condition of the implanted femur construct by means of radiographic assessment. Gruen *et al.* (1979) (389 hips, 3 years post operatively), Stauffer (1982) (231 hips, 10 years post operatively) and Paterson *et al.* (1986) (882 hips, mean of 6.8 years post operatively) provide a comprehensive combined study, totalling over 1,500 hips. Of the prostheses considered loose, Gruen *et al.* (1979) found the majority (57%) to exhibit loosening at the bone/cement interface. Stauffer (1982) quoted a much lower figure – 19%, and Paterson *et al.* (1986) only found bone/cement interface loosening in "severely infected secondary loosenings excluded from the series". These apparent differences may have been due to different cementing techniques employed in the different centres (Gruen *et al.*– Division of Orthopaedic Surgery, UCLA, CA; Stauffer – Mayo Clinic, Rochester, MN; Paterson *et al.*– Queen Alexandra Hospital, Portsmouth, UK). The influence of cementing technique and cement/bone interdigitation is discussed in Section 2.3.1, page 62. Gruen *et al.* (1979), Stauffer (1982) and Paterson *et al.* (1986) found agreement on the stem/cement interface – they all reported radiolucency between the cement and the superolateral part of the stem (see Figure 2.10, page 31) in components that were considered loose. Gruen *et al.* (1979) considered 53%, Stauffer (1982) 81% and Paterson *et al.* (1986) 100% of loose components to exhibit lucency in this region. The cement mantle itself was also inspected in these follow-up studies – but the number of critical defects reported was low. Of the components considered loose, Gruen *et al.* (1979), Stauffer (1982) and Paterson *et al.* (1986) only observed cement mantle fractures in 22%, 26% and 26% of cement mantles respectively. However, that is not to say that critical defects were not present – the study by Reading *et al.* (1999) suggested that radiographs were unable to show even potentially serious defects in the cement mantle. Indeed, Stauffer (1982) comments on the difficulty of seeing cracks radiographically that were clearly visible at revision surgery, and Paterson notes that the out of plane fractures in the cement would not be detected by the radiograph. Stauffer (1982) goes on to conclude that the most common type of loosening was that resulting from complete cement mantle fractures, i.e. cracks extending from the stem/cement interface to the bone/cement interface and in the longitudinal plane (Figure 2.11).

A post-mortem study by Jasty *et al.* (1991) examined 16 femora between 2 weeks and 17 years post operatively. In all cases, patients were asymptomatic and only in one case was radiographic evidence of loosening observed, at the stem/cement interface. The cadaveric specimens were sectioned at 5mm intervals, and sections were examined by scanning electron microscope and contact radiograph. In none of the 16 specimens was there evidence of loosening at the bone/cement interface; rather the trabecular bone was intimately associated and interdigitated with the cement. The stem/cement interface was another matter; some debonding was seen in every specimen. Debonding was generally more extensive in the specimens retrieved latest. Fractures in the cement mantle were found on cut sections; specimens less than 10 years in situ showed incomplete cement mantle fractures (for example Figure 2.12), while specimens in place more than 10 years had complete cement mantle fractures (Figure 2.13).

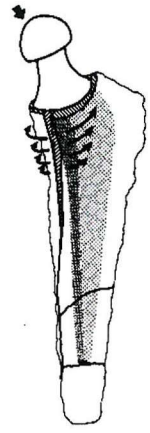

Figure 2.11: Schematic of cement mantle cracking that facilitates prosthesis loosening (Stauffer, 1982).

In some cases, evidence of fatigue in the form of discontinuous crack growth bands were identified on the fracture surfaces (Figure 2.14). Cracks in the cement mantle were observed at the stem/cement interface and appeared to grow radially into the cement (Figure 2.12). Pores and voids in the cement mantle were also associated with crack initiation and propagation (see Figure 2.15). Cement cracks were found to be progressive, increasing in number and extent with time, so that eventually more of the specimens may have shown loosening. Complete cement mantle fractures were only found in 10-year to 17-year specimens. Considering these results, Jasty *et al.* (1991) proposed that the cement mantle experienced a process of damage accumulation

before clinical loosening was apparent. Cracks in the cement could grow by means of fatigue, and eventually combine to form fractures through the thickness of the cement mantle. Only one specimen in this study had signs of radiographic loosening at the stem/cement interface, i.e. evidence of stem/cement separation. Indeed, Figure 2.13 suggests that complete cement mantle fractures are necessary for stem cement separation.

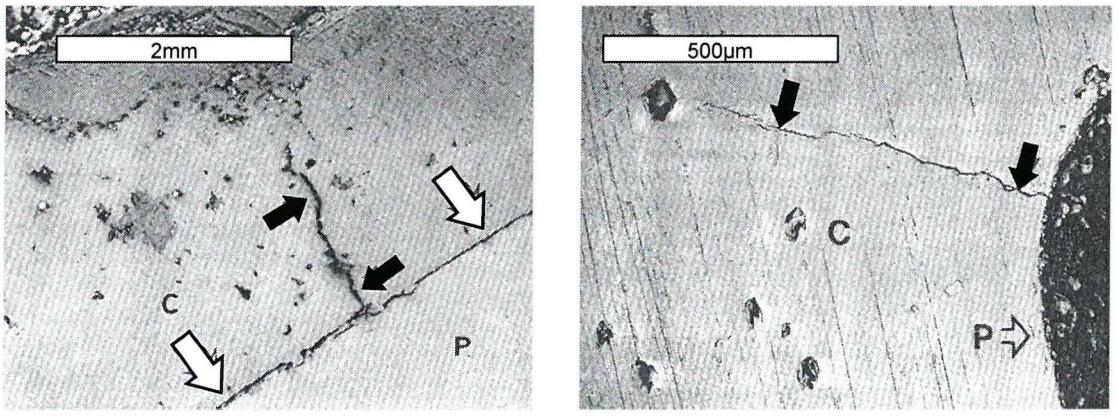

Figure 2.12: Scanning electron micrograph showing incomplete cement mantle fractures originating at the stem/cement interface (small solid arrows) and propagating in the radial direction. P = prosthesis stem, C = cement (Jasty *et al.*, 1991).

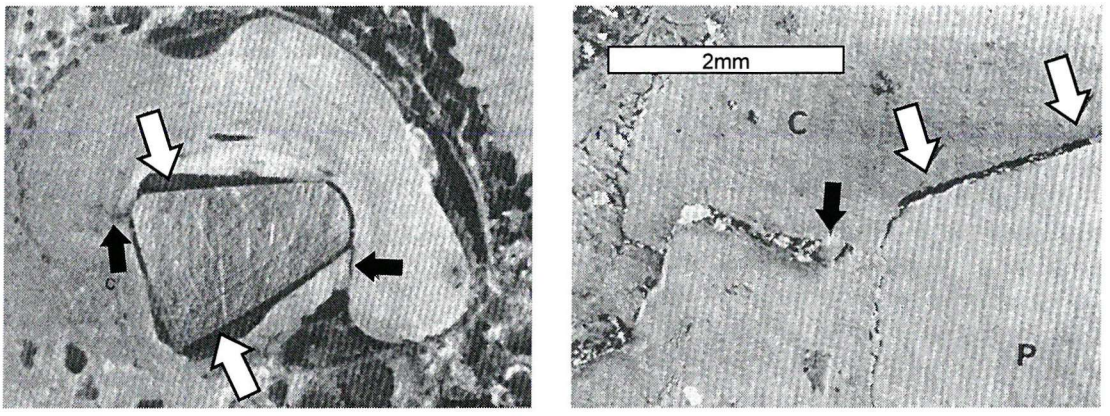

Figure 2.13: Scanning electron micrograph showing complete cement mantle fractures (small dark arrows). White arrows indicate separation at the stem/cement interface (Jasty *et al.*, 1991).

In a further clinical study, Topoleski *et al.* (1990) obtained specimens of bone cement from 12 failed replacements. Only pieces of fractured cement that were removed easily were included in the study, thus minimising artefacts on the fracture surface caused by instrument damage. Fracture surfaces were examined, and compared to *in vitro* fracture surfaces of bone cement tested to failure under the following conditions:

1. 3-point bend fatigue
2. Rotating-bend fatigue
3. 3-point bend (constant displacement rate)

The *in vivo* fracture surfaces were "remarkably similar" to the *in vitro* fracture surfaces. The role of pores was highlighted as having a clear influence on a propagating crack, on both *ex vivo* and *in vitro* specimens. Topoleski *et al.* (1990) concluded that fatigue crack growth was most likely the leading *in vivo* complete cement mantle fracture mechanism and that methods to prevent sub-critical crack propagation would be important for improving the mechanical performance of cement.

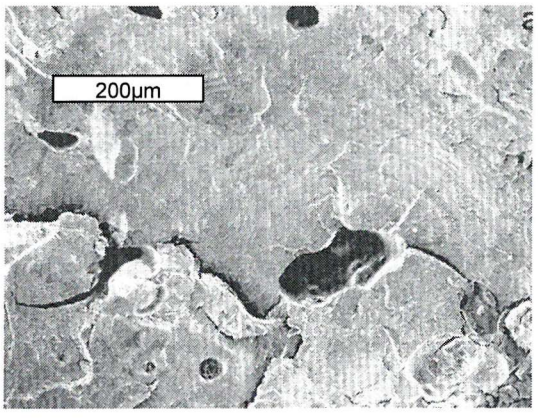

Figure 2.14: Scanning electron micrograph of discontinuous crack growth on a cement mantle fracture (Jasty *et al.*, 1991).

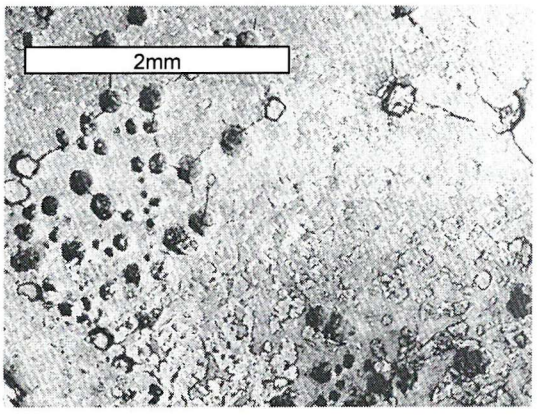

Figure 2.15: Scanning electron micrograph showing numerous small cracks through pores/voids near the distal end of the femoral stem (Jasty *et al.*, 1991).

The studies discussed in this section provide the main clinical evidence for the damage accumulation failure scenario. The radiographic assessment studies by Gruen *et al.* (1979), Stauffer (1982) and Paterson *et al.* (1986) all cite lucency at the stem/cement interface as a sign of implant loosening, and this has become universally adopted with the Harris loosening criteria (Table 2.5). Debonding of the stem/cement interface may occur within a short time postoperatively (Jasty *et al.*, 1991), but this would not be visible radiographically. Indeed Jasty *et al.* (1991) suggests that lucency at the stem/cement interface (i.e. separation at that interface) is only made possible by complete cement mantle fractures. Both Jasty *et al.* (1991) and Topoleski *et al.* (1990) propose that complete cement mantle fractures are formed by a process of fatigue crack growth, with pores and flaws in the cement mantle heavily influencing the crack growth process.

The clinical studies in this section rely either on radiographs or data gained at time of revision or posthumously. Although there is evidence to support the damage accumulation failure scenario, clinical studies have unavoidable limitations: for example it hasn't been possible to monitor fatigue crack growth *in vivo*. *In vitro/silico* testing, discussed in the following sections, allows more information to be gained regarding damage accumulation failure mechanisms, however, as with all investigations of this nature, *in vivo* conditions may not be adequately replicated.

2.2.3 *Cement mantle failure: in vitro studies and initial conditions*

In vitro studies of the cement mantle can be divided into two sections: those that assess the initial conditions (representing the immediate postoperative period), and those that simulate the construct under a fatigue load. The former are discussed in this section.

A number of *in vitro* studies have made use of strain gauges to assess the cement mantle under load. Crowninshield and Tolbert (1983) implanted femoral prostheses into cadaveric femora and embedded strain gauges in the proximal and distal cement mantle. The prosthesis/cement interface was either completely bonded or unbonded. A debonded interface was achieved by coating the prosthesis stem with a release agent prior to implantation. It was possible to remove the prosthesis without disturbing the cement mantle; reinserting with a coating of epoxy on (a) the whole stem and (b) the proximal part only created a fully bonded and proximally bonded stem/cement interface respectively. A joint reaction force was applied to the femoral head of the prosthesis and strains recorded for the different interface conditions. For the proximal gauges, both the fully and proximally bonded stems exhibited lower strains than the unbonded case. The greatest reduction in strain was measured in the anterior cement mantle, in the medial-lateral direction – 84% and 68% reduction for the fully bonded and proximally bonded stem respectively. Distal strain gauges measured little difference in strain for the different interface conditions. The authors proposed that a proximally bonded stem could have a similar effect on the cement strains as a fully bonded stem, with the advantage that it may be easier to remove should a revision operation be necessary. The authors also mention that this interface may become debonded over time, and that the consequences of this are not addressed in the study.

The study by Crowninshield and Tolbert (1983) only investigated the strains in the proximal and distal cement. O'Connor *et al.* (1996) used bone cement strain gauge carriers to position gauges throughout the cement mantle. In this way, cement strains could be recorded throughout the cement mantle for two loadcases – the stance phase of gait and stair climbing. The joint reaction and abductor muscle forces were used to simulate these loadcases. Perhaps surprisingly, in many areas of the cement mantle there was not a great difference between strains for these two loadcases, but in the

proximal cement, the stair climbing loadcase produced strains 300% greater than gait loading. For both loadcases, high localised strains were observed at the proximal and distal ends of the prosthesis, and the authors suggest that efforts should be made to protect the cement mantle in these sites. Three methods were proposed to achieve this: maintaining an adequate thickness of cement mantle, porosity reduction and changes to implant design.

Fisher *et al.* (1997) used embedded strain gauges to investigate the effect of cement mantle thickness on the strains in the cement mantle by implanting synthetic composite femurs with two different sizes of femoral stem. Different broach sizes were used to prepare the femur, generating a total of four different cement mantle thicknesses. Three biaxial strain gauges were embedded in the medial cement and three in the lateral cement. An axial load was applied to the head of the prosthesis, and strain gauge data was recorded. Increasing the cement mantle thickness from 2.4mm to 3.7mm reduced the distal lateral and distal medial axial strains by 40% and 49% respectively. In addition, the hoop strains in the mid-stem medial and mid-stem lateral cement were reduced by 29% and 44% respectively. Based on the results of this study, the authors proposed that a slightly thicker cement mantle (up to 3.7mm) could be used to protect areas of the cement mantle vulnerable to failure. A similar conclusion was reached by Mann *et al.* (2004), who performed *in vitro* fatigue simulations of cadaveric implanted femora. Through cement mantle cracks, most likely associated with loosening (Section 2.2.1, page 30) were mostly associated with a thin cement mantle, under 2mm thick (Mann *et al.*, 2004).

A combined experimental/finite element study of the strains in the cement mantle was undertaken by Harrigan *et al.* (1992). An intact cadaver femur was implanted with a femoral prosthesis, and strain gauges attached to the bone at three locations – below the prosthesis collar, half way down the prosthesis stem and at the stem tip. Gauges were also embedded in the cement mantle in the proximal, middle and distal regions. Strains were recorded for gait and stair climbing loadcases. A finite element model of the structure was generated, boundary conditions applied to simulate the experimental loading and pores simulated in the cement (see Section 2.3.5, page 100, for pore simulation details). The strains predicted by the finite element analysis were compared to the experimental data, and there was 'good but not excellent' agreement.

The finite element model predicted the correct sign of strain (tensile versus compressive), but the magnitude of strain was sometimes quite different. In the proximal cement mantle, strains differed by 10% to 40%. In the middle section, strains differed by 15% to 40% and in the distal cement strains differed by 30% to 40%. The authors suggested that these discrepancies could be due to local prosthesis/cement debonding or slipping at the prosthesis tip in the experimental specimens. The finite element model did not consider this, as the prosthesis/cement interface was modelled as fully bonded. The finite element model exhibited different stress fields for the different loading configurations. For gait loading, the maximum stress was 13MPa, and occurred at a pore distal to the prosthesis tip. The peak stress for the stair climbing loadcase was 22MPa, at a pore in the proximal postero-medial region, while the stress at a pore distal to the prosthesis tip was 15MPa.

Another combined finite element/experimental study by Wheeler *et al.* (1997) used two stainless steel tapered stems (one polished, one grit blasted) implanted into epoxy resin bone substitutes. Five strain gauges were embedded in the cement mantle from the proximal to distal ends (Figure 2.16). A compressive load was applied to the top of the stem and strains recorded. Axisymmetric finite element models of the structure were generated, and boundary conditions applied to simulate the experimental loading. The polished stem was simulated with an unbonded stem/cement interface and a coefficient of friction of 0.2, and a fully bonded interface was used to model the grit blasted stem. The finite element predictions compared well with the experimental data (Figure 2.16), for both bonded and unbonded stem cement interface conditions. For both interface conditions, peak strain was recoded towards the distal end of the cement mantle, approximately 500 microstrain and 30 microstrain for the unbonded and bonded interface respectively.

Migration, stem shape and surface finish was the subject of a study by Huiskes (1988). Two different prostheses were included – a 'shape-closed' and a 'force-closed' design. Bonding with the cement is desired for the shape-closed design, and the shape of the prosthesis attempts to minimise stress in the cement. An unbonded prosthesis/cement interface is desired by the force-closed design, and stability is achieved when the frictional force on the unbonded interface balances the applied load, i.e. the implant becomes wedged tightly in the cement mantle. Subsidence in finite element and *in*

vitro models of these types of prosthesis were analysed and compared to clinical radiostereophotogrammetric analysis. Clinical data was limited to 12 months post operatively; hence the study was limited to the initial conditions of the reconstructions. Finite element analysis predicted greater subsidence for the force-closed design; this was in agreement with the *in vitro* tests and clinical observations. In the finite element models, cement stresses were assessed as a function of cement volume. Assuming a fatigue limit of 2.4MPa (fatigue strength at 10 million cycles), the authors reported 1.8% and 0.3% of the cement volume above this limit for the force-closed and shape-closed designs respectively. This study did not attempt to determine which prosthesis type is the best for clinical use. Rather, it was demonstrated that the migration and stress transfer behaviour of a force-closed and shape-closed design are different. The authors highlighted this, and concluded that indications of *in vivo* migration could be gained from preclinical testing (finite element and *in vitro* models), but must be judged against the design philosophy of the prosthesis.

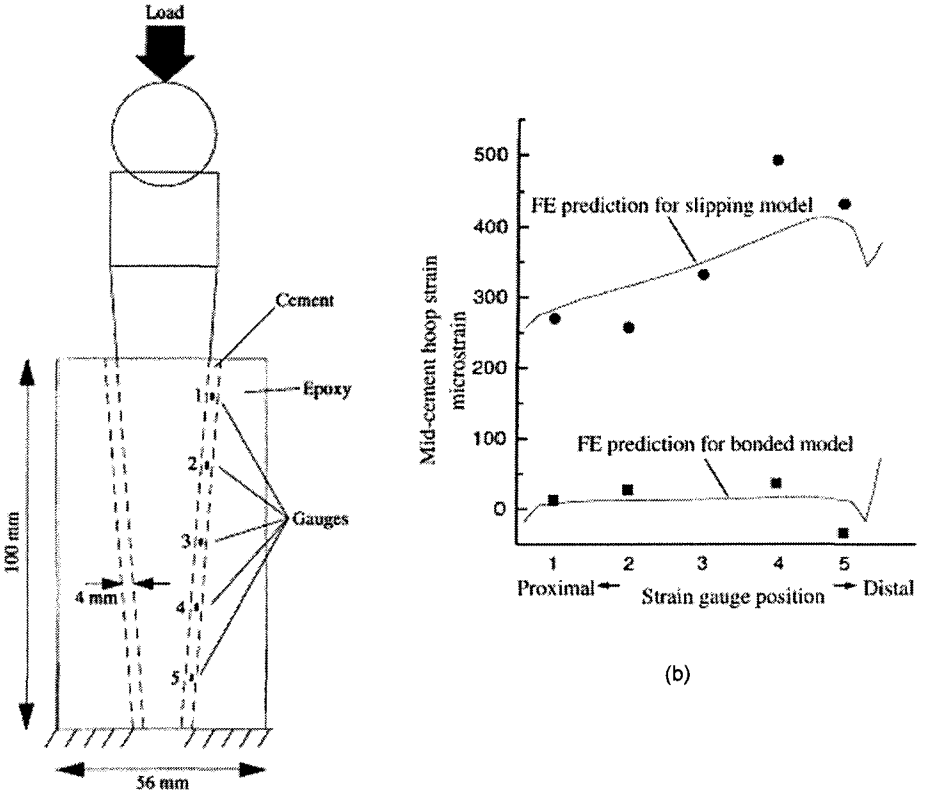

Figure 2.16: Experimental model of Wheeler *et al.* (1997) and comparison of finite element predictions with experimental data.

2.2.4 *Cement mantle failure: in silico studies and initial conditions*

The study of Harrigan *et al.* (1992), discussed in the previous section (page 39), was able to predict the correct sign of strain in implanted femur models using finite elements, but there was significant error in terms of the magnitude of the predicted strains. While finite element studies can provide useful information for the biomechanist, results should be considered alongside clinical and experimental findings.

Prendergast *et al.* (1989) used the finite element approach to investigate the influence of different stem and cement material properties on the stress distribution in the implanted femur structure. Increasing prosthesis stiffness tended to reduce the stresses in the cement, while increasing the cement stiffness increased the cement stresses. The maximum stresses in the cement were observed proximally. These results were gained with a stem/cement interface assumed as being completely bonded. Although fatigue was not simulated in this study, the authors presented a factor of safety by dividing the peak stress in each material by the fatigue limit of that material. In this way fatigue loading was addressed, if not simulated. Mann *et al.* (1995) also investigated the effect of prosthesis material properties. Increasing prosthesis stiffness (Ti alloy to CoCr, 110GPa to 210GPa) increased the cement stresses by 11% in the posterior lateral cement mantle, but by less than 5% in the rest of the cement mantle. These results were gained with the stem/cement interface modelled as completely debonded. The difference in interface conditions may explain the difference in results as compared to Prendergast *et al.* (1989).

Prosthesis design has also received attention in several finite element studies. Mann *et al.* (1997a) investigated the effect a longer stem would have on the stresses in the cement mantle. This was to simulate the situation where a primary replacement had failed. Increasing the stem length such that it was slightly longer than the failed primary replacement (33mm longer) reduced the maximum principal stress in the proximal cement from 7.7MPa to 5.5MPa, but increased stresses in the distal cement from 7.9MPa to 10.7MPa. Further increases in stem length reduced the distal cement stresses. A risk of failure parameter was discussed in this study, based on dividing the peak stresses by previously reported fatigue strengths. In this case, the fatigue

strength used for the cement was 8MPa. The risk of cement mantle failure was higher in the distal region, and indicated fatigue failure in this location was likely.

Prosthesis stem cross-sectional geometry was the focus of a study by Mann *et al.* (1997b), where a Charnley prosthesis was compared to a modified Charnley prosthesis. The cross section of a Charnley prosthesis is rectangular, with rounded ends, similar to the perimeter of an Olympic running track (See Figure 2.17C). The distal section of the modified Charnley was circular in cross section. Both stems were modelled as proximally bonded. The modified Charnley stem was less able to transfer torsional loads to the bone, and generated increased shear stresses at the proximal stem/cement interface bond. The authors concluded that the distal prosthesis geometry had an influence on debonding at the proximal stem/cement interface, which, when debonded, would create higher cement mantle stresses. This in turn could influence failure within the cement mantle. The Charnley and modified Charnley stems were also the subject of a study by Chang *et al.* (1998). In this case, the influence of neck length on the stresses in the cement mantle was also investigated. The Charnley cross-section was thought to be superior to the modified Charnley cross-section (in agreement with Mann *et al.* (1997b)), and the neck length was found to have a negligible effect on the stresses in the cement.

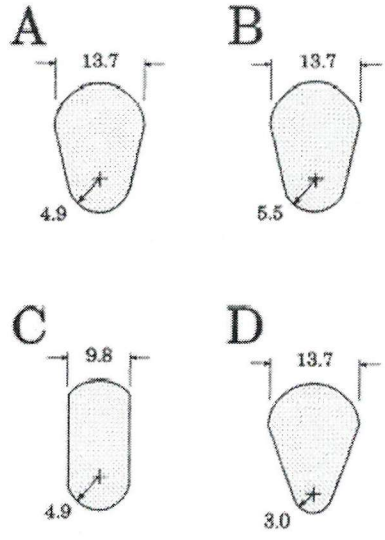

Figure 2.17: Cross sectional geometry of four cemented stem component designs evaluated by Mann *et al.* (1995). The medial radius is shown. All units in mm.

Four different stem cross-sectional geometries were included in a study by Mann *et al.* (1995), as shown in Figure 2.17, with stem A representing the baseline case. The maximum principal stress in the proximal cement decreased by 16% for stem B, but increased by 18% for stem D under the same applied load. Reducing the medial radius served to increase the stresses in the cement. The maximum principal stress in the proximal cement for stem C was 11% below the baseline case.

Finite element studies have also investigated the effects of prosthesis surface finish on the cement stresses in the cement mantle. Generally, a rough surface finish is simulated as a bonded stem/cement interface, while a polished finish is simulated as a debonded stem/cement interface with a coefficient of friction between the two surfaces. One such study was performed by Lennon and Prendergast (2001) for three different scenarios – bonded stem/cement interface, debonded stem/cement interface and debonded interface with no distal cement (see Figure 2.18a). A coefficient of friction of 0.32 was used to model the debonded interface. Joint reaction, abductor and iliotibial forces were simulated to represent the stance phase of normal gait. The stresses in the cement mantle were analysed, but instead of only reporting peak or average stresses, a distribution plot was employed to represent cement stresses in the whole cement volume (shown in Figure 2.18b). Stresses were highest in the debonded cases, and removing the distal cement more than halved the peak stress in the cement for the debonded cases. However, while the peak stress was reduced, removing the distal cement also served to increase the volume of cement above a certain threshold (3MPa). Different interface conditions also generated different locations for peak stresses in the cement (see Figure 2.18a). A probability of failure analysis was performed on the cement mantle, using probability data from Murphy and Prendergast (2000). The results of this study are shown in Figure 2.19; the debonded case appears more likely to have failed volumes of cement after 10 million cycles. However, this probability of survival does not consider any cracking or stress relaxation that may occur during that 10 million cycles. For example, in Figure 2.18a(*ii*), the maximum stress is at the distal tip of the prosthesis. Cracking is therefore likely in this location, and once a through cement mantle crack has formed, the stress distribution in the cement mantle would be different. This would in turn influence the predicted fatigue performance.

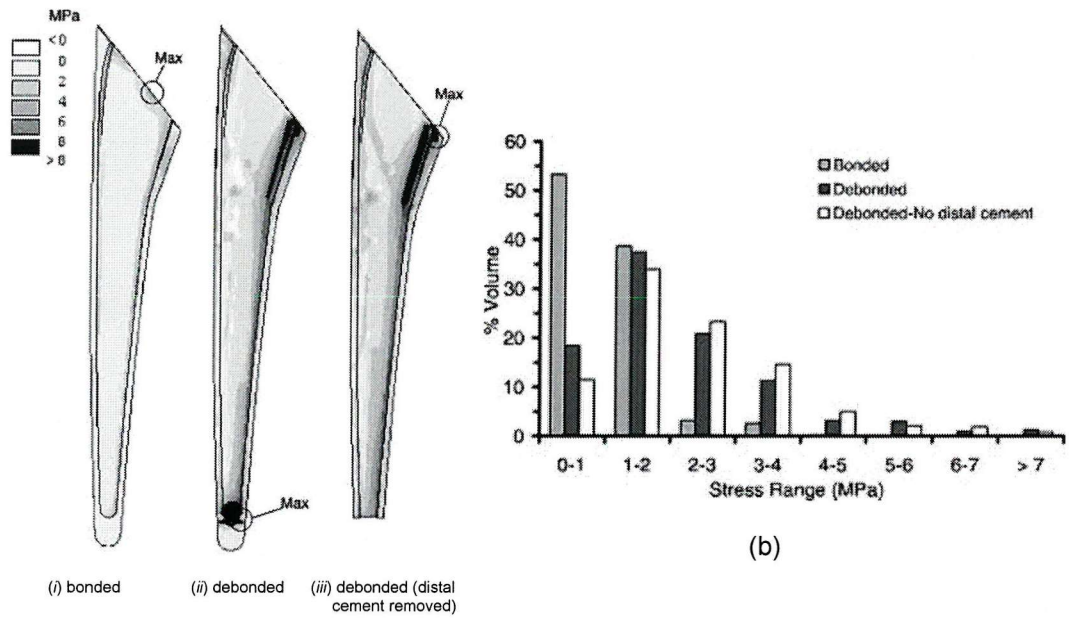

Figure 2.18: (a) Comparison of maximum tensile principal stresses in the anterior half of the cement for (*i*) bonded, (*ii*) debonded, and (*iii*) debonded with distal cement removed. (b) Distribution plot of percent volume of cement over a stress range of 0-8MPa for the three scenarios simulated (Lennon and Prendergast, 2001).

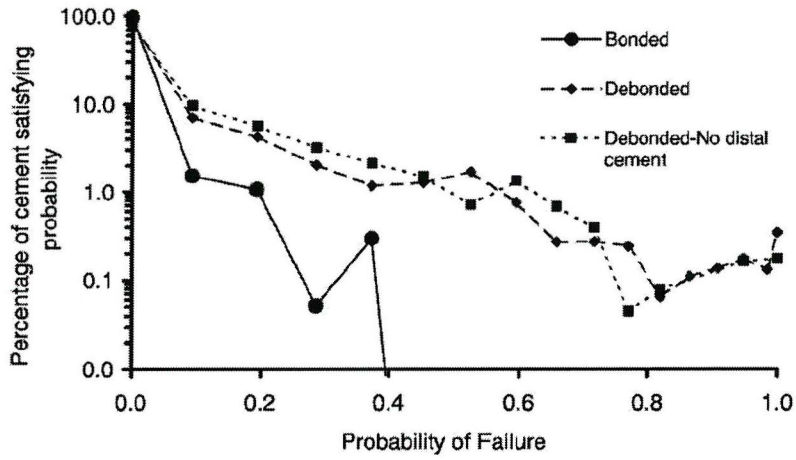

Figure 2.19: Percentage volume of cement satisfying probability of failure survival at 10 million cycles (P_f=1 predicts failure within 10 million cycles and P_f=0 predicts survival for the same time period) (Lennon and Prendergast, 2001).

Harrigan and Harris (1991) also used finite element techniques to investigate the influence of the prosthesis/cement interface on stresses in the cement mantle. Models were generated with fully bonded, partially bonded and completely debonded prosthesis/cement interfaces. The partially debonded case was modelled by debonding the proximal interface to a distance of 35mm, 62.5mm and 82.5mm below the prosthesis collar. A frictionless interface was assumed for the debonded regions, thought to be a worst-case scenario. Pores were also simulated in the cement mantle (see Section 2.3.5, page 100, for pore simulation details). For gait loading, stresses in the cement were found to be lowest for the fully bonded interface and highest for the fully debonded case. Stresses in the cement for the partially bonded interface conditions were between these two extremes (fully bonded/debonded). For gait loading, the maximum stress in the cement was located at a pore below the prosthesis tip and was 13.6MPa for the fully bonded case and 20.2MPa for a fully debonded interface. For stair climbing loads, the stresses were again lowest for the fully bonded case. The location of the peak stress was in the proximal cement, at a pore near the postero-medial corner of the prosthesis. This stress had a magnitude of 22.5MPa for the bonded interface, rising to 69.4MPa for the 82.5mm partially debonded interface. The fully debonded interface was not simulated for stair climbing loads. The authors concluded that under gait loading, the cement distal to the prosthesis tip was most as risk of failure. Under stair climbing loads, the proximal cement mantle was more at risk of failure, as this was the location of the maximum stress.

Partial prosthesis/cement debonding was also simulated by Chang *et al.* (1998), but with a proximal bonded and distal unbonded region, the opposite of the study by Harrigan and Harris (1991). The unbonded distal interface was modelled with a coefficient of friction of 0.3. When compared to a fully unbonded interface, a proximal bond reduced the peak cement mantle stresses by 30% to 60% for two different implant designs and loading configurations. A fully bonded stem/cement interface was not considered. Similar reductions in peak stress were observed by Mann *et al.* (1997b), who compared a proximally bonded and fully unbonded prosthesis. A coefficient of friction of 0.3 was used for the unbonded interface. A 60% to 70% reduction in cement mantle stress in the proximal region was obtained by introducing the proximal bond.

Fully bonded and unbonded prosthesis/cement interface conditions were simulated by Mann *et al.* (1995). For the unbonded case, the friction coefficient of the interface was set as 0.3. When gait loading was applied, the stresses in the bone were almost identical for both interface conditions. Maximum stresses in the prosthesis were also similar. However, the cement mantle stress field was quite different. For the fully bonded case, the peak cement mantle stress was in the distal cement mantle, with a magnitude of 7.5MPa. The corresponding region for the fully debonded interface had a stress magnitude of 5.6MPa. The peak stress for the fully debonded interface was in the medial cement mantle, at the postero-lateral corner of the implant, with a magnitude of 10.8MPa. The corresponding region for the fully bonded interface had a stress magnitude of 1.4MPa. In this study, although the peak cement mantle stress was higher in the fully unbonded interface model (unbonded 10.8MPa, bonded 7.5MPa), the fully bonded interface model exhibited higher distal cement stresses.

The matter of implant surface finish is still open to debate. The studies in this section generally predict that a bonded prosthesis/cement interface will reduce cement mantle stresses and therefore prolong the life of the cement mantle. Predictions made on initial conditions do not consider that a prosthesis may become debonded from the cement regardless of the surface finish, and this may be a negative factor for the rough surface finish. If a roughened prostheses/cement interface becomes unbonded, the subsequent rubbing can generate a greater level of debris than a polished interface. Verdonschot and Huiskes (1998) demonstrated this with two metal tapers (one polished, one grit blasted) implanted in a cement mantle and loaded with a 7kN compressive fatigue load for 1.7×10^6 cycles. Scanning electron microscopy of the interface in control specimens identified the polished interface as a clean line (Figure 2.20a), but the grit blasted interface had gaps at the interface of about 10μm where the bone cement had not interdigitated with the roughened surface (Figure 2.20b). After loading, a large level of damage was observed for the roughened interface, but the polished interface was relatively intact (Figure 2.20c & 2.20d). The level of damage shown in Figure 2.20d may not be representative of *in vivo* conditions, as the applied load was so high. However, the point that interface debris can be greater if a roughened prosthesis becomes debonded is nicely illustrated.

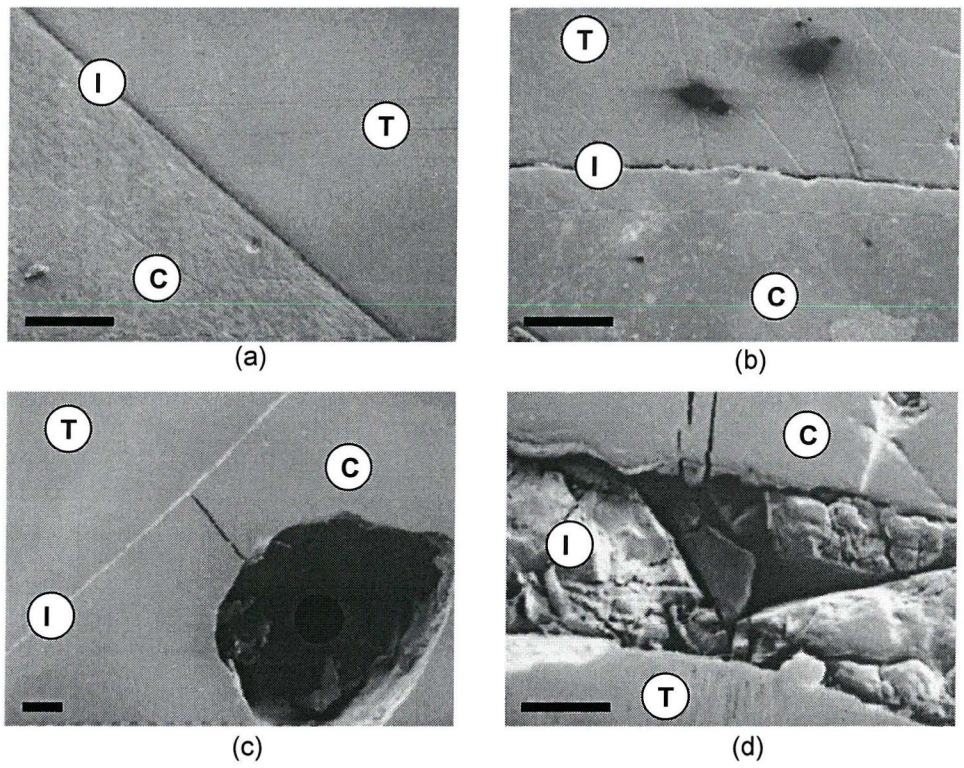

Figure 2.20: Scanning electron micrographs of taper/cement interface before and after loading. The black lines in the bottom left represent 50μm. I: interface, C: cement and T: taper. (a) Polished control specimen, (b) grit blasted control specimen, (c) polished specimen after $1.7x10^6$ load cycles and (d) grit blasted specimen after $1.7x10^6$ load cycles (Verdonschot and Huiskes, 1988).

The initial conditions can provide useful information regarding the stresses in the cement mantle, but should not be considered in isolation when predicting the performance of the cement mantle in the implanted femur reconstruction. A number of the studies in this section compare the initial stresses to known fatigue data for the cement. While this gives an idea of the fatigue performance, it does not consider that the stress distribution in the cement may change over time. This may occur due to cracking of the cement, debonding of the prosthesis/cement interface, viscoelastic effects of the cement or indeed biological parameters, not considered here, such as bone remodelling or wear debris that may evoke the particulate reaction failure scenario (discussed at the beginning of Section 2.2.1, page 30). It may not always be appropriate to compare prosthesis designs with different interface conditions – both Verdonschot and Huiskes (1998) and Huiskes (1988) suggest that results should be interpreted as a function of prosthesis design goals, i.e. shape-closed versus force-closed. An interesting manifestation of shape-closed design has been discussed in this

section – a prosthesis with a proximal bond but unbonded distally. This has been realised commercially as a roughened, or PMMA pre-coated proximal section with a polished distal section. Although this does not seem to fit into the shape-closed design category, the work discussed in this section by Crowninshield and Tolbert (1983), Chang *et al.* (1998) and Mann *et al.* (1997b) suggests that a proximal bond closely approximates the cement mantle stresses found with a fully bonded interface. Indeed, a polished distal section may be advantageous as there is a strong likelihood of distal debonding even shortly post operatively (Jasty *et al.*, 1991). Interface debris due to rubbing at the interface would therefore be minimised, as described by Verdonschot and Huiskes (1998). The literature discussed in this section suggests this is the optimum shape-closed design. However, little information can be gained regarding the performance of this design (or indeed any design) of prosthesis under the fatigue loading experienced *in vivo*. To better represent the *in vivo* conditions, preclinical testing has been developed to apply fatigue loads to the construct; this is discussed in the following section.

2.2.5 *Cement mantle failure: in vitro studies and fatigue loading*

Two *in vitro* methods that have been used to investigate damage accumulation in the cement mantle of implanted femur models are sectioning and dye penetrant. McCormack *et al.* (1999) developed an implanted femur model with a constant cross-section stem cemented into a tube with similar torsional rigidity as the diaphysis of the femur (Figure 2.21).

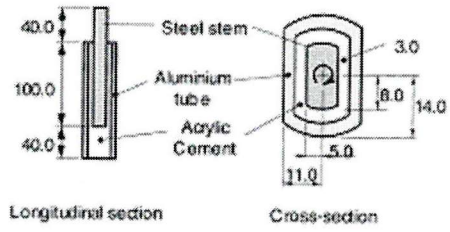

Figure 2.21: Simulated implanted femur of (McCormack *et al.*, 1999). Dimensions in mm.

Sixteen specimens were assembled, divided into groups of four, and each group tested for a different number of cycles. The applied load was torsional, of similar magnitude to that measured with instrumented prostheses (50Nm & 80Nm, see Table 2.3, page 21), and applied to the stem cyclically, zero to maximum at a frequency of 7Hz. Specimens were sectioned and treated with dye penetrant to highlight cracks and pores. The resulting micrographs (see Figure 2.22) exhibited damage in the cement mantle similar to that observed in the post-mortem study of Jasty *et al.* (1991) (Figures 2.12-2.15, pages 36-37). Specimens subject to a greater number of loading cycles had more cracks in the cement, supporting the damage accumulation failure hypothesis. Cracks were found to mainly originate from pores on the interfaces (see Figure 2.22). A large variability was noted between specimens tested under the same conditions, and thought to be due to the random distribution of pores in the cement and at the interfaces.

Stolk *et al.* (2003) performed a sectioning study to investigate the damage accumulation in the cement mantle of physiological implanted femur models (Figure 2.23). Two different implant designs were considered – the Lubinus SPII and the

Müller curved stem. The Swedish hip register puts the revision rate for these implants at 4% and 16% respectively after 10 years. A joint reaction force was applied to the head of the implant, and specimens loaded in fatigue. After $2x10^6$ load cycles the specimens were sectioned, treated with dye-penetrant and cement surfaces analysed. Far more cracks in the cement were observed in the Müller specimens, and stem migration was also greater. Porosity was found to have a marked influence on the damage in the cement. A partner study by Maher *et al.* (2002) found, using the same *in vitro* models, the inducible displacement (displacement recovered when implant is unloaded) increased with time for the Müller prosthesis, but decreased with time for the Lubinus SPII stem, and it was proposed that increasing inducible displacement was therefore a sign of early loosening. In this study, linear variable displacement transducers (LVDTs) measured inducible displacement by monitoring the motion of spheres rigidly connected to the prosthesis through holes in the femur (Figure 2.23).

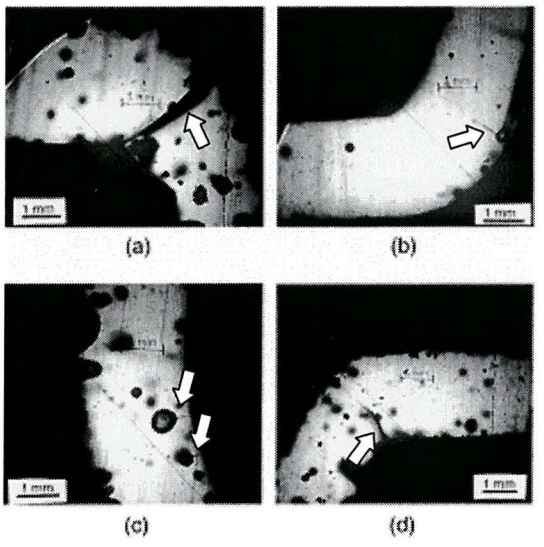

Figure 2.22: Micrographs showing crack types observed under torsional fatigue: (a) through cement mantle crack; (b) crack from a pore at the cement/tube interface; (c) cracks from the stem/cement interface; (d) crack passing through a pore. Cracks are indicated by white arrows (McCormack *et al.*, 1999).

The physiological femur models of Stolk *et al.* (2003) and Maher *et al.* (2002) only included the joint reaction force in the loading history. Britton *et al.* (2003) made an improvement on this loading configuration by including the action of the abductors,

vastus lateralis and the tensor fasciae latae (Figure 2.24). Specimens were loaded for $1x10^6$ load cycles, and sectioned longitudinally. The majority of the damage consisted of partial cement mantle cracks, usually originating at the stem/cement interface. Once again, porosity was associated with crack initiation and coalescence. When examining the cement of an unloaded control specimen, damage was observed and thought to be caused by the curing of the cement (Britton *et al.*, 2003).

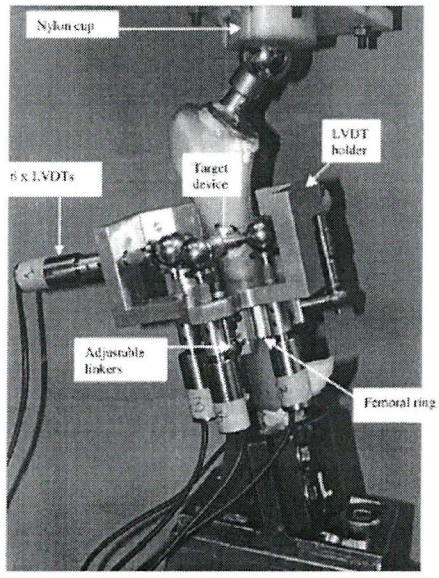

Figure 2.23: Photograph of the implanted femur model of Maher *et al.* (2002) and Stolk *et al.* (2003).

Another sectioning study was performed by Mann *et al.* (2004) to investigate any association between cement mantle cracking and cement mantle thickness. Eight cadaveric femora were implanted with prostheses, fatigue loading was applied to the femoral head (the loading simulated an aggressive stair climbing regime) and the specimens were sectioned at 10mm intervals after 300,000 cycles. Microcracking was not specifically associated with thin areas (<2mm) of the cement mantle, but an association between through cement mantle cracks and a thin cement mantle was made. Microcracks were also observed in two control specimens that were not subject to an applied load. Based on these observations, Mann *et al.* (2004) proposed that microcracks were generated during cement polymerisation and 'over-represented' in thin cement mantle regions. While the propagation rate of these cracks was no different to those in thicker cement mantle regions (>2mm), they formed through cement mantle cracks first (alo discussed in Section 2.3.4, page 95).

The *in vitro* studies discussed thus far have relied on sectioning to assess the cement mantle. A couple of limitations with this method are that artefacts may be generated during the sectioning process, and analysis can only be performed at the end of the test. Non-destructive evaluation (NDE) methods overcome these limitations and have been used to characterise cement damage. Two examples of NDE methods are acoustic emission (AE) and dye penetrant. AE has the advantage that damage within the volume of the specimen can be detected while dye-penetrant can only detect damage that intersects the surface of the specimen (Browne *et al.* 2005). Dye penetrant also usually requires the test to be interrupted to observe cracks. Sugiyama *et al.* (1989) used the AE technique to monitor the cement mantle of an implanted femur under torsional loads, but could not distinguish cement damage AE from interface motion noise or load application noise. Kohn (1995) had greater success, and was able to discriminate between loose and well-fixed prostheses *in vivo* by attaching AE sensors to the patient's skin at the greater trochanter. Good signal filtering was required to avoid noises due to skin friction and transducer motion being recorded. No attempt was made in this study to monitor cracking in the cement mantle of the reconstruction.

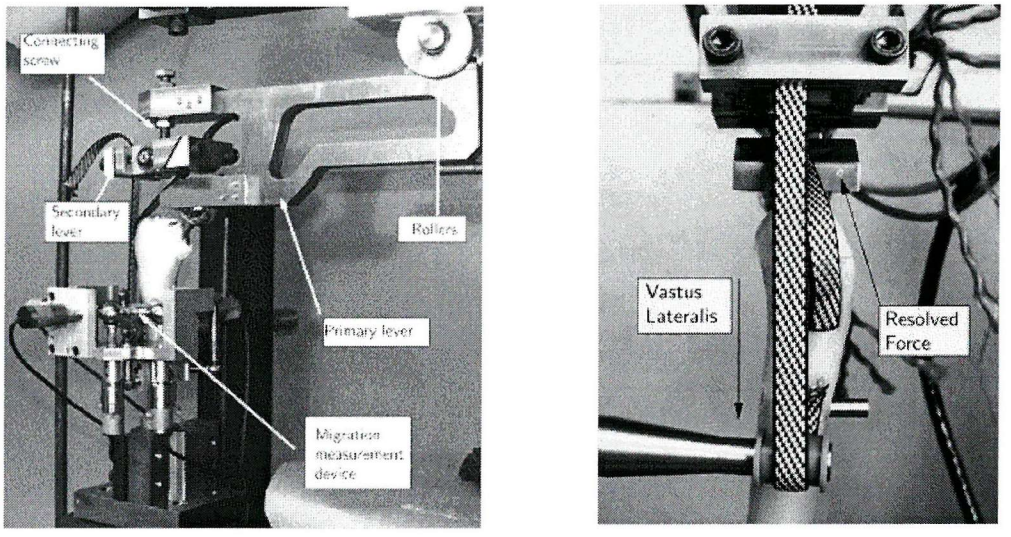

Figure 2.24: Photograph of the implanted femur model of Britton *et al.* (2003) with muscle loading.

Successful AE use in relation to bone cement has so far been restricted to experimental specimens. Qi *et al* (2000) used six sensors to locate damage in notched

tensile fatigue specimens, and reported good damage location ahead of the notch tip. This study was based on AE wavelet analysis (i.e. frequency analysis of each burst of AE activity) using self-written location software, and has been the subject of controversy. In particular, the accuracy of their location algorithm was criticised, as damage appeared to be located in the specimen notch, where there was no material. However, the ability of the technique to detect damage was not brought into question (Akkus, 2002; Pujol and Qi, 2002). A different approach to Qi *et al* (2000) was taken by Roques *et al.* (2004a), who performed an analysis based on the parameters of the detected AE (e.g. duration of AE event, peak amplitude). Parameters most suited to bone cement failure characterisation were presented to allow differentiation of cement damage from other sources of AE activity (this may have allowed Sugiyama *et al.* (1989) to differentiate cement damage from other AE data, see previous paragraph). The study by Roques *et al* (2004a) also demonstrated the capability of the AE method to locate critical (that led to eventual failure) and non-critical damage in 4-point bend fatigue tests. This parametric approach (rather than the frequency approach) has become the method of choice in the civil and aerospace engineering fields, where AE is an established test method (Browne *et al*, 2005).

Dye penetrant techniques have been applied to *in vitro* models of the implanted femur allowing individual cracks in the cement to be monitored. McCormack and Prendergast (1999) developed a layer based quasi 2-D model of the implanted femur to monitor cement damage (Figure 2.25). Windows in the model allowed the dye-penetrant to be applied and surfaces to be analysed without sectioning. There are limitations associated with this structure – hoop stresses are not considered, only surface damage can be detected and no muscle forces are applied. However, it allowed the cement mantle to be assessed during the loading history, and the effects of porosity and preload damage, noticed in the studies discussed above, to be considered. Cyclic loading was applied to the femoral head and the test was stopped periodically to assess the cement mantle. The damage accumulation process was evident, with the number of, and length of cracks increasing as a function of loading cycles. Pre-load cracks were also evident. All the pre-load cracks and cracks caused by fatigue loading originated from pores within the bulk cement and not from the interfaces. Specimens with a greater amount of pre-load damage were found to have accelerated damage accumulation rates.

Lennon *et al.* (2003) developed the model of McCormack and Prendergast (1999) to include an abductor force (Figure 2.26), and investigated the effects of a rough vs. polished stem. Specimens (5x rough, 5x smooth) were fatigued for $2x10^6$ load cycles, and the cement mantle was examined using the dye penetrant technique at the beginning and end of the test. There was a definite relationship between the level of pre-load damage and damage at the end of the tests. Porosity was again cited as having an influence on the damage accumulation process. In fact, the role of pre-load damage (possibly caused by residual stress) and porosity were so dominant that there was no significant difference between stem surface finishes. Figure 2.26 shows the correlation between cement damage (measured in total length of detected cracks) and prosthesis inducible displacement at the end of the tests, supporting the use of inducible displacement as a means to discriminate between prosthesis designs.

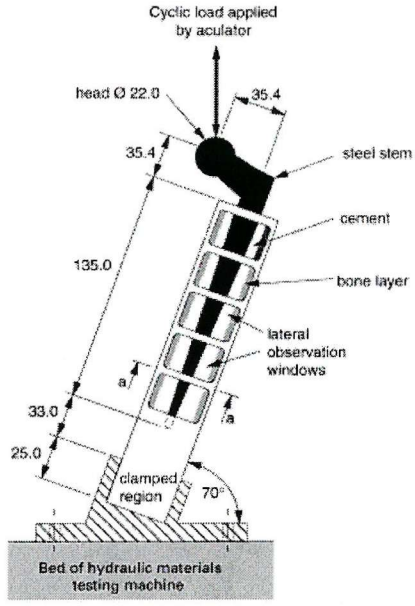

Figure 2.25: Schematic of the experimental model of McCormack and Prendergast (1999). All dimensions are in mm.

The *in vitro* studies discussed in this section provide information on the damage accumulation failure scenario that could not be gained from clinical studies. For example, torsional loads can cause cracks originating at the stem/cement interface, while bending loads can cause cracks to grow within the bulk cement. All the *in vitro* studies regarded porosity as having a strong influence on the fatigue of the cement mantle by acting as crack initiators or as a means to ease crack coalescence (the

effects of porosity on cracking are further discussed in Section 2.3.2). A significant amount of pre-load damage was observed in the cement, and specimens with greater pre-load damage tended to have greater levels of damage at the end of the tests. However, all the studies discussed had limitations, whether it was a simplified geometry to allow visualisation of the cement mantle, neglecting muscle forces or only assessing the cement mantle at the end of the test. These limitations can be overcome with finite element modelling and continuum damage mechanics techniques.

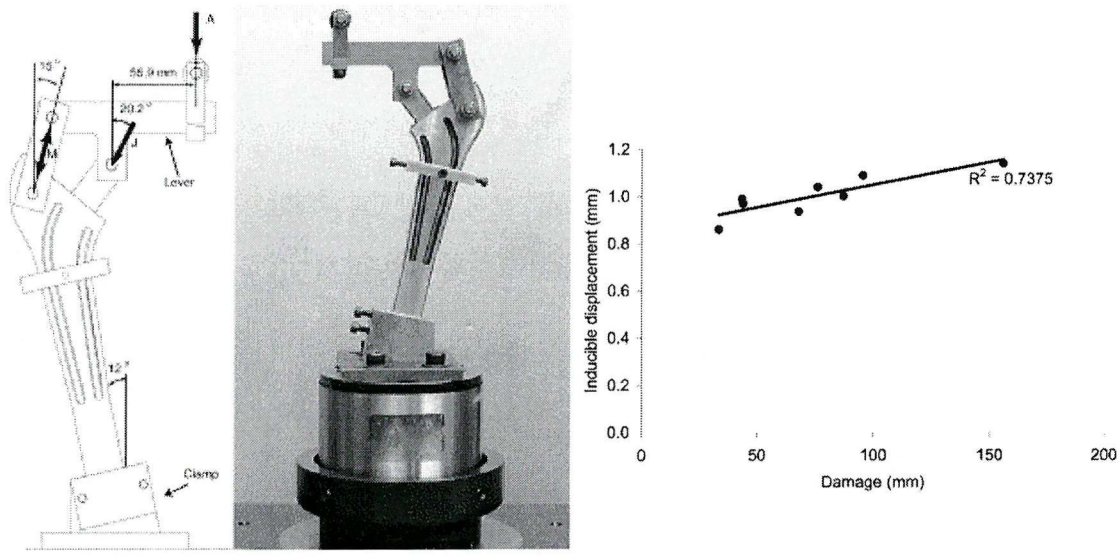

Figure 2.26: Schematic of the model of Lennon *et al.* (2003), photograph of the assembled rig mounted on the testing machine and inducible displacement plotted as a function of cement damage.

2.2.6 *Cement mantle failure: in silico studies and fatigue loading*

The continuum damage mechanics method calculates the fatigue life of each element/integration point in the cement mantle based on the stress experienced by that element. When the number of cycles simulated exceeds the number of cycles to failure for an individual element/integration point, a modulus reduction (to zero, or a small value that would not contribute any stiffness to the model) takes place to simulate a crack on a continuum level. The fatigue life of the element/integration point is taken from an experimental tensile fatigue S-N curve, and therefore assumes the fatigue life of each element (or part thereof) to be the same as the tensile test specimen. However, the cement mantle of the implanted femur is a complicated structure, and any given volume is subject to a multi-axial stress state. The fatigue life of cement under multi-axial stress has been shown to be significantly lower than under uniaxial conditions (Murphy and Prendergast, 2003, discussed fully in Section 2.3.2). This is a limitation of the computational method, but it can still provide useful preclinical testing information, as the studies in this section demonstrate.

Using the continuum damage mechanics method, Verdonschot and Huiskes (1997a) simulated cement mantle damage in a finite element model of an implanted femur with a bonded and unbonded stem/cement interface (Figure 2.27a). Debonding the stem/cement interface caused the stresses in the cement to rise by a factor of two to three. These elevated stress levels accelerated the simulated damage accumulation in the cement mantle (see Figure 2.27b), leading the authors to conclude that a bonded stem/cement interface would be beneficial to the life of the reconstruction. However, the consequences of debonding of the bonded stem/cement interface (realised clinically as a roughened stem) were not considered, but have been shown to be relevant (Figure 2.20, page 49). This study also reported the peak stress in the cement mantle as a function of loading cycles (Figure 2.27c), which reduced as the simulation progressed for both bonded and unbonded analyses. This suggests that studies based on initial stress have poor predictive capabilities regarding the long-term performance of the cement mantle.

Stolk *et al.* (2002) developed the method of Verdonschot and Huiskes (1997a) to include cement creep, and investigated the influence of stair climbing loading on the

damage in the cement mantle. Constitutive laws used to represent fatigue and creep were taken from experimental studies of vacuum mixed Palacos R (Murphy and Prendergast, 2001) and hand mixed Simplex P (Verdonschot and Huiskes, 1994) respectively. Damage was simulated in the cement for a reconstruction with a simulated gait only loadcase, a stair climbing only loadcase and a combined loadcase (gait load cycles to stair climbing load cycles ratio of 9:1). The stem/cement interface was simulated as being polished and therefore unbonded in all tests. Relative to gait loading, the stair climbing loadcase increased the amount of cement damage by a factor of 6. Even the combined loadcase increased the amount of damage by 47% relative to the gait only loading. The authors propose that the loadcase is critical when simulating damage in the cement mantle, and realistic loading (i.e. the combined loadcase in their study) should be applied for a more realistic representation of *in vivo* conditions.

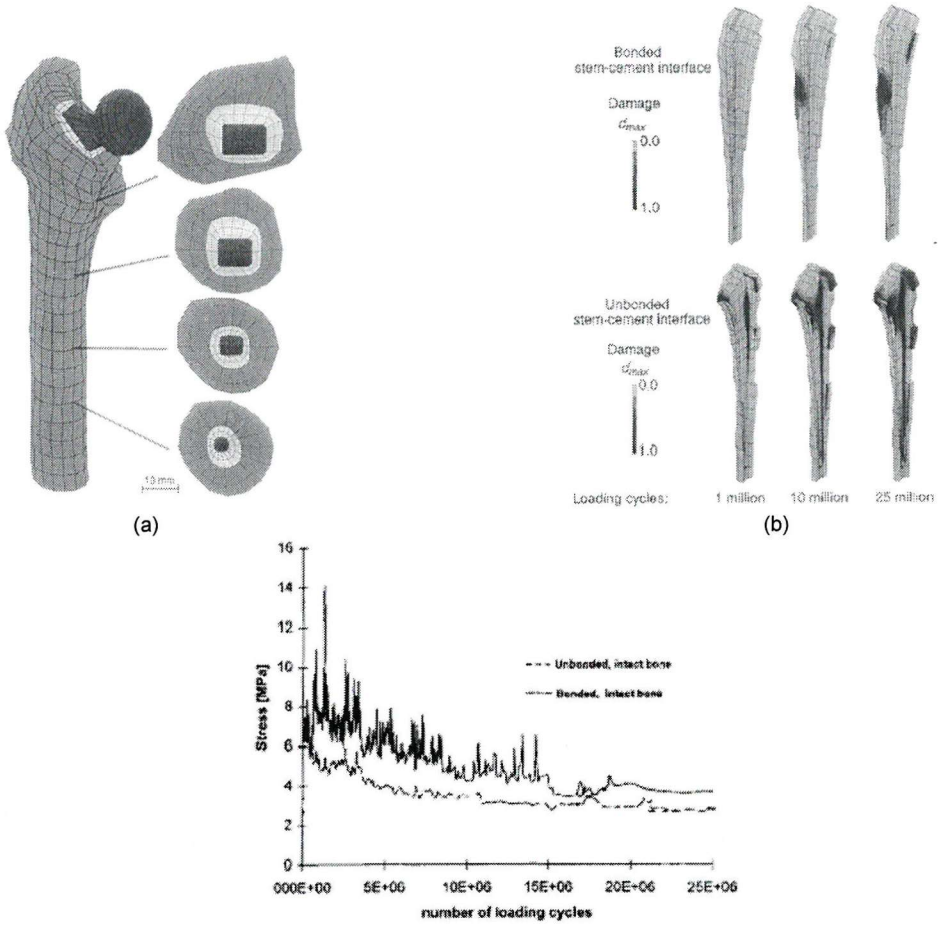

Figure 2.27: (a) Finite element model used by Verdonschot and Huiskes (1997a). (b) Damage in the cement at 1, 10 and 25 million simulated load cycles for bonded and unbonded stem/cement interfaces. (c) Peak tensile stress levels in the cement as a function of loading cycles for the both analyses.

Stolk *et al.* (2003) demonstrated the ability of the computational method to differentiate between different prostheses in agreement with the Swedish Hip Register study (Herberts and Malchau, 2000), and to predict damage patterns similar to experimental observations. A Lubinus SPII and Muller Curved stem were selected for analysis in this study (i.e. Stolk *et al.*) as they have a marked difference in clinical loosening rates. The experimental part of this study has been discussed previously (page 51) – five Lubinus SPII and five Muller Curved stems were implanted into composite femora, gait loading applied for $2x10^6$ load cycles and specimens sectioned to observe cement damage. Finite element models of the Lubinus SPII and Muller Curved specimens were generated, and damage simulated in the cement mantles using a continuum damage mechanics approach. For the same number of loading cycles ($25x10^6$ load cycles), more damage was predicted in the Muller Curved model. This correlated well with both the experimental tests and data from the Swedish Hip Register (Herberts and Malchau, 2000). The *in silico* predicted damage patterns were also similar to the damage patterns observed in the experimental specimens upon sectioning. These were positive results for the analysis, but the analysis required $25x10^6$ to generate levels of damage observed experimentally after $2x10^6$ load cycles. This difference in timescale was attributed to the absence of pores, pre-cracks and other cement irregularities in the finite element models.

A further study by Stolk *et al.* (2004) simulated the fatigue of uniaxial tensile fatigue specimens, using the same method as Stolk *et al.* (2002) and Stolk *et al.* (2003). The predicted fatigue lives were compared to experimental data, and good agreement was reported. Creep strains were also compared to the experimental data, with good agreement. This study suggests that the computational method is capable of simulating a realistic fatigue life for uniaxial tensile loading, but not for the implanted femur structure. This may be the case, as the cement mantle of the implanted femur is subject to multi-axial stress whereas the constitutive laws were from uniaxial data. However, it must be considered that the analysis *was* capable of ranking implants according to their clinical survival rates. Regarding the failure timescale, all the *in vitro* studies discussed in Section 2.2.4 identified porosity and pre-load cracks as having a negative impact on cracking in the cement mantle. Neither of these factors were considered in the studies by Stolk and co-workers.

A further limitation with the *in silico* methods discussed in this section is that deterministic results are generated. For example, Stolk *et al.* (2003) used five Lubinus SPII and five Muller Curved experimental specimens, but only one finite element model of each. When simulating uniaxial tensile fatigue (Stolk *et al.*, 2004), only one number of cycles to failure was generated for each stress level. This is in contrast to the experimental data, where data scatter was observed in the fatigue life results. Deterministic results from the computational method may therefore not provide the most realistic representation of experimental tests.

2.3 Bone cement in orthopaedic surgery

2.3.1 Chemical composition and preparation techniques

Bone cement has no adhesive properties, but provides an interlock between the prosthesis and the bone that is capable of transferring load from the former to the latter (Figure 2.28). Prior to use, bone cement comprises a powder and separate liquid. Different brand names have different compositions; these are detailed in Table 2.6.

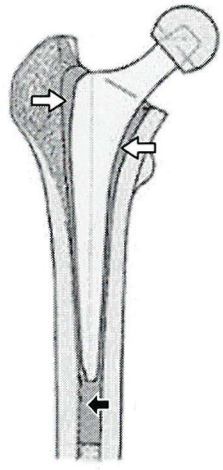

Figure 2.28: Schematic of total hip replacement identifying the proximal (white arrows) and distal (black arrow) areas of the cement mantle.

Taking CMW-1 (DePuy, UK) as an example, the powder contains pre-polymerised polymethylmethacrylate (PMMA) beads, which act as a substrate around which further polymer chains can form. A small amount of benzoyl peroxide (BPO) and barium sulphate ($BaSO_4$) act as an initiator for polymerisation and a radiopacifying agent respectively. The radiopacifying agent allows the bone cement to be identified on radiographic images (see Figure 2.10, page 31). The liquid contains methacrylate (MMA) monomer, with a small amount of *N,N*–dimethyl-p-toluidine (DMPT) and hydroquinone (HQ) to act as an accelerator and stabiliser to respectively. When the powder and liquid are mixed, the methacrylate (MMA) is polymerised via free radical polymerisation to form PMMA. BPO molecules are broken into free radicals by

DMPT (Figure 2.29a), and each free radical can then bond with a MMA molecule (Figure 2.29b) to form an initiator-dimer radical (Figure 2.29c). The initiator-dimer radical can then bond with another MMA molecule to form a polymer chain. Further MMA molecules bond to the chain until termination, when either two free ends of different chains bond, or when the free end of a chain bonds with a free radical.

	Powder constituents							Liquid constituents		
Brand name	PMMA	P(MMA/ MA)	P(MMA/ BMA)	P(MMA/ sty)	BPO	$BaSO_4$	ZrO_2	MMA	DMPT	HQ†
Boneloc	-	-	90.0	-	0.7	-	10	50.0*	0.5	-
Cemex RX	88.3	-	-	-	2.7	9.0	-	99.1	0.9	75
CMW-1	88.9	-	-	-	2.0	9.1	-	98.7	0.4	20
Palacos R	-	84.2	-	-	0.8	-	15	97.9	2.0	64
Simplex P	15.0	-	-	75.0	0.3	10.0	-	97.5	2.5	80

Polymers
PMMA: polymethylmethacrylate
P(MMA/MA): poly(methylmethacrylate/methacrylate) copolymer
P(MMA/BMA): poly(methylmethacrylate/butylmethacrylate) copolymer
P(MMA/sty): poly(methylmethacrylate/styrene) copolymer
Initiator
BPO: Benzoyl peroxide
Radiopacifying agents
$BaSO_4$: Barium sulphate
ZrO_2: Zirconium dioxide
Monomers
MMA: methylmethacrylate
*also contains 30%w/w *n*-decyl methacrylate and 20%w/w isobornyl methacrylate
Accelerator and stabiliser
DMPT: *N,N* –dimethyl-p-toluidine
HQ: Hydroquinone

Table 2.6: Formulations of Boneloc and four commercially available bone cements (Lewis, 1997). Values are in %w/w except † in ppm.

Once the cement is mixed, it is left for a short time (dough or pick-up time, Figure 2.30) allowing it to become doughy and easily manipulated by the surgeon. The surgeon then has a few minutes (working time) to introduce the cement into the bone and position the prosthesis. The prosthesis is held in position until the cement is solid enough to support it. The polymerisation process is exothermic and can be influenced by the ambient temperature. Higher ambient temperatures serve to accelerate polymerisation, and may not allow the surgeon enough working time to position the prosthesis correctly. Conversely, lower temperatures increase the working time,

making it difficult to maintain prosthesis position while the cement cures. The peak temperature reached by the bone cement during polymerisation has been cited as a critical parameter – at 60°C bone cell necrosis is thought to occur after as little as 30 seconds exposure (Nzihou *et al.*, 1999). Once polymerisation is complete, the phases present in the cement are: PMMA beads, a PMMA matrix, with $BaSO_4$ particles dispersed in the matrix. However, this represents an ideal scenario, because the matrix inevitably includes a certain amount of porosity, as air bubbles are trapped in the cement during mixing and delivery to the bone (see Figure 2.14 & 2.15). In practice, the cement mixing technique has evolved to minimise the entrapment of air. The latest generation of mixing apparatus involves a syringe pre-filled with the correct amount of cement powder. The liquid is added and a vacuum applied to the syringe. Mixing takes place in the syringe barrel, and once complete, the syringe is transferred to a cement gun ready for delivery into the femoral canal.

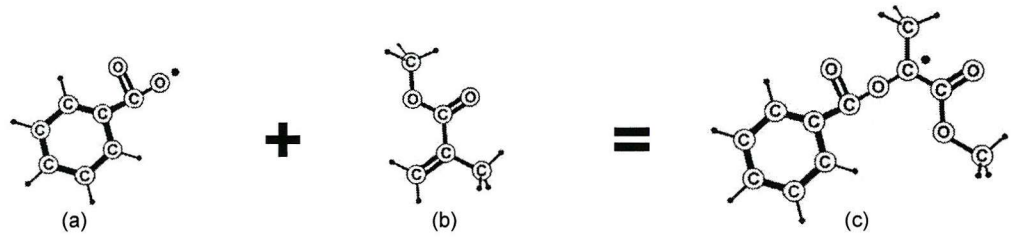

Figure 2.29: (a) Benzoyl peroxide free radical, (b) methylmethacrylate monomer and (c) initiator-dimer radical.

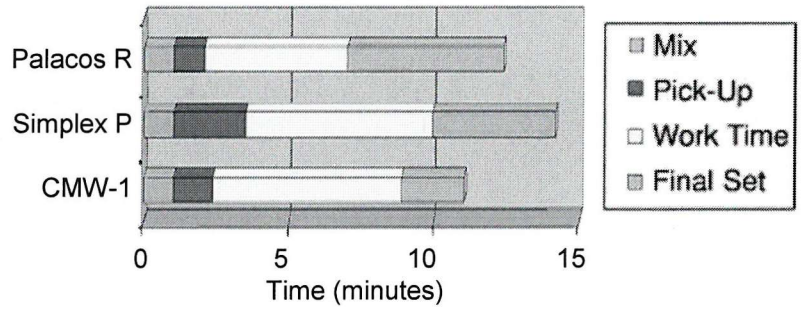

Figure 2.30: Overall set time for three different cements at 18°C (Lewis, 1997).

Vacuum mixing the cement is just one part of the 'third generation cementing technique'. Prior to implantation, the femoral canal is brushed, washed and dried.

This leaves the femoral canal free from debris that may have been created during reaming. The removal of (some) cancellous bone allows a stronger bone/cement interface to be created. A distal cement restrictor prevents cement passing to the distal femur, and allows pressurisation of the applied cement. Cement pressurisation is required to fully interdigitate the cement with the remaining cancellous bone, i.e. to overcome the bleeding pressure. The distal cement restrictor can also act as a centraliser, which allows the prosthesis to be positioned in a neutral position, with an even cement mantle. Proximal centralisers are also part of the third generation cementing technique, and facilitate the optimum positioning of the prosthesis. The differences between third generation and previous generation cementing techniques are described by Haydon *et al.* (2004) and summarised in Table 2.7. It is thought that the improvements in cementing technique are a major reason for the high survival rates recently reported in current hip register studies (Malchau *et al.*, 2002).

First generation (<1980)	Second generation (1980-1990)	Third generation (>1990)
Hand mix cement	Hand mix cement	Vacuum mix cement
Leave cancellous bone	Remove cancellous bone to near endosteal surface	Remove cancellous bone to near endosteal surface
No distal cement restrictor	Distal cement restrictor	Distal cement restrictor
Irrigate and suction canal	Brushing, pulsatile irrigation, pack and dry canal	Brushing, pulsatile irrigation, pack with adrenaline soaked sponges and dry canal
Digital cement insertion	Retrograde injection with cement gun	Retrograde injection with cement gun and pressurisation
Manual positioning of stem	Manual positioning or early centralisation methods	Distal and proximal centralisers

Table 2.7: First, second and third generation cementing techniques, as described by Haydon *et al.* (2004).

The static mechanical properties of popular brands of bone cement are well studied, and there exist a number of comprehensive reviews on the subject (Lewis, 1997; Saha and Pal, 1984). The brand of bone cement used throughout this thesis is CMW-1

(DePuy, Blackpool, UK). The uniaxial and flexural (4-point bend) properties of CMW-1 are summarised in table 2.8.

Tensile	Strength (MPa)	30 – 52[a]
	Modulus (GPa)	2.1 – 3.3[a]
Compressive	Strength (MPa)	86 – 89[b]
	Modulus (GPa)	2.4 – 2.7[b]
Flexural	Strength (MPa)	64 – 67[c]
	Modulus (GPa)	2.5 – 2.7[c]

Table 2.8: Static material properties for CMW-1 bone cement. [a] Roques (2004), vacuum mixed. [b] Linden (1991), centrifuged. [c] Hansen and Jensen (1992), vacuum mixed.

2.3.2 *Bone cement and fatigue*

The repetitive loading experienced by the hip replacement during normal activities, for example walking or stair climbing, subjects the cement mantle to a fatigue load. There have been numerous studies investigating bone cement fatigue, and several review articles (Krause and Mathis, 1988; Lewis, 1997; Lewis, 2003). Four phases of bone cement that may have an influence on fatigue were identified by Topoleski *et al.* (1993):

- Pre-polymerised beads
- Interbead matrix
- $BaSO_4$ particles
- Porosity

In their study, notched Simplex P and Zimmer LVC specimens were subjected to a 3-point bend fatigue load at 10Hz, with a peak load of 133N and R-ratio of 0.2. After a set number of loading cycles that did not result in failure, a static 3-point bend load was applied to the specimens to open the crack slightly. While this static load was applied, the damage zone was examined by light and scanning electron microscopy. Microcracks were visible in the damage zone ahead of the crack tip, and observed in the interbead matrix rather than the pre-polymerised beads (Figure 2.31). The presence of $BaSO_4$ in the matrix was thought to facilitate microcrack growth in the interbead matrix, as these particles did not seem to bond with the matrix. A second hypothesis was that matrix shrinkage during polymerisation could generate residual stresses and strains in the matrix that could promote microcracking. In the matrix, porosity was found to act as a nucleation site for microcracks, but it was proposed that porosity could also provide a positive contribution by dispersing energy at the crack tip, forming a larger damage zone and effectively blunting the crack.

Bhambri and Gilbertson (1995) studied unnotched cylindrical specimens under a fully reversed tension-compression fatigue load (max. stress 5-15MPa, R-ratio of –1 and frequency of 1Hz, tested in Ringer's soln. at 37°C). Fracture surfaces were examined using a scanning electron microscope. The fatigue cracks were seen to originate from the following sites: (i) large voids showing multiples of pre-polymerised beads on their interior surface; (ii) small voids, and (iii) agglomerates of $BaSO_4$. The crack

initiation region was generally smooth, and the defect was at the centre of river pattern tributaries, pointing to the crack origin. In the smooth crack initiation region, pre-polymerised beads were not well differentiated from the matrix, possibly due to surfaces rubbing together during slow crack growth. Further away from the origin, crack growth through the beads was distinguishable as a smooth fracture surface. As the crack growth rate increased (at a greater distance from the origin), a pattern was recognisable on the bead fracture surface. The following mechanism was proposed for bead fracture: as the advancing crack approached a bead surrounded by $BaSO_4$ particles, microcracks originated at these particles and propagated into the bead at different planes from various directions. These microcracks may have either resulted in a completely brittle fracture of the bead, or in beads where a ligament remains unbroken, the final separation may have occurred by tensile tearing.

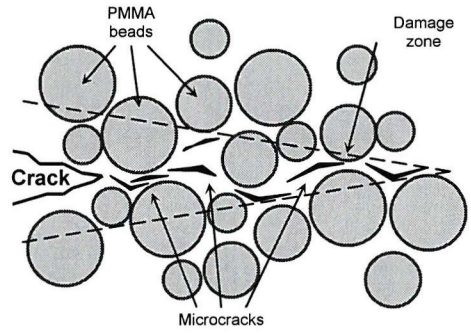

Figure 2.31: Schematic of microcracking ahead of a propagating fatigue crack (Topoleski *et al.*, 1993).

To further investigate the effect $BaSO_4$ may have on fatigue, Molino and Topoleski (1996) fabricated notched tensile test specimens of radiopaque (with $BaSO_4$) and radiolucent (without $BaSO_4$) Simplex P cement. Testing was performed in air at 5Hz, with a maximum and minimum load of 170N and 10N respectively. A crack gauge measured the length of the crack from the tip of the notch. Fracture surfaces were examined by scanning electron microscope. The fracture surface of the radiolucent cement was relatively smooth, and consistent with indiscriminate crack propagation through both pre-polymerised beads and matrix. Contrary to this, the fracture surface of the radiopaque cement was consistent with the model of interbead matrix fracture (see Figure 2.31). The crack growth rate of the radiopaque cement was one order of

magnitude less than that of radiolucent. However the authors did not believe the $BaSO_4$ acted to directly reinforce the cement. Indeed, scanning electron microscope analysis of the fracture surface revealed that the $BaSO_4$ particles did not bond with the cement matrix. It was proposed that $BaSO_4$ weakened the matrix, resulting in a longer crack path as the crack preferentially grew in the matrix, and helping to slow propagation. Another proposal was that $BaSO_4$ acted to blunt the crack tip and thus retarded crack growth. In this study, the region of fast catastrophic failure was smooth for both types of cement.

It is evident from *in vitro* studies that porosity influences damage accumulation in the cement mantle; as a result efforts are now made to minimise porosity in the cement mix (see Section 2.3.1, page 62). Several studies have attempted to elucidate the role of porosity in greater detail. One such study was presented by James *et al.* (1992), who compared centrifuged and uncentrifuged Simplex P specimens subject to a fully reversed tension-compression sinusoidal load (at 2Hz and a 37°C water bath). Scanning electron microscopy was used to examine fatigue surfaces. On all fatigue surfaces, cracks initiated at interior pores and travelled out to the edge of the specimen. River patterns were found to originate at pores for most specimens. The fracture surface was relatively smooth towards the initiating pores, but towards the edge of the specimen where fast fracture occurred, the surface was much rougher. The size and distribution of pores was also thought to have an impact on the fatigue life. Large pores initiated more and larger fatigue cracks than smaller pores. Small pores in close proximity to a large pore caused a larger stress concentration than the large pore alone, and led to many large fatigue cracks originating at the smaller pores. The small pores in this case effectively sharpened the edge of the large pore. Porosity therefore had a negative effect on the fatigue of the material, which is reflected in the fatigue lives of the centrifuged vs. uncentrifuged cement (Table 2.9). Centrifuging served to reduce the porosity in the specimens, thus increasing the fatigue life. Similar conclusions were drawn by Davies *et al.* (1987), who tested centrifuged and uncentrifuged Simplex P at 2Hz and initial strain levels of 0.01, 0.008, 0.005, 0.003 and 0.002. Further testing was performed at an initial strain level of 0.001, but at 20Hz. All tests were fully reversed uniaxial tension-compression and performed at 37°C. Prior to testing, specimens were radiographed, and centrifuging was seen to

reduce specimen porosity (Figure 2.32). S-N data was presented from the fatigue tests, and regression lines fitted to the data (see Figure 2.33):

Uncentrifuged: $\log N_f = -4.68 \log \sigma + 8.77$ **Equation 2.1**

Centrifuged: $\log N_f = -4.74 \log \sigma + 9.91$ **Equation 2.2**

where N_f was the number of cycles to failure and σ was the stress level. A 2-parameter Weibull analysis of the data was performed (details of the analysis on page 74), and yielded the survival probability curves shown in Figure 2.34. These curves illustrated the increased resistance of the centrifuged specimens, something that was not immediately apparent from the S-N data due to the large level of scatter. The constants of the Weibull analysis were not presented.

Uncentrifuged Specimens	Centrifuged Specimens
3,830	21,080
83,690	28,230
4,010	11,730
7,290	14,260
680	37,560
63,740	24,650
20,150	52,300
930	40,000
3,020	
9,430	

Table 2.9: Number of cycles to failure for uncentrifuged and centrifuged cement specimens (James *et al.*, 1992).

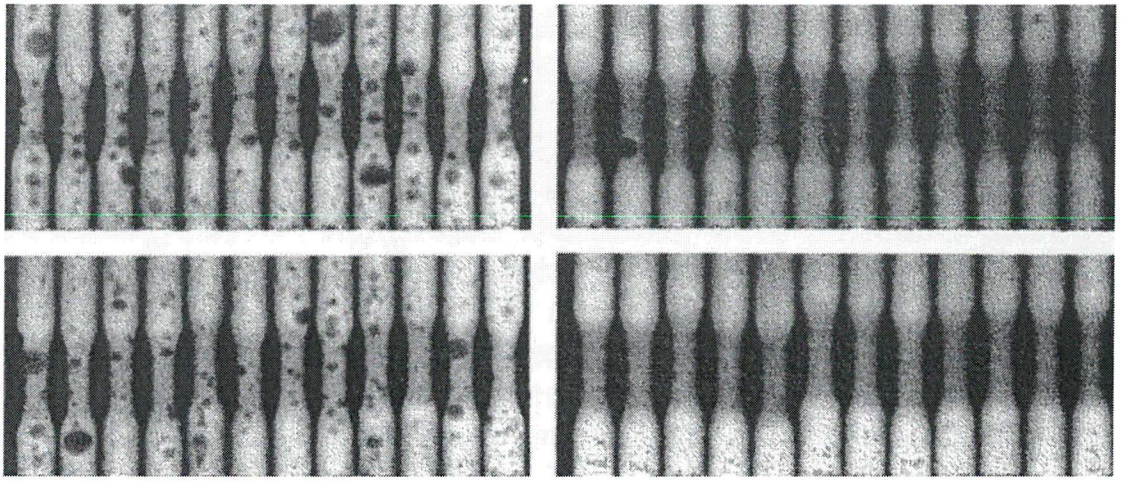

(a) (b)

Figure 2.32: Radiographs of (a) uncentrifuged and (b) centrifuged Simplex P fatigue test specimens (Davies *et al.*, 1987).

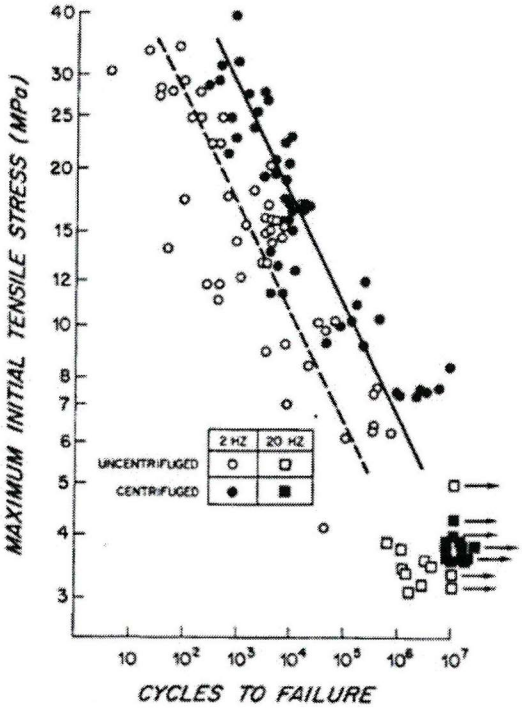

Figure 2.33: Stress versus cycles to failure for centrifuged and uncentrifuged cement specimens (Davies *et al.*, 1987).

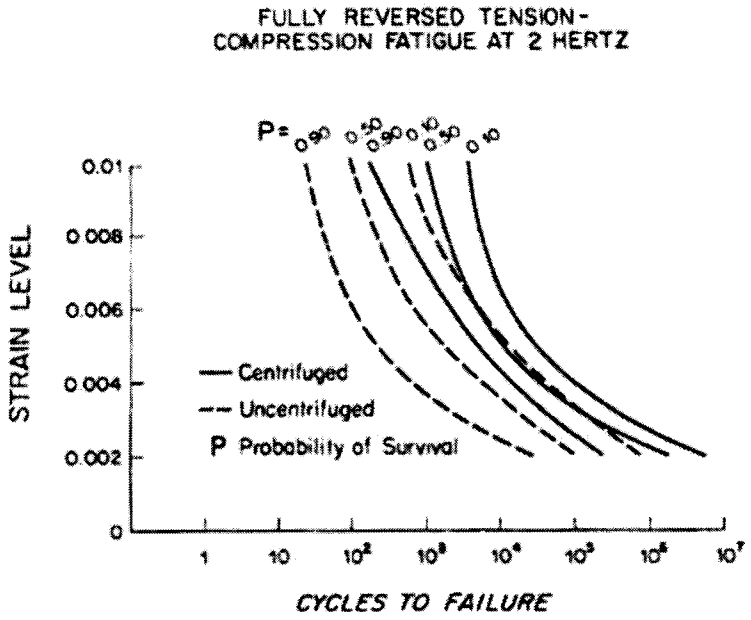

Figure 2.34: Strain level versus cycles to failure curves for centrifuged and uncentrifuged Simplex P at the 90%, 50% and 10% probability if survival levels (Davies *et al.*, 1987).

An alternative to centrifuging, and currently the more popular technique, is vacuum mixing. By reducing porosity, vacuum mixing should improve the fatigue behaviour when compared to hand mixing. Graham *et al.* (2000) performed uniaxial sinusoidal fatigue tests of hand and vacuum mixed Palacos R (in air, at 2Hz, a peak stress of 20MPa and an R-Ratio of 0.3). It was apparent from scanning electron microscopy of the fracture surfaces that the vacuum mixing reduced the internal porosity of the specimen. Improved fatigue resistance was reported for the vacuum mixed group, but specimens with large pores were discarded from the results. Lewis (1999) prepared hand and vacuum mixed cement Palacos R specimens, and performed fully reversed tension-compression fatigue tests with a maximum stress of 15MPa at 2Hz in air. The fatigue life of the vacuum mixed specimens was significantly superior to hand mixed (see Table 2.10). A 3-parameter Weibull statistical analysis was performed on the data, and values were presented for the *minimum* or *guaranteed fatigue life*, and the characteristic fatigue life. However, this study discarded specimens with any radiographic sign of porosity. The *minimum fatigue life* presented was therefore a misleading number, as it only represented a subset of specimens, and was not representative of the *in vivo* case where large pores may be present.

Vacuum mixed specimens	Hand mixed specimens
81,634	31,257
105,450	38,177
120,572	49,021
140,084	53,104
171,099	71,682

Table 2.10: Number of cycles to failure for vacuum and hand mixed cement specimens (Lewis, 1999).

Murphy and Prendergast (2000) performed a similar study, comparing vacuum mixed versus hand mixed Cemex Rx cement with a 2-parameter Weibull statistical analysis. No specimens were discarded in this study, so the true variability of the fatigue life was captured. Dog bone specimens were tested under sinusoidal tension at 13MPa, 17MPa, 21MPa and 25MPa, with an R-ratio of 0.1 at 10Hz (and a 37°C water bath). S-N curves for hand mixed and vacuum mixed cement were generated (Figure 2.35), and regression lines plotted through the average fatigue life at each stress level:

Hand mixed: $\sigma = -4.8 \log N_f + 39.3$ **Equation 2.3**

Vacuum mixed: $\sigma = -4.4 \log N_f + 40.4$ **Equation 2.4**

where σ was the stress level and N_f the number of cycles to failure. Correlation coefficients were 0.89 and 0.76 for hand and vacuum mixing respectively.

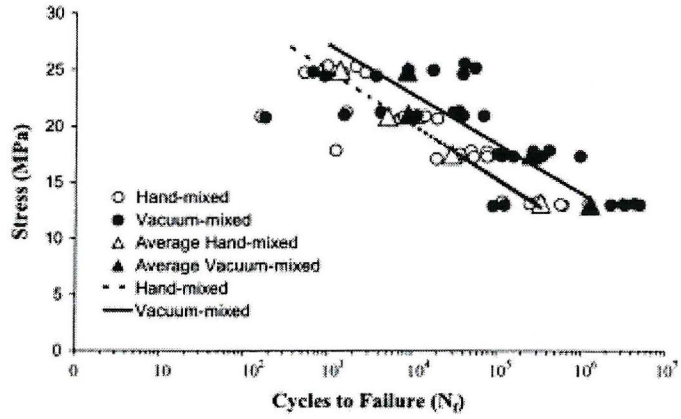

Figure 2.35: S-N curves for hand and vacuum mixed cement (Murphy and Prendergast, 2000).

The Weibull analysis allowed the probability of survival to a given number of cycles under a known stress level:

$$P_s = \exp\left[-\left(\frac{N}{\beta}\right)^{\alpha}\right] \qquad \textbf{Equation 2.5}$$

where P_s was the probability of survival, N the number of cycles and α and β empirical constants. Higher values of shape parameter (α) indicate a narrower distribution of data and therefore less variability. Higher values of location parameter (β) indicate a higher mean strength. These constants were calculated from the S-N data (Table 2.11), and allowed the probability of survival to 10 million load cycles to be plotted against stress level (Figure 2.36).

Stress (MPa)	Hand mixed cement		Vacuum mixed cement	
	α	β	α	β
13	1	593,366	0.53	2,842,535
17	0.67	49,998	1.39	361,968
21	0.6	9,412	0.5	18,519
25	1.92	1,564	0.58	16,008

Table 2.11: Weibull distribution constants (Murphy and Prendergast, 2000).

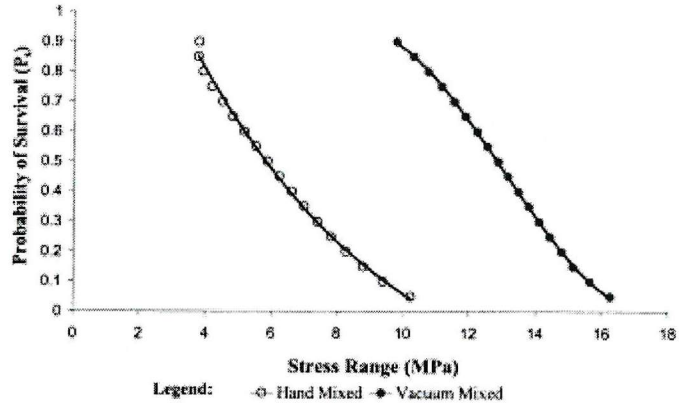

Figure 2.36: Probability of survival to $10x10^6$ cycles as a function of stress for hand and vacuum mixed cement (Murphy and Prendergast, 2000).

These curves display a clear distinction between hand mixed and vacuum mixed cement, which was not immediately obvious from the S-N data due to the large amount of scatter (Figure 2.35). Fracture surfaces were examined under scanning electron microscope, and distinct differences were observed between hand mixed and vacuum mixed fracture surfaces. A distribution of small pores with some relatively large pores was characteristic of the hand mixed specimens (Figures 2.37(a) & 2.37(b)). Small pores immediately adjacent to a large pore caused a stress concentration greater than the large pore alone (similar to observations by James *et al.* (1992)), effectively sharpening the large pore. This allowed fatigue cracks to initiate (Figure 2.37 (c) & 2.37(d)). Vacuum mixed specimens typically exhibited a single defect on the fracture surface, without the distribution of pores (Figure 2.38(a)). River patterns were observed propagating away from pores, implicating them in crack initiation (Figure 2.38(b). Vacuum mixed specimens occasionally contained a large pore, causing a significantly reduced fatigue life (Figures 2.38(c) & 2.38(d)) and greater variability in the vacuum mixed fatigue lives. This was also observed by Dunne *et al.* (2003), who compared the fatigue lives of Palacos R specimens mixed with different mixing devices and tested in air at 2Hz. Applied load was tension-tension with an upper load of 22MPa and an R-ratio of 0.01. A 3-parameter Weibull analysis of the data allowed the distribution parameter to be calculated for each mixing method, which gave an indication of the data scatter (Figure 2.39).

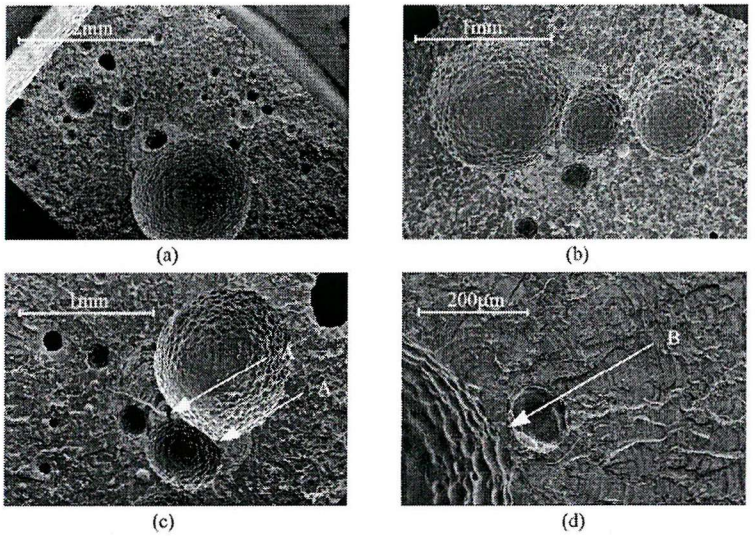

Figure 2.37: Hand mixed cement fracture surfaces. Arrows A and B identify the initiation of fatigue cracks (Murphy and Prendergast, 2000).

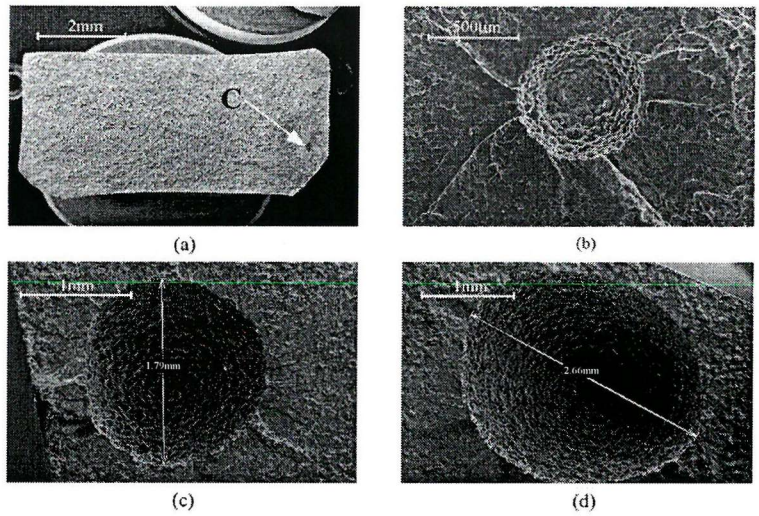

Figure 2.38: Vacuum mixed fracture surfaces. Arrow C points to the initiation of fatigue failure (Murphy and Prendergast, 2000).

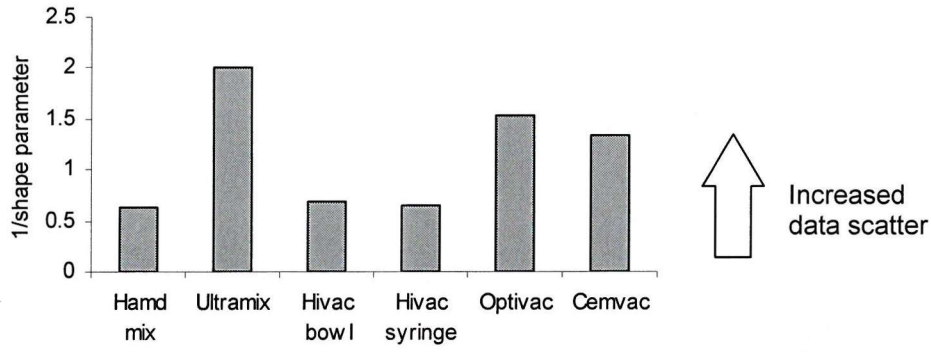

Figure 2.39: Inverse shape parameter from the Weibull analysis of fatigue data for cement mixed with different devices. Higher values indicate increased data scatter (Dunne *et al.*, 2003).

A further study by Murphy and Prendergast (2003) investigated the fatigue of bone cement under multi-axial conditions. Tubular specimens were formed that could be tested in uniaxial tensile fatigue, but also subjected to internal pressure (Figure 2.40). In this way, the cement specimens were subject to both tensile and hoop stress. Testing was performed at 0-11MPa sinusoidal tensile load, with internal pressure to produce hoop stresses of 0MPa, 11MPa and 16.5MPa on the internal walls of the specimen, and 0-15MPa tensile load with 0MPa and 15MPa hoop stress. All testing was performed at 37°C and 5Hz.

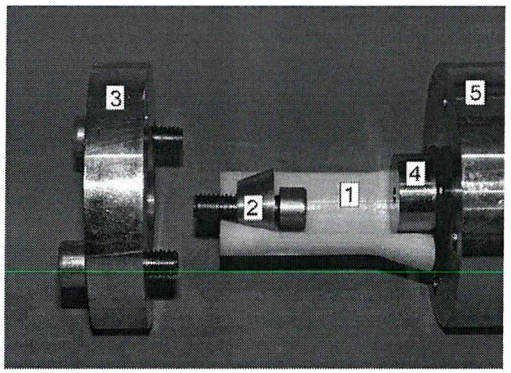

Figure 2.40: Schematic of the specimen gripping arrangement identifying: (1) pressure chamber, (2) internal specimen grip, (3&5) external grips and (4) pressure inlet (Murphy and Prendergast, 2003)

Taking the 0-11MPa and 0MPa hoop stress as the baseline, at 0-11MPa and hoop stress of 11MPa, the mean fatigue life increased by 16% (p=0.41) . At 0-11MPa and hoop stress of 16.5MPa, the mean fatigue life decreased by 30% from the baseline (p=0.06). The p values indicate the null hypothesis (i.e. that hoop stress does not influence fatigue) could not be rejected in either case. A 2-parameter Weibull analysis was used to further investigate the data (Figure 2.41). From this, the reduced fatigue life of the 16.5MPa hoop case was clear, but also the increased data scatter (indicated by a lower shape parameter or flatter curve). However, the 11MPa hoop case gave an almost identical cumulative Weibull distribution to the 0MPa hoop case. The authors suggest that this may have been due to the change in volume of the pressurised cavity during cyclic loading. This change in volume caused a cyclic hoop fluctuation of 0.6MPa for the 11MPa hoop case, but 1.6MPa for the 16.5MPa hoop case. The authors suggest this greater fluctuation in hoop stress may have allowed hoop stress to initiate fatigue cracks. For the higher axial stress of 0-15MPa, the average fatigue life was reduced by 40%, but the null hypothesis could again not be rejected (p=0.09). However, the cumulative Weibull distribution indicated a statistical likelihood of inferior fatigue live as well as increased variability (Figure 2.41). The increased variability was explained by considering pore orientation relative to the stress. Introducing hoop stress led to failures being initiated from pores due to the hoop stress (as well as the axial stress).

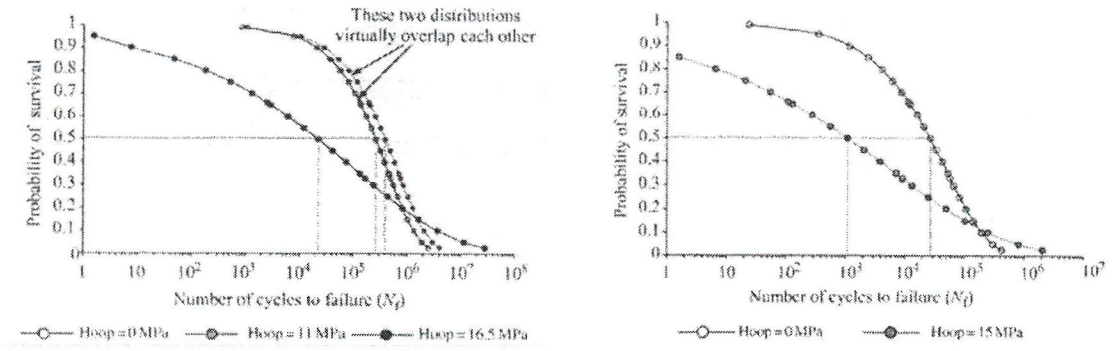

(a) (b)

Figure 2.41: Cumulative Weibull distributions for fatigue tests with axial stress of (a) 11MPa and (b) 15MPa.

From the studies discussed in this section, porosity is seen to have a dramatic influence on the fatigue properties of cement. However, porosity is not the only controlling parameter, as was demonstrated by Healey *et al.* (2002). Four different brands of cement (Simplex P, Palacos R, Endurance and Osteopal) were prepared with the same type of mixing device, and fatigued at 15MPa, 12.5MPa, 10MPa and 9MPa (fully reversed tension-compression at 10Hz and 37°C). Specimens were radiographed prior to testing. The average radiographic porosity did not necessarily predict the survival rates seen in the fatigue experiment, leading the authors to conclude that porosity was not the only factor influencing fatigue performance. Other properties such as cement chemistry and interaction with radiopacifiers and various enhancing drugs may have played a factor in the resistance to fatigue loads, and these should be considered when evaluating bone cements.

A good example of factors other than porosity influencing fatigue was presented by Harper and Bonfield (2000) who performed fatigue tests of 10 brands of cement (Palacos R, Sulfix-60, Simplex P, CMW-3, CMW-1, Duracem-3, Boneloc, Osteobond, Endurance and Zimmer dough type). All cement was hand mixed and tested in tension-tension with an upper stress level of 22MPa and an R-ratio of 0.01 (in air at a frequency of 2Hz). A 2-parameter Weibull analysis allowed a 50% probability of survival value to be determined for each cement (Table 2.12).

Cement Brand	Weibull 50% probability of survival
Simplex P	36,677
Palacos R	27,892
CMW-3	16,441
Osteobond	16,162
Duracem-3	15,031
Sulfix-60	9,816
CMW-1	4,407
Endurance	4,355
Zimmer dough type	781
Boneloc	164

Table 2.12: 50% Probability of survival for ten different bone cements. See text for testing details (Harper and Bonfield, 2000).

The differences in fatigue life were attributed to a range of parameters: variations in both composition of polymer and monomer, particle (e.g. $BaSO_4$, ZrO_2) size, morphology and molecular weight of powder, strength of polymer bead/matrix interface, powder to liquid ratios and sterilisation method. Most of the fracture surfaces displayed clear distinctions between pre-polymerised beads and interbead matrix, with evidence of radiopaque agent ($BaSO_4$ or ZrO_2) pullout upon failure (Figure 2.42). No evidence of $BaSO_4$ agglomeration was observed, unlike that observed with ZrO_2 in the Palacos R (Figure 2.43). The fracture surface of Boneloc was noticeably different from the other cements. Fracture surfaces showed regions where there appeared to be separate layers of material (Figures 2.44(a) & 2.44(b)). Circular holes were also observed on the fracture surface, assumed to contain ZrO_2 particles prior to failure (Figure 2.44(b)). There was no increased number of pores in the Boneloc cement, suggesting the low fatigue life was not related to porosity. The chemical composition of Boneloc is quite different from the other cements tested (Table 2.6, page 63), and may have been more influential than porosity in the fatigue tests. The poor performance of Boneloc was to be expected; many early failures of hip replacement with this brand of cement were reported leading to its withdrawal from the market (Havelin and Espehaug, 1995).

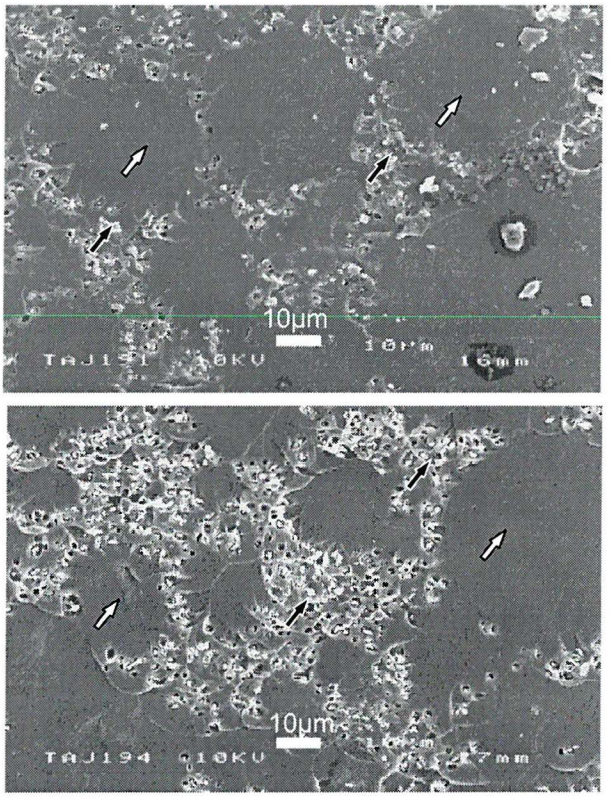

Figure 2.42: Scanning electron micrograph of (a) Simplex P and (b) CMW-1 cement. White arrows identify pre-polymerised beads, black arrows identify $BaSO_4$ particles in the interbead matrix (Harper and Bonfield, 2000).

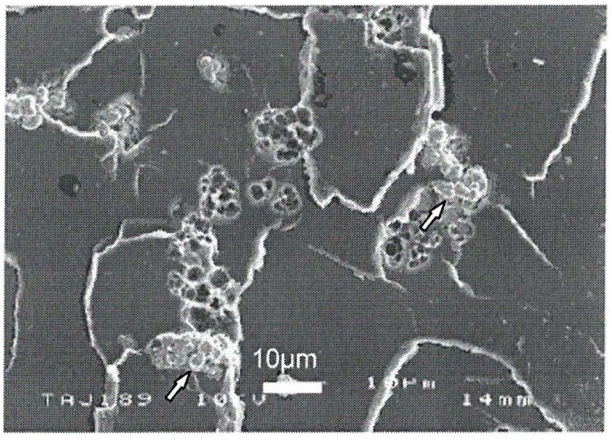

Figure 2.43: Scanning electron micrograph of Palacos R fatigue fracture surface showing agglomerates of ZrO_2 particles (white arrows) (Harper and Bonfield, 2000).

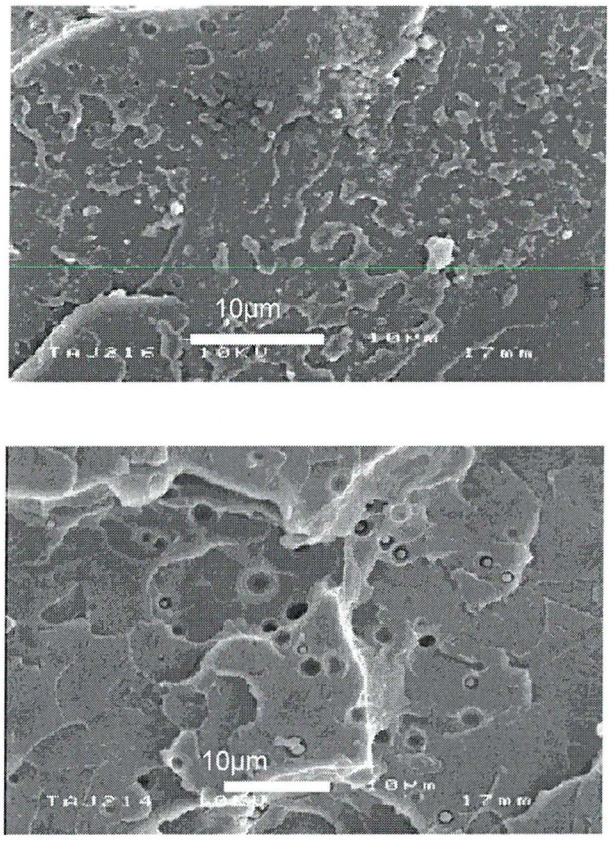

Figure 2.44: Scanning electron micrograph of Boneloc cement fracture surface (a) displaying layers of material and (b) circular holes where ZrO_2 particles may have pulled out (Harper and Bonfield, 2000).

The studies in this section have presented results in a number of ways. Presenting the equations of S-N regression lines is useful, as it allows different cements to be compared by a third party. For example, it would be quite easy to compare the fatigue results of Davies *et al.* (1987) and Murphy and Prendergast (2000). In this particular case, the testing conditions were not the same so this would be an inappropriate comparison. Murphy and Prendergast (2000) presented the Weibull constants (α and β), which allows any further Weibull study (of a different cement brand perhaps) to compare statistical results. Of course testing conditions and specimen geometry would need to be similar.

Many factors influence the fatigue of bone cement, and currently porosity is thought of as the dominant influence (this is the case for most commercially available bone cements, Boneloc is an exception). There are, however, a number of other factors that

may influence fatigue that have not been explored in detail yet. These include creep and residual stress, and are discussed in the following sections, along with a section on how pores are generated in the cement.

2.3.3 *Bone cement and viscoelasticity*

The influence of cement viscoelasticity is of interest, as (a) creep may allow subsidence of the femoral component or (b) stress relaxation may dissipate high stresses within the cement, resulting in a more favourable stress distribution (Verdonschot and Huiskes, 1997b). Creep strain depends on the applied stress, but also testing time and environment. Lee *et al.* (2002) tested cement creep under static tensile, compressive and 4-point bend loads using hand mixed cement specimens, and the following factors were identified as having the potential to influence creep.

- *Age of specimens.* The lower the age of the specimen (aged in saline at 37°C), the greater the creep/stress relaxation rate. This was thought to be due to the presence of residual monomer shortly after mixing acting as a plasticiser. Further polymerisation as the specimens aged removed this residual monomer.
- *Testing environment.* At 37°C, testing in saline produced a greater level of creep than testing in air, but less than testing in an environment containing fat. The reasons for this were uncertain, but the saline or fat environment probably acted as a plasticiser in the same way as residual monomer.
- *Temperature.* The glass transition temperature of bone cement is about 95°C, while it is required to function at about 37°C. Testing at elevated temperatures significantly increased creep strains. Compared to testing at room temperature, strain rates were 3.55 and 4.43 times higher at 37°C and 40°C respectively.
- *Stress level and load application time.* In common with all conventional materials, bone cement creep strain is greater for a greater applied stress. Also, the creep strain increases depending on the time the load is applied.
- *Cement brand.* Seven different cement brands were tested, Simplex P, Palacos R, Palacos LV40, CMW-1, CMW-2, CMW-3 and Boneloc (Figure 2.45). The creep strains were similar for all cements apart from Boneloc, which has a glass transition temperature of about 55°C. Boneloc was found to have viscoelastic properties "very much more pronounced than those of the PMMA based cements". The poor performance of Boneloc cement in clinical trials is

widely reported (Abdel-Kader *et al.*, 2001; Havelin and Espehaug, 1995; Walczak *et al.*, 2000).

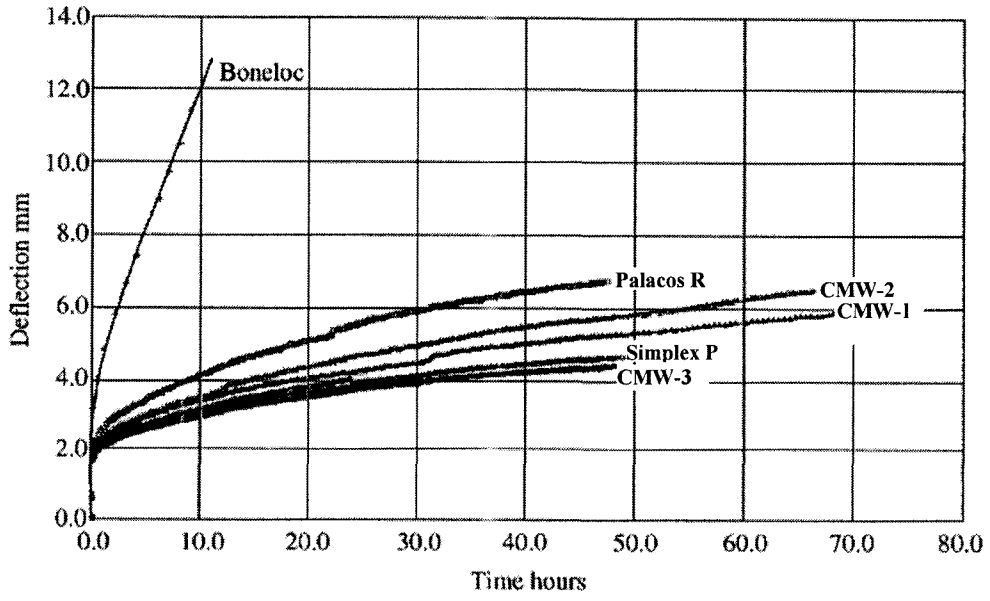

Figure 2.45: Creep of various bone cements – 4-point bending, central deflection versus time at body temperature. Different cements exhibit different creep rates, with Boneloc being quite different to the others (Lee *et al.*, 2002).

Displacement controlled tests can investigate the stress relaxation associated with viscoelasticity. Stress relaxation was reported by Lee *et al.* (2002) for hand mixed Palacos R under 4-point bending (constant displacement) in saline at 37°C (Figure 2.46). Over a period of 50 hours, the stress in the cement was found to reduce from 25MPa to about 10MPa. A similar magnitude of stress relaxation was reported by Yetkinler and Litsky (1998), who tested cylindrical specimens (hand mixed) under constant compressive displacement in water at 37°C. The initial applied stress was about 14MPa, which reduced to about 6MPa after 50 hours (Figure 2.47).

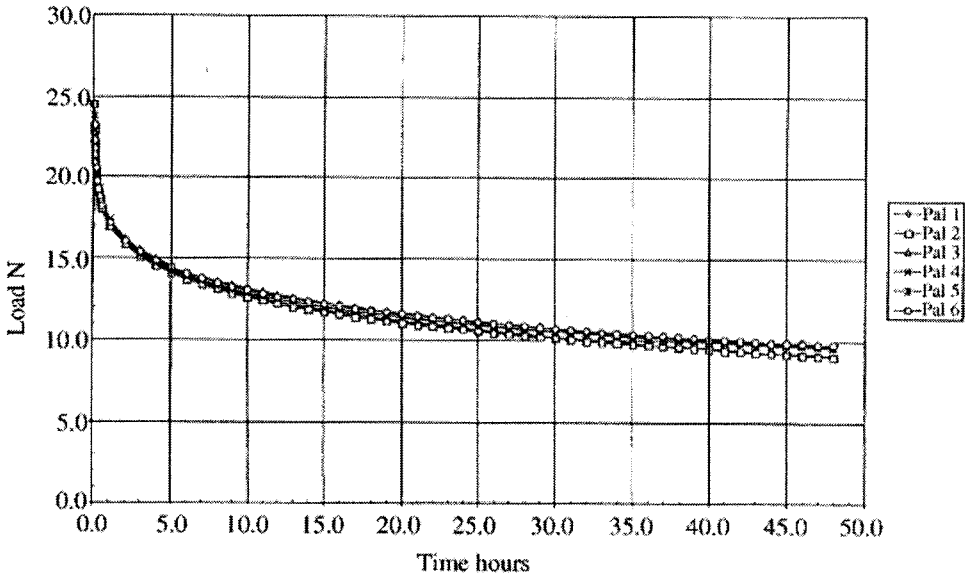

Figure 2.46: Stress relaxation of Palacos R, 4-point bending, constant central deflection, specimens 7 days old at start of tests, in saline at body temperature (Lee *et al.*, 2002).

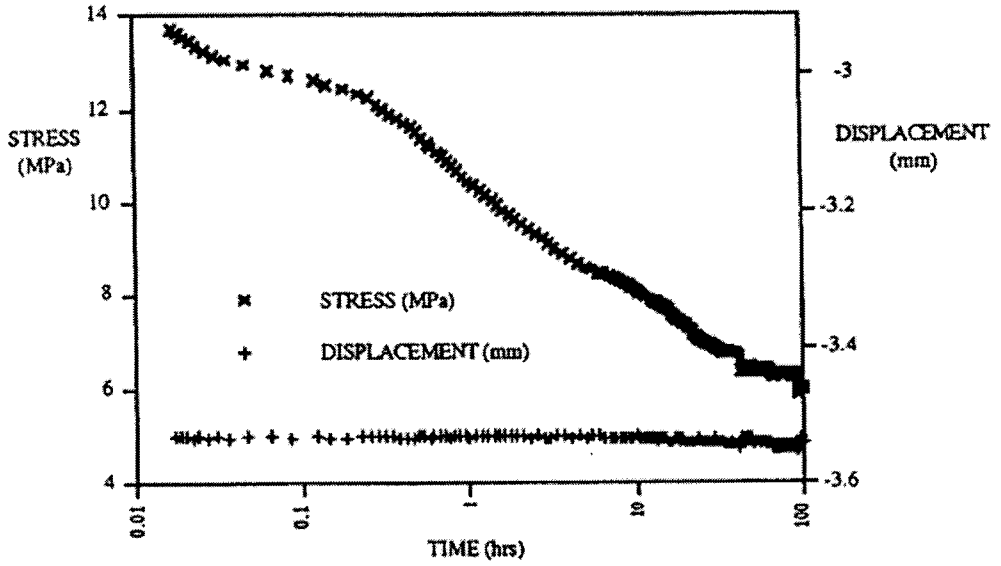

Figure 2.47: Stress relaxation of Simplex P specimen, 4-point bending, central deflection, tested in water at body temperature. Note logarithmic scale on x-axis (Yetkinler and Litsky, 1998).

Several studies have presented empirical models for bone cement creep. Chwirut (1984) measured the creep of hand mixed Zimmer regular cement under a static compressive load in saline at 37°C. A power law time function was fitted to the data, with parameters determined by a least squares fit to the experimental data:

$$\frac{\varepsilon}{t^n} = k\sigma^m \qquad \textbf{Equation 2.6}$$

where ε was the creep strain, t the time in hours, n was the average time coefficient calculated from the data (0.283, calculated by fitting $\varepsilon=ct^n$ to the data by least squares, where c was a stress dependant constant) and coefficients k ($1.76\text{x}10^{-9}$) and m (1.858) calculated from the data by least squares. A second function was evaluated, namely the exponential stress function:

$$\frac{\varepsilon}{t^n} = a\exp(b\sigma) \qquad \textbf{Equation 2.7}$$

where σ was the stress level, coefficients a ($3.02\text{x}10^{-4}$) and b ($9.37\text{x}10^{-4}$) were computed from the data by least squares, and other parameters were as described above (n=0.283) . The exponential stress function provided a better representation of the experimental data, predicting strains within 10% for periods up to 1000 hours. However, this function suffered the limitation that creep strain was not zero at zero stress, so the low stress predictions were necessarily not correct.

The work by Chwirut (1984) dealt solely with creep under a static compressive load. Verdonschot and Huiskes (1995) expanded on this, by measuring creep under a cyclic compressive load. Cylindrical specimens of hand mixed Simplex P were exposed to a sinusoidal compressive load at 7MPa, 11MPa, 15MPa and 20MPa, at 38.5°C and an R-ratio of 0.1. A similar model to Equation 2.7 was used to model creep, replacing the time parameter with the number of loading cycles:

$$\log\varepsilon = b_0 \log N + b_1 \qquad \textbf{Equation 2.8}$$

where ε was creep strain, N the number of loading cycles and b_0 and b_1 parameters dependant on stress level. Equation 2.8 was applied to the experimental data, plotted on a double logarithmic strain versus loading cycles graph. The slopes of the creep curves were similar for all stress levels, such that the b_0 parameter could be assumed a constant value of 0.314 (standard deviation 0.036). From the experimental data, the dependency of b_1 on stress was virtually linear and described by:

$$b_1 = 0.033\sigma - 4.9117 \qquad \textbf{Equation 2.9}$$

where σ was the stress level and b_1 the stress dependant parameter. Creep strain represented by this model is displayed in figure 2.48.

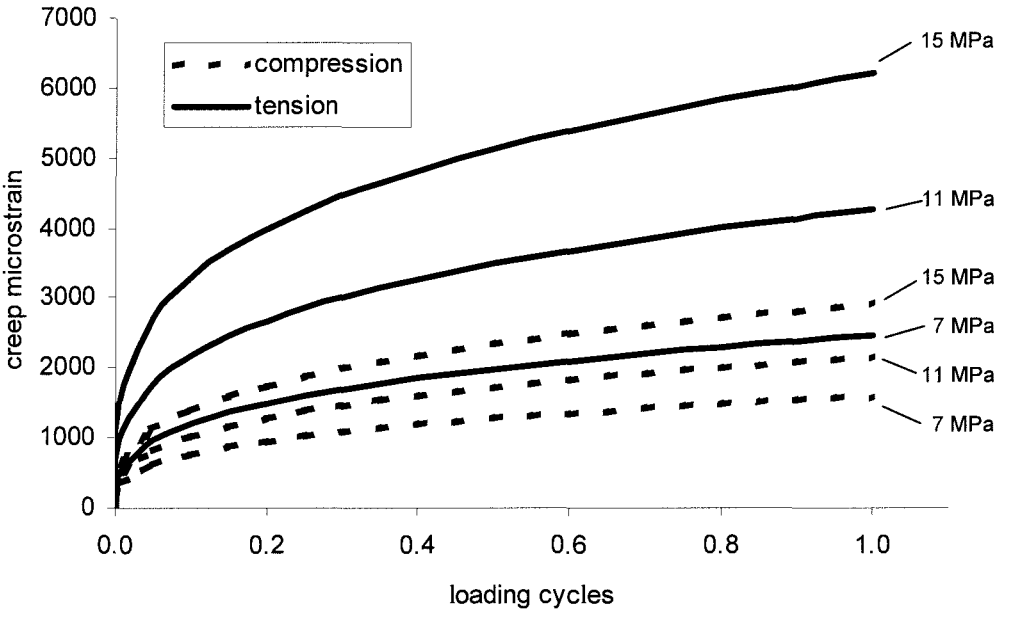

Figure 2.48: Creep strain as a function of loading cycles under cyclic tension and compression. A double logarithmic relationship between strain and number of loading cycles was used to model experimental data (Verdonschot and Huiskes, 1994; Verdonschot and Huiskes, 1995).

Boneloc exhibits greater levels of creep than more conventional PMMA based cements (see Figure 2.45). It is therefore reasonable to suggest that preclinical testing of bone cement should include creep tests as these may identify an inferior cement, as Boneloc turned out to be. This was the reasoning behind the study by Verdonschot and Huiskes (2000), who performed compressive creep tests of three relatively new bone cement brands – Cemex Rx, Cemex System and Cemex Isoplastic, and compared results to a conventional bone cement (Simplex P). Hand mixed specimens were tested in saline at 38.5°C under a cyclic compressive load of peak magnitude 20MPa and an R-ratio of 0. The data was modelled as described by Equations 2.8 and

2.9. Creep rates of the new cements were higher than the conventional cement, but were not considered excessive, and the creep properties deemed adequate for clinical use.

Another study by Verdonschot and Huiskes (1994) investigated the creep of Simplex P under a cyclic tensile load. Hand mixed specimens were tested in saline at 38.5°C at stress levels of 3MPa, 7MPa and 11MPa, and creep measured with an extensometer. No specimens were discarded. A double logarithmic function was proposed to model the creep:

$$\log \varepsilon = A \log N + B \qquad \textbf{Equation 2.10}$$

where ε was creep strain, N the number of loading cycles and A and B stress dependant constants. A logarithmic relationship was used to evaluate the relationship between A and B and stress:

$$A = a_1 + a_2 \log \sigma \qquad \textbf{Equation 2.11}$$

$$B = b_1 + b_2 \log \sigma \qquad \textbf{Equation 2.12}$$

where A and B were the constants to be determined, and a_1, a_2, b_1 and b_2 were determined as 0.41, -0.12, -0.10 and 1.91 respectively from the experimental data. Creep strain for cyclic tensile loading by this method is plotted in Figure 2.48. A limitation of the logarithmic creep function was that tertiary creep was not included. This was considered acceptable as specimens usually fractured before signs of tertiary creep were recorded by the extensometer.

The creep models presented by Chwirut (1984), Verdonschot and Huiskes (1994) and Verdonschot and Huiskes (1995) were for bone cement, but creep models have also been presented for industrial PMMA, which may be of use to the biomechanist. Berthoud *et al.* (1999a) used Paraglas brand commercial PMMA to perform uniaxial compression tests and depth sensing indentation tests. Creep models were derived for both tests based upon:

$$\dot{\varepsilon} = \dot{\varepsilon}_1 \exp\left(\frac{\sigma}{S_1}\right) \qquad \textbf{Equation 2.13}$$

where $\dot{\varepsilon}$ is creep strain rate, σ the stress level and $\dot{\varepsilon}_0$ and S_1 constants defined for a uniaxial creep test. For the compression model, the hydrostatic compression was included in the σ component and was able to replicate experimental data. For the indentation tests, creep was analysed by relating the average stress and the strain rate in the deformed volume. The resulting model could account for the multi-axial stress and strain fields under the indenter and again replicate the experimental data. In a further study, Berthoud *et al.* (1999b) used the same logarithmic relationship (Equation 2.13) to model interfacial creep (i.e. creep of load bearing asperities). This was then incorporated in a simple model of a static frictional interface. Other methods have been presented for modelling creep of commercial PMMA, for example Dooling *et al.* (1998) used a generalised Maxwell model for the linear viscoelastic region, and included the onset of nonlinearity based on differential representations in which the stress activating non-Newtonian flow was an internal variable. Further investigation of such studies may be outside the scope of the thesis, but the constitutive models employed could certainly be used in relation to bone cement.

The empirical models presented for bone cement creep allowed the process to be simulated in finite element analyses. However, the empirical models discussed above (for bone cement) were for uniaxial stress conditions, seldom encountered *in vivo*. It was therefore necessary to assess the suitability of using uniaxial creep data in a 3-dimensional stress field. Verdonschot and Huiskes (1996) considered this by developing a polished metal tapered stem surrounded by a cement mantle and applying a sinusoidal axial force to the stem tip (see Figure 2.49). Testing took place in saline at 38°C, with a maximum and minimum load of 7kN and 0kN respectively. Strains in the cement mantle and stem subsidence were recorded. An axisymmetric finite element model of the structure was generated (see Figure 2.49), with creep simulated according to Equation 2.8 and 2.10 for elements with a compressive and tensile maximum principal stress respectively. Two tapered stems were used in the study, and although the subsidence *patterns* were the same, the *magnitude* of subsidence was different (380μm versus 630μm). The finite element model was able

to generate a similar subsidence pattern to the experimental models (see Figure 2.50) using two different coefficients of friction (μ=0.25 and 0.5). The lower coefficient represented a highly polished taper, but the higher was chosen arbitrarily. The stepwise subsidence pattern seen in Figure 2.50 was thought to be due to slip-stick mechanisms at the interface starting distally and gradually working towards the proximal. It was concluded that finite element models, extended to incorporate cement creep, could produce realistic results. However, there was a degree of uncertainty regarding the interface conditions of the experimental models (hence the different friction coefficients in the computational model). For each, specimen preparation was the same, and the surface roughness of each taper was similar – 0.033μm (standard deviation 0.0025) and 0.039μm (standard deviation 0.0019). Including more specimens in the study to provide a subsidence data envelope may have allowed better comparison between the experimental subsidence and the deterministic computational result.

In addition to the subsidence effect, viscoelasticity may also serve to relax stresses in the cement mantle, and generate a more favourable stress distribution. Verdonschot and Huiskes (1997b) investigated this by generating a finite element model of the implanted femur (see Figure 2.51) and simulating cement viscoelasticity as the model was subjected to gait loading. The stem/cement interface was assumed debonded with a friction coefficient of 0.25. The subsidence of the implant was small (about 50μm), but the cement stresses were relaxed over time for both bonded and unbonded interfaces (see Figure 2.51). A similar analysis was performed by Lu and McKellop (1997), who generated a simplified implanted femur model to investigate the influence creep had on implant subsidence and cement stresses (Figure 2.52). Cement creep was simulated with an exponential function. (Prior to simulating creep in the FE model seen in Figure 2.38, creep was simulated in a cylindrical specimen, and compared to experimental results of Chwirut (1984). Good agreement was reported.) The reduction in cement mantle stress is shown in Figure 2.52(b), for a debonded stem/cement interface with a friction coefficient of 0.22. Fully bonded and frictionless debonded analyses were also performed; a similar stress reduction was found. Subsidence caused by creep was small; the analysis was repeated *without* the effects of creep, and subsidence was reduced by 2μm, 2μm and 190μm for the bonded, frictional and frictionless stem/cement interface respectively.

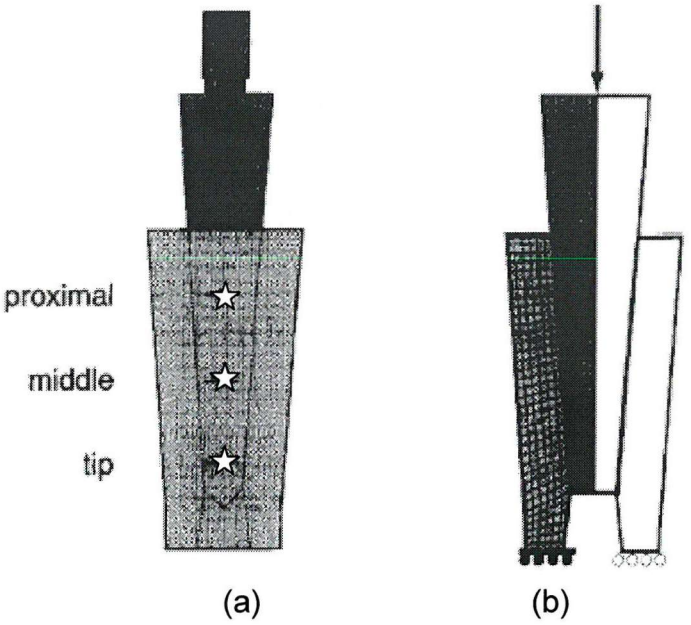

Figure 2.49: (a) Experimental model of metal taper surrounded by a cement mantle with three strain gauges attached identified by stars and (b) the axisymmetric FE model of the structure (Verdonschot and Huiskes, 1996).

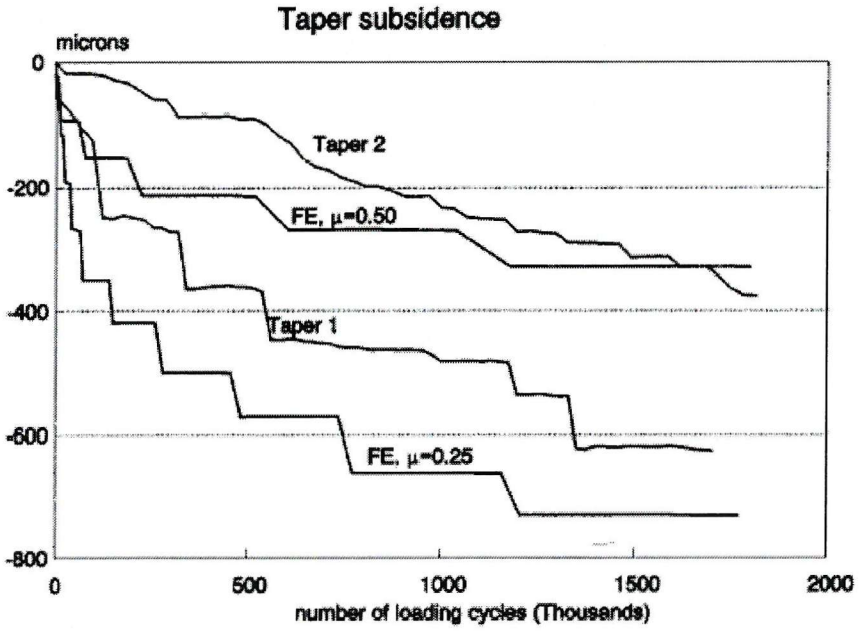

Figure 2.50: Experimental and computational subsidence of the taper illustrated in Figure 5. Two different coefficients of friction (μ) were used in the finite element analysis (Verdonschot and Huiskes, 1996).

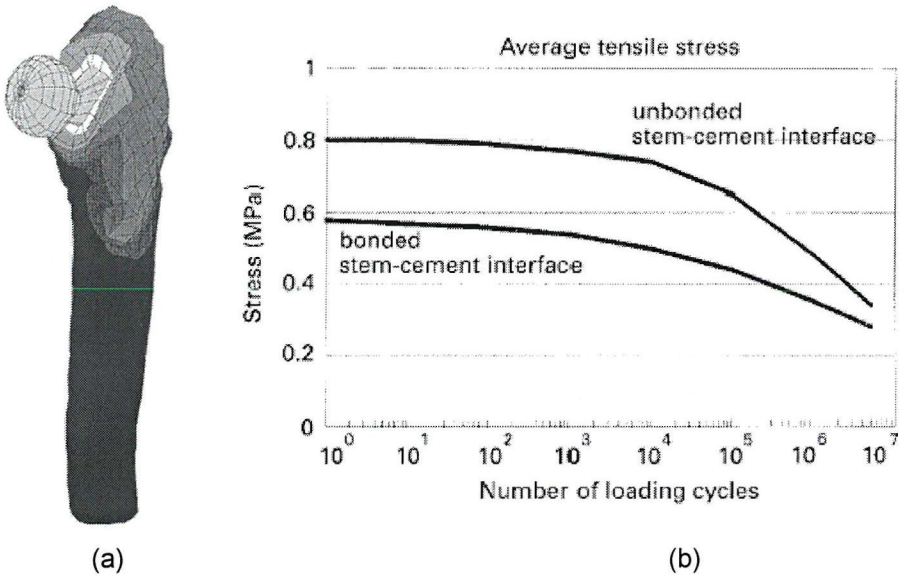

Figure 2.51: (a) Finite element model used by Verdonschot and Huiskes (1997b) to simulate cement creep under a fatigue load and (b) average tensile stress in the cement mantle of (a) as a function of loading cycles. The stress reduced as a function of time due to creep being simulated in the analysis.

Similar levels of creep-induced subsidence (for the same interface conditions) were reported by Norman *et al.* (2001) in a finite element study. A power law function was used to describe creep strain (Equation 2.6), and the stress monitored while gait loading was simulated. The peak stress in the cement reduced over time, as was observed in previous studies. The stress normal to the stem/cement interface was found to be the highest for the debonded frictionless case, inducing a so-called 'taper lock' as the stem got tighter in the cement mantle (Figure 2.53). The authors proposed that the stem tightening was mainly caused by prosthesis subsidence within the cement mantle, and creep induced subsidence had only a minimal contribution.

The studies in this section either (a) generated creep data using hand mixed specimens (Chwirut, 1984; Verdonschot and Huiskes, 1994; Verdonschot and Huiskes, 1995) or (b) simulated creep using data from (a) (Verdonschot and Huiskes, 1996; Verdonschot and Huiskes, 1997b; Lu and McKellop, 1997; Norman *et al.*, 2001). Therefore, all the finite element simulations simulate creep for hand mixed cement. Previously it has been discussed that the mixing method has a drastic influence on the fatigue performance of the cement (Section 2.3.2, page 67). It follows that mixing method should also influence the viscoelastic properties of the cement. This hypothesis was

investigated by Norman *et al.* (1995) in a study that compared hand and vacuum mixed cement under constant compressive loads at room temperature. Two brands were tested, Zimmer regular and Palacos R. The cement specimens were kept moist with a drip-feed mechanism. Vacuum mixing was found to reduce the creep strain for both cement brands. For example, hand mixed Zimmer specimens loaded at 50MPa for 6 hours exhibited a creep strain of 14% (SD 0); vacuum mixing reduced this value to 6.7% (SD 0.48). The reduction in internal porosity was cited as being the reason for the reduction in creep strains.

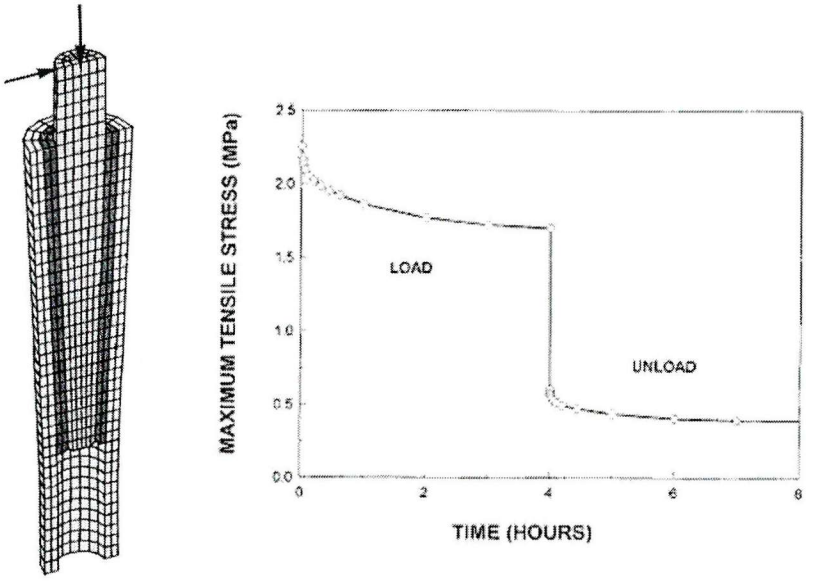

Figure 2.52: (a) Finite element model used by Lu and McKellop (1997) to investigate the influence of cement creep on stem subsidence and stress relaxation in the cement and (b) maximum tensile stress as a function of time within the cement mantle of (a) during the load and unload period.

The literature reviewed in this section informs us that cement creeps under a static and dynamic load under simulated *in vivo* conditions. This creep may not cause a great deal of implant subsidence, but could play a favourable role by reducing peak stresses in the cement. That is not to say increased creep rates are always favourable – Boneloc exhibited a high creep rate (Figure 2.45), but did not perform well in clinical trials. Certainly *in vitro* creep tests alone do not provide enough information to preclinically assess a new brand of cement. The experimentally generated creep laws under tension and compression allow creep to be simulated in finite element models, but currently data is only available for hand mixed cement. This means data from

different cement mixing conditions, and even different brands are currently being used in computational studies. For example, Stolk *et al.* (2003) simulated fatigue and creep in the cement mantle of the implanted femur, using fatigue data for vacuum mixed Cemex Rx, and creep data for hand mixed Simplex P cement. According to Norman *et al.* (1995), the porosity reduction associated with vacuum mixing reduces the magnitude of creep strain, and Lee *et al.* (2002) considers different cement brands to have different creep properties (Figure 2.45). There is therefore a gap in the literature, in that no single study reports both the fatigue *and* creep properties of a particular brand of vacuum mixed cement in the same specimens subjected to the same loading conditions.

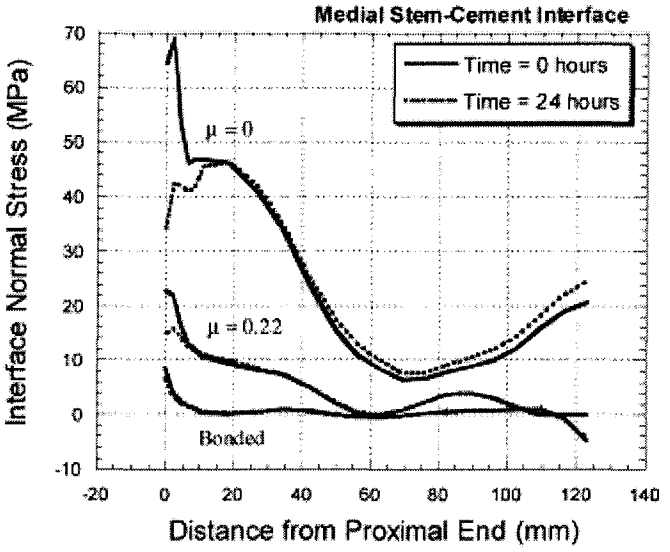

Figure 2.53: Normal stem/cement interface stress plotted for the length of the cement mantle (proximal to distal end) for bonded, frictional and frictionless cases (Norman *et al.*, 2001).

2.3.4 *Bone cement and residual stress*

During the polymerisation process of bone cement, the liquid monomer MMA polymerises to form the solid polymer PMMA. This process involves a density change as PMMA has a higher density than MMA. This density change causes the cement to reduce in volume, or shrink. The polymerisation process is exothermic, and shrinkage can also occur when the cement cools from the peak temperature reached. Cement shrinkage by both mechanisms has been proposed as a means of inducing a stress state in the cement (Gilbert *et al.*, 2000; Orr *et al.*, 2003). This induced stress is known as residual stress.

Residual stress was the focus of a study by Li *et al.* (2003), who simulated the thermal shrinkage process using computational methods. The residual stress in a ring of cement curing around a hollow aluminium stem was simulated, and compared to an experimental model. The photoelastic method was used to obtain cement stresses in the experimental model. Stresses were assumed 'locked' in the cement from the peak exotherm. The computational results were in good agreement with the experimental, thus providing some validation of method. The peak stress in this study was about 12MPa, in the hoop direction, close to the stem/cement interface. Also investigated was the effect of preheating the stem. Preheating the stem to 45°C increased the peak residual stress to about 14MPa, but shifted the position of peak stress away from the stem/cement interface, and actually lowered the stress at the interface. As cracks in the cement mantle have been found originating at the stem/cement interface (see Figure 2.12, page 36), it was proposed that minimising the residual stress at this location (by preheating the stem) might prolong the life of the cement mantle.

Another combined computational/experimental study was presented by Orr *et al.* (2003), who simulated the polymerisation process by cooling a polymerised ring of cement on a Morse taper mandrel. The cracks generated by this operation were similar to those observed *in vivo* (compare Figure 2.54 to Figure 2.12, page 36). This cooling process was simulated computationally for hand mixed cement, and hoop stresses of between about 8MPa and 25MPa were calculated, depending on the initial temperature. Residual stress values for vacuum mixed cement were slightly higher, between about 10MPa and 30MPa for the same initial temperature range. A second

part of this study calculated the residual stresses again, but this time including the physical shrinkage due to density change of the material as it polymerises and assuming an axial restraint. This increased the calculated residual stresses to between 20MPa and 70MPa for the same initial temperatures. These values are greatly in excess of the tensile strength of the material and must be considered overestimates. Shrinkage due to density change occurs partly while the cement is in the liquid phase and can flow to accommodate the volume changes; this was neglected in this study. However, the results suggest that cracks due to cement shrinkage may be present in the cement mantle prior to functional loading. Also, while the reduction in porosity may be desirable to increase the fatigue life, the increased density of vacuum mixed cement may generate residual stresses of higher magnitude.

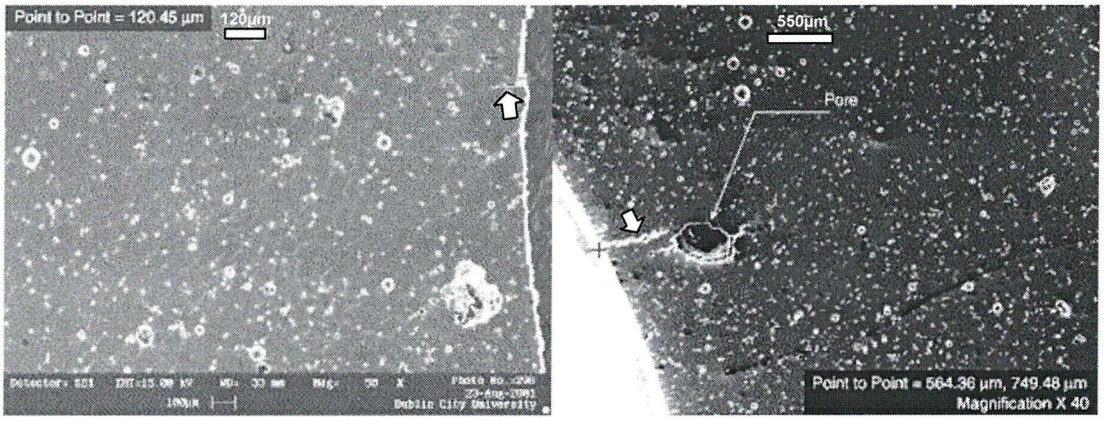

Figure 2.54: Scanning electron micrographs of the cement/mandrel interface, with white arrows showing cracks originating at the interface and propagating into the cement (Orr *et al.*, 2003).

Acoustic emission equipment and strain gauges were used by Roques *et al.* (2004b) to investigate residual stress. A hollow stem was equipped with the strain gauges and implanted into a composite femur with bone cement. The acoustic emission sensor was attached to the stem, to monitor any cracking in the cement or sliding at the stem/cement interface. Strains measured inside the stem were correlated to stresses in the cement with a finite element model. A peak residual stress of 9.8MPa was calculated using this method, in the hoop direction and close to the stem/cement interface. The strain gauges revealed that the cement was shrinking onto the stem, i.e. the stem was restricting shrinkage, hence the high hoop stresses. Acoustic emissions were detected from the time of peak exotherm, and demonstrated that strains in the

cement were partly relieved by cracking and sliding of the cement against the stem after this time.

A different approach to simulating residual stress was taken by Nuno and Cristofolini (2001), who allowed a cement mantle to polymerise around a titanium alloy stem. Once the cement had polymerised, the stem was removed, leaving a hollow cylinder of bone cement. Strain gauges were applied to the outside surface of the cement, and the stem re-inserted. Strain gauge data was recorded. A finite element model of the experimental model was then created, and an interference fit applied to the stem/cement interface such that the strains at the outer surface were similar to those recorded by the strain gauges. This generated a stress field in the cement mantle that simulated residual stress, with peak values in the hoop direction between 10MPa and 15MPa. Although these values are similar to those discussed above, the method of residual stress generation did not facilitate stress generation in the longitudinal direction.

The studies discussed thus far deal with cement polymerising around a rigid metallic stem. To investigate the residual stress in unconstrained cement, Whelan *et al.* (2000) measured the internal strains in polymerising blocks of bone cement (75mm x 17.8mm x 7.9mm), using optical fibre Bragg grating sensors. A thermocouple was used to monitor the temperature of the cement during polymerisation. The strains in the cement were induced only from the time of peak exotherm, providing evidence that stresses are locked in the material from this time. A companion study by (Lennon *et al.*, 2000) simulated the polymerisation process for the bone cement block with embedded optical fibre. Temperature and strain history closely matched the results of (Whelan *et al.*, 2000), and a peak stress in the optical fibre of 3.1MPa was calculated. This is considerably less than reported in the studies discussed above, as the cement blocks were unconstrained by a metallic stem, and could therefore shrink freely.

The experimental/computational study by Mann *et al.* (1991) used a simplified thermal contraction method to simulate residual stress. The entire cement mantle was assigned a thermal expansion coefficient of 47×10^{6}, and cooled from a uniform peak temperature (of 85°C to 25°C). Hoop and longitudinal residual stresses were dominant, with the majority of the cement experiencing a magnitude of 5MPa to

6MPa. The residual stress was simulated in axisymmetric models of straight and tapered push-through tests – titanium alloy stems surrounded by the cement mantle. The push-through tests were simulated, including residual stress and friction at the stem/cement interface. The resulting load/displacement curves were similar to experimental tests, and the study concluded that friction at the interface and residual stress were the controlling parameters in the computational models.

The final study discussed in this section is a finite element based simulation of thermal shrinkage performed by Lennon and Prendergast (2002). The model calculated the polymerisation fraction of each element and the subsequent temperature change. Shrinkage was simulated from the maximum temperature reached by each element, and generated a peak residual stress level of 7MPa, but simulating a pore in each element increased the peak stress to 24MPa (see Section 2.3.5, page 100 for pore simulation details). While a pore in *every* element may be unrealistic, a threefold increase in stress suggests porosity should be at least considered in finite element studies. The finite element model in this study was generated to the same dimensions as an experimental model based on layers to facilitate visualisation of the cement mantle (see Figure 2.26, page 57). Dye penetrant analysis of the experimental model revealed cracks perpendicular to the orientation of the stresses predicted by the computational model. However, hoop stresses could not be simulated by this method. This may be why the peak value predicted (without porosity, 7MPa) was slightly lower than the other studies discussed, where hoop stresses were usually dominant.

Considering the studies discussed in this section, we may conclude that residual stress is present in the cement mantle of the implanted femur immediately post operatively. Studies that have measured residual stress from experimental models report peak magnitudes of 12MPa (Li *et al.*, 2003), 10MPa (lower bound estimation) (Orr *et al.*, 2003), 9.8MPa (Roques *et al.*, 2004b), and 10MPa – 15MPa (Nuno and Cristofolini, 2001). These studies all simulate cement constrained by a femoral stem, which serves to restrict shrinkage and generate the dominant hoop stresses. These magnitudes are significant, especially as they are present prior to functional loading of the replacement. It is possible that stress relaxation may reduce the magnitude of residual stress over a period of time, but it may not be entirely dissipated. As would be expected, unconstrained cement exhibits a lower magnitude of residual stress –

3.1MPa was reported by Whelan *et al.* (2000) and Lennon *et al.* (2000). As observed by Orr *et al.* (2003), residual stress may cause pre-load damage in the cement mantle. This has been observed *in vitro* and thought to accelerate fatigue cracking in the cement (Section 2.2.5, page 51). Residual stress should therefore at least be considered when analysing the stress state in the cement mantle of orthopaedic devices; it is not exclusive to the femoral component in hip replacement.

2.3.5 *Bone cement and porosity*

As the cement is prepared by the surgeon in the operating theatre, air can be trapped in the final mix and form pores in the resulting material. General opinion is that porosity should be reduced in bone cement, and modern cement mixing now takes place under a vacuum to minimise the likelihood of pores. Although vacuum mixing can reduce porosity in the cement, it does not eliminate it entirely.

Jasty *et al.* (1990) assessed porosity by sectioning cement specimens at 5mm intervals and spray-painting the surfaces, allowing the fractional porosity to be determined. Four different cement brands were analysed by this method: Simplex P, Zimmer Regular, CMW and AKZ. Fractional porosity was between 9% and 10% for hand mixing at room temperature, dropping by about a factor of two when the cement was centrifuged. Muller *et al.* (2002) measured the fractional porosity of CMW-1 using a similar sectioning method. The mean measured value from six hand mixed specimens was 6.7%; vacuum mixing reduced this value to 1.3%. Norman *et al.* (1995) measured the porosity of Zimmer Regular and Palacos R in a similar fashion. A fractional porosity of 4.8% was reported for hand mixed specimens, reducing to 1.7% for vacuum mixed specimens.

The principal of Archimedes was used by Dunne and Orr (2001) to quantify the percentage porosity in rectangular specimens of Palacos R. Six different mixing devices were used to prepare the specimens, at reduced pressure levels recommended by the device manufacturer. Porosity levels (of the same cement brand, Palacos R) were between 10.3% and 1.4% for the six different mixing devices (see Table 2.13). A porosity level of 16.4% was reported for hand mixed cement.

The number of pores in a given volume of cement is another, possibly more useful, way to quantify porosity. Murphy and Prendergast (2001) were able to count the pores on the surface of vacuum mixed bone cement specimens using dye penetrant methods. A total of 398 pores in 15 specimens was reported (counted in gauge section, volume 896mm^3). This should perhaps be considered a lower bound value, as only pores that intersected the specimen surface could be counted.

Mixing system	Mixing method	Mean resultant porosity % (SD)
Howmedica Mix Kit 1	Hand	16.40(0.78)
Zimmer Osteobond	Vacuum	10.30(0.81)
Summit LoVac Bowl	Vacuum	9.86(1.24)
Cemvac	Vacuum	4.37(1.55)
Summit HiVac Syringe	Vacuum	3.17(1.54)* 1.70(0.76)†
Mitab Optivac	Vacuum	1.44(0.24)

Table 2.13: Porosity generated in Palacos R cement specimens using six different mixing apparatus (Dunne and Orr, 2001). *Reduced pressure of –72kPa. †Reduced pressure of –86kPa.

Porosity then, is generated during the mixing process, and vacuum mixing can minimise the level of porosity in the cement. However, cement also shrinks during the polymerisation process (this has been discussed in the residual stress section, 2.3.4, page 95), and as well as inducing residual stress, this shrinkage can also be a source of porosity, as proposed by Gilbert *et al.* (2000), with the following concept. They considered a hypothetical cube of bone cement, 1000mm^3, allowed to cure such that the external dimensions of the cube were fully constrained, and in which existed an infinitesimal pore at the centre of the cube. If the cement underwent shrinkage, the pore would increase in size to accommodate this shrinkage. Gilbert *et al.* (2000) calculated that cement shrinkage of 7.8% would grow the pore to a diameter of 5.3mm, assuming all shrinkage occurs at the pore site. Experimental models were built to achieve a similar situation to this, and porosity was indeed observed to develop as the cement polymerised when the external dimensions of the cement were constrained. When the cement was not constrained, no pores developed. It was also noticed that for the unconstrained case, vacuum mixed cement generated a greater level of shrinkage than hand mixed cement. This was also noticed by Muller *et al.* (2002), who presented the relationship between porosity and shrinkage in Figure 2.55. Lower porosity was found to correspond to a higher shrinkage, while higher porosity was associated with less shrinkage, suggesting that reducing porosity in the cement (i.e. vacuum mixing) serves to not only reduce porosity, but may also increase the residual stress experienced *in vivo*. Muller *et al.* (2002) proposed that the thermal

characteristics of the cement were altered by the level of porosity, and may explain the difference in shrinkage.

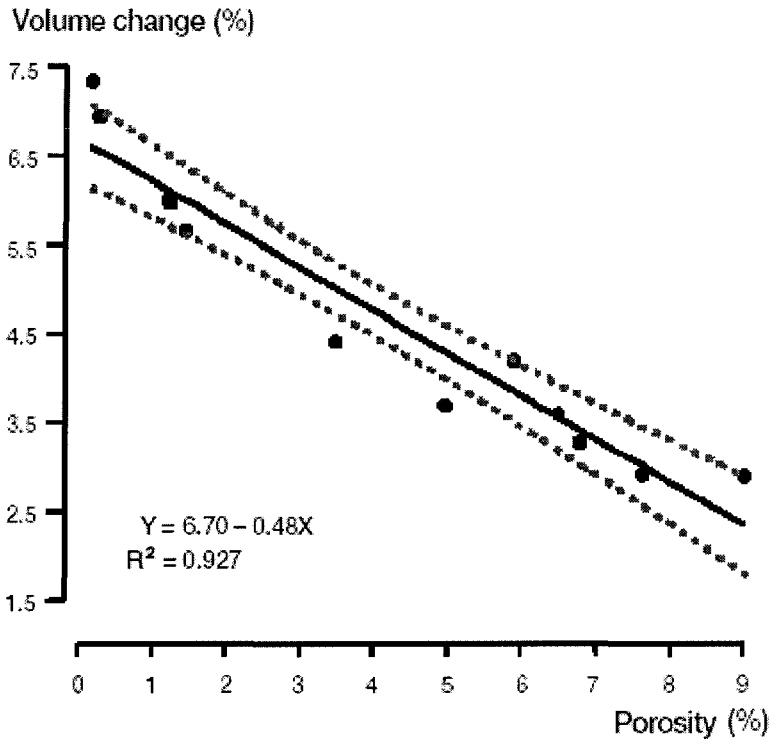

Figure 2.55: Plot of shrinkage as a function of porosity (Muller *et al.* 2002).

Porosity generates a level of variability in the mechanical properties of bone cement, which is especially apparent in fatigue tests (Section 2.3.2, page 67). To reduce this variability and determine the mechanical properties of the bulk material itself, a number of fatigue studies have rejected specimens with any macro pores (diameter >1mm) visible radiographically (Cristofolini *et al.*, 2000; Healey *et al.*, 2002; Lewis, 1999). This practice has been criticised by Prendergast *et al.* (2002), who feel specimen rejection leads to "the true variability of the fatigue study (being) missed".

A similar argument could be put to finite element based studies that neglect porosity distributions. Modelling the cement mantle as a homogeneous material free from flaws and voids will generate deterministic results. For example, the finite element simulation of bone cement fatigue by Stolk *et al.* (2004) simulated fatigue in uniaxial tensile specimens and compared the results to experimental data. The finite element

models were free from pores, flaws and voids, and therefore generated only *one* value of fatigue life at both stress levels considered, i.e. deterministic results. Porosity in finite element models has been simulated by Harrigan *et al.* (1992), Harrigan and Harris (1991) and Lennon *et al.* (2003), using the theoretical elasticity solution for a spherical pore in an infinite medium under remote stress. This theory was developed by Timoshenko and Goodier (1970), and shows that the stresses at the surface of a pore (under the conditions described above) do not depend on pore size. Simulating pores in this manner has the limitation that the pore is much smaller than the region in which it is found. However, even if a pore of diameter d was located a distance $3d$ from an interface or another pore, the errors caused by this assumption are small, less than ~10% (Timoshenko and Goodier, 1970). Under a uniaxial stress, the stress concentration caused by a pore (σ_{max}) is defined as:

$$\sigma_{max} = \left(\frac{27 - 15\nu}{2(7 - 5\nu)} \right) S \qquad \textbf{Equation 2.14}$$

where S is the maximum principal stress in a uniaxial stress field (applied stress) and ν the Poisson's ratio. This can be expanded to include a multi-axial stress state:

$$\sigma_{max} = Max \begin{bmatrix} \sigma_{1max} = Max \begin{bmatrix} B\sigma_1 + A\sigma_2 + C\sigma_3 \\ B\sigma_1 + C\sigma_2 + A\sigma_3 \end{bmatrix} \\ \sigma_{2max} = Max \begin{bmatrix} A\sigma_1 + B\sigma_2 + C\sigma_3 \\ C\sigma_1 + B\sigma_2 + A\sigma_3 \end{bmatrix} \\ \sigma_{3max} = Max \begin{bmatrix} A\sigma_1 + C\sigma_2 + B\sigma_3 \\ C\sigma_1 + A\sigma_2 + B\sigma_3 \end{bmatrix} \end{bmatrix} \qquad \textbf{Equation 2.15}$$

where σ_1, σ_2 and σ_3 are the principal stresses and A, B and C are defined as:

$$A = \frac{-(3 + 15\nu)}{2(7 - 5\nu)};\ B = \frac{27 - 15\nu}{2(7 - 5\nu)};\ C = \frac{15 - 3\nu}{2(7 - 5\nu)} \qquad \textbf{Equation 2.16}$$

Porosity was simulated in the finite element studies by Harrigan *et al.* (1992), Harrigan and Harris (1991) and Lennon *et al.* (2003) using Equations 2.15 & 2.16, but

the results generated were still deterministic. A pore was simulated at either every integration point Harrigan *et al.* (1992), Harrigan and Harris (1991), or the centroid of every element Lennon *et al.* (2003). The nature of a porosity *distribution* was therefore not considered. It may be useful to use mathematical methods to simulate a random distribution of pores in finite element bone cement studies. This would allow stochastic (rather than deterministic) results to be generated that would better reflect *in vitro* tests.

2.3.6 *Bone cement and industrial PMMA*

It is reasonable to suggest that similarities could exist between the properties of bone cement and commercial grade PMMA. This may be advantageous to the biomechanist, as the properties of commercial PMMA have been well studied. Industrial manufacture of PMMA is by free radical polymerisation of MMA, the same process as for bone cement. However, the process is performed in a controlled environment, including high temperatures (140-150°C) and pressures ($2x10^7$Pa). The resulting material does not contain any residual monomer, and is void and pore free. There is no radiopaque agent added, and the molecular weight is much higher than that of bone cement (approximately $1x10^6$ g/mol for commercial PMMA and $1.7x10^5$ for bone cement).

A study by Molino and Topoleski (1996) compared fatigue of vacuum mixed (radiopaque) Simplex P bone cement to Plexiglas (a brand of commercial PMMA). Notched specimens were loaded in uniaxial tension at 5Hz, with a maximum and minimum load of 170N and 10N respectively (at 37°C). A crack gauge measured the length of the crack from the notch tip. The crack growth rate was plotted against the stress intensity factor on a logarithmic scale and regression lines fitted to the data. Correlation coefficients of 0.994 and 0.869 were reported for the Plexiglas and cement regression lines respectively. At every value of stress intensity factor, the crack growth rate of the cement was approximately one order of magnitude less than that of Plexiglas. A fractographic analysis identified apparent fatigue striations on all fracture surfaces, but the fracture surface of Plexiglas was much smoother than that of the cement.

A similar study was performed by Beaumont and Young (1975), with comparable results. The crack growth rate in hand mixed Simplex P was compared to that in Perspex. Time to failure was calculated for specimens subject to a stress level of 2.7MPa in air at 20°C, and was three orders of magnitude greater for Simplex P. Fracture surfaces were observed under scanning electron microscope, and a much smoother fracture surface for Perspex was observed. The authors concluded that the bone cement fatigue crack grew primarily in the weaker interbead matrix, and the

presence of pre-polymerised PMMA beads effectively toughened the bone cement by deviating the propagating crack.

In these studies, evidence of discontinuous crack growth was observed on the fracture surfaces of both bone cement and industrial PMMA. This has also been reported in other bone cement fatigue studies (see Section 2.3.2, page 67). According to Skibo *et al.* (1977), the discontinuous crack growth patterns observed in industrial PMMA are not fatigue striations; as (for polymers) striations refer to the crack growth in one loading cycle. Instead, the accumulation of damage ahead of the fatigue crack over many cycles causes the crack to jump suddenly (see Figure 2.56). The surface morphology of this crack jumping would resemble fatigue striations, but with a greater spacing between successive peaks. Suresh (1998) described the following possible mechanism for crack growth. During cyclic loading, the crack tip is stationary, but damage is accumulating in the craze zone. When the craze zone opens by a critical amount, crack growth occurs in one spurt (Figure 2.56). The crack propagates initially along the craze/matrix interface and subsequently along the fibril midrib until crack arrest (Figure 2.57). This process repeats itself causing dark bands of discontinuous crack growth to appear on the fracture surface. This proposed fatigue crack propagation model relates to industrial PMMA, but there is evidence that this mode of crack propagation also occurs in cement – Roques *et al.* (2004a) monitored fatigue test specimens with the acoustic emission technique, and found that bursts of fatigue crack growth occurred separated by periods of apparent inactivity.

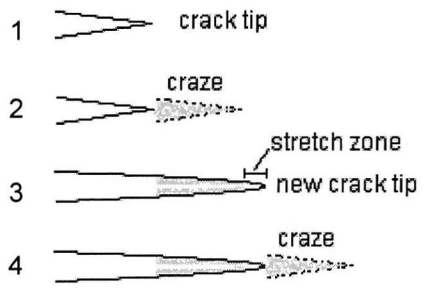

Figure 2.56: A schematic representation of discontinuous crack growth. The crack jumps between stages 2 and 3. From Suresh (1998), reproduced with permission from Cambridge University Press.

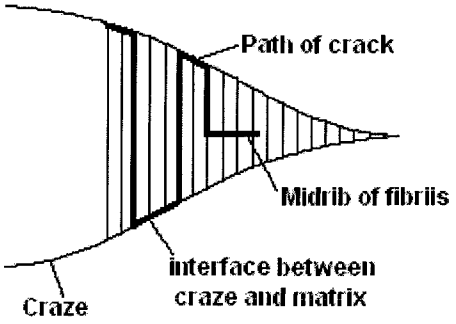

Figure 2.57: An idealisation of the path of a fatigue crack within the craze zone. From Suresh (1998), reproduced with permission from Cambridge University Press.

2.4 Literature summary and aims of thesis

Can initial conditions (i.e. without considering fatigue loading, cement viscoelasticity or cement cracking) predict the performance of the hip replacement over its working life? If so, complex *in vitro* and *in silico* fatigue simulations described in Sections 2.2.5 (page 51) and 2.2.6 (page 58) would become obsolete. The literature review has discussed factors that influence the stress distribution in the implanted femur over time, for example cement fatigue (Section 2.3.2, page 67) and creep (Section 2.3.3, page 83). These cannot be predicted by assessing the initial conditions in isolation. For example, Boneloc cement has a Young's modulus similar to CMW-1 (2.26GPa versus 2.96GPa). Initial stresses in the implanted femur with these cements would therefore be similar, and one could predict that the performance over the working life of the reconstruction would also be similar. However this would not be the case – the inferior performance of Boneloc has been mentioned several times already (Section 2.3.2, page 67; Section 2.3.3, page 83). Only by considering the performance of the cement as a function of time (for example through creep and fatigue testing) does the inferior performance of Boneloc become apparent.

A predominant cause of prosthesis loosening is fatigue cracking of the cement mantle (Section 2.2.1, page 30). Considering this, *in silico* simulations of cement mantle cracking may be a useful tool for the design and preclinical testing of prostheses and bone cements. The first such study was performed by Verdonschot (1995) and developed to include cement creep by Stolk (2003). Although these studies had limitations, their capability to differentiate between superior and inferior prostheses designs was demonstrated by Stolk (2003) (Section 2.2.6, page 58). However, the results generated were deterministic, and did not include the effects of cement porosity and pre-load cracking caused by residual stress. These two factors have been identified as having a critical role in cement mantle cracking (Section 2.2.5, page 51).

The fatigue algorithm described by Stolk (2003) used S-N data for vacuum mixed Cemex RX and creep data for hand mixed Simplex P bone cements, but the fatigue and creep properties have been shown to depend on both cement brand and mixing conditions (Section 2.3.2, page 67; Section 2.3.3, page 83). The first aim of this thesis is to gather creep and S-N data simultaneously for a single brand of bone cement

(vacuum mixed CMW-1). This data can then be implemented in a damage simulation based on the methods of Verdonschot (1995) and Stolk (2003). The acoustic emission non-destructive evaluation technique will be employed in this series of fatigue/creep tests.

The second aim of the thesis is to develop the *in silico* simulation of bone cement fatigue by including the influence of cement pore distributions. This will firstly be attempted by simulating uniaxial tensile and 4-point bend fatigue tests and comparing the stochastic (due to the pore distributions) results with those of experimental testing. Subsequently, the *in silico* analysis will be applied to a quasi-3D model of the implanted femur (similar to the model of Lennon *et al.* (1998), Figure 2.26, page 57), and predicted fatigue results compared to experimental tests. Finally the computational process will be applied to an implanted femur model, and the influence of various cement parameters (porosity, creep, initial stress) investigated. In addition, the fatigue failure of the cement mantle can be compared to clinically observed failure modes. For the implanted femur construct, the boundary conditions are applied as described by Bergmann (2001), discussed in detail in Section 2.1.2 (page 18) and 2.1.3 (page 22).

2.5 References

Abdel-Kader, K.F.M., Allcock, S., Walker, D.I. and Chaudhry, S.B., 2001. Boneloc bone-cement - experience in hip arthroplasty during a 3-year period. Journal of Arthroplasty, 16(7): 811-819.

Akkus, O., 2002. Comments on acoustic emission visualization of bone cement fatigue locations. Journal of Biomedical Materials Research, 59(2): 398-399.

Anthony, P.P., Gie, G.A., Howie, C.R. and Ling, R.S.M., 1990. Localised endosteal bone lysis in relation to the femoral components of cemented total hip arthroplasties. Journal of Bone and Joint Surgery-British Volume, 72(6): 971-979.

Athanasou, N.A., Quinn, J. and Bulstrode, C.J.K., 1992. Resorption of bone by inflammatory cells derived from the joint capsule of hip arthroplasties. Journal of Bone and Joint Surgery-British Volume, 74(1): 57-62.

Beaumont, P.W.R. and Young, R.J., 1975. Failure of brittle polymers by slow crack growth. Part 1: Crack propagation in polymethylmethacrylate and time-to-failure predictions. Journal of Materials Science, 10: 1334-1342.

Bergmann, G., Graichen, F. and Rohlmann, A., 1993. Hip joint loading during walking and running measured in two patients. Journal of Biomechanics, 28(8): 969-990.

Bergmann, G., Graichen, F. and Rohlmann, A., 1995. Is staircase walking a risk for the fixation of hip implants? Journal of Biomechanics, 28(5): 535-553.

Bergmann, G., Deuretzbacher, G., Heller, M., Graichen, F., Rohlmann, A., Strauss, J. and Duda, G.N., 2001. Hip contact forces and gait patterns from routine activities. Journal of Biomechanics, 34(7): 859-871.

Bergmann, G.E., 2001. Hip98, loading of the hip joint. Published as a CD-ROM attachment to the Journal of Biomechanics: ISBN 3-9807848-0-0.

Berthoud, P., Baumberger, T., G'Sell, C. and Hiver, J.M., 1999. Physical analysis of the state and rate dependant friction law: static friction. Physical Review B, 59(22): 14313-14327.

Berthoud, P., G'Sell, C. and Hiver, J.M., 1999. Elastic-plastic indentation creep of glassy poly(methyl methacrylate) and polystyrene: characterisation using uniaxial compression and indentation tests. Journal of Physics D: Applied Physics, 32: 2923-2932.

Bhambri, S.K. and Gilbertson, L.N., 1995. Micromechanisms of fatigue-crack initiation and propagation in bone cements. Journal of Biomedical Materials Research, 29(2): 233-237.

Brand, R.A., Pedersen, D.R., Davy, D.T., Kotzar, G.M., Heiple, K.G. and Goldberg, V.M., 1994. Comparison of hip force calculations and measurements in the same patient. Journal of Arthroplasty, 9(1): 45-51.

Britton, J.R., Walsh, L.A. and Prendergast, P.J., 2003. Mechanical simulation of muscle loading on the proximal femur: Analysis of cemented femoral component migration with and without muscle loading. Clinical Biomechanics, 18: 637-646.

Browne, M., Roques, A. and Taylor, A., 2005. The acoustic emission technique in orthopedics - a review. Journal of Strain Analysis for Engineering Design, 40(1): 59-79.

Chang, P.B., Mann, K.A. and Bartel, D.L., 1998. Cemented femoral stem performance - effects of proximal bonding, geometry, and neck length. Clinical Orthopaedics and Related Research, 355: 57-69.

Chwirut, J., 1984. Long term compressive creep deformation and damage in acrylic bone cements. Journal of Biomedical Material Research, 18: 25-37.

Cristofolini, L., Viceconti, M., Toni, A. and Giunti, A., 1995. Influence of thigh muscles on the axial strains in a proximal femur during early stance in gait. Journal of Biomechanics, 28(5): 617-624.

Cristofolini, L., Minari, C. and Viceconti, M., 2000. A methodology and criterion for acrylic bone cement fatigue tests. Fatigue & Fracture of Engineering Materials & Structures, 23(11): 953-957.

Crowninshield, R.D., Johnston, R.C., Andrews, J.G. and Brand, R.A., 1978. A biomechanical investigation of the human hip. Journal of Biomechanics, 11: 75-78.

Crowninshield, R.D. and Brand, R.A., 1981. A physiologically based criterion of muscle force prediction in locomotion. Journal of Biomechanics, 14(11): 793-801.

Crowninshield, R.D. and Tolbert, J.R., 1983. Cement strain-measurement surrounding loose and well-fixed femoral component stems. Journal of Biomedical Materials Research, 17(5): 819-828.

Davies, J.P., Burke, D.W., O'Connor, D.O. and Harris, W.H., 1987. Comparison of the fatigue characteristics of centrifuged and uncentrifuged Simplex P bone cement. Journal of Orthopaedic Research, 5(3): 366-371.

Davy, D.T., Kotzar, G.M., Brown, R.H., Heiple, K.G.S., Goldberg, V.M., Heiple, K.G.J., Berilla, J. and Beurstein, A.H., 1988. Telemetric force measurements across the hip after total arthroplasty. Journal of Bone and Joint Surgery-American Volume, 70: 45-50.

Dooling, P.J. and Buckley, C.P., 1988. The onset of nonlinear viscoelasticity in multiaxial creep of glassy polymers: a constitutive model and its application to PMMA. Polymer Engineering and Science, 38(6): 892-904.

Duda, G.N., Heller, M., Albinger, J., Schulz, O., Schneider, E. and Claes, L., 1998. Influence of muscle forces on femoral strain distribution. Journal of Biomechanics, 31(9): 841-846.

Dunne, N.J. and Orr, J.F., 2001. Influence of mixing techniques on the physical properties of acrylic bone cement. Biomaterials, 22(13): 1819-1826.

Dunne, N.J., Orr, J.F., Mushipe, M. and Eveleigh, R., 2003. The relationship between porosity and fatigue characteristics of bone cements. Biomaterials, 24: 239-245.

Fender, D., Harper, W.M. and Gregg, P.J., 1999. Outcome of Charnley total hip replacement across a single health region in England - the results at five years from a regional hip register. Journal of Bone and Joint Surgery-British Volume, 81(4): 577-581.

Fisher, D.A., Tsang, A.C., Paydar, N., Milionis, S. and Turner, C.H., 1997. Cement-mantle thickness affects cement strains in total hip replacement. Journal of Biomechanics, 30(11/12): 1173-1177.

Gilbert, J.L., Hasenwinkel, J.M., Wixson, R.L. and Lautenschlager, E.P., 2000. A theoretical and experimental analysis of polymerisation shrinkage of bone cement: A potential major source of porosity. Journal of Biomedical Materials Research, 52(1): 210-218.

Glitsch, U. and Baumann, W., 1997. The three-dimensional determination of internal loads in the lower extremity. Journal of Biomechanics, 30(11-12): 1123-1131.

Gough, J.E. and Downes, S., 2001. Osteoblast cell death on methacrylate polymers involves apoptosis. Journal of Biomedical Materials Research, 57(4): 497-505.

Graham, J., Pruitt, L., Ries, M. and Gundiah, N., 2000. Fracture and fatigue properties of acrylic bone cement - the effects of mixing method, sterilization treatment, and molecular weight. Journal of Arthroplasty, 15(8): 1028-1035.

Gruen, T.A., McNeice, G.M. and Amstutz, H.C., 1979. Modes of failure of cemented stem-type femoral components. Clinical Orthopaedics & Related Research, 141: 17-27.

Hansen, D. and Jensen, J.S., 1992. Mixing does not improve mechanical properties of all bone cements. Acta Orthopaedica Scandinavica, 63: 13-18.

Harper, E.J. and Bonfield, W., 2000. Tensile characteristics of ten commercial acrylic bone cements. Journal of Biomedical Materials Research, 53(5): 605-616.

Harrigan, T.P. and Harris, W.H., 1991. A three-dimensional non-linear finite element study of the effect of cement-prosthesis debonding in cemented femoral total hip components. Journal of Biomechanics, 24(11): 1047-1058.

Harrigan, T.P., Kareh, J.A., O'Connor, D.O., Burke, D.W. and Harris, W.H., 1992. A finite-element study of the initiation of failure of fixation in cemented femoral total hip components. Journal of Orthopaedic Research, 10(1): 134-144.

Harris, W.H., McCarthy, J.C. and O'Neill, D.A., 1982. Femoral component loosening using contemporary techniques of femoral cement fixation. Journal of Bone and Joint Surgery-American Volume, 64(7): 1063-1067.

Havelin, L. and Espehaug, B., 1995. The effect of the type of cement in early revision of Charnley total hip prostheses. Journal of Bone and Joint Surgery-American Volume, 77(10): 1543-1550.

Havelin, L.I., Engesaeter, L.B., Espehaug, B., Furnes, O., Lie, S.A. and Vollset, S.E., 2000. The Norwegian arthroplasty register - 11 years and 73,000 arthroplasties. Acta Orthopaedica Scandinavica, 71(4): 337-353.

Haydon, C.M., Mehin, R., Burnett, S., Rorabeck, C.H., Bourne, R.B., McCalden, R.W. and MacDonald, S.J., 2004. Revision total hip arthroplasty with use of a cemented femoral component - results at a mean of ten years. Journal of Bone and Joint Surgery-American Volume, 86(6): 1179-1185.

Healey, R., Perona, P., Dimaio, F. and Coutts, R., 2002. Porosity and fatigue properties of emerging bone cements. In Transactions of the 48th annual meeting of the Orthopaedic Research Society, Dallas, Texas.

Heller, M.O., Bergmann, G., Deuretzbacher, G., Durselen, L., Pohl, M., Claes, L., Haas, N.P. and Duda, G.N., 2001. Musculo-skeletal loading conditions at the hip during walking and stair climbing. Journal of Biomechanics, 34(7): 883-893.

Herberts, P. and Malchau, H., 2000. Prognosis of total hip replacement, Goteborg University, http://www.jru.orthop.gu.se.

Herberts, P., Malchau, H., Garellick, G., Soderman, P. and Eisler, T., 2002. Prognosis of total hip replacement, Goteborg Universityhttp://www.jru.orthop.gu.se.

Huiskes, R., 1988. Migration, stem shape and surface finish in cemented total hip arthroplasty. Clinical Orthopaedics & Related Research, 355: 103-112.

Huiskes, R., 1993. Failed innovation in total hip replacement - diagnosis and proposals for a cure. Acta Orthopaedica Scandinavica, 64(6): 699-716.

Inman, V.T., Rolston, H.J. and Todd, F., 1981. Human walking. Williams & Wilkins.

James, S.P., Jasty, M., Davies, J., Piehler, H. and Harris, W.H., 1992. A fractographic investigation of PMMA bone-cement focusing on the relationship between porosity reduction and increased fatigue life. Journal of Biomedical Materials Research, 26(5): 651-662.

Jasty, M., Davies, J.P., O'Connor, D.O., Burke, D.W., Harrigan, T.P. and Harris, W.H., 1990. Porosity of various preparations of acrylic bone cements. Clinical Orthopaedics and Related Research(259): 122-129.

Jasty, M., Maloney, W.J., Bragdon, C.R., O'Connor, D.O., Haire, T. and Harris, W.H., 1991. The initiation of failure in cemented femoral components of hip arthroplasties. Journal of Bone and Joint Surgery-British Volume, 73(4): 551-558.

Karachalios, T., Tsatsaronis, C., Efraimis, G., Papadelis, P., Lyritis, G. and Diakoumopoulos, G., 2004. The long-term clinical relevance of calcar atrophy caused by stress shielding in total hip arthroplasty - a 10-year, prospective, randomised study. Journal of Arthroplasty, 19(4): 469-475.

Kohn, D., 1995. Acoustic emission and nondestructive evaluation of biomaterials and tissues. Critical reviews in Biomedical Engineering, 22(3/4): 221-306.

Krause, W. and Mathis, R.S., 1988. Fatigue properties of acrylic bone cements - review of the literature. Journal of Biomedical Materials Research-Applied Biomaterials, 22(1): 37-53.

Lee, A.J.C., Ling, R.S.M., Gheduzzi, S., Simon, J.P. and Renfro, R.J., 2002. Factors affecting the mechanical and viscoelastic properties of acrylic bone cement. Journal of Materials Science-Materials in Medicine, 13(8): 723-733.

Lengsfeld, M., Kaminsky, J., Merz, B. and Franke, R.P., 1996. Sensitivity of femoral strain pattern analyses to resultant and muscle forces at the hip joint. Medical Engineering & Physics, 18(1): 70-78.

Lennon, A.B., McCormack, B.A.O. and Prendergast, P.J., 1998. Development of a physical model of a cemented hip replacement for investigation of cement damage accumulation. In: Proceedings of the 12th Conference of the European Society of Biomechanics, Dublin, Ireland.

Lennon, A.B., Prendergast, P.J., Whelan, M.P., Kenny, R.P. and Cavalli, C., 2000. Modelling of temperature history and residual stress generation due to curing in polymethylmethacrylate. In: Proceedings of the 12th Conference of the European Society of Biomechanics, Dublin, Ireland.

Lennon, A.B. and Prendergast, P.J., 2001. Evaluation of cement stresses in finite element analyses of cemented orthopaedic implants. Journal of Biomechanical Engineering, 123: 623-628.

Lennon, A.B. and Prendergast, P.J., 2002. Residual stress due to curing can initiate damage in porous bone cement: Experimental and theoretical evidence. Journal of Biomechanics, 35(3): 311-321.

Lennon, A.B., McCormack, B.A.O. and Prendergast, P.J., 2003. The relationship between cement fatigue damage and implant surface finish in proximal femoral prostheses. Medical Engineering & Physics, 25: 833-841.

Lewis, G., 1997. Properties of acrylic bone cement: State of the art review. Journal of Biomedical Materials Research, 38(2): 155-182.

Lewis, G., 1999. Effect of mixing method and storage temperature of cement constituents on the fatigue and porosity of acrylic bone cement. Journal of Biomedical Materials Research Part B-Applied Biomaterials, 48: 143-149.

Lewis, G., 2003. Fatigue testing and performance of acrylic bone-cement materials: State-of-the-art review. Journal of Biomedical Materials Research Part B-Applied Biomaterials, 66: 457-486.

Li, C., Wang, Y. and Mason, J., 2003. The effects of curing history on residual stress in bone cement during hip arthroplasty. Journal of Biomedical Material Research Part B-Applied Biomaterials, 70: 30-36.

Linden, U., 1991. Mechanical-properties of bone-cement - importance of the mixing technique. Clinical Orthopaedics and Related Research, 272: 274-278.

Lu, T.W., Taylor, S.J.G., O'Connor, J.J. and Walker, P.S., 1997. Influence of muscle activity on the forces in the femur: An *in vivo* study. Journal of Biomechanics, 30(11-12): 1101-1106.

Lu, Z. and McKellop, H., 1997. Effects of cement creep on stem subsidence and stresses in the cement mantle of a total hip replacement. Journal of Biomedical Materials Research, 34(2): 221-226.

Lucht, U., 2000. The Danish hip arthroplasty register. Acta Orthopaedica Scandinavica, 71(5): 433-439.

Maher, S.A. and Prendergast, P.J., 2002. Discriminating the loosening behavior of cemented hip prostheses using measurements of migration and inducible displacement. Journal of Biomechanics, 35: 257-265.

Malchau, H., Herberts, P., Garellick, G., Soderman, P. and Eisler, T., 2002. Prognosis of total hip replacement: Update of results and risk-ratio analysis for revision and re-revision from the Swedish national hip arthroplasty register 1979-2000. Goteborg University, Sweden. Presented at the 69th annual meeting of the AAOS, February 2002, Dallas, USA. Available from www.jru.orthop.gu.se.

Mann, K.A., Bartel, D.L., Wright, T.M. and Ingraffea, A.R., 1991. Mechanical characteristics of the stem-cement interface. Journal of Orthopaedic Research, 9(6): 798-808.

Mann, K.A., Bartel, D.L., Wright, T.M. and Burstein, A.H., 1995. Coulomb frictional interfaces in modelling cemented total hip replacements - a more realistic model. Journal of Biomechanics, 28(9): 1067-1078.

Mann, K.A., Ayers, D.C. and Damron, T.A., 1997a. Effects of stem length on mechanics of the femoral hip component after cemented revision. Journal of Orthopaedic Research, 15(1): 62-68.

Mann, K.A., Bartel, D.L. and Ayers, D.C., 1997b. Influence of stem geometry on mechanics of cemented femoral hip components with a proximal bond. Journal of Orthopaedic Research, 15(5): 700-706.

Mann, K.A., Gupta, S., Race, A., Miller, M.A., Cleary, R.J. and Ayers, D.C., 2004. Cement microcracks in thin-mantle regions after *in vitro* fatigue loading. Journal of Arthroplasty, 19(5): 605-612.

Martini, F.H. and Bartholomew, E.F., 2000. Essentials of Anatomy and Physiology. Prentice-Hall Inc.

McCormack, B.A.O. and Prendergast, P.J., 1999. Microdamage accumulation in the cement layer of hip replacements under flexural loading. Journal of Biomechanics, 32(5): 467-475.

McCormack, B.A.O., Prendergast, P.J. and O'Dwyer, B., 1999. Fatigue of cemented hip replacements under torsional loads. Fatigue & Fracture of Engineering Materials & Structures, 22(1): 33-40.

Molino, L.N. and Topoleski, L.D.T., 1996. Effect of $baso_4$ on the fatigue crack propagation rate of PMMA bone cement. Journal of Biomedical Material Research, 31(1): 131-137.

Muller, S.D., Green, S.M. and McCaskie, A.W., 2002. The dynamic volume changes of polymerising polymethylmethacrylate bone cement. Acta Orthopaedica Scandinavica, 73(6): 684-687.

Murphy, B.P. and Prendergast, P.J., 2000. On the magnitude and variability of the fatigue strength of acrylic bone cement. International Journal of Fatigue, 22: 855-864.

Murphy, B.P. and Prendergast, P.J., 2001. The relationship between stress, porosity and nonlinear damage accumulation in acrylic bone cement. Journal of Biomedical Materials Research, 59: 646-654.

Murphy, B.P. and Prendergast, P.J., 2003. Multi-axial fatigue failure of orthopaedic bone cement - experiments with tubular specimens. Journal of Materials Science-Materials in Medicine, 14(10): 857-861.

Norman, T.L., Kish, V., Blaha, J.D., Gruen, T.A. and Hustosky, K., 1995. Creep characteristics of hand-mixed and vacuum-mixed acrylic bone-cement at elevated stress levels. Journal of Biomedical Materials Research, 29(4): 495-501.

Norman, T.L., Thyagarajan, G., Saligrama, V.C., Gruen, T.A. and Blaha, J.D., 2001. Stem surface roughness alters creep induced subsidence and 'taper-lock' in a cemented femoral hip prosthesis. Journal of Biomechanics, 34(10): 1325-1333.

Nuno, N. and Cristofolini, L., 2001. Sensitivity analysis on the uncertainties of metal-PMMA interface characteristics. In: Proceedings of the 3rd International symposium on computer methods in biomechanics and biomedical engineering, Barcelona, Spain.

Nzihou, A., Sharrock, P. and Ricard, A., 1999. Reaction kinetics and heat transfer studies in thermoset resins. Chemical Engineering Journal, 72(1): 53-61.

O'Connor, D.O., Burke, D.W., Jasty, M., Sedlacek, R.C. and Harris, W.H., 1996. *In vitro* measurement of strain in the bone cement surrounding the femoral component of total hip replacements during simulated gait and stair-climbing. Journal of Orthopaedic Research, 14(5): 769-777.

Orr, J.F., Dunne, N.J. and Quinn, J.C., 2003. Shrinkage stresses in bone cement. Biomaterials, 24: 2933-2940.

Paterson, M., Fulford, P. and Denham, R., 1986. Loosening of the femoral component after total hip replacement. Journal of Bone and Joint Surgery-British Volume, 68(3): 392-397.

Patriarco, A.G., Mann, R.W., Simon, S.R. and Mansour, J.M., 1981. An evaluation of the approaches of optimisation models in the prediction of muscle forces during human gait. Journal of Biomechanics, 14: 513-525.

Pauwels, F., 1980. Biomechanics of the locomotor apparatus: Contributions on the functional anatomy of the locomotor apparatus. Springer-Verlag.

Pedersen, D.R., Brand, R.A. and Davy, D.T., 1997. Pelvic muscle and acetabular contact forces during gait. Journal of Biomechanics, 30(9): 959-965.

Prendergast, P.J., Monaghan, J. and Taylor, D., 1989. Material selection in the artificial hip joint using finite element stress analysis. Clinical Materials, 4: 361-376.

Prendergast, P.J., Murphy, B.P. and Taylor, D., 2002. Discarding specimens for fatigue testing of orthopaedic bone cement: A comment on Cristofolini *et al.* (2000). Fatigue & Fracture of Engineering Materials & Structures, 25(3): 315-316.

Pujol, J. and Qi, G., 2002. Comments on acoustic emission visualization of bone cement fatigue locations - reply. Journal of Biomedical Materials Research, 59(2): 399-401.

Puolakka, T.J.S., Pajamaki, K.J.J., Halonen, P.J., Pulkkinen, P.O., Paavolainen, P. and Nevalainen, J.K., 2001. The Finnish arthroplasty register - report of the hip register. Acta Orthopaedica Scandinavica, 72(5): 433-441.

Qi, G., Pujol, J. and Fan, Z.F., 2000. 3-D AE visualization of bone-cement fatigue locations. Journal of Biomedical Materials Research, 52(2): 256-260.

Reading, A.D., McCaskie, A.W. and Gregg, P.J., 1999. The inadequacy of standard radiographs in detecting flaws in the cement mantle. Journal of Bone and Joint Surgery-British Volume, 81(1): 167-170.

Reilley, D.T., Burstein, A.H. and Frankel, V.H., 1974. The elastic modulus for bone. Journal of Biomechanics, 7: 271-275.

Roques, A., 2004. Novel approaches to the structural integrity assessment of acrylic bone cement as part of the bone/cement/stem construct. PhD Thesis, University of Southampton, United Kingdom.

Roques, A., Browne, M., Thompson, J., Rowland, C. and Taylor, A., 2004a. Investigation of fatigue crack growth in acrylic bone cement using the acoustic emission technique. Biomaterials, 25(5): 769-778.

Roques, A., Browne, M., Taylor, A., New, A. and Baker, D., 2004b. Quantitative measurement of the stresses induced during polymerisation of bone cement. Biomaterials, 25(18): 4415-4424.

Saha, S. and Pal, S., 1984. Mechanical properties of bone cement - a review. Journal of Biomedical Material Research, 18(4): 435-462.

Schmalzreid, T.P., Jasty, M. and Harris, W.H., 1992. Periprosthetic bone loss in total hip arthroplasty. Journal of Bone and Joint Surgery-American Volume, 74(6): 849-863.

Simoes, J.A., Vaz, M.A., Blatcher, S. and Taylor, M., 2000. Influence of head constraint and muscle forces on the strain distribution within the intact femur. Medical Engineering & Physics, 22(7): 453-459.

Skibo, M.D., Hertzberg, R.W., Manson, J.A. and Kim, S., 1977. On the generality of discontinous fatigue crack growth in glassy polymers. Journal of Materials Science, 12: 531-542.

Stauffer, R.N., 1982. Ten-year follow up study of total hip replacement. Journal of Bone and Joint Surgery-American Volume, 64(7): 983-990.

Stolk, J., Verdonschot, N. and Huiskes, R., 2001. Hip-joint and abductor-muscle forces adequately represent *in vivo* loading of a cemented total hip reconstruction. Journal of Biomechanics, 34(7): 917-926.

Stolk, J., Verdonschot, N. and Huiskes, R., 2002. Stair climbing is more detrimental to the cement in hip replacement than walking. Clinical Orthopaedics and Related Research(405): 294-305.

Stolk, J., 2003. A computerized pre-clinical test for cemented hip prostheses based on finite element techniques. PhD thesis, University of Nijmegen, the Netherlands.

Stolk, J., Maher, S.A., Verdonschot, N., Prendergast, P.J. and Huiskes, R., 2003. Can finite element models detect clinically inferior cemented hip implants? Clinical Orthopaedics and Related Research, 409: 138-150.

Stolk, J., Verdonschot, N., Murphy, B.P., Prendergast, P.J. and Huiskes, R., 2004. Finite element simulation of anisotropic damage accumulation and creep in acrylic bone cement. Engineering Fracture Mechanics, 71(4-6): 513-528.

Sugiyama, H., Whiteside, L.A. and Kaiser, A.D., 1989. Examination of Rotational Fixation of the Femoral Component in Total Hip-Arthroplasty - a Mechanical Study of Micromovement and Acoustic-Emission. Clinical Orthopaedics and Related Research(249): 122-128.

Suresh, S., 1998. Fatigue of materials. Cambridge University Press.

Taylor, M.E., Tanner, K.E., Freeman, M.A.R. and Yettram, A.L., 1996. Stress and strain distribution within the intact femur: Compression or bending. Medical Engineering & Physics, 18(2): 122-131.

Taylor, S.J.G., Perry, J.S., Meswania, J.M., Donaldson, N., Walker, P.S. and Cannon, S.R., 1997. Telemetry of forces from proximal femoral replacements and relevance to fixation. Journal of Biomechanics, 30(3): 225-234.

Timoshenko, S.P. and Goodier, J.N., 1970. Theory of elasticity, 3rd edition. McGraw-Hill.

Topoleski, L.D.T., Ducheyne, P. and Cuckler, J.M., 1990. A fractographic analysis of *in vivo* poly(methylmethacrylate) bone-cement failure mechanisms. Journal of Biomedical Materials Research, 24(2): 135-154.

Topoleski, L.D.T., Ducheyne, P. and Cuckler, J.M., 1993. Microstructural pathway of fracture in poly(methylmethacrylate) bone-cement. Biomaterials, 14(15): 1165-1172.

Verdonschot, N. and Huiskes, R., 1994. Creep-behaviour of hand-mixed simplex-p bone-cement under cyclic tensile loading. Journal of Applied Biomaterials, 5(3): 235-243.

Verdonschot, N., 1995. Biomechanical failure scenarios for cemented total hip replacement. PhD Thesis, University of Nijmegen, the Netherlands.

Verdonschot, N. and Huiskes, R., 1995. Dynamic creep-behaviour of acrylic bone-cement. Journal of Biomedical Materials Research, 29(5): 575-581.

Verdonschot, N. and Huiskes, R., 1996. Subsidence of THA stems due to acrylic cement creep is extremely sensitive to interface friction. Journal of Biomechanics, 29(12): 1569-1575.

Verdonschot, N. and Huiskes, R., 1997a. The effects of cement-stem debonding in tha on the long-term failure probability of cement. Journal of Biomechanics, 30(8): 795-802.

Verdonschot, N. and Huiskes, R., 1997b. Acrylic cement creeps but does not allow much subsidence of femoral stems. Journal of Bone and Joint Surgery-British Volume, 79(4): 665-9.

Verdonschot, N. and Huiskes, R., 1998. Surface roughness of debonded straight-tapered stems in cemented THA reduces subsidence but not cement damage. Biomaterials, 19(19): 1773-1779.

Verdonschot, N. and Huiskes, R., 2000. Creep properties of three low temperature-curing bone cements: A preclinical assessment. Journal of Biomedical Materials Research, 53(5): 498-504.

Walczak, J.P., D'Arcy, J.C., Ross, K.R., James, S.E., Bonnici, A.V., Koka, S.R. and Morris, R.W., 2000. Low-friction arthroplasty with Boneloc bone-cement - outcome at 2 to 4 years. Journal of Arthroplasty, 15(2): 205-209.

Wheeler, J.P.G., Miles, A.W. and Clift, S.E., 1997. The influence of the stem-cement interface in total hip replacement -a comparison of experimental and finite element approaches. Proceedings of the Institution for Mechanical Engineers Part H, 211: 181-186.

Whelan, M.P., Kenny, R.P., Cavalli, C., Lennon, A.B. and Prendergast, P.J., 2000. Application of optical fibre Bragg grating sensors to the study of PMMA curing. In: Proceedings of the 12th Conference of the European Society of Biomechanics, Dublin, Ireland.

Yetkinler, D. and Litsky, A., 1998. Viscoelastic behaviour of acrylic bone cements. Biomaterials, 19: 1551-1559.

CHAPTER 3

DAMAGE ACCUMULATION, FATIGUE AND CREEP OF VACUUM MIXED BONE CEMENT[1]

Damage in the cement mantle of orthopaedic implants can accumulate under *in vivo* loads and eventually form critical defects resulting in implant loosening. The behaviour of bone cement under fatigue loading is therefore of interest to assess the long-term *in vivo* performance. In this study, uniaxial tensile fatigue tests were performed on CMW-1 bone cement. Acoustic emission sensors and an extensometer were attached to monitor damage accumulation and creep respectively. The S-N data exhibited the scatter synonymous with bone cement fatigue, with large pores generally responsible for premature failure. Acoustic emission data revealed a non-linear accumulation of damage with respect to time, with increasing non-linearity at higher stress levels. The damage accumulation process was not continuous, but occurred in bursts separated by periods of inactivity. Damage in the specimen was located by acoustic emissions, and allowed the failure site to be predicted. Acoustic emission data could also be used to predict when failure was not imminent. When this was the case at 3 million load cycles, the tests were terminated. Bone cement creep was plotted against the number of load cycles and a linear relationship was found when a double logarithmic scale was employed. The results can be used to characterise CMW-1 in computational simulations of the damage accumulation process, and further evidence is provided for the condition-monitoring capabilities of the acoustic emission technique in orthopaedic applications.

[1]Accepted for publication in Biomaterials. Presented at the 14th European Society of Biomechanics conference, 's-Hertogenbosch, the Netherlands, 4th – 7th July 2004.

3.1 Introduction

The repetitive loading experienced by a hip replacement during normal activities, for example walking or stair climbing, subjects the cement mantle (which fixes the prosthesis in the bone) to spectrum loading which may lead to fatigue failure. Fatigue failure of the cement mantle has been identified as a possible loosening mechanism for the prosthesis, which in turn can lead to revision surgery (Jasty et al., 1991; Topoleski et al., 1990). Numerous studies have found that the method used to mix the cement influences its fatigue life. For example, Graham et al. (2000), Lewis (1999) and Murphy and Prendergast (2000) all found vacuum-mixed cements have a longer fatigue life compared to hand-mixed cements. In addition, fatigue varies between different cement brands. Harper and Bonfield (2000) found significant differences in fatigue performance for 10 different cement brands.

Bone cement fatigue data are useful, for example, S-N data have been used to compare different brands and mixing methods (Murphy and Prendergast, 2000). Also of interest is the manner of damage accumulation in the cement specimens that leads to fatigue failure. This has been assessed using the dye-penetrant technique (Murphy and Prendergast, 2001), but with the disadvantages that only surface damage was detected and that the test had to be stopped for the specimen to be analysed. An alternative to dye penetrant is the acoustic emission (AE) technique. This has previously been used to monitor bone cement under fatigue loads (Roques et al., 2004a), and has the advantage of being passive, thus allowing the tests to run continuously.

Bone cement is a polymer with a glass transition temperature of about 95°C, and is liable to creep at *in vivo* temperatures (about 37°C). Empirical models for creep have been presented for static and dynamic loading, under uniaxial tension and compression. Chwirut (1984) presented a stress dependent power law relationship between creep strain and time for cement under a static compressive load. Verdonschot and Huiskes (1995) measured creep strain under uniaxial compressive cyclic loading, and presented a stress dependent double logarithmic relationship between creep strain and number of loading cycles. A similar relationship, under uniaxial cyclic tensile loading, was observed by Verdonschot and Huiskes (1994). The empirical creep models presented in these studies were for hand mixed cement, and may not be representative of current mixing methods.

Norman et al. (1995) found that vacuum mixing could reduce creep strains in bone cement compression tests by as much as 48%.

One of the uses to which information on fatigue and creep deformation could be put is for the development of computational simulations of these processes. In the literature, simulations have been performed for cement fatigue only (Verdonschot and Huiskes, 1997), cement creep only (Lu and McKellop, 1997; Norman et al., 2001) and cement fatigue and creep simultaneously (Stolk et al., 2003). All these studies relied on experimental constitutive laws to simulate fatigue and creep, and therefore simulated the behaviour of the cement from which the constitutive laws were generated. Simultaneous fatigue and creep simulation therefore requires the constitutive laws to be generated from the same brand of bone cement, mixed and tested in the same manner. This data is currently not available in the literature; for example Stolk et al. (2003) used fatigue data for vacuum mixed Palacos R and creep data for hand mixed Simplex P.

The first aim of the present work was to provide experimental data that could aid the development of simultaneous fatigue and creep simulations as described by Stolk et al. (2003). The second aim was to present this data in a format that would allow comparison to previous fatigue and creep studies. The third aim was to use the AE technique to monitor damage accumulation in the specimens prior to failure and investigate the capability of this technique to locate critical damage and predict the likelihood of imminent failure.

3.2 Materials and methods

3.2.1 Specimen preparation

For all specimens, CMW-1 radiopaque bone cement was used (DePuy CMW, Blackpool, UK). Vacuum mixing was performed using the VacuMix vacuum mixing apparatus (DePuy CMW). Mixing was performed as per manufacturers instructions, at room temperature. The time from first contact between liquid (monomer) and powder (polymer) to injection into the mould was approximately 100sec. The mould used to fabricate the specimens consisted of a central polyethylene (PE) plate, with the profile of two specimens machined from it, a PE plate above and below the central plate, held together between two stainless steel external plates for rigidity. Cement was injected into the open mould cavity, the top PE and steel plates were positioned and the mould was clamped. Specimens were allowed to cure in the mould for two hours before being aged in Ringer's solution at 37°C until required for testing. The ageing period of the specimens was between 18 and 30 days. To provide the best representation of cement *in vivo*, all specimens (regardless of porosity) were included in the testing. However, specimens that failed to fill the mould (and were, therefore, of an irregular geometry) were discarded. A schematic drawing of the specimen is shown in Figure 3.1.

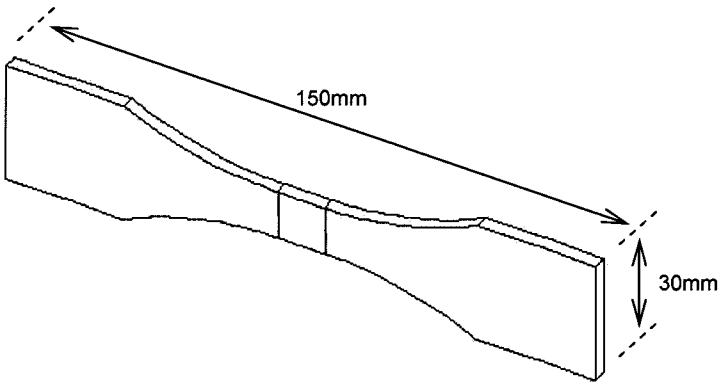

Figure 3.1: Dimensioned view of a test specimen. The gauge section was 12mm x 12 mm and specimen thickness was 3.5mm.

3.2.2 Test setup

Prior to testing, one acoustic emission (AE) sensor was attached to each end of the gauge length of the specimen (Figure 3.2). A waterproof 12.5mm extensometer (Instron Ltd.) was attached to the specimen to monitor creep deformation. Specimens were lightly clamped in custom made grips, which were coupled to the testing machine via a pin linkage system to help ensure a pure tensile load (Figure 3.2). A small amount of tension was applied to align the specimen before final clamping. All testing took place using an Instron 8874 servohydraulic testing machine equipped with an environmental chamber, which contained distilled water at 37°C and was electrostatically insulated from the testing machine to prevent any interference with the monitoring equipment (Figure 3.2). Testing was performed in load control, at a frequency of 5Hz. Four stress levels were considered: 20MPa, 15MPa, 11MPa and 7MPa, where the stress level was the peak stress experienced under a cyclic sinusoidal load, at an R-ratio of 0.1. Five specimens were tested at each stress level. Applied load, extensometer displacement and crosshead displacement were recorded during the test, along with the AE parameters described in section 3.2.3.

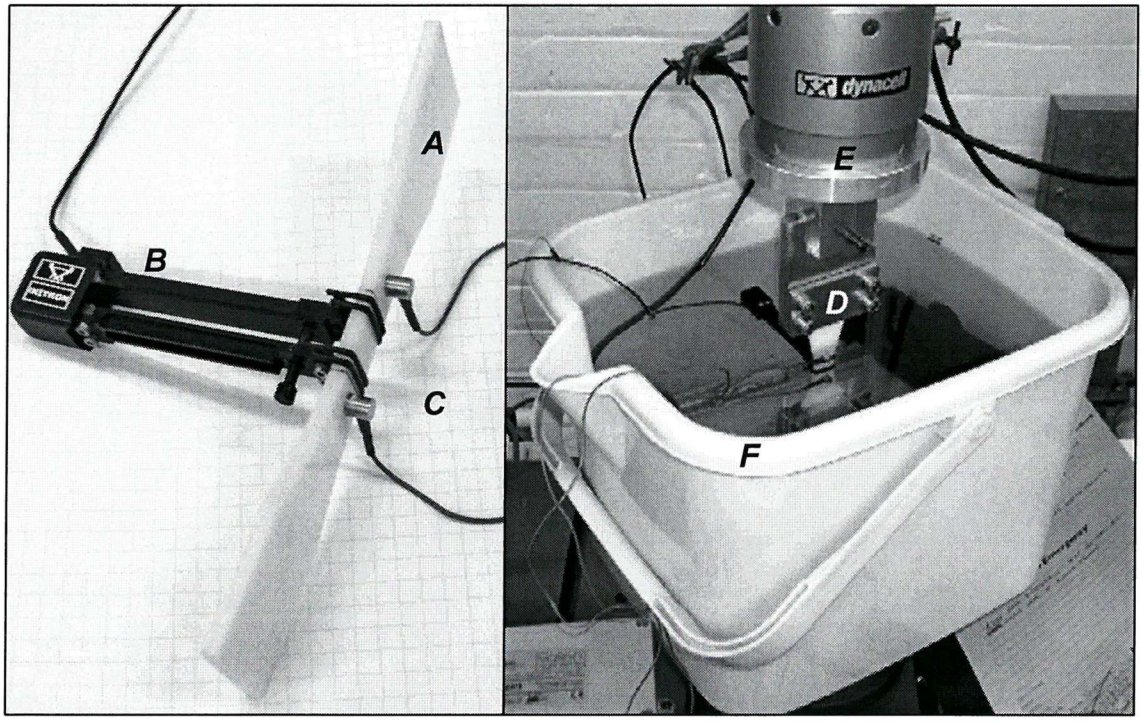

Figure 3.2: Instrumented fatigue test specimen (A), with extensometer (B) and acoustic emission sensors (C), and specimen in grips (D) connected to the load cell (E) and in the environmental chamber (F).

3.2.3 Acoustic emission

The instrumentation used in this study was the AMSY4 four-channel PC based data acquisition with Visual AE software (Vallen Systeme GmbH, Munich). AE sensors were Vallen Z-series, bandwidth 100kHz – 1MHz. Preamplifiers were fixed 40dB gain, with 100kHz – 1MHz filters.

Prior to testing, the AE sensors were attached to the hydraulic testing machine to measure any noise generated by the machine. Acoustic activity was detected up to 32dB; a lower bound threshold was set at 40dB to avoid recording this noise during the test. Previous AE studies of bone cement cracking have used thresholds of 40dB (Qi et al., 2000; Roques et al., 2004a,b) and 45dB (Qi, 2000). Acoustic activity detected above this threshold had the following parameters (see Figure 3.3): peak amplitude, rise time, duration, ring down counts (i.e. the number of threshold crossings) and energy.

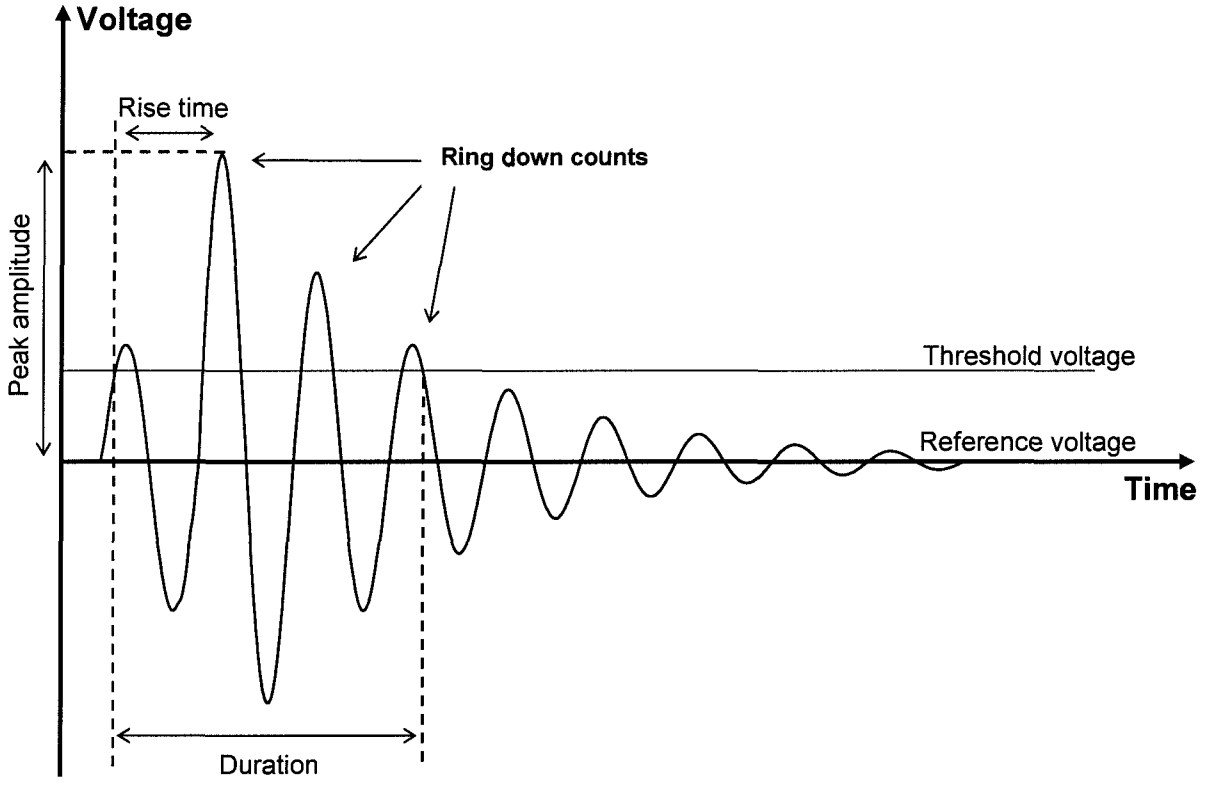

Figure 3.3: Schematic of acoustic emission hit on a voltage versus time plot. Acoustic emission parameters are shown.

In this study, the duration of the AE was used as a damage parameter, as it gave information as to the magnitude of the detected signal (Figure 3.2). The speed of sound in the material was determined by breaking a high polymer graphite pencil lead (this produces a broadband step-release transient wave, known as a Hsu-Neilsen source) at one sensor, and recording the time taken for the elastic wave to reach the second sensor. Measuring the distance between sensors allowed the speed of sound in the material to be calculated. Once this was known, a hit could be located between the two sensors, based on the time lag between arrival at each sensor. A located event was defined by the following time parameters: (i) the first-hit channel discrimination time (FCDT), used to separate events. If a hit was detected, and the time to the previous hit was greater than FCDT, a new event was defined. (ii) The maximum time between first and last hit allowed within one event (DT1). (iii) Maximum time to the previous hit within one event (DT2). The settings for these parameters were taken from Roques (2004) and are summarised in Table 3.1.

Parameter	Value
Threshold	40dB
FCDT	0.2ms
DT1	0.2ms
DT2	0.2ms

Table 3.1: AE parameters used in the current study.

3.3 Results

In all cases, the fracture surface contained a pore or defect of some kind (see Figures 3.4 & 3.5 for examples). Cracks were observed at pore boundaries, and evidence of microcracking was also seen (Figure 3.4). Discontinuous crack growth bands were identified on the fracture surfaces, and indicated the source of the crack (Figure 3.5). This was usually a pore or number of pores, but in one instance was an agglomerate of $BaSO_4$ particles.

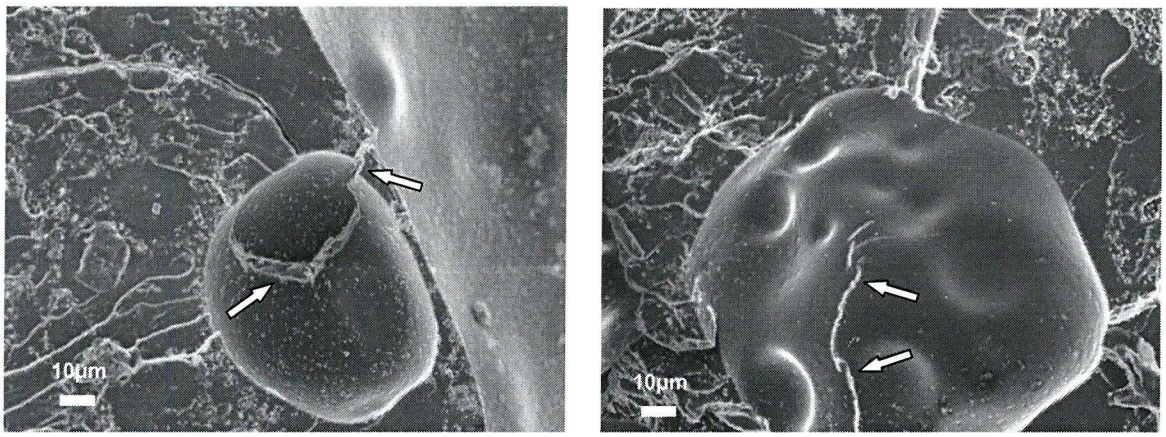

Figure 3.4: Scanning electron micrographs identifying (a) cracks and (b) microcracks at pores in the cement (white arrows).

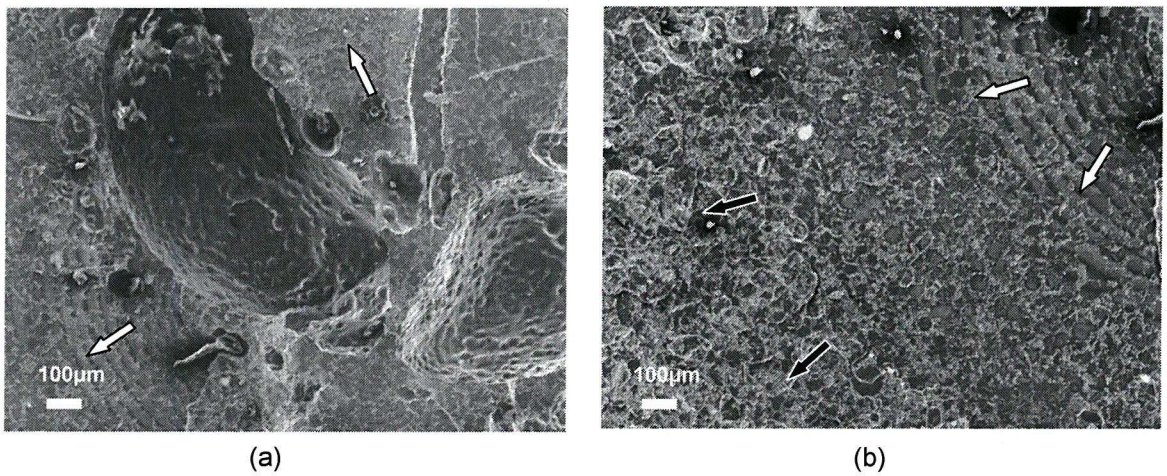

Figure 3.5: Scanning electron micrographs identifying discontinuous crack growth bands close to source of failure (white arrows) and rougher fast fracture surface further away from failure source (black arrows). Arrows indicate the direction of crack growth.

The S-N data were characterised by variability in the number of cycles to failure at any given stress level (Figure 3.6). As with previous bone cement fatigue studies, the presence of large pores (approx diameter >1mm) was responsible for early fatigue failure (Murphy and Prendergast, 2000). The best fit regression line (Figure 3.6) that was fitted to the average number of cycles to failure at each stress level, is:

$$\log N_f = (41.99 - \sigma)/5.13 \qquad \textbf{Equation 3.1}$$

where N_f is the number of cycles to failure and σ is the stress level.

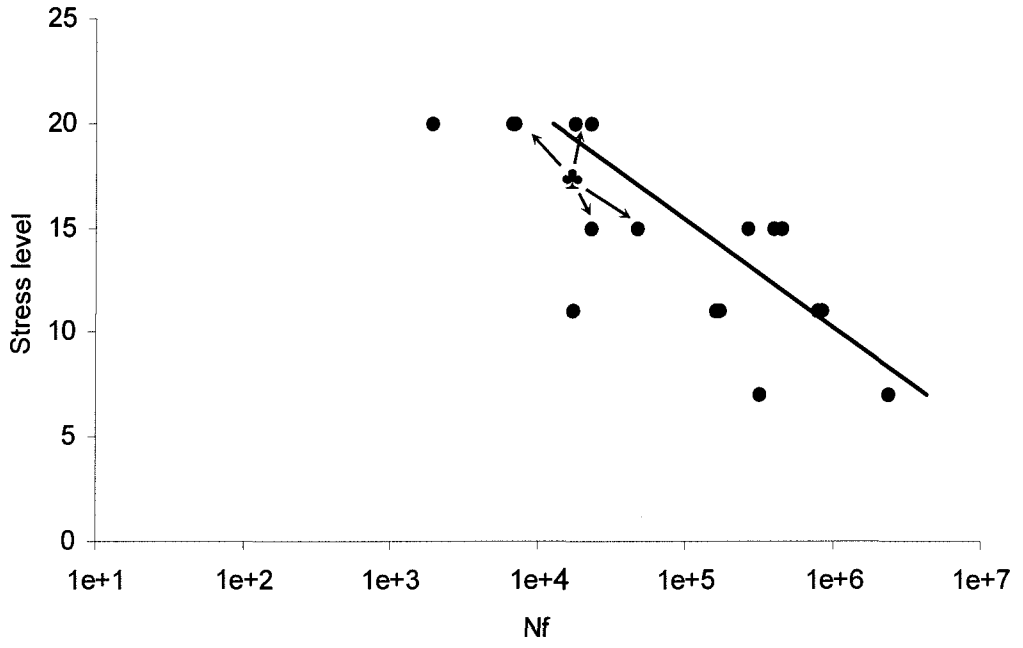

Figure 3.6: Stress versus load cycles to failure (S-N) curve for CMW-1. Data points are only plotted for specimens that failed, hence n=2 @ 7MPa. Specimens in which an initial burst of AE activity was recorded are identified by ♣. Regression line plotted through average fatigue life at each stress level.

To allow the fatigue data to be compared to Murphy and Prendergast (2000), a two-parameter Weibull analysis was performed on the fatigue data to determine the probability of survival to a given number of cycles at a certain stress level:

$$P_s = \exp\left[-\left(\frac{N_f}{\beta}\right)^{\alpha}\right] \qquad \textbf{Equation 3.2}$$

where P_s was the probability of survival, N_f the number of cycles to failure and α and β the shape and location parameters respectively. Applying a linearised form of Equation 3.2 to the data yielded values for α and β as given in Table 3.2. For each of the stress levels, and a given P_s, the corresponding Weibull life can be calculated from Equation 3.2, taking α and β from Table 3.2. This can be repeated for different values of P_s, and by extrapolating the data a plot of probability of survival to $1x10^6$ load cycles as a function of stress level can be obtained (Figure 3.7). The method is described in full by Murphy and Prendergast (2000).

Stress (MPa)	α	β
20	1.04	13,171
15	0.73	269,479
11	0.63	435,172
7	-	-

Table 3.2: Weibull distribution constants: α, shape parameter; β location parameter. Only two specimens were tested to failure at 7MPa, therefore a statistical analysis could not be performed at this stress level.

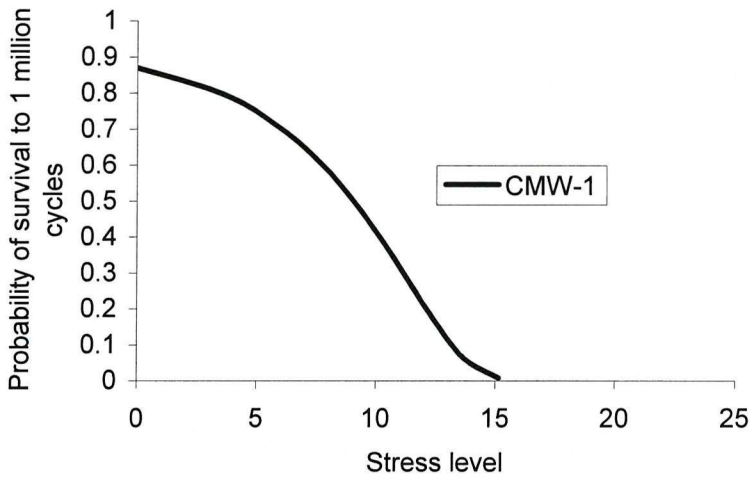

Figure 3.7: Probability of survival as a function of stress for a Weibull life of $1x10^6$ load cycles.

Three specimens that were tested at 7MPa did not fail after $3x10^6$ load cycles. By plotting the duration of the AE events against their energy (Figure 3.8), it was possible to predict that specimen failure was not imminent. As the fatigue test progressed, the duration and energy of the detected AE increased, and the plot built up as shown in Figure 3.8a until failure occurred. For all specimens (at all stress levels), the final event was of high duration (approx 4000μs) and high energy (approx 10^4nVs), and was easily identifiable on the graph (Figure 3.8a). Plots from failed specimens (Figures 3.8a) could be compared (in real time) to those of specimens that had not failed after $3x10^6$ load cycles (Figure 3.8b). From this it could be predicted that failure was not imminent, and the tests were stopped.

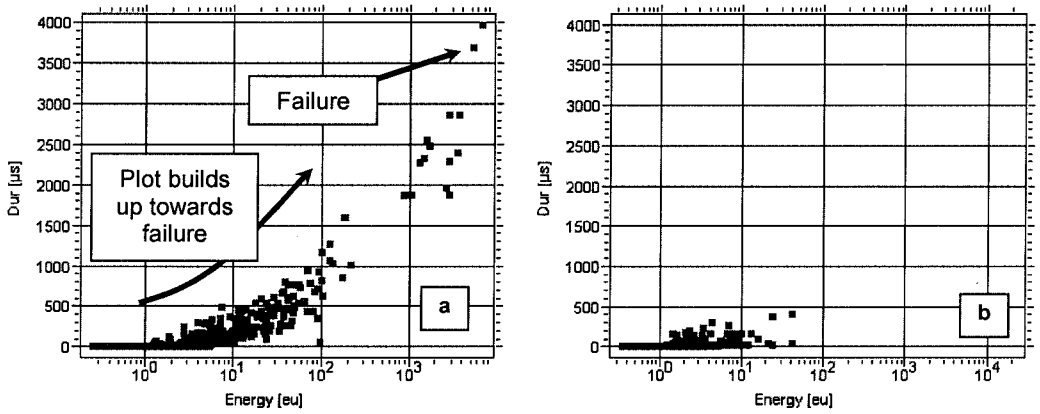

Figure 3.8: Duration versus energy plots for two different specimens: (a) Failed specimen at 7MPa; data points built up until failure occurs. (b) Specimen not failed at 7MPa after $3x10^6$ load cycles. Data points on the plot had not built up, predicting failure was not imminent, and the test was stopped.

Plotting hits as a function of time revealed the discontinuous nature of bone cement damage accumulation (Figure 3.9). The four plots in Figure 3.9 represent specimens in which an initial burst of AE activity was recorded (marked by ♣). These specimens are identified on the S-N data curve (Figure 3.6). The duration of the detected AE was used to represent damage in the cement. For each specimen, the normalised damage was calculated as ω/ω_f, where ω represented the cumulative durations of the detected AE at a number of cycles (n), and ω_f represented the cumulative durations of the detected AE at failure. The normalised life of each specimen was calculated as n/N_f where n was the number of cycles completed and N_f the number of cycles to failure. Plotting normalised damage against normalised life allowed the damage accumulation curves to be compared (Figure 3.10). The nonlinearity of the damage accumulation was evident, and the

'stepping' nature of the curves indicated that damage was a discontinuous process (see also Figure 3.9). There was a trend for increasing non-linearity at higher stress levels, but this was masked slightly by an initial burst of AE activity for two specimens at 15MPa and two at 20MPa (marked by ♣ in Figures 3.9 & 3.10). This phenomenon was not observed at the lower stress levels.

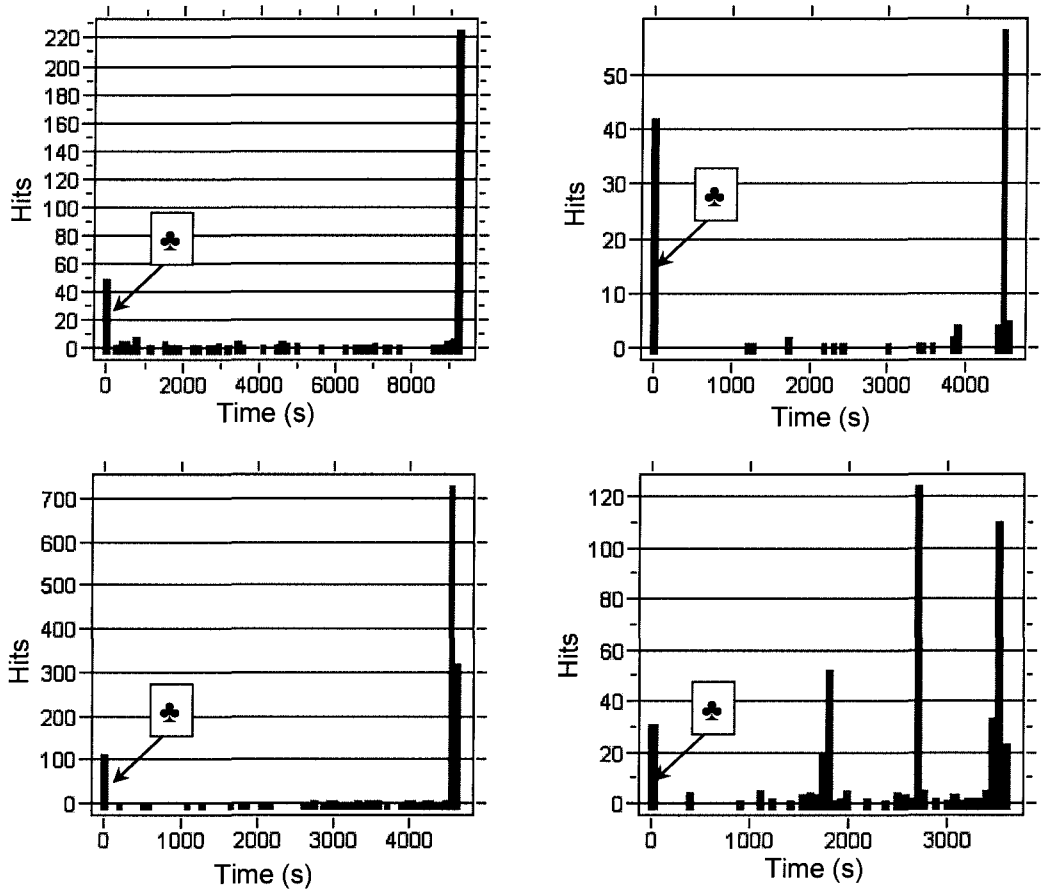

Figure 3.9: AE hits as a function of time for specimens exhibiting discontinuous damage accumulation and an initial burst of AE activity upon loading (♣). Only 4 specimens exhibited this initial burst of AE activity, but all exhibited discontinuous damage accumulation.

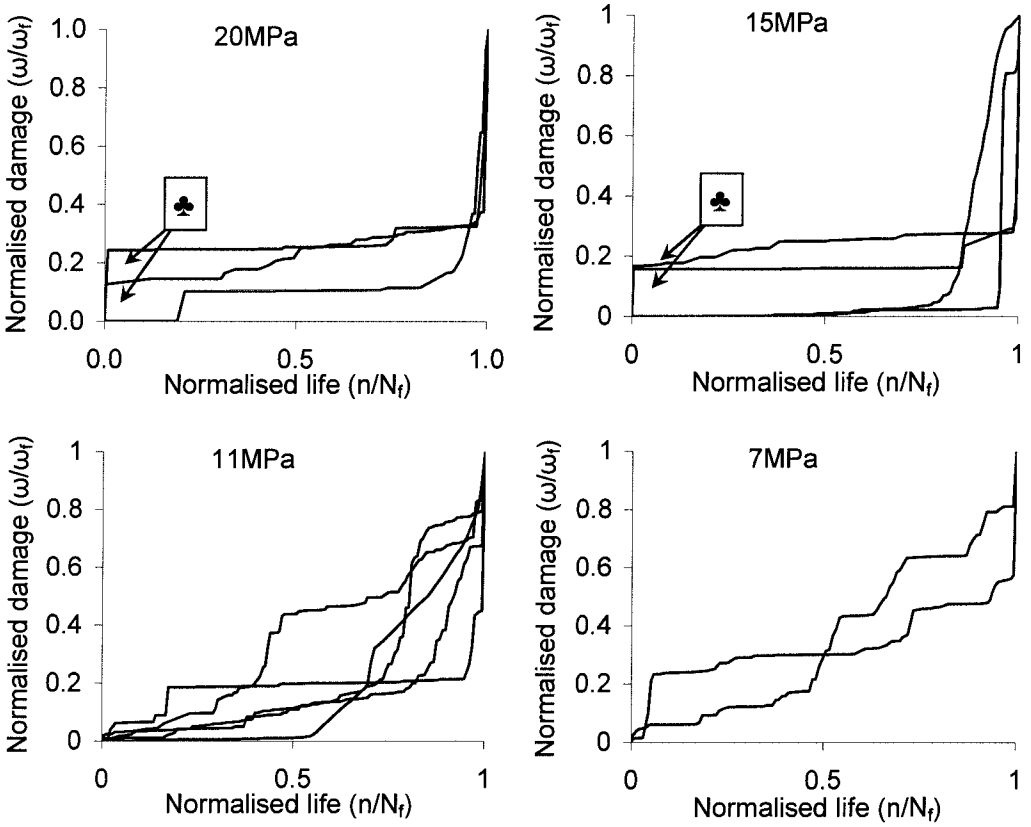

Figure 3.10: Damage as a function of time for the four stress levels considered. The damage parameter was the duration of the acoustic event. Although five specimens were tested at each stress level, AE sensors became loose for two tests at 20MPa and one at 15MPa, generating erroneous data. Only two specimens at 7MPa were tested to failure. None of these are included in the graphs. Initial bursts of AE activity are highlighted (♣) for two specimens at 20MPa and two at 15MPa.

By monitoring the location of detected damage, it was possible to predict the failure location in the specimen, as shown in Figure 3.11. As time progressed (z-axis, Figure 3.11), the majority of damage was occurring 10mm from sensor #1. This correlated well to the position of final fracture, as observed on the failed specimen. The final fracture site was well located by the AE method throughout the fatigue tests (see Figure 3.12).

Creep deformation was recorded for specimens tested at 20MPa, 15MPa and 11MPa. Creep strain was plotted against number of loading cycles on a double logarithmic scale (Figure 3.13a,b,c). The resulting relationship was represented by:

$$\log \varepsilon = A \log N + B \qquad \textbf{Equation 3.3}$$

where ε is the creep strain, N is number of load cycles and A and B are constants whose values are dependant on the stress level. In this case:

$$A = -0.13\log(\sigma) + 0.42 \qquad \textbf{Equation 3.4a}$$

$$B = 3.12\log(\sigma) - 2.61 \qquad \textbf{Equation 3.4b}$$

where A and B are the stress dependant constants (see Equation 3.3), and σ is the stress level. The creep strains calculated using Equation 3.3 are shown in Figure 3.13d.

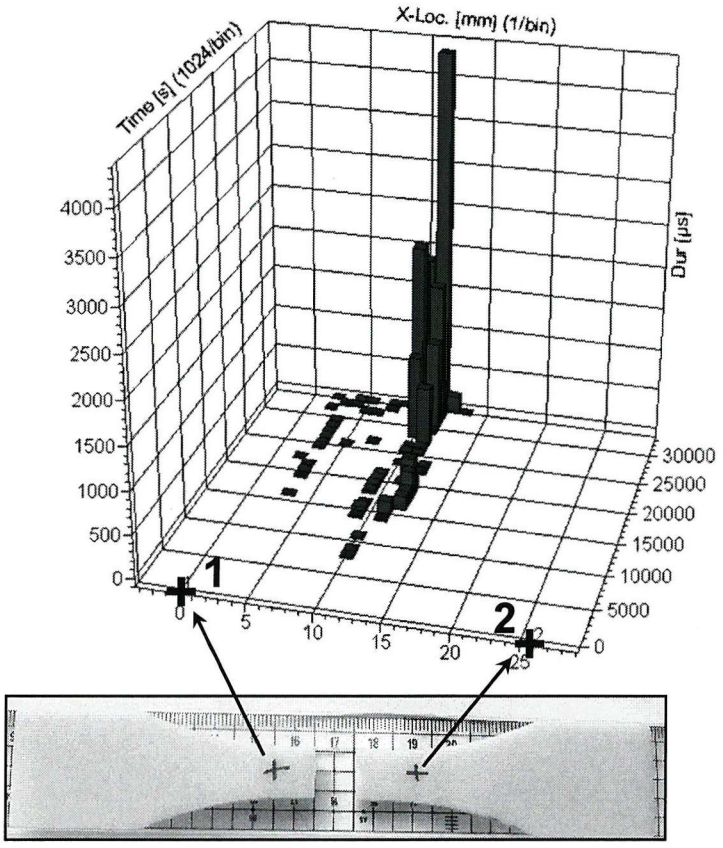

Figure 3.11: Damage (y-axis) as a function of time (z-axis) and location (x-axis), and an image of the specimen from which the data was recorded.

3.4 Discussion

This study investigated the number of cycles to failure, damage accumulation and creep of bone cement under tensile fatigue loading. Damage accumulation was monitored with the AE technique allowing the tests to run without interruption, which in turn allowed creep strain to be monitored throughout the test. Tests were terminated at $3x10^6$ load cycles, but not before checking the AE damage/energy plots to ensure failure was not imminent (see Figure 3.8). All specimens failed at a pore or void, indicating the critical nature of porosity for this specimen geometry and loading configuration. Pores reduced the cross-sectional area of the specimen, thus increasing the apparent stress level. Pores also acted as stress concentrations, which may have acted to initiate crack growth. There was considerable scatter in the S-N data, and a relatively low number of cycles to failure could be correlated with the presence of a large pore in the specimen. The variability in fatigue life is indicated by the Weibull curve (Figure 3.7) where a stress range of 0MPa – 14MPa covers the P_s value from 0.9 to 0.1. By presenting the shape and location parameters (α and β, Table 3.2), a direct comparison of Weibull life can be made with the results of Murphy and Prendergast (2000) (who also presented data for α and β) by using Equation 3.2.

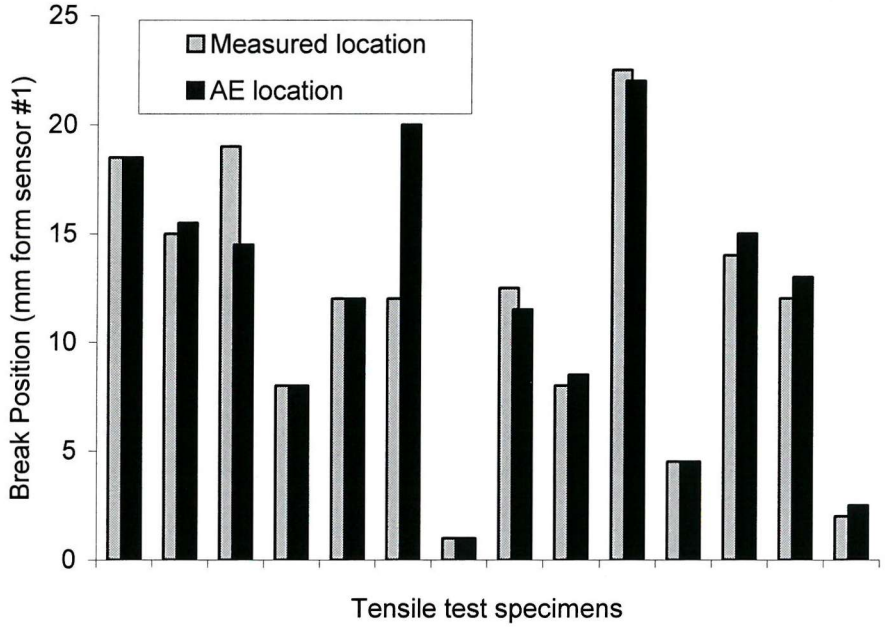

Figure 3.12: Measured fracture location and AE predicted fracture location for different specimens.

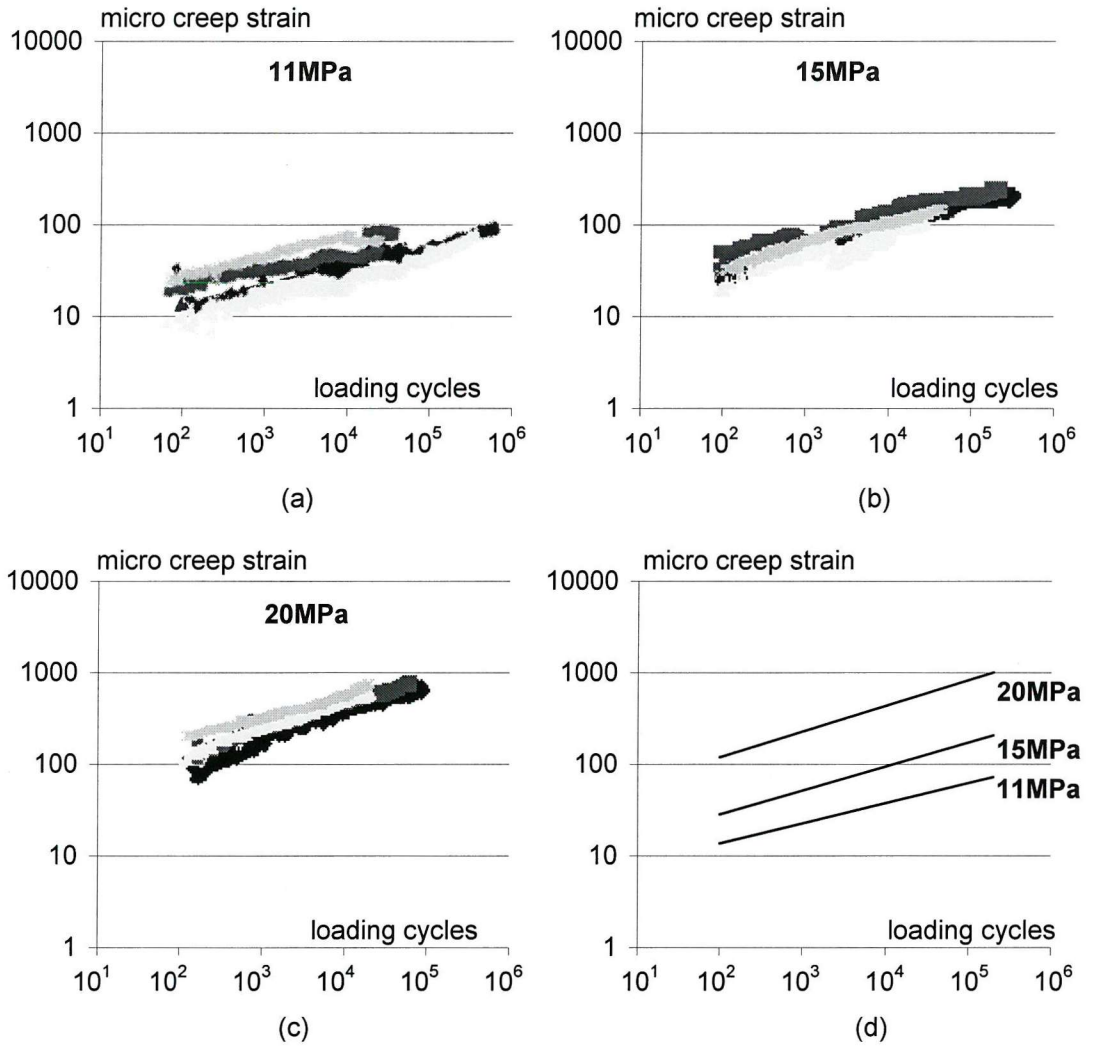

Figure 3.13: Micro creep strain experimental data as a function of loading cycles for (a) 11MPa, (b) 15MPa and (c) 20MPa. (d) Creep strain versus loading cycles as modelled by the empirically derived double logarithmic function for 11MPa, 15MPa and 20MPa.

Damage accumulation (as monitored by AE) was a non-linear process with respect to the number of loading cycles, and there was a trend for increasing non-linearity at higher stress levels (see Figure 3.10). This is in good agreement with Murphy and Prendergast (2001) who used the dye penetrant method to monitor damage accumulation. The possibility of a relationship between damage rate and fatigue life was investigated. For the higher stress levels (20MPa, 15 MPa and 11MPa) damage accumulated at a low rate early in the loading history and a higher rate towards failure. At 20MPa and 15MPa, the damage rate only increased immediately prior to failure, but at 11MPa, the damage accumulation rate increased more progressively such that the increasing damage rate

could predict the onset of failure. However, as can be seen in Figure 3.10 this was not the case for all specimens. At 7MPa the damage accumulation rate was relatively constant throughout the fatigue test. There therefore did not appear to be a relationship between damage rate and fatigue life.

The non-linearity of damage accumulation was masked by an initial burst of AE activity for two specimens at 20MPa, and two at 15MPa (see ♣, Figures 3.9 & 3.10). At 15MPa, the specimens with an initial burst of activity had a noticeably shorter fatigue life than others at that stress level (see ♣, Figure 3.6), suggesting that the initial activity could be a sign of premature fatigue failure. These specimens both had large pores clearly visible on the fracture surface. At 20MPa, the specimens with the initial burst of activity had average fatigue lives and no large pores on the fracture surfaces. Indeed, the specimen with the shortest fatigue life at 20MPa contained a large pore and no initial burst of activity was recorded by the AE, suggesting that initial AE activity was not an indicator of poor fatigue life. This is corroborated when it is considered that at lower stress levels, no initial burst of activity was recorded for any specimens. It is unlikely that the initial burst of activity was indicative of a residual stress field or pre-load damage caused by residual stress in the specimen, given that the specimens were unconstrained (in contrast to cement constrained by a metallic stem *in vivo*) and free to shrink in the mould during polymerisation. In addition, the fact that initial activity was only recorded in 4 out of 20 specimens (fabricated under the same conditions) indicates it was caused by another mechanism. Bone cement is prone to craze formation (Topoleski et al, 1990), which can occur in the first load cycle if the stress amplitude is high enough (Suresh, 1998). The absence of initial activity at lower stress levels suggests the initial burst of AE activity at higher stress levels may have been due to crazing. Another possibility for the initial activity is specimen slippage at the grips, which may have occurred if specimens were not aligned properly during the gripping procedure.

For all specimens, damage was found to be a discontinuous process (see Figure 3.9), where periods of AE activity occurred in a stop-start manner. Evidence of discontinuous growth bands were observed on the fracture surfaces and the spacing of successive bands were approximately 80μm, too large to be fatigue striations. A similar phenomenon has been observed for commercial grade PMMA, and Suresh (1998) described the following possible mechanism for crack growth: during cyclic loading, the crack tip is stationary,

but damage is accumulating in a craze zone (Figure 3.14b). When this craze zone opens by a critical amount, crack growth occurs in one spurt (Figure 3.14c). This process repeats itself causing dark bands of discontinuous crack growth to appear on the fracture surface. This would explain the large spacing of the discontinuous growth bands.

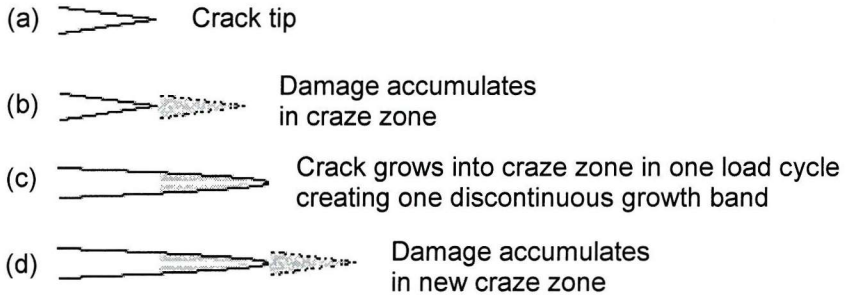

Figure 3.14: A schematic representation of discontinuous crack growth under fatigue loading. Reproduced from Suresh (2000) with permission from Cambridge University Press.

AE was capable of locating damage in the fatigue tests. The good location capability of the AE method has also been commented on previously (Qi et al., 2000; Roques et al., 2004a). For higher stress levels, as damage accumulated rapidly, location could only be predicted immediately before failure. For lower stress levels fracture site prediction was possible long before failure occurred. In either case, the site of final fracture was always located, and the fracture site located by the AE compared well to the actual location (see Figure 3.12), within a tolerance of approx +/- 0.5mm. The AE was able to locate critical damage (i.e. at the site of final fracture), but there was evidence that non-critical damage was also located (for example between 3mm and 8mm in Figure 3.11). It is unlikely that all damage was located, as the elastic AE wave may have lost energy as it propagated through the specimen (attenuation). One way to overcome attenuation is to apply more sensors to the specimen. Certainly for more complex geometries, eg. the cement mantle of an implanted femur model, more sensors would be necessary to detect all damage occurring, and while some of this would inevitably remain unlocated due to attenuation (as location requires detection by more than one sensor), it could still be related to sensor position.

Cement creep is an important characteristic of bone cement, as it allows the relaxation of high stresses. The data in this study were analysed in the same manner as Verdonschot and Huiskes (1994) who tested hand mixed Simplex P, but the creep strains observed were significantly lower. According to the creep study by Lee et al. (2002), the creep rates of CMW-1 and Simplex P are similar for identical testing conditions and mixing methods. Although the testing conditions used in the present study were similar to those used by Verdonschot and Huiskes (1994), these workers used hand-mixed cement while the present specimens were fabricated using vacuum-mixed cement. Norman et al. (1995) found that vacuum mixing reduced the creep strain by almost half when compared to hand mixing (at 50MPa compression, for 6hrs). Reduced creep strain for vacuum mixed cement was therefore expected. The double logarithmic creep model presented (Equations 3.3 & 3.4) includes primary and secondary creep but not tertiary creep. This is considered acceptable because specimen failure occurred before any tertiary creep deformation was recorded.

There are a number of limitations with the current study. Although the specimen shape was similar to that of previous studies, different specimen sizes were employed in these studies (Murphy and Prendergast, 2000; Murphy and Prendergast, 2001; Verdonschot and Huiskes, 1994). As bone cement contains pores, larger volumes are statistically more likely to contain a greater number of pores or weak regions. As failure usually occurs from such regions, the fatigue data may not be comparable with specimens of different volume. The specimens in the current study were vacuum mixed, therefore a comparison between the creep data presented here for CMW-1 and that by Verdonschot and Huiskes (1994) for hand mixed Simplex P is perhaps inappropriate. Another limitation involves gripping of the specimens. It may have been the case that a number of specimens (identified by an initial burst of AE activity) were not aligned properly in the fatigue testing, despite precautions taken to prevent this occurring. Murphy and Prendergast (2000) aligned their specimens by applying a small tensile load with pins through the grip and specimen before final clamping; this may have alleviated the gripping problem. A further limitation involves the test frequency of 5Hz. This frequency would seldom be experienced *in vivo*, but fatigue testing at realistic frequencies was not practical. However, a study by Lewis et al. (2003) suggests testing frequency does not have a statistically significant effect on fatigue life (see Section 2.3.2, page 67). A final limitation regards the application of the constitutive laws in computational simulations.

This data is for vacuum mixed CMW-1 cement, aged for a time and tested at 37°C. The properties of acrylic bone cement are influenced by a host of variables such as cement brand, mixing method and testing environment. While the testing conditions in the current work were applied to represent the *in vivo* situation, they may not represent the conditions experienced by the cement mantle of *in vitro* models. Caution must therefore be exercised in applying these constitutive laws to simulate fatigue and creep in the cement mantle of *in vitro* models.

The motivation for this study came from three areas. First, different cement brands can only be compared when testing conditions are the same, and the results are presented in a similar manner. In this study, the creep and fatigue data for CMW-1 were presented in the same manner as previous studies, allowing CMW-1 to be compared directly to the other brands tested. Second, the simultaneous simulation of creep and fatigue has been developed for bone cement, but until now the creep and fatigue data required by the computational method has been taken from different cement brands and different mixing methods (Stolk et al., 2003). The current study has presented the data necessary to simulate both the creep and fatigue behaviour of vacuum mixed CMW-1. Third, it was further demonstrated that AE can be used as a condition-monitoring tool for bone cement. Damage could be monitored continuously, without visualisation of the cement, and AE data could be used to locate damage in the specimens and predict likely failure sites. AE has been used previously to monitor material failure during loading of cemented implanted cadaveric femora, but the difficulties of measurement through the bone limited its effectiveness, as data was recorded from the entire construct (for example the load application, bone microcracking and rubbing at the stem/cement interface) rather than just the bone cement (Sugiyama et al., 1989). By characterising the AE activity due to cement microcracking, it may be possible to filter out the unwanted AE data and transfer the benefits of the AE method discussed in the current work to more complicated models.

3.5 Conclusions

The present study has characterised the fatigue, damage accumulation and creep properties of vacuum mixed CMW 1 bone cement. As with previous bone cement fatigue studies, porosity was observed to be the controlling factor of fatigue life and caused a large amount of data scatter. Damage accumulation was monitored using the AE technique and was a non-linear process, the degree of non-linearity depending on stress level. Creep strain was dependant on the number of loading cycles and the stress level. Empirical models were generated from the fatigue and creep data for use in computational simulations of the processes. Evidence has been presented of the capability of AE to be used as a condition-monitoring tool for bone cement fatigue. AE data was capable of locating damage in the specimens, predicting the site of final fracture and the immanency of failure.

3.6 References

Chwirut, J., 1984. Long term compressive creep deformation and damage in acrylic bone cements. Journal of Biomedical Material Research, 18: 25-37.

Graham, J., Pruitt, L., Ries, M. and Gundiah, N., 2000. Fracture and fatigue properties of acrylic bone cement - the effects of mixing method, sterilization treatment, and molecular weight. Journal of Arthroplasty, 15(8): 1028-1035.

Harper, E.J. and Bonfield, W., 2000. Tensile characteristics of ten commercial acrylic bone cements. Journal of Biomedical Materials Research, 53(5): 605-616.

Jasty, M., Maloney, W.J., Bragdon, C.R., O'Connor, D.O., Haire, T. and Harris, W.H., 1991. The initiation of failure in cemented femoral components of hip arthroplasties. Journal of Bone and Joint Surgery-British Volume, 73(4): 551-558.

Lee, A.J.C., Ling, R.S.M., Gheduzzi, S., Simon, J.-P. and Renfro, R.J., 2002. Factors affecting the mechanical and viscoelastic properties of acrylic bone cement. Journal of Materials Science-Materials in Medicine, 13(8): 723-733.

Lewis, G., 1999. Effect of mixing method and storage temperature of cement constituents on the fatigue and porosity of acrylic bone cement. Journal of Biomedical Materials Research Part B-Applied Biomaterials, 48: 143-149.

Lewis, G., Janna, S. and Carroll, M., 2003. Effect of test frequency on the *in vitro* fatigue life of acrylic bone cement. Biomaterials, 24(6): 1111-1117.

Lu, Z. and McKellop, H., 1997. Effects of cement creep on stem subsidence and stresses in the cement mantle of a total hip replacement. Journal of Biomaterials Research, 34(2): 221-226.

Murphy, B.P. and Prendergast, P.J., 2000. On the magnitude and variability of the fatigue strength of acrylic bone cement. International Journal of Fatigue, 22: 855-864.

Murphy, B.P. and Prendergast, P.J., 2001. The relationship between stress, porosity and nonlinear damage accumulation in acrylic bone cement. Journal of Biomedical Materials Research, 59: 646-654.

Norman, T.L., Kish, V., Blaha, J.D., Gruen, T.A. and Hustosky, K., 1995. Creep characteristics of hand-mixed and vacuum-mixed acrylic bone-cement at elevated stress levels. Journal of Biomedical Materials Research, 29(4): 495-501.

Norman, T.L., Thyagarajan, G., Saligrama, V.C., Gruen, T.A. and Blaha, J.D., 2001. Stem surface roughness alters creep induced subsidence and 'taper-lock' in a cemented femoral hip prosthesis. Journal of Biomechanics, 34(10): 1325-1333.

Qi, G., 2000. Attenuation of acoustic emission body waves in acrylic bone cement and synthetic bone using wavelet time-scale analysis. Journal of Biomedical Materials Research, 52(1): 148-156.

Qi, G., Pujol, J. and Fan, Z.F., 2000. 3-D AE visualization of bone-cement fatigue locations. Journal of Biomedical Materials Research, 52(2): 256-260.

Roques, A., Brown, M., Thompson, J., Rowland, C. and Taylor, A., 2004a. Investigation of fatigue crack growth in acrylic bone cement using the acoustic emission technique. Biomaterials, 25(5): 769-778.

Roques, A., Browne, M., Taylor, A., New, A. and Baker, D., 2004b. Quantitative measurement of the stresses induced during polymerization of bone cement. Biomaterials, 25(18): 4415-4424.

Stolk, J., Maher, S.A., Verdonschot, N., Prendergast, P.J. and Huiskes, R., 2003. Can finite element models detect clinically inferior cemented hip implants? Clinical Orthopaedics and Related Research, 409: 138-150.

Sugiyama, H., Whiteside, L.A. and Kaiser, A.D., 1989. Examination of rotational fixation of the femoral component in total hip-arthroplasty - a mechanical study of micromovement and acoustic-emission. Clinical Orthopaedics and Related Research, 249: 122-128.

Suresh, S., 1998. Fatigue of materials. Cambridge University Press.

Topoleski, L.D.T., Ducheyne, P. and Cuckler, J.M., 1990. A fractographic analysis of *in vivo* poly(methyl methacrylate) bone-cement failure mechanisms. Journal of Biomedical Materials Research, 24(2): 135-154.

Verdonschot, N. and Huiskes, R., 1994. Creep behaviour of hand-mixed Simplex P bone cement under cyclic tensile loading. Journal of Applied Biomaterials, 5(3): 235-243.

Verdonschot, N. and Huiskes, R., 1995. Dynamic creep-behaviour of acrylic bone-cement. Journal of Biomedical Materials Research, 29(5): 575-581.

Verdonschot, N. and Huiskes, R., 1997. The effects of cement-stem debonding in THA on the long-term failure probability of cement. Journal of Biomechanics, 30(8): 795-802.

CHAPTER 4

TENSILE AND 4-POINT BEND FATIGUE: IN SILICO MODELS AND EXPERIMENTAL TESTS[1]

In this study, experimental tensile and 4-point bend fatigue tests were performed. The tensile fatigue S-N data was used to drive the computational simulation of fatigue in finite element models of the tensile and 4-point bend specimens. Porosity was simulated in the finite element models according to the theory of elasticity and using Monte Carlo methods. The computational fatigue simulations generated variability in the fatigue life at any given stress level, due to each model having a unique pore distribution. The fracture site also varied between specimens. Good agreement between computational models and experimental tests was achieved for tensile and 4-point bend loading, but, for the latter, only when porosity was included. The 4-point bend test was slightly more complicated than the uniaxial test, as a stress gradient was generated through the specimen. That fatigue of this structure could only be modelled by including porosity in the model indicates that porosity should be included in further analyses.

[1]Accepted for publication in the Journal of Biomechanical Engineering. Presented at the 51st Meeting of the Orthopaedic Research Society, Washington DC, 20th-23rd February 2005.

4.1 Introduction

Porosity has been identified as having a negative effect on the fatigue resistance of bone cement. Jasty et al. (1991) and Topoleski et al. (1990) both examined ex vivo cement specimens, and found evidence that cement mantle cracking could be associated with porosity. *In vitro* testing has also found porosity to have a strong influence on cement fatigue cracking. McCormack et al. (1999), McCormack and Prendergast (1999), Britton et al. (2003) and Lennon et al. (2003) have all examined the cement mantle of implanted femur models under a fatigue load. Although these models were quite different, pores in the cement were thought to initiate or facilitate fatigue cracking in all cases. Porosity has also been identified as a critical parameter in uniaxial tensile fatigue testing. James et al. (1992), Davies et al. (1987), Murphy and Prendergast (2000) and Roques et al. (2004) all performed fatigue testing of bone cement specimens, and found porosity to have a negative impact on fatigue life. Murphy and Prendergast (2000) also found the distribution of pores to have an influence on the fatigue life of the specimen.

Attempts to reduce the level of porosity in bone cement have included centrifuging the cement and mixing under a vacuum. Although these techniques can reduce porosity when compared to hand mixed cement, they do not eliminate it entirely. Jasty et al. (1990), Muller et al. (2002) and Norman et al. (1995) sectioned specimens at regular intervals to determine the level of porosity in hand and vacuum mixed specimens. Dunne and Orr (2001) and Muller et al. (2002) used the principle of Archimedes, and Murphy and Prendergast (2001) counted pores on the surface of specimens to achieve the same goal. In all these studies, a statistical probability was associated with the number of pores/percentage porosity for each specimen, and for specimens of a given size a mean porosity and standard deviation could be found. This means mathematical techniques (Monte Carlo simulations) can be used to simulate the number of pores in finite element models of bone cement, and better reflect the realities of experimental test specimens. Porosity has been simulated in finite element studies, using the theoretical elastic solution for a spherical pore in an infinite medium under a remote stress (Harrigan and Harris, 1991; Harrigan et al., 1992; Lennon et al., 2003). In these studies, a pore was simulated at each integration point (Harrigan and Harris, 1991; Harrigan et al., 1992), or at the centroid of each element (Lennon et al., 2003). Because a pore was simulated in *every*

element, these studies did not represent the porosity distributions observed experimentally.

Cement mantle cracking under a fatigue load has been simulated using a combined finite element/continuum damage mechanics approach. Using this method, the effect of factors such as prosthesis type (Stolk et al., 2003) and stem surface finish (Verdonschot and Huiskes, 1997) have been investigated. A limitation of these studies is that the cement mantles were modelled as being completely free from voids, pores, flaws or defects of any kind. *In vitro* testing has presented evidence that pores and pre-load damage has a strong influence on cement mantle cracking (Section 2.2.5, page 51). The aim of the current study is to develop the computational simulation of fatigue, similar to that used by Stolk et al. (2003) and Verdonschot and Huiskes (1997), to include the effects of porosity for simple load cases – uniaxial tensile fatigue and 4-point bend fatigue. The results of the computational model will be compared to experimental tests to see if a correlation can be made. By including unique pore distributions in each of the models, stochastic results should be generated by the computational method.

4.2 Materials and methods

4.2.1 Specimen preparation & experimental testing

CMW-1 radiopaque cement (DePuy CMW, Blackpool, England) was mixed using the Vacu-Mix vacuum mixing apparatus (DePuy CMW, Blackpool, England) according to the manufacturers instructions. Tensile and 4-point bend specimens were fabricated using a polyethylene and stainless steel mould respectively. The tensile test specimens were dog-bone shaped, with a rectangular cross section, and a gauge section volume of 504mm^3 (see Figure 3.1, page 125). The 4-point bend specimens were rectangular with dimensions 6mm x 20mm x 100mm. Specimens were aged in Ringers' solution at 37°C until required for testing. The ageing period of specimens was between 18 and 30 days. No specimens were discarded in this study; even when large pores (>1mm) were evident.

All testing was performed in a water bath at 37°C on an Instron 8874 servohydraulic testing machine. Tensile tests were performed in load control, with a sinusoidal applied load, at an R-ratio of 0.1 and a frequency of 5Hz. Four stress levels were considered: 20MPa, 15MPa, 11MPa and 7MPa; these were the peak stresses experienced (in the gauge length) during fatigue loading. Sixteen specimens were tested, four at each stress level, as reported in Chapter 3.

4-point bend tests were performed under sinusoidal load control, at an R-ratio of 0.1 and a frequency of 2Hz. The peak stress levels considered were 40MPa, 30MPa, 25MPa and 19MPa. These stresses were tensile in nature and located on the bottom surface of the specimen. Twelve specimens were tested, three at each stress level. The 4-point bend experimental tests were performed by Roques (2004).

4.2.2 Computational analysis – tensile fatigue

A best-fit regression line was fitted to the data of the tensile fatigue tests, plotted through the average fatigue life at each stress level and given by Equation 4.1:

$$\log N_f = (41.99 - \sigma)/5.13 \qquad \textbf{Equation 4.1}$$

where N_f is the number of cycles to failure and σ is the stress level. Only two specimens were tested to failure at 7MPa, these data points were not included in the regression line (see Figure 4.1).

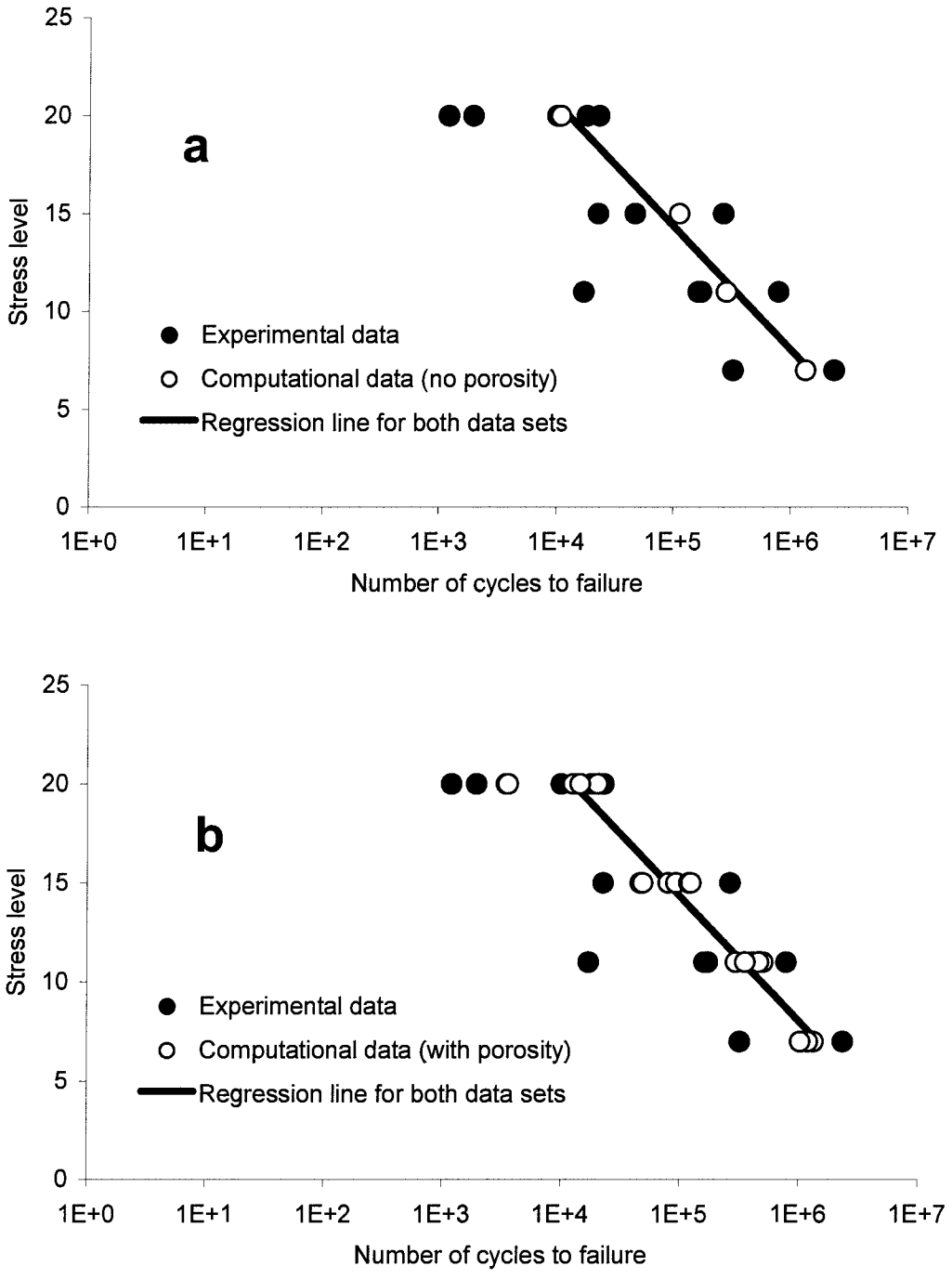

Figure 4.1: Stress versus number of cycles to failure for uniaxial tension (a) *without* porosity and (b) *with* porosity simulated in the computational data. Regression lines are coincident and plotted through average fatigue life at each stress level.

Finite element models (n=20, 5 at each stress level) of the tensile test were generated, each consisting of 19,000 tetrahedral elements. The volume of each specimen was $1.17 \times 10^4 mm^3$, giving an average element volume of $0.6mm^3$. A number of pores was generated for each specimen by Monte Carlo methods, and randomly distributed through the specimens (see Section 4.2.4, page 151). Boundary conditions were applied to simulate the experimental tensile fatigue test, and fatigue simulated in the model as described in Section 4.2.5 (page 157). Equation 4.1 was used in the simulation algorithm. The results of the finite element simulations were plotted as an S-N curve, but it was not in agreement with experimental data for the following reason. Equation 4.1 represents the fatigue life of a specimen volume of $504mm^3$ (the volume of the gauge section). The volume of an individual element in the finite element model was almost 10x smaller ($0.6mm^3$). That bone cement contains pores means a larger volume of cement is statistically more likely to contain a greater number of pores or weak regions. As fatigue failure is usually caused by such weak regions, larger volumes of cement are expected to have shorter fatigue lives. The S-N curve for uniaxial tensile fatigue specimens of volume $504mm^3$ (i.e. Equation 4.1) was therefore not valid for simulating fatigue of elements of volume $0.6mm^3$. Experimental fatigue testing of such a small volume of cement was not practical, but an S-N curve representing fatigue of $0.6mm^3$ of cement could be derived. The slope and intersect parameters of the finite element generated S-N curve were multiplied by variables a and b such that the curve was the same as the experimental. The slope and intersect parameters of Equation 4.1 were then multiplied by the same variables a and b and used in the computational simulation again. This process was repeated until the S-N curve predicted by the finite element method converged to two decimal places with the experimental S-N curve (see Figure 4.1b). This new equation gave a low probability of a critical pore being present in each element, and was therefore suitable for calculating fatigue of elements of volume $0.6mm^3$:

$$\log_{10} N_f = (78.39 - \sigma)/11.22 \qquad \textbf{Equation 4.2}$$

where N_f is the number of cycles to failure and σ is the stress level. Equation 4.2 was also used in the simulation of 4-point bend fatigue (Section 4.2.3, next page).

4.2.3 Computational analysis –4-point bend fatigue

Finite element models of the 4-point bend tests were generated (n=20, 5 at each stress level). Porosity was simulated as described in Section 4.2.4. The volume of each model was $1.2x10^4mm^3$, and each consisted of 20,500 elements giving an average element volume of $0.6mm^3$. Boundary conditions were set to simulate the experimental 4-point tests, and fatigue simulated as described in Section 4.2.5.

To check the hypothesis that both porosity and element size must be considered when simulating fatigue, simulations were repeated for the tensile test and 4-point bend tests using the method of previous deterministic studies (Stolk et al., 2003; Verdonschot and Huiskes, 1997), i.e. no pores in the models, and using Equation 4.1 in the fatigue simulation (Section 4.2.5, page 157).

4.2.4 Simulating porosity

A Monte Carlo simulation technique was used to generate the number of pores in each specimen. The name Monte Carlo itself means nothing, and merely refers to the city in Monaco where the primary attractions are casinos containing games of chance (Figure 4.2).

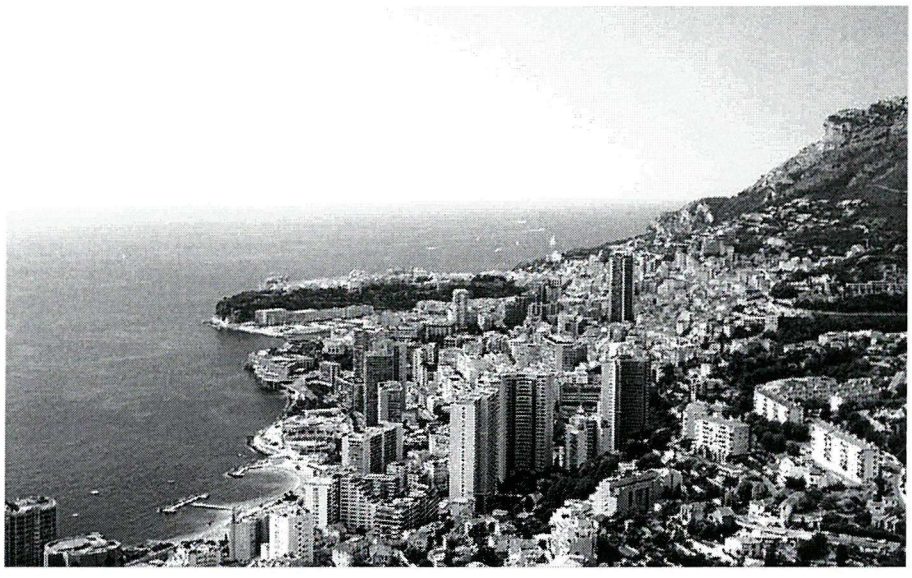

Figure 4.2: Monte Carlo.

The Monte Carlo simulation technique employed was the inverse transformation technique. Firstly the number of pores in the models were assumed to have a lognormal distribution, as this prevents negative values of porosity being generated. The probability density function indicates the nature of randomness of the distribution. For a lognormal distribution:

$$f_X(x) = \frac{1}{\sqrt{2\pi}\zeta_X x} \exp\left[-\frac{1}{2}\left(\frac{\ln x - \lambda_X}{\zeta_X}\right)^2\right], 0 \leq x < \infty \qquad \textbf{Equation 4.3}$$

where x is the random variable (number of pores), and λ_X and ζ_X are the two parameters of the lognormal distribution. If a random variable has a lognormal distribution, then its natural logarithm has a normal distribution. The mean (μ_X) and standard deviation (σ_X) of the normal distribution can be used to calculate λ_X and ζ_X (Haldar and Mahadevan, 2000):

$$\lambda_X = \ln \mu_X - \frac{1}{2}\zeta_x^2 \qquad \textbf{Equation 4.4}$$

and:

$$\zeta_X^2 = \ln\left[1 + \left(\frac{\sigma_X}{\mu_X}\right)^2\right] \qquad \textbf{Equaiton 4.5}$$

To calculate the probability of an event where the underlying distribution of a random variable is lognormal, it is convenient to use procedures for a random variable with normal distribution. As the natural logarithm of the random variable has a normal distribution, the set of lognormal random variables (X) can be transformed to a set of standard normal variables (S) with zero mean and unit standard deviation:

$$S = \frac{\ln X - \mu_X}{\sigma_X} \qquad \textbf{Equation 4.6}$$

The probability density function of this normal distribution can be expressed as:

$$f_S(s) = \frac{1}{\sqrt{2\pi}} \exp\left[-\frac{1}{2}s^2\right], -\infty < s < +\infty \qquad \textbf{Equation 4.7}$$

The probability of S being less than or equal to s is found by calculating the area under the curve described by equation 4.7. Integrating for all values of S less than or equal to s gives:

$$F_S(s) = \int_{-\infty}^{s} \frac{1}{\sqrt{2\pi}} \exp\left[-\frac{1}{2}s^2\right] ds = \Phi(s) \qquad \textbf{Equation 4.8}$$

This is called the cumulative distribution function and gives the probability of a random variable having a value less than or equal to a specific value.

The inverse transformation technique converts a set of uniformly distributed random numbers to random numbers with a lognormal distribution as shown by the dashed line in Figure 4.3. A set of uniformly distributed pseudorandom numbers (not true random numbers, as they do follow a pattern depending upon the initial seed value, and repeatability can occur after generation of ~10^9 numbers. Each finite element model required a unique seed value to ensure a unique set of random numbers, and repeatability was not an issue for this study) were created using the FORTRAN built in RAND function. The set of uniformly distributed random numbers U was converted to a set of lognormally distributed random numbers X according to:

$$x_i = \exp\left[\lambda_X + \zeta_X \Phi^{-1}(u_i)\right] \qquad \textbf{Equation 4.9}$$

where x_i is a number in set X, u_i a number in set U, λ_X and ζ_X are the two parameters of the lognormal distribution (Equation 4.4 & 4.5) and Φ is the cumulative distribution function as defined in Equation 4.8. This set of lognormally distributed random numbers could then be used to simulate a number of pores in each finite element model, but firstly data regarding the mean number of pores in a given volume and standard deviation was required.

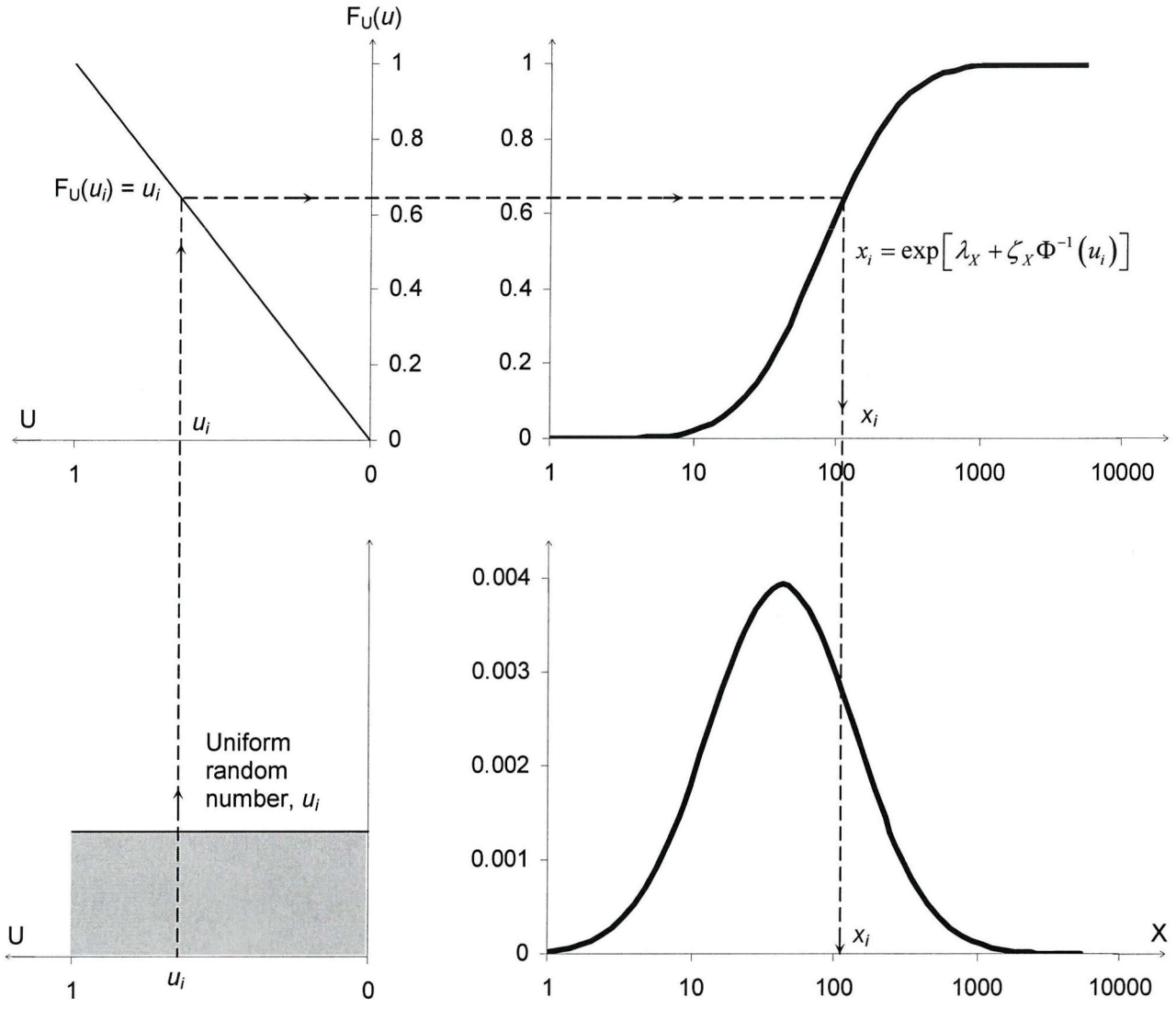

Figure 4.3: Mapping for simulation. The dashed line follows the progression of mapping uniformly distributed random numbers U to lognormally distributed random numbers X.

Alhough there are numerous studies that have determined the percentage porosity in cement specimens, the number of pores in a specimen is not reported (Jasty et al., 1990; Muller et al., 2002; Norman et al., 1995). However, the number of pores on the surface of experimental specimens was reported by Murphy and Prendergast (2001). By estimating the number of pores in the volume from these figures and assuming a linear relationship between porosity and volume, a mean number of pores and standard deviation could be determined for the tensile and 4-point bend models respectively (Table 4.1).

Using these values, the Monte Carlo simulation generated a number of pores for twenty tensile and twenty 4-point bend finite element models (see Figure 4.4). Once the number of pores was determined, they were randomly distributed throughout the finite element models. Each element was assigned a pseudorandom number (uniformly distributed from 0 to 1; RAND function). For n pores, the elements with the n greatest random numbers were selected and the stress concentrating effects of a pore applied as described on the next page.

	Murphy and Prendergast (2001)	Tensile test FE model	4-point bend FE model
Volume (mm^3)	896	11,700	9,600
Mean no. pores	99	1307	1281
Standard deviation	57	747	732

Table 4.1: Average number and standard deviation of pores in the finite element models.

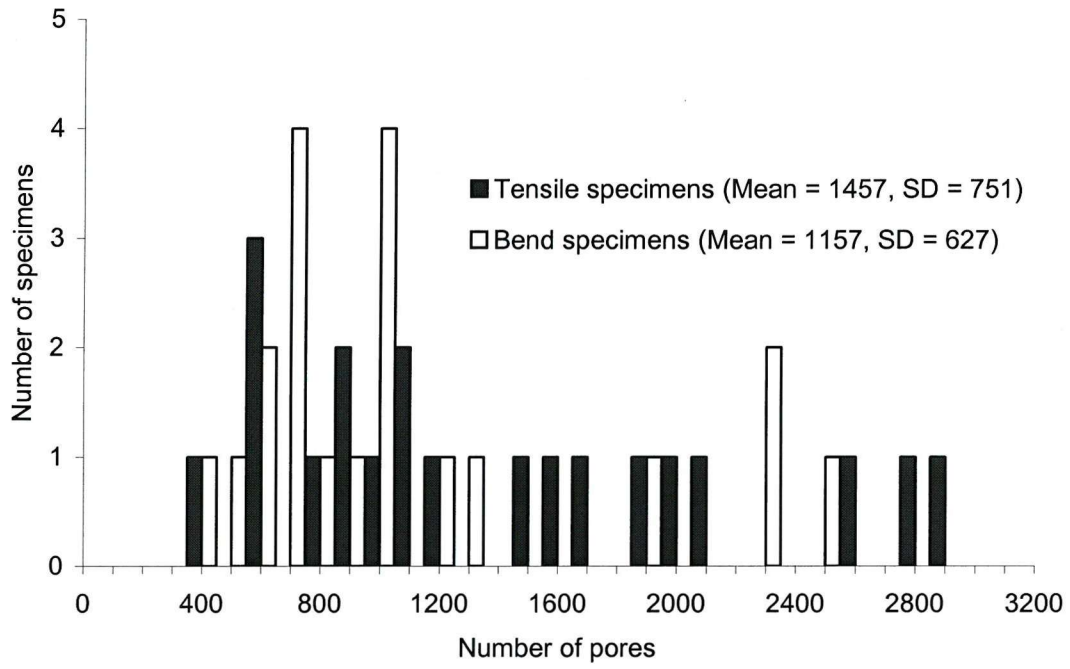

Figure 4.4: The number of pores simulated in the tensile and 4-point bend FE models. The sample mean and SD are given.

The theoretical elastic solution for a spherical pore in an infinite medium under remote stress was used to represent a pore in the finite element models. This theory was

developed by Timoshenko and Goodier (1970), and shows that the stresses at the surface of a pore (under the conditions described above) do not depend on pore size. Under a uniaxial stress, the stress concentration caused by a pore (σ_{max}) is defined as:

$$\sigma_{max} = \left(\frac{15\nu - 3}{2(7 - 5\nu)} \right) S \qquad \textbf{Equation 4.10}$$

where S is the maximum principal stress in a uniaxial stress field and ν the Poisson's ratio. Although Equation 4.10 is adequate for the simulations described in this chapter, for multi-axial stress states (further chapters) it requires modifying to:

$$\sigma_{max} = Max \begin{bmatrix} \sigma_{1max} = Max \begin{bmatrix} B\sigma_1 + A\sigma_2 + C\sigma_3 \\ B\sigma_1 + C\sigma_2 + A\sigma_3 \end{bmatrix} \\ \sigma_{2max} = Max \begin{bmatrix} A\sigma_1 + B\sigma_2 + C\sigma_3 \\ C\sigma_1 + B\sigma_2 + A\sigma_3 \end{bmatrix} \\ \sigma_{3max} = Max \begin{bmatrix} A\sigma_1 + C\sigma_2 + B\sigma_3 \\ C\sigma_1 + A\sigma_2 + B\sigma_3 \end{bmatrix} \end{bmatrix} \qquad \textbf{Equiation4.11}$$

where σ_1, σ_2 and σ_3 are the principal stresses and A, B and C are defined as:

$$A = \frac{-(3 + 15\nu)}{2(7 - 5\nu)};\ B = \frac{27 - 15\nu}{2(7 - 5\nu)};\ C = \frac{15 - 3\nu}{2(7 - 5\nu)} \qquad \textbf{Equation 4.12}$$

This method has been used previously to simulate pores in finite element studies (Harrigan and Harris, 1991; Harrigan et al., 1992; Lennon et al., 2003). Simulating pores in this manner has the limitation that the pore is much smaller than the region in which it is found. However, even if a pore of diameter d was located as close as $3d$ from a surface edge or another pore, the errors caused by this assumption are small, less than ~10% (Timoshenko and Goodier, 1970). For our purposes, the pore size is not defined, but is intrinsically linked to element size; bigger elements means bigger pores. Therefore, element size must be kept uniform for all meshes.

4.2.5 Fatigue simulation

Damage was simulated in the tensile test and 4-point bend models using a continuum damage mechanics approach, based on similar techniques employed by Verdonschot and Huiskes (1997) and Stolk et al. (2004). A damage scalar, d, was allocated to each element. At the beginning of the analysis, d was set to zero for all elements, meaning the cement was completely undamaged. While damage may occur continuously or otherwise in cement subject to fatigue loading, it is not necessary to simulate every loading cycle. To increase the efficiency of the analysis, an iterative solution procedure was employed, each iteration representing the action of tens to tens of thousands of loading cycles depending on the stress level in the elements. At the beginning of each iteration, the load was applied to the finite element model and the maximum tensile stress was calculated for each element by the solver. Based on this stress level, N_f was calculated for each element in the cement mantle using either equation 4.2 (equation 4.1 was only used for demonstration purposes, see Section 4.2.3, page 151), assuming no failure in compression (it should be noted that the computational method *always* uses data from uniaxial tension to calculate fatigue, regardless of the applied loadcase). The number of loading cycles simulated in each iteration (Δn) could then be determined, based on a predefined percentage (20%, found to be acceptable with a convergence study) of the lowest N_f of the elements in the mesh. Damage was incremented for each element according to the linear Palmgren-Miner rule: $\Delta d = \Delta n / N_f$, and added to the damage already accumulated (d) for each element. When $d \geq 0.9$, the element was deactivated (removed from the model) and the load transferred to the surrounding elements.

Cement creep was also included in the fatigue simulation. For an element with tensile maximum principal stress:

$$\log \varepsilon = A \log N + B \qquad \textbf{Equation 4.13}$$

where ε is the creep strain, N is number of load cycles and A and B are constants whose values are dependant on the stress level. In this case (from Chapter 3):

$$A = -0.13 \log(\sigma) + 0.42 \qquad \textbf{Equation 4.14a}$$

$$B = 3.12\log(\sigma) - 2.61$$ **Equation 4.14b**

For an element with compressive maximum principal stress:

$$\varepsilon_c = Cn^{b_0}10^{S\sigma}$$ **Equation 4.15**

where ε_c = compressive creep strain, C = 1.225e-5; b_0 = 0.314; S = 0.33; n is the number of cycles completed and σ is the stress level (Verdonschot and Huiskes, 1995). Creep strain values were returned to the FE solver at the end of each increment, along with a list of elements that were to be deactivated (those with $d \geq 0.9$). This marked the end of the iteration; the loads were applied again to begin the next iteration.

The fatigue simulation was checked for mesh dependency by simulating fatigue without pores for tensile and 4-point bend models. Doubling the number of elements in the mesh altered the predicted fatigue life by less than 3.5%. This was considered acceptable.

The finite element models underwent between 150 and 400 iterations before specimen failure (i.e. damage linking up such that a through specimen crack was formed). The time taken for the analysis was approximately 10mins for each tensile model (n=20) and 30mins for each 4-point bend model (n=20).

4.3 Results

4.3.1 Experimental results

There was considerable scatter in the results of the tensile fatigue tests (Figure 4.2); data had an R^2 correlation coefficient of 0.67. The 4-point bend tests produced less scatter than the tensile tests, with an R^2 value of 0.87 (Figure 4.5). In all specimens (tensile and 4-point bend), fracture originated from a critical defect, either a pore within the material, or a flaw on the surface.

4.3.2 Computational results

A good agreement was found between the 4-point bend S-N curve as predicted by the computational method and the experimental S-N curve (see Figure 4.5b). Figure 4.6 shows three failed finite element models at 35MPa, each with a different number of cycles to failure (due to the porosity distributions). The fracture site was different for each model, and damage was also generated in sites other than that of eventual failure, indicative of the damage accumulation failure process. Using a 2-parameter Weibull model (see Section 2.3.2, page 67 for method) the 4-point bend experimental and computational S-N data were compared (figure 4.7). The location of the two curves was similar; a 50% probability of survival to 1 million load cycles occurred at 15.6MPa and 17.2MPa for the experimental and computational data respectively. However, the shape of the curves was quite different – there was less variability with the FE/CDM data, which was manifest as a steeper Weibull curve.

There was also a degree of data scatter in the tensile finite element models (R^2=0.90), but not as much as observed experimentally (R^2=0.67). Figure 4.8 shows three different failed finite element models at 20MPa. The failure location was different for each model, and damage was also generated in sites other than eventual failure. Model A (3,564 cycles) had a short life compared to Model C (20,341 cycles). This was due to a couple of pores in close proximity in Model A, causing premature failure. This is reflected in the relatively low level of damage elsewhere in the specimen.

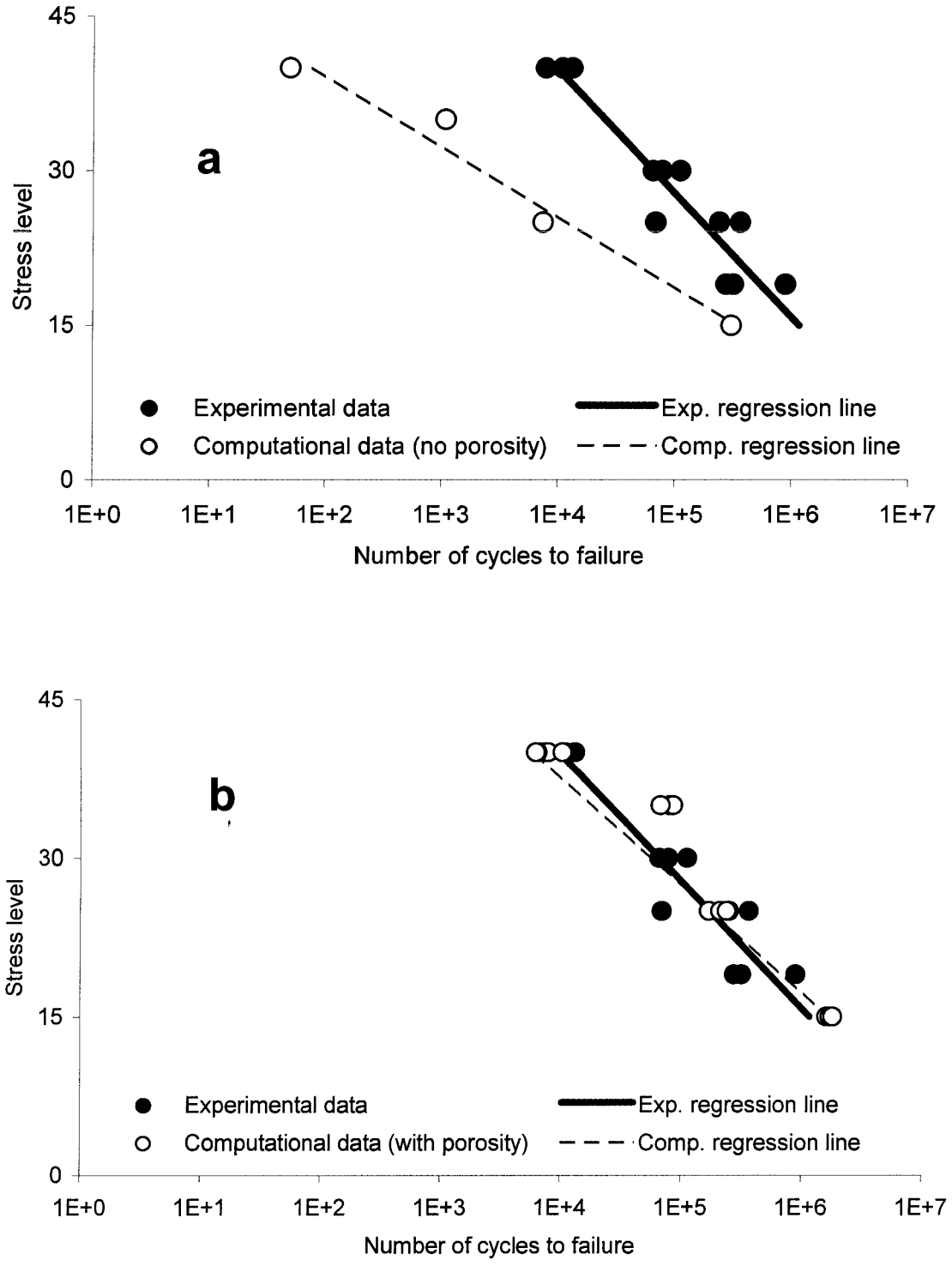

Figure 4.5: Stress versus number of cycles to failure for 4-point bend loading (a) *without* porosity and (b) *with* porosity simulated in the computational data. Regression lines plotted through average fatigue life at each stress level.

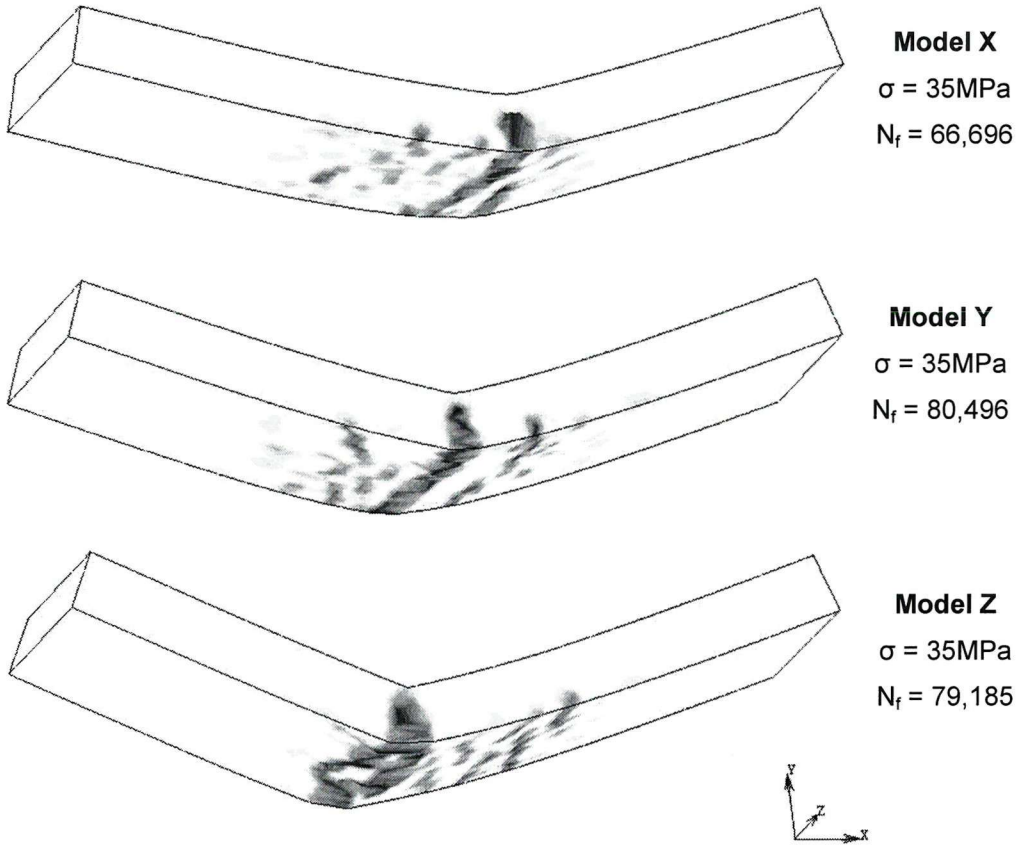

Figure 4.6: Damage in three different 4-point bend finite element models (with porosity) after failure (all tested at 35MPa). The damage accumulation failure scenario is apparent, with damage (dark regions) occurring at sites other than that of eventual failure. Element edges are not shown for the sake of clarity.

To check the hypothesis that porosity and element size must be considered to simulate non-uniaxial fatigue, the tensile and 4-point bend fatigue simulations were repeated in a similar manner to existing studies (Stolk et al., 2003; Verdonschot and Huiskes, 1997). Simulating fatigue in this manner generated good results for the tensile fatigue, but under-predicted fatigue life for the 4-point bend fatigue tests (Figures 4.3a & 4.5a). In addition, no data scatter was generated by this method; the results were deterministic.

4.4. Discussion

This study provides two improvements in the computational simulation of bone cement fatigue. Firstly, the computational method, driven by uniaxial fatigue data, was able to model the 4-point bending. This was only possible by including the effect of element volume and the influence of porosity in the models. Secondly, the computational method was capable of generating stochastic fatigue results, i.e. the pore distributions generated unique fatigue lives for each finite element model.

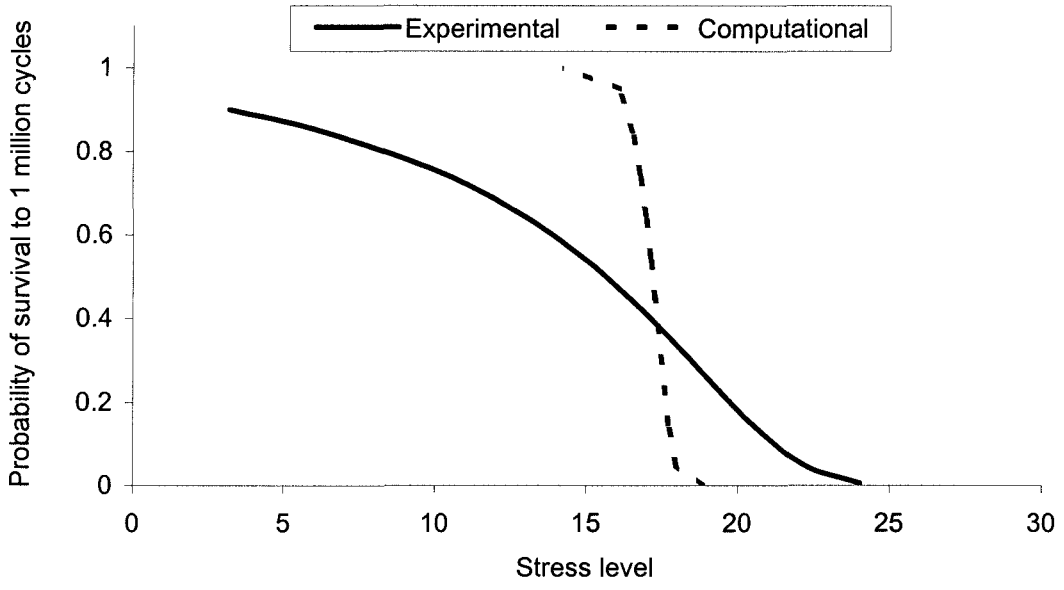

Figure 4.7: Experimental and computational probability of survival to 1 million load cycles (Weibull life) as a function of stress for the 4-point bend test.

In the experimental tests, the cement failed from a critical pore or defect in all specimens, but damage probably occurred around other less critical pores without causing failure (this is the basis of the damage accumulation failure scenario). The critical nature of porosity caused scatter in the fatigue data, to a greater extent with the tensile tests (R^2(tensile)= 0.67 vs. R^2(bend)=0.87), suggesting that the tensile test is more sensitive to porosity. Assuming failure by tensile stress only, a critical crack is not going to originate from above the neutral axis in the 4-point bend specimens. A critical pore may therefore be present in this region and not influence the fatigue life. With the tensile tests, a critical

flaw *anywhere* within the gauge section or the shoulders of the specimen could cause failure. This may explain the increased scatter in the tensile fatigue tests.

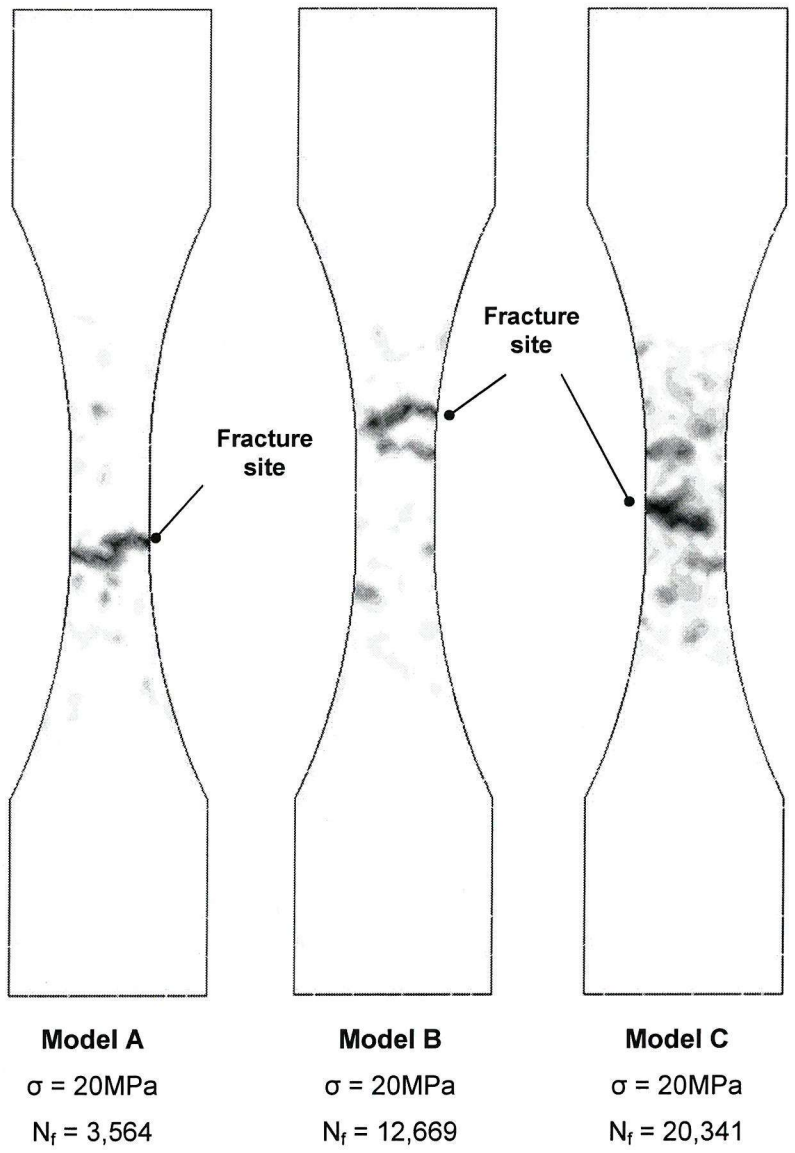

Figure 4.8: Damage in three different tensile test finite element models (with porosity) after failure (all tested at 20MPa). The number of cycles to failure and fracture site is different for each model. Element edges are not shown for the sake of clarity.

Including porosity in the finite element models had two effects. Firstly, the fracture site varied depending on the pore distribution (Figures 4.6 & 4.8), and in the tensile simulations there were even examples of specimens breaking outside the gauge length (Figure 4.8b). Damage was also evident at sites other than that of eventual failure

(Figures 4.6 & 4.8), thus providing a good representation of the damage accumulation scenario. Secondly, a degree of scatter in the fatigue life was generated due to the variability in number and distribution of pores. The best example of this was for the tensile fatigue finite element models at 20MPa, where the number of cycles to failure varied between 3,564 cycles and 20,341 cycles (see Figure 4.8).

There were a number of limitations with this study:

1. The number of pores in a volume of cement was estimated from the number observed on the surface (Murphy and Prendergast, 2001). The number of pores on the surface may not be representative of the internal porosity, as pores can be generated at the interface between cement and mould during specimen fabrication. This can be due to the difference in thermal properties of the polymerising cement and the mould. If this is the case, the finite element models in the current study overestimated the porosity distribution. Other porosity studies have presented results in terms of percentage volume rather than number of pores, making the results unsuitable for use here (Jasty et al., 1990; Muller et al., 2002; Norman et al., 1995).

2. The computational method deactivated (removes from model) elements to simulate damage. This method did not allow stress to be transferred in the plane normal to the crack, nor did it allow the transferral of compressive or shear stress upon crack closure. However, for the tests considered (tensile and 4-point bend) the case of stress transfer in the plane normal to the crack should not occur. More sophisticated anisotropic damage algorithms have been presented (Stolk et al., 2003; Stolk et al., 2004; Verdonschot and Huiskes, 1997), but the loadcases considered in this study would not take advantage of these. Regarding crack closure, Stolk et al. (2004) argued that the reversal of loads that cause crack closure are rare in a structure subject to constant amplitude loading conditions.

3. Pores are simulated as being located in an infinite volume. The method of simulating pores does not define a pore size, but simulates the stress concentration caused by a pore that is small in relation to its surroundings. The stress concentration caused by one of these pores drops to 5% of the maximum value at a distance of d from the pore centre, where d is the diameter of the pore

(Timoshenko and Goodier, 1970). Therefore, a pore can reside within an element, with a distance of d from the pore centre to the element edge and not introduce errors greater than 5%. Exceptions to this are elements (a) at the specimen edge or (b) adjacent to other pore containing elements. In these cases, a distance of $3d$ is required between (a) the pore centre and edge of specimen or (b) the centre of two adjacent pores to keep errors below 10% (Timoshenko and Goodier, 1970).

4. Only small pores are simulated. Although the pore size is not defined, pores are smaller than element volume. Large pores (approx diameter > 1mm) cause large scatter in experimental data (Prendergast et al., 2002), due to (a) the stress concentration generated by the pore and (b) the pore significantly reducing the cross sectional area of the test specimen. In this study, pore induced stress concentrations were simulated, but the absence of material associated with a pore or void was not considered. This may be an acceptable simulation for small pores, but means large pores were not modelled. There are two possible ways to approach this problem. Firstly, rejecting tensile test specimens with large pores would reduce the scatter of the experimental data, and *apparently* improve the computational scatter. This glosses over a limitation with the computational analysis and is perhaps inappropriate. A second approach is to simulate large pores in the FE models, by deleting clusters of elements. A distribution of large pores could be then superimposed on the existing pore distribution, with another Monte Carlo simulation. This would require more information regarding the distribution of pores with respect to pore size.

5. Differences in tensile and 4-point bend testing. Tensile tests were performed at 5Hz, while 4-point bend tests were performed at 2Hz. However, a recent study by Lewis *et al.* (2003) compared uniaxial tensile fatigue tests at 1Hz and 10Hz and found no statistical difference between fatigue lives due to high levels of variability. Another limitation was that the 4-point bend fatigue tests were performed at a higher stress level than the tensile fatigue tests. This was unavoidable, as specimens had to fail within a reasonable timeframe.

The issue of mesh dependency is important in a study such as this and can be divided into three criteria. Firstly, mesh dependency of the fatigue simulation, putting porosity aside –

when one element fails and is deleted, does the mesh density influence the damage accumulation process? This question was answered by simulating fatigue in models (tensile and 4-point bend) with twice the number of elements. The predicted fatigue lives were within 3.5%, which was considered acceptable.

The second mesh dependency criterion was related to element size and the derivation of Equation 4.2. Equation 4.2 was derived to give the theoretical S-N curve for tensile fatigue specimens the same size as the finite elements. Therefore Equation 4.2 represented S-N data for the element size used in the tensile test models only ($0.6mm^3$). The element size was the same for the 4-point bend models, but Equation 4.2 is not transferable to larger (or indeed smaller) elements (this was investigated with a convergence test). A new version of Equation 4.2 would be required for different sized elements.

The third mesh criteria deals with percentage porosity. Assuming a maximum pore size within each element according to the criteria detailed in limitation 3, the percentage porosity should not exceed that observed experimentally. For vacuum mixed cement, Dunne and Orr (2001) found percentage porosity of between 1.3% and 10.3% depending on the mixing device. In none of the finite element models (20x tensile, 20x 4-point bend) did the volume of *elements* containing pores exceed 15% specimen volume (and only 7 models exceeded 10%). Given that pore volume is smaller than element volume, the percentage porosity will be well within the values found by Dunne and Orr (2001). For a set number of pores, reducing the number of elements (increasing element size) would increase the volume of elements containing pores. If the pore size is scaled with the element size, there will be a limit where the percentage porosity exceeds that observed experimentally. There is therefore a critical limit for an acceptable mesh density, but the meshes in this study appear to be well within this limit.

Porosity plays a major role in the fatigue failure of bone cement. This is not only the case for experimental specimens, but for *in vitro* models of the implanted femur and also the cement mantle *in vivo*. In this study, we have demonstrated the simulation of porosity in simple structures, and the generation of stochastic fatigue results. The computational method was driven by uniaxial tensile fatigue, and was able to model this loadcase, and also the 4-point bend loadcase. The stresses in the 4-point bend are essentially uniaxial,

with shear stresses present, but minimal at the outer edges where failure initiated from. The multi-axial stress distribution in the *in vivo* cement mantle is more complex, and this must be considered when applying the method to more complex structures. However, the non-deterministic approach may allow further development of the fatigue simulations described by Stolk et al. (2004) and Verdonschot and Huiskes (1997).

4.5 Conclusions

Computational simulation of cement fatigue was performed for uniaxial tensile and 4-point bend fatigue loads. Good comparisons could be made with experimental tests. Pore distributions were included in the finite element models, which generated a degree of data scatter. There was variability in the predicted fatigue lives at any given stress level and location of fracture site.

4.6 References

Britton, J.R., Walsh, L.A. and Prendergast, P.J., 2003. Mechanical simulation of muscle loading on the proximal femur: Analysis of cemented femoral component migration with and without muscle loading. Clinical Biomechanics, 18: 637-646.

Davies, J.P., Burke, D.W., O'Connor, D.O. and Harris, W.H., 1987. Comparison of the fatigue characteristics of centrifuged and uncentrifuged simplex p-bone cement. Journal of Orthopaedic Research, 5(3): 366-371.

Dunne, N.J. and Orr, J.F., 2001. Influence of mixing techniques on the physical properties of acrylic bone cement. Biomaterials, 22(13): 1819-1826.

Haldar, A. and Mahadevan, S., 2000. Probability, reliability and statistical methods in engineering design. John Wiley & Sons Inc.

Harrigan, T.P. and Harris, W.H., 1991. A three dimensional non linear finite element study of the effect of cement-prosthesis debonding in cemented femoral total hip components. Journal of Biomechanics, 24(11): 1047-1058.

Harrigan, T.P., Kareh, J.A., Oconnor, D.O., Burke, D.W. and Harris, W.H., 1992. A finite-element study of the initiation of failure of fixation in cemented femoral total hip components. Journal of Orthopaedic Research, 10(1): 134-144.

James, S.P., Jasty, M., Davies, J., Piehler, H. and Harris, W.H., 1992. A fractographic investigation of PMMA bone-cement focusing on the relationship between porosity reduction and increased fatigue life. Journal of Biomedical Materials Research, 26(5): 651-662.

Jasty, M., Davies, J.P., O'Connor, D.O., Burke, D.W., Harrigan, T.P. and Harris, W.H., 1990. Porosity of various preparations of acrylic bone cements. Clinical Orthopaedics and Related Research(259): 122-129.

Jasty, M., Maloney, W.J., Bragdon, C.R., O'Connor, D.O., Haire, T. and Harris, W.H., 1991. The initiation of failure in cemented femoral components of hip arthroplasties. Journal of Bone and Joint Surgery-British Volume, 73(4): 551-558.

Lennon, A.B., McCormack, B.A.O. and Prendergast, P.J., 2003. The relationship between cement fatigue damage and implant surface finish in proximal femoral prostheses. Medical Engineering & Physics, 25: 833-841.

Lewis, G., Janna, S. and Carroll, M., 2003. Effect of test frequency on the *in vitro* fatigue life of acrylic bone cement. Biomaterials, 24(6): 1111-1117.

McCormack, B.A.O. and Prendergast, P.J., 1999. Microdamage accumulation in the cement layer of hip replacements under flexural loading. Journal of Biomechanics, 32(5): 467-475.

McCormack, B.A.O., Prendergast, P.J. and O'Dwyer, B., 1999. Fatigue of cemented hip replacements under torsional loads. Fatigue & Fracture of Engineering Materials & Structures, 22(1): 33-40.

Muller, S.D., Green, S.M. and McCaskie, A.W., 2002. The dynamic volume changes of polymerising PMMA bone cement. Acta Orthopaedica Scandinavica, 73(6): 684-687.

Murphy, B.P. and Prendergast, P.J., 2000. On the magnitude and variability of the fatigue strength of acrylic bone cement. International Journal of Fatigue, 22: 855-864.

Murphy, B.P. and Prendergast, P.J., 2001. The relationship between stress, porosity and nonlinear damage accumulation in acrylic bone cement. Journal of Biomedical Materials Research, 59: 646-654.

Norman, T.L., Kish, V., Blaha, J.D., Gruen, T.A. and Hustosky, K., 1995. Creep characteristics of hand-mixed and vacuum-mixed acrylic bone-cement at elevated stress levels. Journal of Biomedical Materials Research, 29(4): 495-501.

Prendergast, P.J., Murphy, B.P. and Taylor, D., 2002. Discarding specimens for fatigue testing of orthopaedic bone cement: A comment on Cristofolini et al. (2000) Fatigue & Fracture of Engineering Materials & Structures, 25(3): 315-316.

Roques, A., Browne, M., Thompson, J., Rowland, C. and Taylor, A., 2004. Investigation of fatigue crack growth in acrylic bone cement using the acoustic emission technique. Biomaterials, 25(5): 769-778.

Stolk, J., Maher, S.A., Verdonschot, N., Prendergast, P.J. and Huiskes, R., 2003. Can finite element models detect clinically inferior cemented hip implants? Clinical Orthopaedics and Related Research, 409: 138-150.

Stolk, J., Verdonschot, N., Murphy, B.P., Prendergast, P.J. and Huiskes, R., 2004. Finite element simulation of anisotropic damage accumulation and creep in acrylic bone cement. Engineering Fracture Mechanics, 71(4-6): 513-528.

Timoshenko, S.P. and Goodier, J.N., 1970. Theory of elasticity, 3rd edition. McGraw-Hill.

Topoleski, L.D.T., Ducheyne, P. and Cuckler, J.M., 1990. A fractographic analysis of *in vivo* poly(methylmethacrylate) bone-cement failure mechanisms. Journal of Biomedical Materials Research, 24(2): 135-154.

Verdonschot, N. and Huiskes, R., 1995. Dynamic creep-behaviour of acrylic bone-cement. Journal of Biomedical Materials Research, 29(5): 575-581.

Verdonschot, N. and Huiskes, R., 1997. The effects of cement-stem debonding in tha on the long-term failure probability of cement. Journal of Biomechanics, 30(8): 795-802.

CHAPTER 5

INITIAL STRESS AND THE LIFE OF THE CEMENT MANTLE IN TOTAL HIP REPLACEMENT[1]

Initial stress, in the form of residual stress can be found in the cement mantle of total hip replacement, as a result of shrinkage during the curing process. To investigate if this stress has implications on the fatigue of the cement mantle, a finite element model of the implanted proximal femur was developed, and an initial stress field simulated in the cement mantle by means of the thermal contraction. This stress field was generated such that the peak and average stresses were of similar magnitude to residual stresses measured experimentally. The long-term structural integrity of the cement mantle was assumed to be governed by damage accumulation, simulated in the finite element model using a continuum damage mechanics approach. The model was loaded to represent normal gait and damage and cement viscoelasticity were simulated in the cement. Damage accumulation was accelerated by a factor of 10 by including the initial stress, thus shortening the simulated life of the cement mantle considerably. It was also shown that cement creep was not capable of dissipating the stress field entirely. These findings suggest that residual stress *in vivo* may not be dissipated by creep and subsequently may accelerate fatigue cracking of the cement.

[1]Presented at the 1st International Congress on Computational Bioengineering, Zaragoza, Spain, 24th-26th September 2003.

5.1 Introduction

When the constituent parts of bone cement are mixed, the liquid methylmethacrylate (MMA) monomer is converted by free radical polymerisation to polymethylmethacrylate (PMMA). This process involves a density change as the liquid monomer converts to a polymer of higher density, resulting in shrinkage of the cement (Gilbert et al., 2000). The polymerisation process is also highly exothermic, and further shrinkage occurs as the cement cools (Orr et al., 2003). As the cement shrinks because of density and thermal changes, stress is 'locked' in the material. This 'locked-in' stress is known as residual stress and has been the subject of several studies in the literature.

Considering the residual stress field, specifically the orientation of stresses, Orr et al. (2003) demonstrated that the predominant residual stress in annular rings of cement was in the hoop direction, and of sufficient magnitude to cause cement cracking. Roques et al. (2004) measured cement residual stress with an instrumented stem, and also found the hoop stress to be dominant over the longitudinal stress. This was also found by Li et al (2003), who used the photoelastic technique to determine the residual stress in a ring of cement surrounding a hollow aluminium stem. Nuno and Cristofolini (2001) cured a cement mantle around a stem, and then removed the stem. There was a decrease in the inner cement mantle diameter after stem removal, indicating that hoop stresses were present at the stem/cement interface. Indeed further investigation of the stresses found that hoop stresses towards the stem/cement interface were the dominant stress.

The magnitude of the residual stresses has also been reported. Orr et al. (2003) calculated a hoop stress of 10MPa in annular rings of cement on a Morse taper mandrel, and this was thought to be a lower bound estimate. Roques et al. (2004) calculated a residual hoop stress of 9.8MPa in the cement mantle of simplified implanted femur models. Li et al (2003) reported a peak stress of 12MPa with the photoelastic method. Nuno and Cristofolini (2001) used the interference fit method and generated residual hoop stresses of between 10MPa and 15MPa at the stem/cement interface. These studies were all related to cement constrained by a metallic stem, but residual stress measurements have been made for unconstrained blocks of cement. Whelan et al. (2000) and Lennon et al. (2000) measured the strains in rectangular blocks of cement and calculated a peak stress

of 3.1MPa, lower than those discussed above, as the cement was not constrained by a metallic stem.

Residual stress has also been simulated in finite element studies. Mann et al (1991) simulated residual stress by cooling the cement mantle from a uniform peak temperature and found hoop stresses of 5MPa – 6MPa to be dominant in the cement mantle. More sophisticated methods of residual stress simulation have been presented, that assume the stress to be 'locked' in the material from some reference temperature. Lennon and Prendergast (2001) simulated residual stress in this way, and found good agreement between the simulated stress and experimental specimens, as the orientation of stresses (peak magnitude of 7MPa) in the finite element model were perpendicular to cracks visible in experimental specimens. In this computational analysis, the entire cement mantle reached its peak temperature within a time interval of 38 seconds, and complete polymerisation of the cement mantle occurred almost simultaneously. Li et al (2003) simulated residual stress in a similar manner to Lennon and Prendergast (2001), assuming stress locked in the material from the peak exotherm, and were able to generate similar a similar stress distribution to experimental specimens (in which residual stress was assessed with the photoelastic technique), with hoop stresses towards the stem/cement interface dominant.

It has been suggested that cement creep serves to reduce peak stresses in the cement mantle under fatigue loading (Lu and McKellop, 1997; Norman *et al.*, 2001; Verdonschot and Huiskes, 1997a). Total hip replacement patients usually have a period of rest before full loading of the reconstructed joint; this may allow creep to dissipate the residual stress in the cement. However, if the residual stress field is not dissipated, it may influence the fatigue life of the cement mantle. Computational simulations of cement mantle cracking have been presented (Stolk *et al.*, 2003; Verdonschot and Huiskes, 1997b), but these have not considered the residual stress that may be present in the cement.

The present study has two aims. The first is to investigate the ability of cement creep to dissipate an initial stress field (to represent residual stress) in the cement mantle of a finite element model. This can then be related to the ability of creep to dissipate residual stress *in vivo.* The second aim is to investigate the effect the initial stress field has on the damage accumulation process in the cement mantle under fatigue loading. This is a

simplified approach as the influence of pre-load cracking, caused by residual stress, is not considered. However, information regarding the influence of residual stress on *in vivo* cement mantle fatigue may be gained. Before the implanted femur model is considered, a mesh convergence study is performed on a simplified implanted femur geometry.

5.2 Materials and methods

5.2.1 Mesh Convergence

Six finite element meshes of a simplified implanted femur construct were generated using first order hexahedral and tetrahedral elements of different sizes (Figure 5.1). The meshes were classified according to the number of elements through the thickness of the cement mantle (Figure 5.2). The following values for Young's modulus and Poisson's ratio were used: stem 200GPa, 0.3; cement 2.8GPa, 0.3 and bone 15.5GPa, 0.28. The stem/cement interface was assumed perfectly bonded throughout the analysis. The distal nodes of the bone were built in to avoid rigid body movements, and a point load of 2100N applied to the proximal tip of the stem at an angle of 16° to its longitudinal axis. Damage accumulation was simulated in the cement mantle as described in Section 4.2.5 (page 157). The initial equivalent von Mises stress and damage as a function of time were compared for the different meshes.

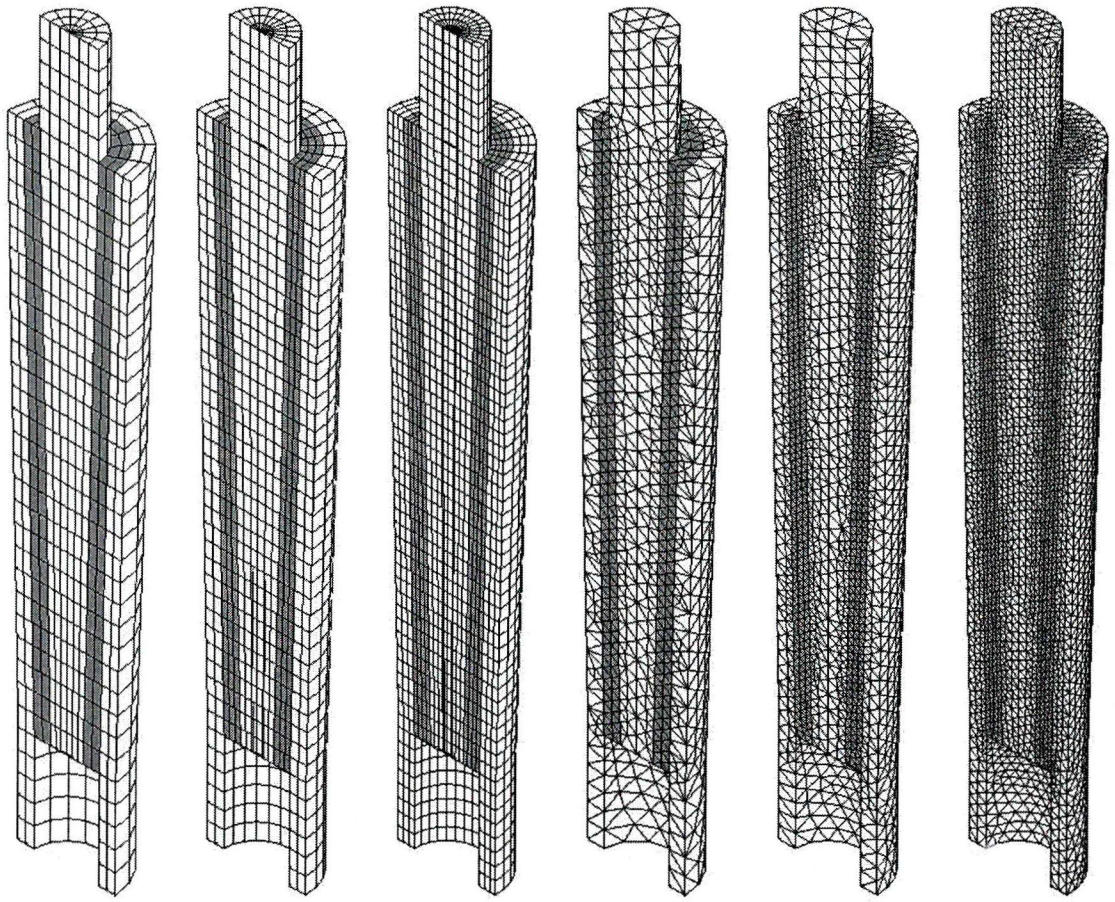

Figure 5.1: Six meshes used in the convergence study.

Figure 5.3 shows the initial von Mises stress in the cement mantle from the proximal end to the distal end measured at the middle of the cement mantle thickness. All meshes produced similar initial von Mises stress patterns. The damage accumulation as a function of loading cycles revealed the TET-2 mesh to have a significantly higher rate of damage accumulation to the others (Figure 5.4). The TET-2 mesh aside, there were similar damage patterns observed for all meshes.

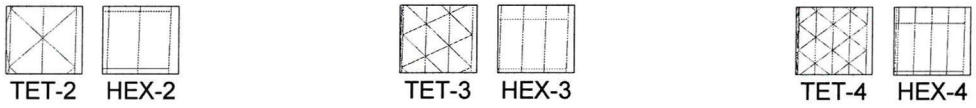

Figure 5.2: Cross sections of the cement mantle for each mesh.

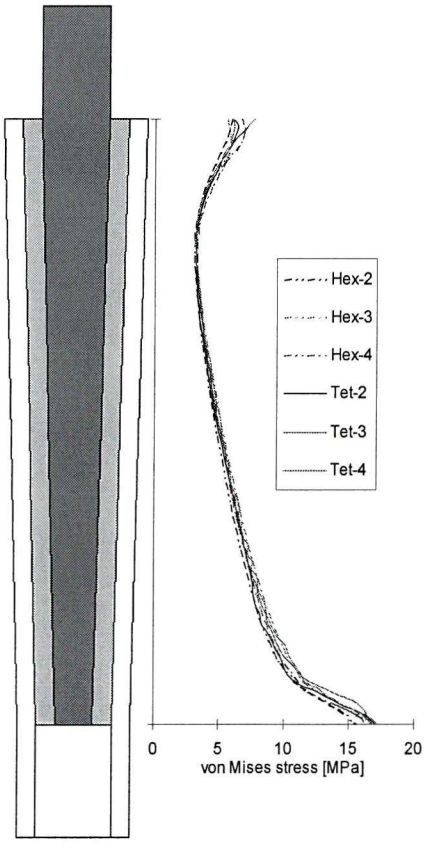

Figure 5.3: Initial von Mises stress in the cement mantle for the different meshes.

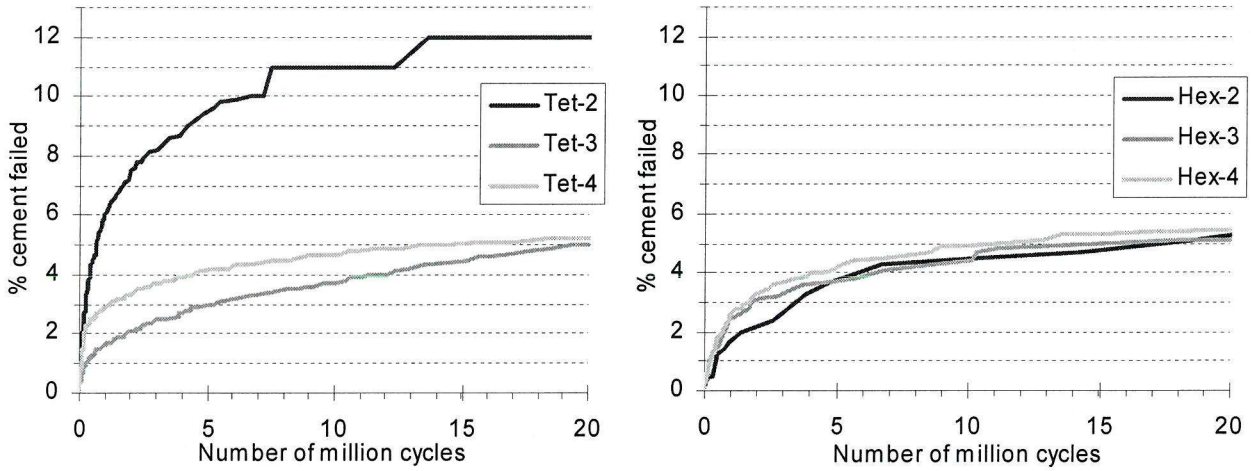

Figure 5.4: Damage as a function of loading cycles for the six different meshes.

For the geometry considered in this convergence analysis, there was no increased difficulty in generating the meshes with good quality hexahedral elements. For more complex geometries, ensuring good quality hexahedral meshes becomes more challenging. For this reason it is preferential to use tetrahedral meshing. The results of this convergence study demonstrate that a TET-3 mesh will generate similar results to meshes of higher refinement. The TET-3 mesh is therefore used in the following study of the implanted femur.

5.2.2 Implanted femur model and initial stress generation

The geometry for the femur was based on the '3rd generation composite femur' (Pacific Research Labs, Vashon Island, WA), and downloaded from the ISB mesh repository (Greer and Wang, 1999). The geometry for the femoral implant was generated using measurements taken from a Charnley Roundback 40 prosthesis (DePuy UK). A 4mm offset surface from the stem of the prosthesis was generated to create a uniform cement mantle. A uniform cement mantle, and the absence of cement below the stem tip (the Charnley is a tip-bearing stem) does not represent a specific clinical scenario, rather a generic implanted femur geometry. Using this geometry, the mesh was generated, using 4 node tetrahedral elements (Figure 5.5); there were 93,000 elements in the model, of which 36,500 were in the cement mantle. The Young's modulus and Poisson's ratio for the materials were as follows: implant, 220GPa and 0.3; cement, 2.8GPa and 0.3;

proximal cancellous bone, 750MPa and 0.28; distal cancellous bone, 5.0GPa and 0.28; cortical bone 15.5GPa and 0.28. The stem/cement interface was modelled as bonded throughout the analysis.

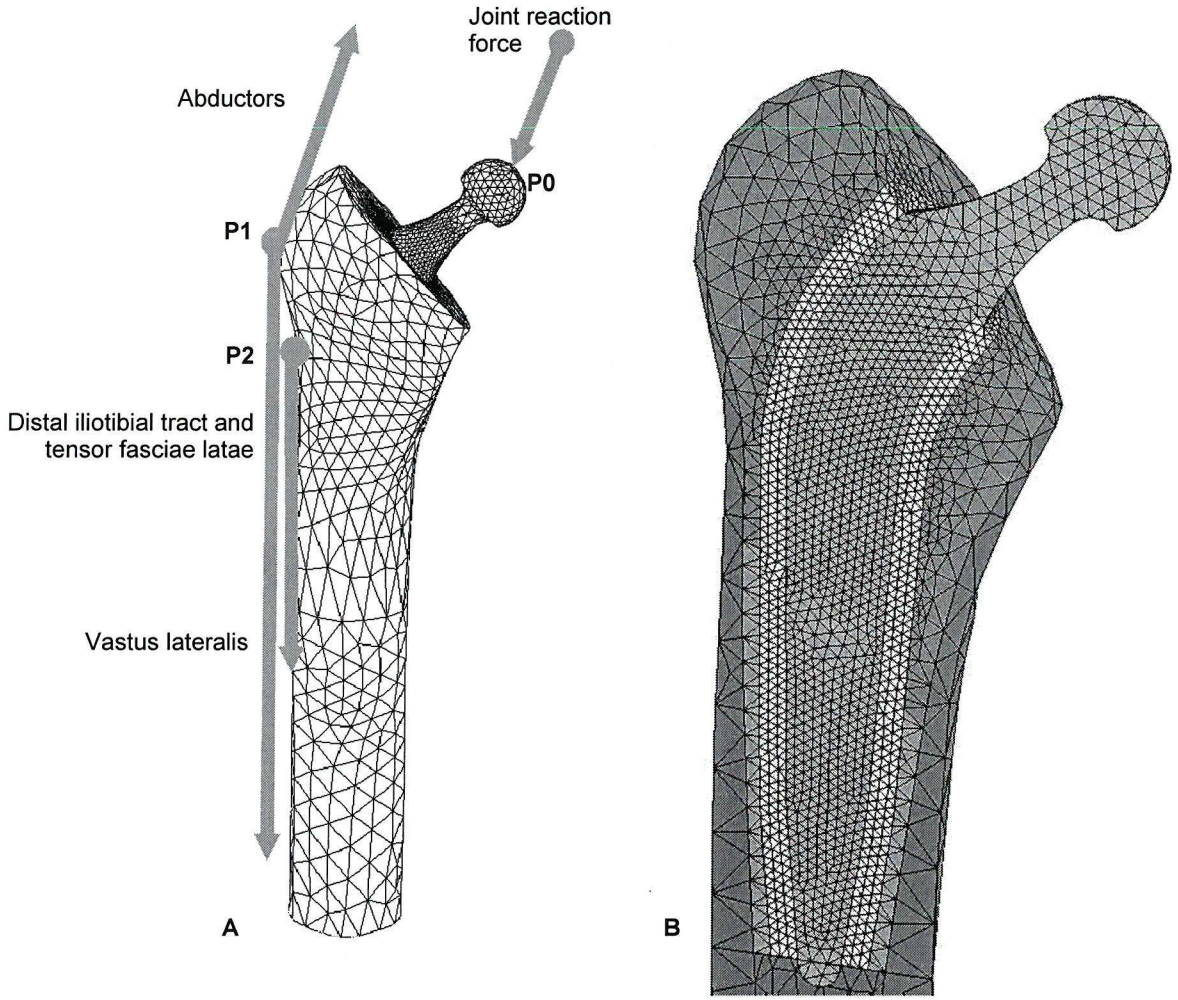

Figure 5.5: The finite element model showing (A) points of load application and (B) a cross-section in the frontal plane, with the cement mantle as white elements.

An initial stress field was generated in the cement, to represent a simplified residual stress field. The cement mantle was assigned a thermal expansion coefficient of 80×10^{-6}, while the rest of the model had a thermal expansion coefficient of zero. By cooling the cement mantle from 31°C to 20°C, a stress field was generated with peak magnitude of 9.6MPa, with over 99% of the cement volume at a stress level lower than 5MPa, and an average stress level of 3.2MPa (Figure 5.6). The peak magnitude (9.6MPa) was less than observed experimentally (Orr et al., 2003; Roques et al., 2004; Nuno and Cristofolini, 2001), and the mean stress level (3.2MPa) was in close agreement to that measured in

unconstrained blocks of cement (Whelan et al., 2000; Lennon et al., 2000). Throughout the cement mantle, the hoop stresses towards the stem/cement interface were dominant (figure 5.7), as the cement was constrained by the metallic stem. Thermal contraction has been used previously as a means to simulate residual stress (Mann et al., 1991).

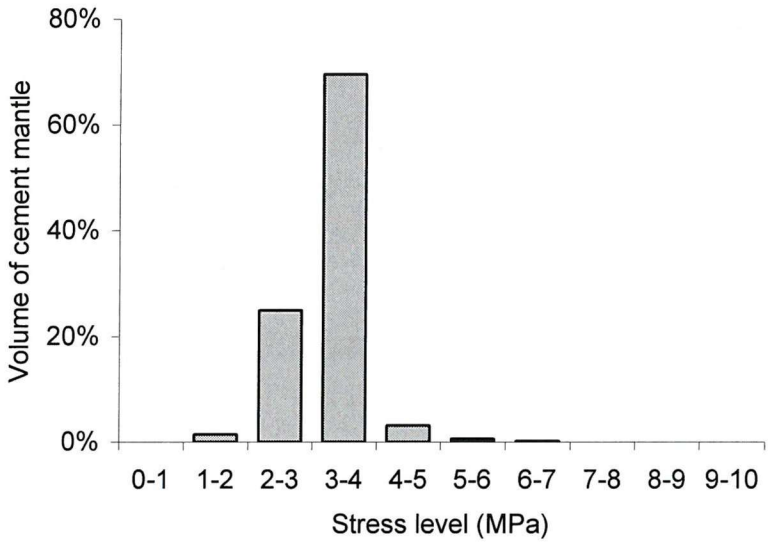

Figure 5.6: The residual stress distribution in the cement mantle. The height of each bar represents the volume of cement experiencing tensile stress within the corresponding stress range.

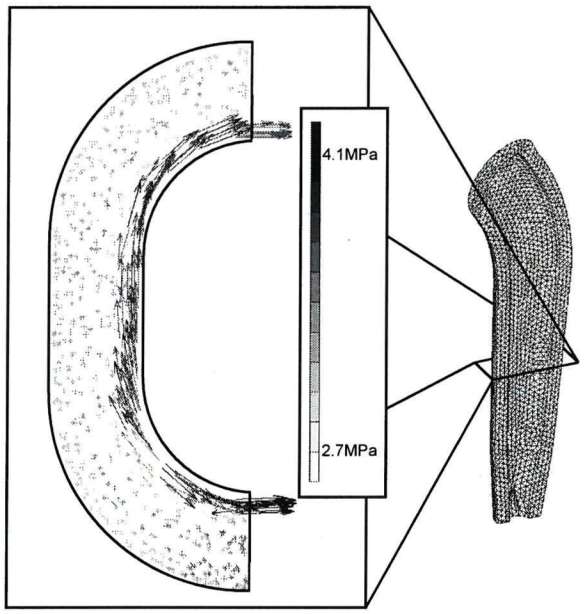

Figure 5.7: Cross-section of the cement mantle showing the direction of the maximum tensile stresses. Towards the stem/cement interface the maximum tensile stresses are in the hoop direction (black arrows). Towards the bone/cement interface, the maximum tensile stresses are in the longitudinal direction (grey crosses), and of lower magnitude than those in the hoop direction.

The model then had loads applied to simulate the stance phase of gait. The appropriate joint reaction force and muscular forces (abductor, proximal and distal tensor fascia lata and vastus lateralis) were taken from the HIP-98 CD-ROM (Bergmann, 2001), as described in Table 2.4 (page 24) and applied for a patient weighing 750N (Figure 5.5).

5.2.3 Simulating cement mantle damage accumulation

Damage accumulation was simulated in the cement mantle as has been described in Section 4.2.5 (page 157), but with a small modification to the method. The method described in chapter 4 calculated damage accumulation assuming an R-ratio (min load/max load) of 0.1. This was the case because the S-N curve used in the simulation algorithm was taken from fatigue tests where the R-ratio was 0.1 (see Chapter 3). When the initial stress field was included in the finite element model, the R-ratio was no longer 0.1. This was considered in the simulation algorithm by considering Goodman's rule:

$$\Delta\sigma_{\sigma m} = \Delta\sigma_0\left(1-\frac{\sigma_m}{\sigma_{TS}}\right) \qquad \textbf{Equation 5.1}$$

where $\Delta\sigma_m$ is the cyclic stress range for failure in N_f cycles under zero mean stress, and $\Delta\sigma_{\sigma m}$ is the same thing for a mean stress of σ_m, and σ_{TS} is the tensile strength of the material (Ashby and Jones, 1988). A graphical representation is shown in Figure 5.8.

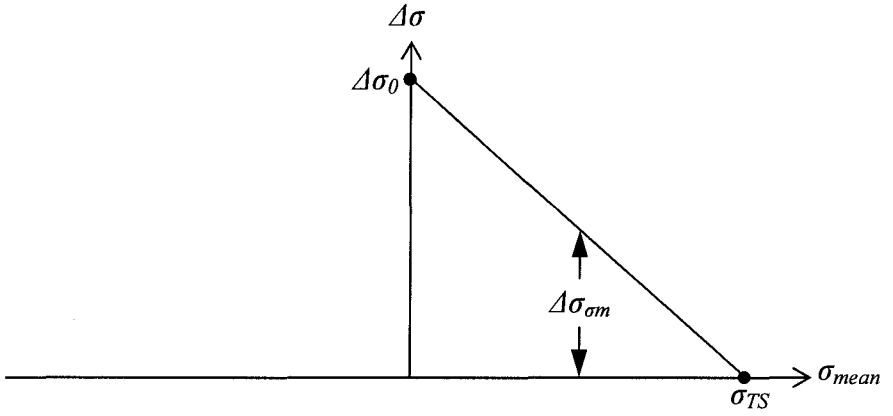

Figure 5.8: Goodman Curve.

Using a modified Goodman curve allows us to predict N_f at different values of σ_m and therefore different R-ratios. Consider a peak stress level of σ_{peak}. With no residual stress

and an R-ratio of 0.1, the mean stress level, $\sigma_{mean(r=0.1)}$, is $0.55(\sigma_{peak})$. For $\sigma_{mean(r=0.1)}$, the number of cycles to failure, $N_{f(r=0.1)}$, can be calculated from the S-N curve. Goodman's rule assumes that the fatigue life is zero cycles when the mean stress equals the tensile strength, σ_{TS}, of the material. These two data points allow a modified Goodman curve to be constructed (Figure 5.9).

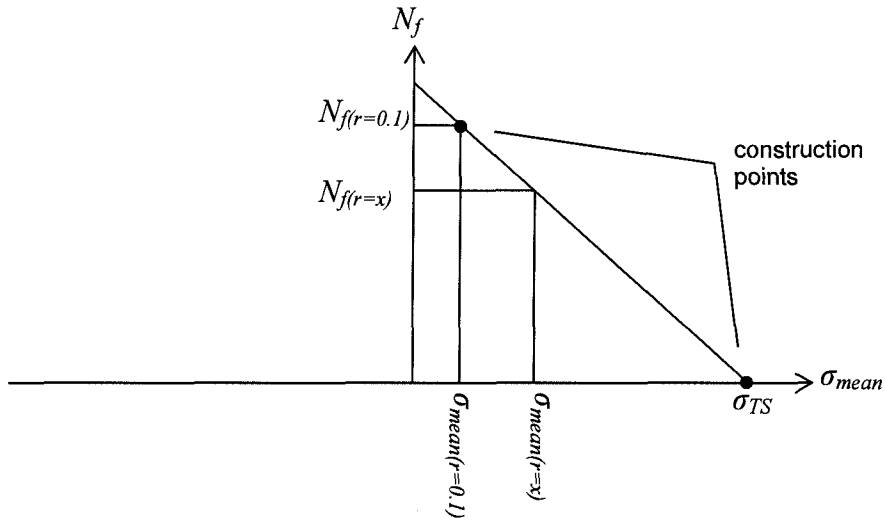

Figure 5.9: Modified Goodman curve.

The slope of the modified Goodman curve is:

$$m = \left(\frac{N_{f(r=0.1)}}{\sigma_{mean(r=0.1)} - \sigma_{TS}} \right) \qquad \textbf{Equation 5.2}$$

Now consider a peak stress level of σ_{peak}, but with a different R-ratio and therefore mean stress, $\sigma_{mean(r=x)}$. The corresponding $N_{f(r=x)}$ can be calculated as:

$$N_{f(r=x)} = N_{f(r=0.1)} \left(\frac{\sigma_{mean(r=x)} - \sigma_{TS}}{\sigma_{mean(r=0.1)} - \sigma_{TS}} \right) \qquad \textbf{Equation 5.3}$$

The computational algorithm for simulating fatigue was as described in Section 4.2.5 (page 157), but using Equation 5.3 to calculate the elemental fatigue life when the R-ratio was not 0.1.

To ascertain the ability of cement creep to dissipate the stress, a second analysis was performed, simulating the initial stress and creep without fatigue or applied load. All analyses performed used the same simulation techniques (for fatigue and creep) described in Chapter 4.

5.3 Results

5.3.1 The initial stress field

The volume of the cement mantle at a given stress level was investigated, from 0MPa to 10MPa in increments of 1MPa (Figure 5.6). For example, 69.5% of the cement mantle volume experienced a tensile stress level of between 3MPa and 4MPa. The peak stress in the cement mantle was set to be 9.6MPa, but over 99% of the cement mantle volume was at a stress level under 5MPa (figure 5.6). The mean stress within the cement was 3.2MPa.

A cross-section of the cement mantle revealed that the direction of the maximum tensile stress was not uniform through the thickness (Figure 5.7). Towards the implant/cement interface, the maximum tensile stress was in the hoop direction, while towards the bone/cement interface, the direction changed to the axial direction. The magnitude of stress in the hoop direction was greater than that in the axial direction. The peak value of hoop stress at this particular cross section was 4.1MPa.

5.3.2 The ability of creep to dissipate residual stress

Creep is known to create a more favourable stress distribution in the cement mantle by relaxing cement stresses (Lu and McKellop, 1997; Verdonschot and Huiskes, 1997a), but can this effect dissipate residual stresses to such an extent that they become insignificant? Simulating residual stress and creep without gait loading, the peak and average stress levels in the cement mantle were plotted as a function of time (Figure 5.10). The peak stress in the cement reduced from 9.6MPa to about 6MPa after a simulated year. The majority of stress reduction occurred within the first 20 days, and any further reduction was minimal. The average stress in the cement followed the same trend, dropping from 3.2MPa to 2.5MPa in the first 20 days, and only dropping a further 0.5MPa after a simulated year.

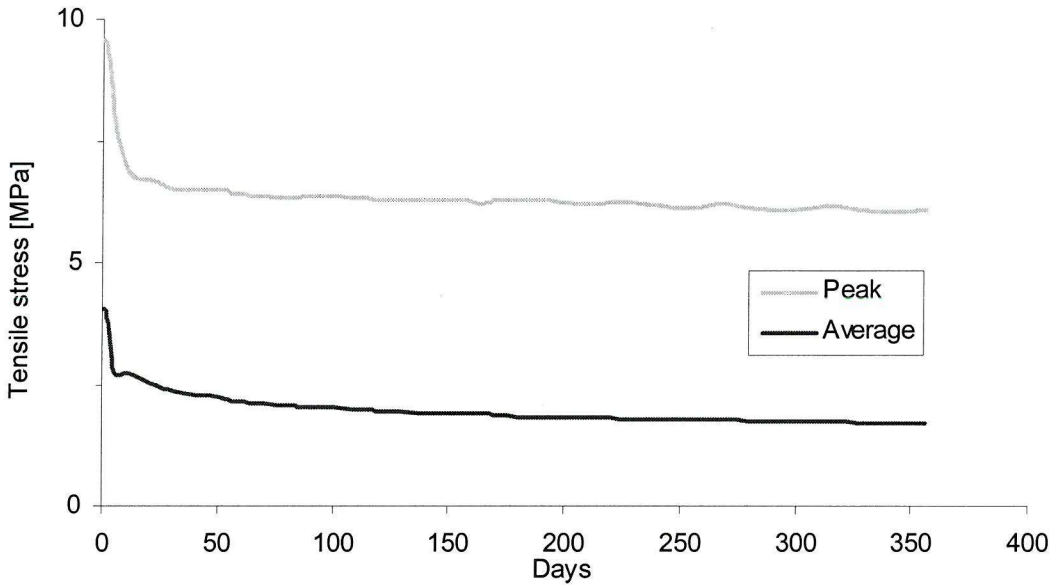

Figure 5.10: Peak and average tensile stresses in the cement mantle as a function of time, simulating initial stress and creep, without fatigue or applied load.

5.3.3 Initial stress and damage accumulation

Damage accumulation was simulated in the cement mantle, with and without the initial stress field, for $25x10^6$ load cycles. The cement mantle was inspected at several stages during loading (Figure 5.11), and the elevated rate of damage for the model that included the residual stress field was evident. For both models, damage occurred mostly towards the stem/cement interface at the distal end and progressed proximally. Including the initial stress caused damage to progress further proximally, and by $25x10^6$ load cycles damage was also observed at the proximal edge and lateral mid section of the cement mantle. The initial stress did not change the failure pattern; rather the timescale for failure was accelerated. The percentage volume of the cement mantle damaged was plotted against number of loading cycles (Figure 5.12). Including the initial stress field increased the damaged volume from approximately 1% to 10% after $25x10^6$ load cycles. At any point during loading, including the initial stress field increased the damage by approximately a factor of 10.

5.4 Discussion

The aim of this study was to investigate whether an initial stress field (to represent residual stress) influenced the damage accumulation process in the cement mantle of the implanted femur construct. The initial stress field generated in this study by thermal contraction from a uniform temperature was a simplified version of the residual stress field *in vivo*. *In vivo*, the cement reaches different peak temperatures depending on its proximity to the prosthesis/bone/exposed proximal surface. The resultant stress field may be influenced by these temperature gradients in the cement mantle, but are neglected in this study. Cement shrinkage occurs due to thermal shrinkage, but also shrinkage as the liquid monomer polymerises to a solid polymer. This phase-change shrinkage is also neglected in the current study, and indicates a further simplification of the residual stress field. It is noted that more sophisticated methods for simulating residual stress have been presented that consider the cure gradient in the cement mantle (Lennon and Prendergast, 2002).

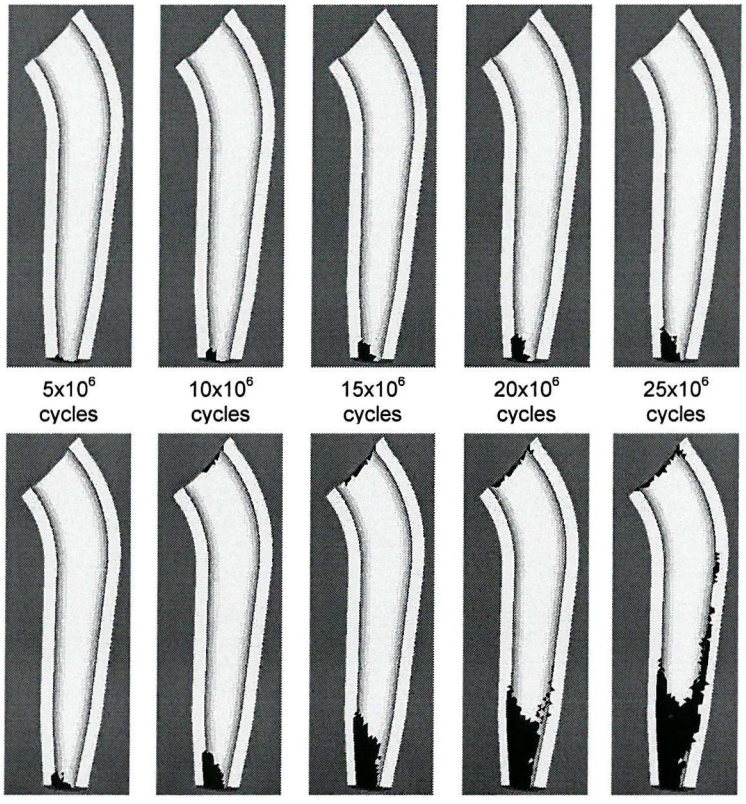

Figure 5.11: Damage accumulation in half the cement mantle over $25x10^6$ simulated load cycles for bone cement neglecting (top row) and including (bottom row) residual stress. Dark elements represent damaged cement. The number of loading cycles is common to both rows.

It was investigated whether cement creep could dissipate the initial stress field, and therefore dissipate residual stress *in vivo*. While the magnitude of the initial stress was reduced by creep, it was not dissipated entirely. The greatest reduction in stress occurred over the first twenty days or so; any reduction thereafter was negligible. It may therefore be that during the first 2-3 weeks after surgery, cement creep is reducing the residual stress field in the cement mantle *in vivo*, but will never dissipate it entirely.

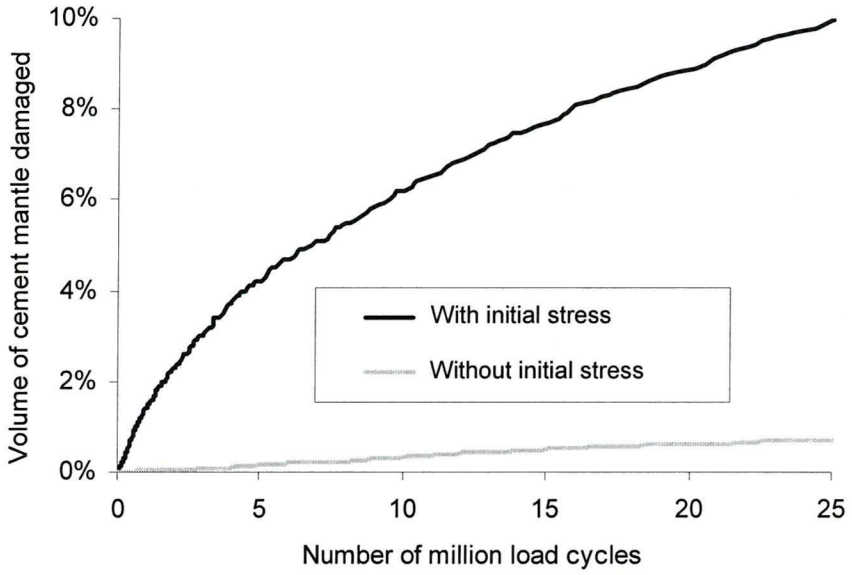

Figure 5.12: Damage accumulation in the cement mantle, represented by the volume of damaged cement as a function of load cycles.

The increased damage levels caused by the initial stress were evident from Figures 5.11 and 5.12. Although the initial stress simulated here was a simplification of residual stress *in vivo*, these results suggest *in vivo* residual stress may serve to accelerate the damage process. However, the action of pre-load cracking, caused by residual stress and not considered in the present study, may relieve the stresses to a certain extent. It may also be the case that residual stress induced pre-load cracking may not have a detrimental effect on cement mantle fatigue owing to the loading state experienced during gait; i.e. pre-load cracks caused by residual stress may reside in areas of low gait-load stress and not be exposed to the maximum principle stress direction.

Simulation of cement mantle damage accumulation has been performed by Stolk et al. (2003), who assessed the performance of two different prosthesis designs, and compared the results to *in vitro* models. The damage patterns in the computational models were found to be similar to those *in vitro*, but the computational models simulated $20x10^6$ load cycles; the *in vitro* models only simulated $2x10^6$ load cycles. No residual stress was simulated in the finite element models. The results of the current study suggest that an initial stress field serves to accelerate the damage accumulation, and may explain, at least partly, the under-prediction of damage by Stolk et al. (2003).

There were a number of limitations with this study; some of these, concerning the computational method, have been discussed in Section 4.4 (page 162) and are not repeated here. Others limitations, not encountered in chapter 4 include:

1. The computational method uses uniaxial data for simulating fatigue and creep, and has only been compared to experimental uniaxial tensile and 4-point bend fatigue tests. The multi-axial stress state in the current study is more complex than these, and the fatigue and creep behaviour for bone cement under multi-axial stress is likely to be different than under uniaxial stress (this was demonstrated by Murphy and Prendergast, 2003). This limitation must be considered when interpreting the data.

2. Stem/cement debonding is a process that begins early in the life of the reconstruction, and may progress until the entire interface is debonded (Jasty et al., 1991). The stem/cement interface in this study is modelled as completely bonded throughout the analysis, and neglects any effect debonding may have on the damage accumulation rate. A debonded stem has been shown to increase the stresses in the cement mantle, and therefore accelerate damage accumulation as modelled by computational simulation (Verdonschot and Huiskes, 1997b). However, experimental studies suggest pre-load damage caused by residual stress and porosity are more dominant causes of cement mantle damage (Lennon et al., 2003). Even if residual stress and porosity are more dominant, the debonded stem would result in different damage patterns within the cement mantle. For this reason, the damage patterns shown in Figure 5.11 do not fully represent cement damage observed *in vivo*. For more realistic simulation of *in vivo* damage patterns, it may be necessary to model the stem/cement interface as being completely unbonded. This interface criterion has been employed previously in

several finite element based studies (Lennon and Prendergast, 2001; Stolk et al., 2003; Verdonschot and Huiskes, 1997b).

3. The cement mantle in this study was considered to be completely free of pores and microcracks that are likely to be present *in vivo*. Chapter 4 demonstrated the importance of including porosity in the finite element models. This thesis does not present the work performed in chronological order; the current study was performed before the work described in Chapter 4.

The initial stress field simulated in the present study served to shorten the life of the cement mantle. Although it was a simplification of the *in vivo* residual stress, it suggests that residual stress may shorten the life of the cement mantle *in vivo*. Residual stress should therefore be considered, as an initial stress field or otherwise, when simulating fatigue of bone cement constrained by a metallic stem.

5.5 Conclusions

Cement creep reduced the magnitude of an applied initial stress field, but did not dissipate it entirely. Therefore, in spite of cement creep, the initial stress field in the cement mantle served to accelerate the damage accumulation process, suggesting that residual stress accelerates the damage accumulation process *in vivo*.

5.6 References

Ashby, M.F. and Jones, D.R.H., 1988. Engineering Materials 1: an inrtoduction to their properties and applications. Butterworth-Heinmann.

Bergmann, G.E., 2001. Hip98, loading of the hip joint. Published as a CD-ROM attachment to the Journal of Biomechanics: ISBN 3-9807848-0-0.

Gilbert, J.L., Hasenwinkel, J.M., Wixson, R.L. and Lautenschlager, E.P., 2000. A theoretical and experimental analysis of polymerization shrinkage of bone cement: A potential major source of porosity. Journal of Biomedical Materials Research, 52(1): 210-218.

Greer, B. and Wang, E.L., 1999. 3rd generation composite femur model. Available for download from: The ISB Finite Element Repository, Istituti Rizzoli, Bologna, Italy, http://www.cineca.it/hosted/LTM-IOR/back2net/index.html.

Jasty, M., Maloney, W.J., Bragdon, C.R., O'Connor, D.O., Haire, T. and Harris, W.H., 1991. The initiation of failure in cemented femoral components of hip arthroplasties. Journal of Bone and Joint Surgery-British Volume, 73(4): 551-558.

Lennon, A.B., McCormack, B.A.O. and Prendergast, P.J., 2003. The relationship between cement fatigue damage and implant surface finish in proximal femoral prostheses. Medical Engineering & Physics, 25: 833-841.

Lennon, A.B. and Prendergast, P.J., 2001. Evaluation of cement stresses in finite element analyses of cemented orthopaedic implants. Journal of Biomechanical Engineering, 123: 623-628.

Lennon, A.B. and Prendergast, P.J., 2002. Residual stress due to curing can initiate damage in porous bone cement: Experimental and theoretical evidence. Journal of Biomechanics, 35(3): 311-321.

Lennon, A.B., Prendergast, P.J., Whelan, M.P., Kenny, R.P. and Cavalli, C., 2000. Modelling of temperature history and residual stress generation due to curing in polymethylmethacrylate. In: Proceedings of the 12th conference of the European Society of Biomechanics, Dublin, Ireland.

Li, C., Wang, Y. and Mason, J., 2003. The effects of curing history on residual stress in bone cement during hip arthroplasty. Journal of Biomedical Material Research Part B: Applied Biomaterials, 70B(1): 30-36.

Lu, Z. and McKellop, H., 1997. Effects of cement creep on stem subsidence and stresses in the cement mantle of a total hip replacement. Journal of Biomaterials Research, 34(2): 221-226.

Mann, K.A., Bartel, D.L., Wright, T.M. and Ingraffea, A.R., 1991. Mechanical characteristics of the stem-cement interface. Journal of Orthopaedic Research, 9(6): 798-808.

Murphy, B.P. and Prendergast, P.J., 2003. Multi-axial fatigue failure of orthopaedic bone cement - experiments with tubular specimens. Journal of Materials Science-Materials in Medicine, 14(10): 857-861.

Norman, T.L., Thyagarajan, G., Saligrama, V.C., Gruen, T.A. and Blaha, J.D., 2001. Stem surface roughness alters creep induced subsidence and 'taper-lock' in a cemented femoral hip prosthesis. Journal of Biomechanics, 34(10): 1325-1333.

Nuno, N. and Cristofolini, L., 2001. Sensitivity analysis on the uncertainties of metal-PMMA interface characteristics. In: Proceedings of the 5th international symposium on computer methods in biomechanics and biomedical engineering. Gordon & Breach, London, pp. 63-68.

Orr, J.F., Dunne, N.J. and Quinn, J.C., 2003. Shrinkage stresses in bone cement. Biomaterials, 24: 2933-2940.

Roques, A., Browne, M., Taylor, A., New, A. and Baker, D., 2004. Quantitative measurement of the stresses induced during polymerisation of bone cement. Biomaterials, 25(18): 4415-4424.

Stolk, J., Maher, S.A., Verdonschot, N., Prendergast, P.J. and Huiskes, R., 2003. Can finite element models detect clinically inferior cemented hip implants? Clinical Orthopaedics and Related Research, 409: 138-150.

Verdonschot, N. and Huiskes, R., 1997a. Acrylic cement creeps but does not allow much subsidence of femoral stems. Journal of Bone and Joint Surgery-British Volume, 79(4): 665-9.

Verdonschot, N. and Huiskes, R., 1997b. The effects of cement-stem debonding in tha on the long-term failure probability of cement. Journal of Biomechanics, 30(8): 795-802.

Whelan, M.P., Kenny, R.P., Cavalli, C., Lennon, A.B. and Prendergast, P.J., 2000. Application of optical fibre Bragg grating sensors to the study of PMMA curing. In: Proceedings of the 12th conference of the European Society of Biomechanics, Dublin, Ireland.

CHAPTER 6

CEMENT MANTLE FATIGUE FAILURE: IN SILICO MODELS AND EXPERIMENTAL TESTS[1]

This chapter investigates the ability of the computational method to predict cement mantle fatigue failure for a simplified implanted femur model. Four *in vitro* specimens of a simplified implanted femur construct were created with an aluminium cortex, rigid polyurethane foam strips to model the cancellous bone, bone cement and a steel stem. Three of the steel stems had a polished finish, were debonded from and reinserted into the specimens prior to testing to ensure an unbonded interface. One of the steel stems had a grit blasted surface finish and was not debonded from the construct prior to testing to ensure a bonded interface. Experimental specimens were loaded to represent gait for $2x10^6$ cycles. Finite element models of the experimental specimens were generated, with stem/cement interface characteristics modelled as completely unbonded (n=3) and bonded (n=1). Porosity and initial stress were simulated in the models prior to simulated fatigue loading. Boundary conditions were applied to simulate the *in vitro* tests and fatigue and creep simulated in the cement mantle over $2x10^6$ load cycles. The predicted cement mantle fracture sites and stem inducible displacements generated by the finite element models were compared to those of the *in vitro* specimens. There was good agreement in fracture location and inducible displacement, demonstrating the capability of the computational method to model this structure.

[1]Presented at the 2005 ASME Summer Bioengineering Conference, Vail, Colorado, 22nd – 26th June, 2005.

6.1 Introduction

The total hip replacement should ideally remain functional for the lifetime of the patient, but unfortunately this is not always the case. A hip replacement is considered to have failed when it causes the patient pain, and requires a revision operation to relieve that pain. According to national hip register studies the most common cause of failure is aseptic loosening of the components (Herberts et al., 2002). There are a number of scenarios that can lead to component loosening; one of these is cracking of the cement mantle. Radiographic follow-up studies consider a cement mantle fracture a sign of definite component loosening (Harris et al., 1982). Inspection of ex vivo fracture surfaces has led to fatigue failure being proposed as a possible failure mechanism (Jasty et al., 1991; Stauffer, 1982; Topoleski et al., 1990).

These clinical observations have led to *in vitro* tests being developed to assess the cement mantle under a fatigue load. McCormack et al. (1999) developed an implanted femur model with a constant cross-section stem cemented into a tube with similar torsional rigidity as the diaphysis of the femur (Figure 2.21, page 51). A torsional fatigue load was applied to the stem and the cement mantle investigated by sectioning the specimen. A disadvantage of this model was that the cement mantle could only be assessed at the end of the test. This was overcome by McCormack and Prendergast (1999), who developed a layer based quasi 3-D model of the implanted femur to monitor cement damage (Figure 2.25, page 56). Windows in the model allowed dye-penetrant to be applied and surfaces to be analysed without sectioning. Lennon et al. (2003) developed the model to include an abductor force and was able to assess the damage accumulation in the cement with different stem surface finishes (Figure 2.26, page 57).

A method for predicting the long-term *in vivo* resistance to prosthesis loosening was proposed by Maher and Prendergast (2002), based on the inducible displacement of the prosthesis. Inducible displacement was defined as the displacement recovered when the prosthesis was unloaded. Two different prostheses were considered – the Lubinus SPII and the Müller curved stem. Of these two, the Lubinus SPII has the superior clinical performance, i.e. increased resistance to loosening. By monitoring inducible displacement of the stem during a fatigue cycle, Maher and Prendergast (2002) observed that the magnitude of inducible displacement *decreased* as loading progressed for the

Lubinus SPII and *increased* for the Müller prosthesis. This led the authors to propose that a prosthesis that exhibits increasing inducible displacement may be prone to early loosening, as the Müller stem was found to be. Lennon et al. (2003) also provided evidence for using inducible displacement as a measure for discriminating between prosthesis designs. Damage was monitored in the cement mantle of *in vitro* implanted femur models, and a correlation was found with stem inducible displacement (Figure 2.26, page 57).

Simulating the damage in the cement mantle has been performed previously, and the effects of stem surface finish and prosthesis design investigated (Verdonschot and Huiskes, 1997; Stolk *et al*, 2003). Using a continuum damage mechanics approach, Stolk *et al.* (2003) were able to rank prostheses according to their performance in the Swedish Hip register. However, the cement mantles in these studies did not include the effects of pores, voids or other defects. From *in vitro* testing, these defects have been observed to be critical in terms of cement fatigue (see Section 2.2.5, page 51). In Chapter 4, using a similar *in silico* method to Stolk *et al* (2003), the effects of pores/defects were included in the computational analysis. The aim of the present study is to apply the same method to models of the implanted femur, and compare the results to experimental tests. The experimental model used in this study is based on that of Lennon *et al* (2003), with bonded (grit blasted) and unbonded (polished) stem/cement interfaces. Different interfaces are considered to test the computational method and not to determine which is superior in clinical practice. Further analysis is performed by comparing the inducible displacements (as described above) of the models with experimental data.

6.2 Materials and methods

6.2.1 Physical model

The physical model consisted of a steel stem fixed in an aluminium femur with acrylic bone cement. The aluminium femur consisted of a back and front cover, which fitted together to enclose the stem and cement. This was based on a similar model developed by Lennon et al. (2003), and had a similar second moment of area measured at the mid section of the stem (25,000mm^4). Cancellous bone was modelled with 3mm solid rigid polyurethane foam strips (Sawbones Europe AB, Sweden), fixed to the aluminium with cyanoacrylate adhesive. Windows in the side of the aluminium femur model allowed visualisation of the cement during fatigue loading. The stem geometry was taken from measurements of a Charnley prosthesis (DePuy, UK). Clamping the stem in position left a uniform 5mm cavity for the bone cement. The bone cement (CMW-1, DePuy CMW, UK) was vacuum mixed as per manufacturers instructions, and injected into the cement cavity from the distal end. This was performed with the top aluminium cover removed, and a polyethylene (PE) sheet with steel backing plate covering the cement cavity. Specimens were left to cure overnight. Once cured, the PE sheet was removed, the stem removed from the cement mantle, grease applied to the sides in contact with the aluminium, and replaced in the cement mantle. This ensured a fully unbonded stem/cement interface, and minimal friction between stem and aluminium. The front aluminium cover was put on the specimens before testing. Three such specimens were built (Figure 6.1).

One further specimen was generated, to simulate a bonded stem/cement interface. This was achieved as described above, but with a grit blasted femoral stem and without removing the stem from the cement.

6.2.1 Mechanical testing

A load horse was designed to allow a joint reaction force of 2.5kN to be applied at 10° to the vertical, and an abductor force of 1.5kN at an angle of 15° to the vertical. This corresponds to 3.5 times bodyweight loading (assuming bodyweight equal to 700N), and was similar to the loading used by Lennon et al. (2003). To determine the dimensions

necessary to allow application of these loads, a simple model of the load horse was drawn (Figure 6.1). The back leg of the horse was connected to the body via a pin at an angle of 15° to the vertical. The back leg was not included in Figure 6.1, but the loads transferred through it (R_C) were included at point C. The load (P) was to be applied at point A, with the joint reaction force (R_B) acting at point B.

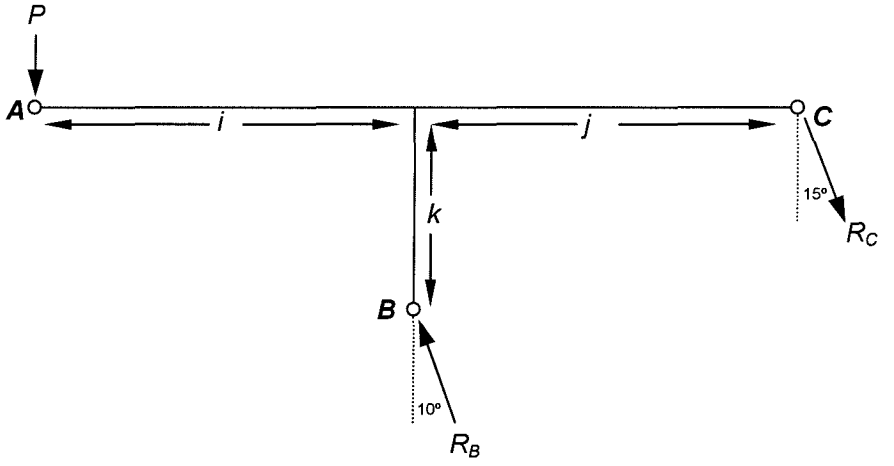

Figure 6.1: Load horse schematic for design.

Resolving the required joint reaction force and abductor force into x and y components gives:

$$R_{Bx} = 0.4kN \quad R_{By} = 2.5kN$$

$$R_{Cx} = 0.4kN \quad R_{Cy} = 1.5kN$$

Balancing vertical forces:

$$\Sigma F_V = 0: \qquad P + R_{Cy} = R_{By} \qquad \textbf{Equation 6.1}$$

Substituting values for R_{Cy} and R_{By} gives P=1kN. Taking moments about B:

$$\Sigma M_B = 0: \qquad iP = jR_{Cy} + kR_{Cx} \qquad \textbf{Equation 6.2}$$

There are geometrical constraints to the model. The back leg of the horse must have the required angle (15° to the vertical), and the front leg must be above the femoral head. Choosing values for j and k allows distance i to be calculated. Defining j=40mm requires k=32mm. Substituting values for j, k, P, R_{Cy} and R_{Cx} gives i=73mm.

A compressive load was applied to the head of the horse via a roller to ensure no bending moment at the point of load application (Figure 6.2). This load was applied sinusoidally for 2 million cycles, at an R-ratio of 0.1 and a frequency of 5Hz. Testing was performed in air at room temperature.

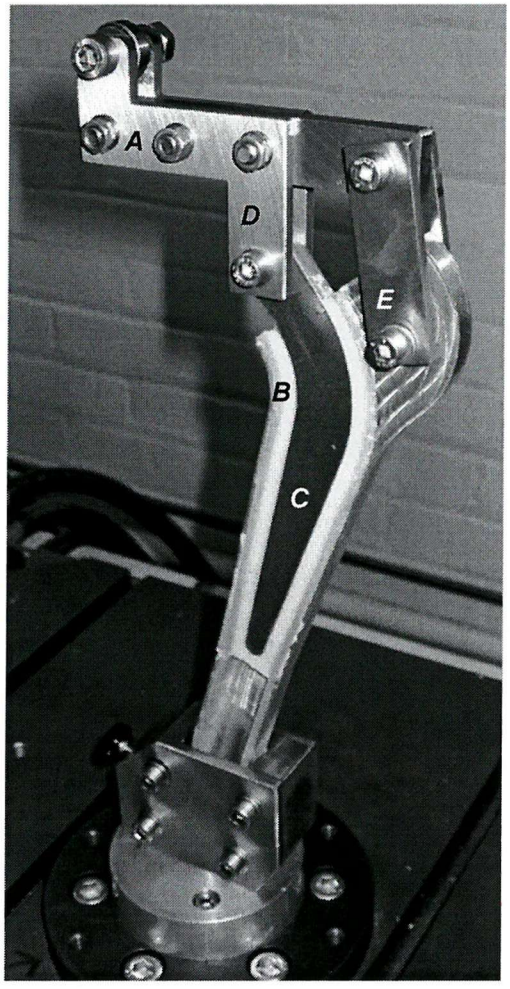

Figure 6.2: Experimental model fixed in testing machine with the front cover removed and the following labels: (A) load horse, (B) cement mantle, (C) stem, (D) joint reaction force point of application and (E) abductor force point of application.

6.2.3 Computational analysis

Four finite element models of the physical model were generated (Figure 6.3). Each consisted of 27,500 tetrahedral elements, 9,200 of which were in the cement mantle. The volume of the cement mantle was 5,800mm^3, giving an average element volume of 0.6mm^3. The material properties used in the finite element models are given in Table 6.1. A number of pores was generated for each finite element model using a Monte Carlo simulation, and distributed randomly throughout the cement mantle. Pores were then simulated using the theoretical elastic solution for a spherical cavity in an infinite medium subject to a remote load, as described in section 4.2.4, page 151. An initial stress distribution was also simulated, of similar magnitude to residual stress measured experimentally, as described in section 5.2.2, page 176. Boundary conditions were applied to replicate the experimental models, and two million loading cycles were simulated. Cement fatigue and creep were simulated using the continuum damage mechanics approach described in Section 4.2.5 (page 157) (using Equation 4.2 in the fatigue algorithm, as the elements in the cement mantle were of the same size as the elements in Chapter 4). Three models simulated an unbonded interface with a coefficient of friction of 0.25; one model simulated a bonded interface.

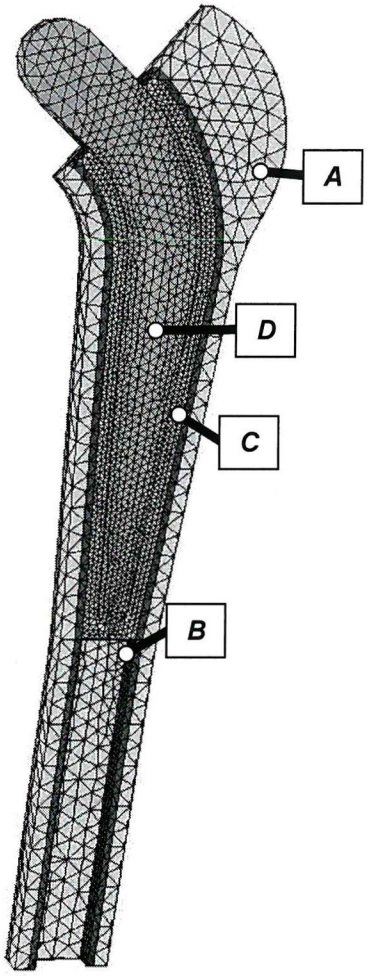

Figure 6.3 The finite element model, identifying (A) aluminium, (B) polyurethane foam, (C) bone cement and (D) steel.

Material	Young's modulus (GPa)	Poisson's ratio
Steel	240.0	0.3
Aluminium	73.0	0.3
Polyurethane foam	2.0	0.28
Cement	2.4	0.3

Table 6.1: Material properties used in the finite element models.

6.3 Results

6.3.1 Mechanical testing

Complete cement mantle fractures occurred in all three unbonded specimens at the distal end of the stem. Fractures occurred between approximately 500 and 100,000 cycles. In two cases the cement fractured at the medial and lateral sides (Figure 6.4a&c), but in one case fractured at the lateral side only (Figure 6.4). Further inspection revealed that, in this specimen, the cyanoacrylate adhesive bonding the cancellous bone substitute to the aluminium had failed, leading to migration of the medial cement rather than fracture at the distal end. Other specimens did not exhibit this failure. For the bonded (grit blasted) stem/cement interface, no cement mantle fractures were observed anywhere in the cement mantle (Figure 6.5).

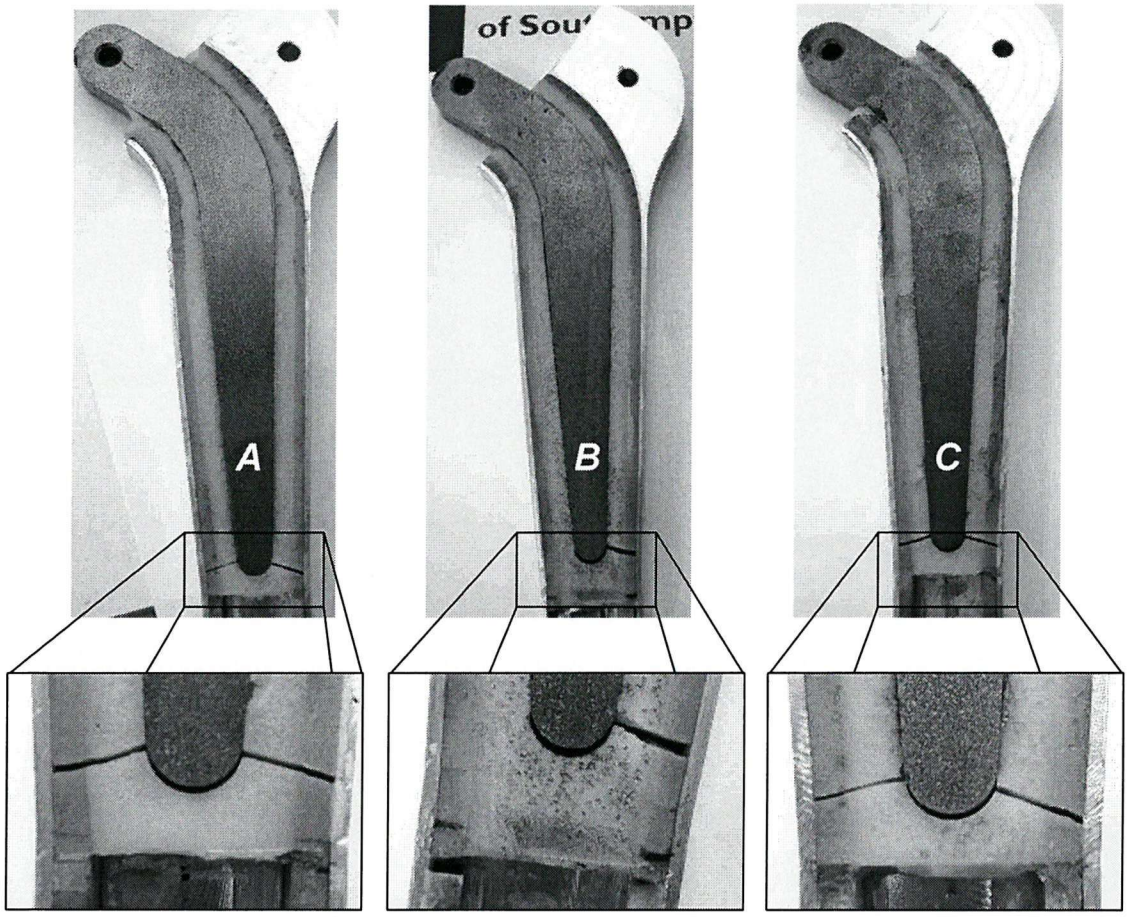

Figure 6.4 Cement mantle fractures in three different specimens after 2 million load cycles (unbonded interface).

6.3.2 Computational analysis

After 2 million simulated load cycles, all three unbonded models had complete cement mantle fractures at the distal tip of the prosthesis on the medial and lateral side (Figure 6.6. In addition, one model had a complete cement mantle fracture in the proximo-medial cement (circled in Figure 6.6a). The fractures at the distal end of the stem were in a similar location to the experimental specimens, and occurred between 10 and 1,000 load cycles. The inducible displacement (displacement recovered when load is removed) was plotted as a function of load cycles, and compared to experimental data (Figure 6.7). Once again, there was a good agreement between the computational and experimental data. One computational specimen experienced a jump in inducible displacement from 1mm to 0.8mm at about 1 million load cycles. This was due to the proximo-medial cement mantle fracture, circled in Figure 6.6a). For the unbonded case, no complete cement mantle fractures were generated, which agreed nicely with the experimental results (Figure 6.5). Inducible displacement for the bonded analysis was of a similar magnitude to the unbonded analyses (bonded inducible displacement magnitude: computational 0.88mm, experimental 0.75-0.80mm) and remained relatively constant throughout the fatigue loading.

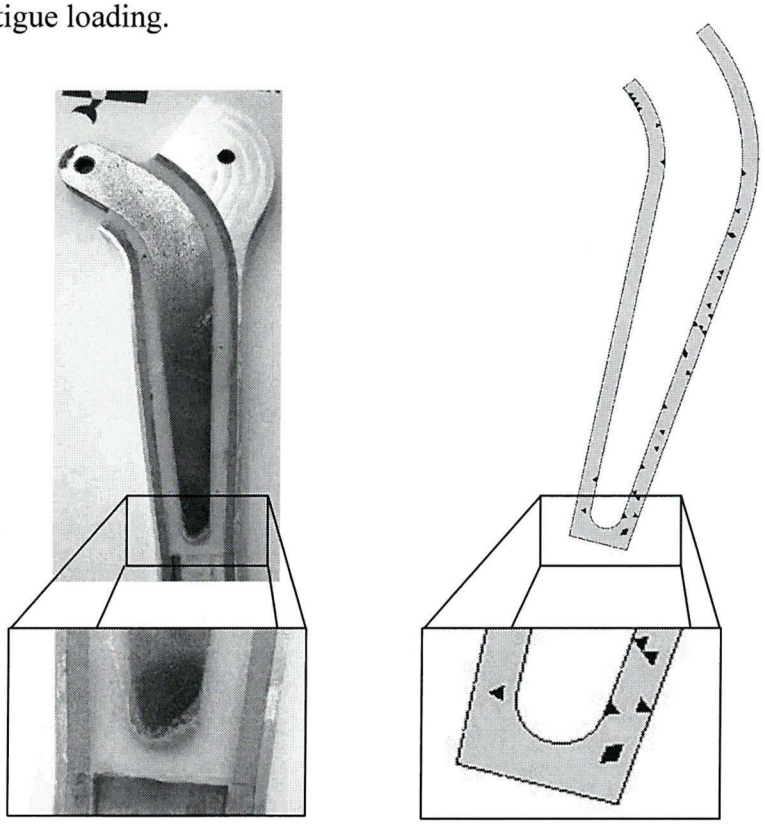

Figure 6.5 Experimental and computational damage in cement mantle after 2 million cycles (bonded stem/cement interface).

6.4 Discussion

The computational damage simulation, developed in Chapter 4 was successfully applied to the implanted femur model in this chapter. Correlations could be drawn between the computational and experimental results – a positive sign for the numerical method. However, although the model was more complex than the structures discussed in Chapter 4, the *in vitro* model employed dictated that cement stresses would not be representative of the triaxial conditions of a 3-D implant construct. As has been discussed previously in Chapter 4, cement fatigue under multi-axial stress may be different to that under uniaxial stress (Murphy and Prendergast, 2003).

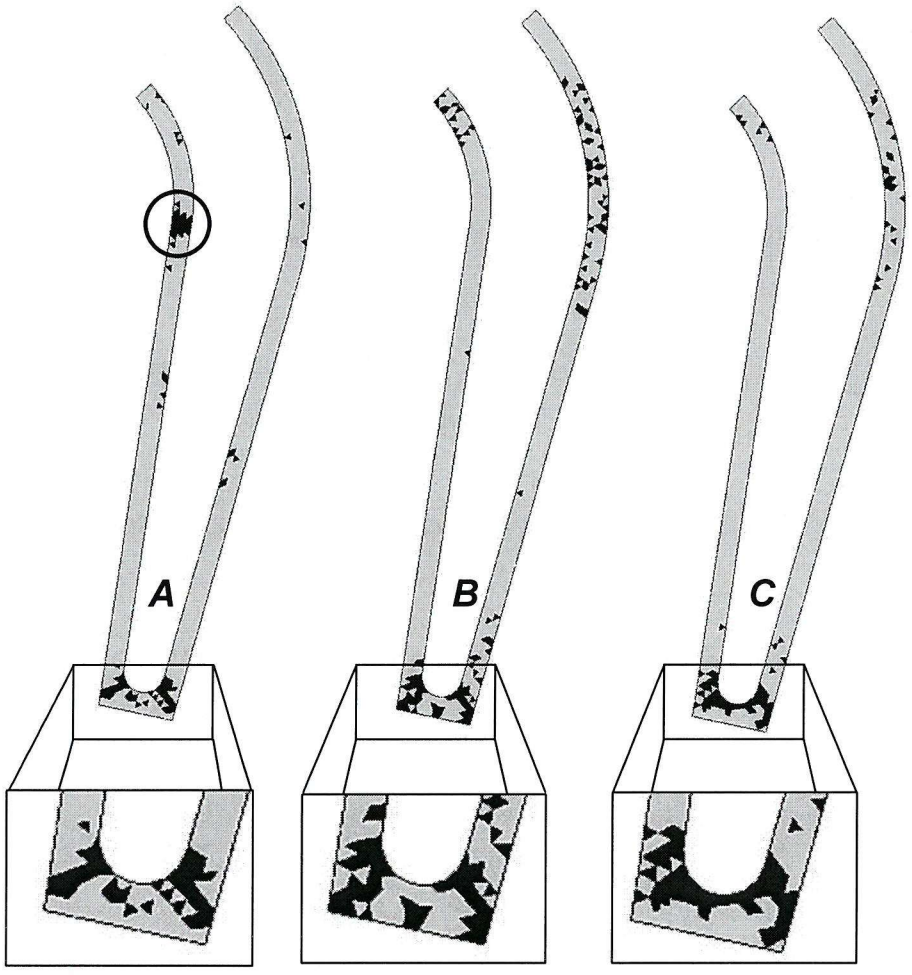

Figure 6.6: Damage in the cement mantle after 2 million load cycles as predicted by the computational method (unbonded interface). Proximo-medial fracture is circled in (a).

The locations of cement mantle fractures were well predicted by the computational method. For the unbonded interface, each finite element model predicted failure at the distal tip of the stem, on both the medial and lateral side (Figure 6.6). This was observed in two of the experimental specimens (Figures 6.4a & 6.4c). The third experimental specimen (Figure 6.4b) only had a cement fracture on the lateral side. This was due to debonding of the polyurethane foam/aluminium interface, causing subsidence of the medial cement mantle rather than fracture of the cement. The finite element models made no provision for debonding of this interface. This specimen also had a thicker distal cement pedestal than the other specimens (and the finite element models), which may have contributed to the foam/aluminium debonding.

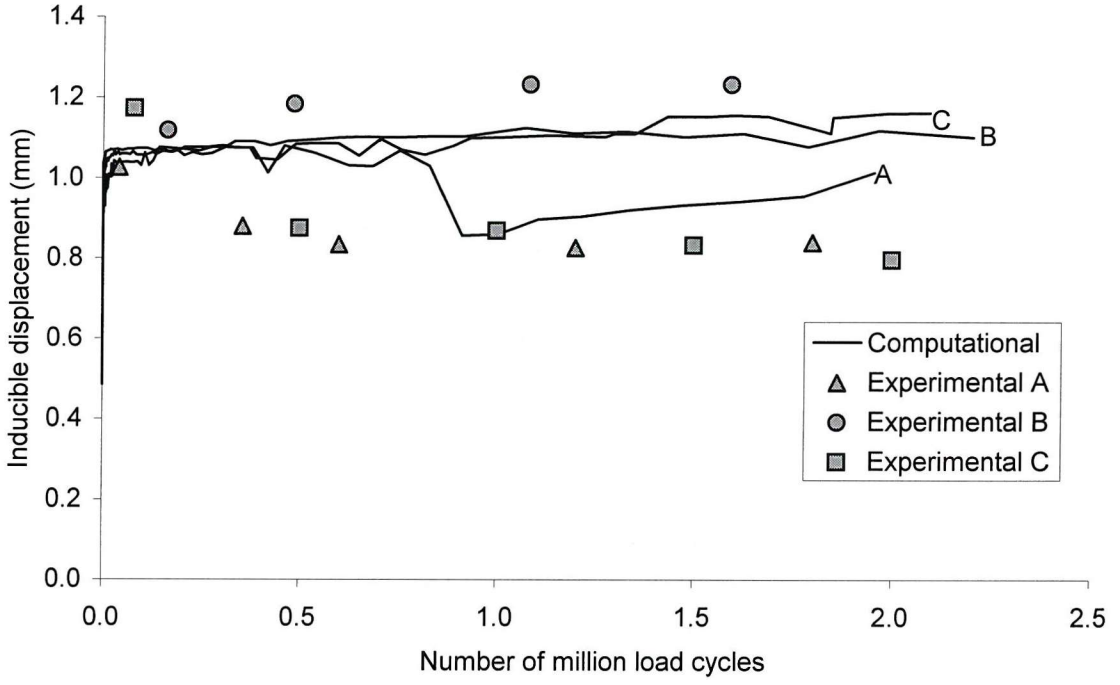

Figure 6.7: Experimental and computational inducible displacement as a function of time.

In each of the finite element models, distal cement fracture originated at the stem/cement interface and progressed towards the bone/cement interface. There also appeared to be a characteristic angle of fracture to the axis of the stem. This was particularly apparent in Figure 6.6b. A similar angle of fracture to the axis of the femoral stem could be observed in the experimental models (Figure 6.4). Inspection of these fracture surfaces revealed evidence of fatigue failure, originating at the stem/cement interface.

In addition to good fracture location prediction, the computational method predicted inducible displacement reasonably well (Figure 6.7). Inducible displacement is the displacement recovered when the load is removed, and has been suggested as a means to assess implant designs (Maher and Prendergast, 2002). The inducible displacement remained relatively constant throughout the analysis (both computational and experimental), between 0.8mm and 1.2mm. One finite element model experienced a jump in inducible displacement at about 1 million cycles (see Figure 6.7). This was caused by a cement mantle fracture in the proximo-medial cement (Figure 6.6a, circled). Lennon et al. (2003) predict this region and the corresponding region on the lateral side to have increased stress when porosity is considered. Inspection of this fracture area in the proximo-medial cement revealed a high localised pore density, which was not present in the other finite element models (Figure 6.8). This model also had the least number of pores, demonstrating that the pore distribution is equally important to the number of pores in the material. This is a good illustration of the stochastic nature of this study, where the results are influenced by the random probability of pores in the cement. Similar findings, i.e. that simulating the stochastic nature of porosity represents experimental models better than the deterministic approach, were presented at a recent conference in the Netherlands by Lennon et al. (2004).

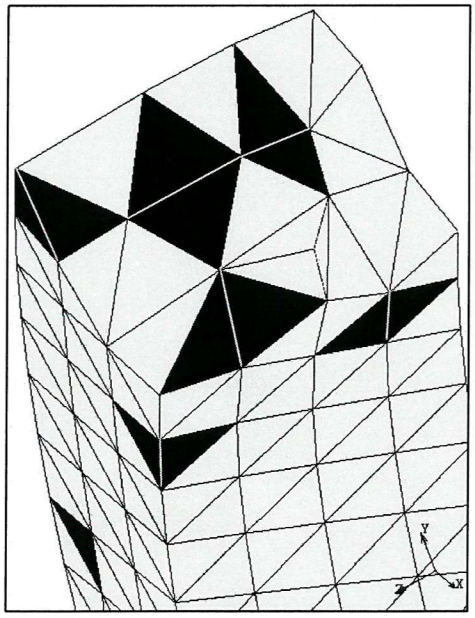

Figure 6.8: Cross section of cement mantle at fracture in the proximo-medial cement (Figure 6.5a). Image shows the elements simulating pores in this location (dark elements).

The bonded stem/cement interface was included to check the computational method, not to ascertain the merits of a smooth or polished stem finish. The cement mantle remained intact in the experimental specimen (grit blasted stem), and this correlated well with the corresponding finite element model. Damage was generated in the finite element cement mantle, but critical fractures were absent (Figure 6.5). The computational method also predicted similar inducible displacement to the experimental model, similar to the unbonded cases, between 0.8 and 1.2mm.

The experimental specimens in the current study were based on those developed by Lennon et al. (2003), so results should be comparable. In the current study, the magnitudes of inducible displacement at the end of the tests (both computational and experimental) were between 0.8mm and 1.2mm (see Figure 6.7). Lennon et al. (2003) reported inducible displacements of between 0.8mm and 1.2mm after 2 million cycles. Also reported by Lennon et al. (2003) was a tendency of increased damage levels for the polished stem (compared to the grit blasted stems). The computational predictions in the current study agreed with these findings (Figures 6.5 & 6.6). In the present study, increased damage levels in the proximo-lateral cement were generally found for the unbonded cases compared to the bonded case (Figure 6.4 & 6.5). A stress analysis of the structure was performed by Lennon et al. (2004), and it was shown that the proximo-lateral area was more susceptible to damage in the unbonded case. The computationally predicted levels of damage in the present study were generally lower than reported by Lennon et al. (2004),possibly due to different cement preparation methods. The present study used vacuum mixed radiopaque cement, while Lennon et al. (2004) used hand mixed radiolucent (without $BaSO_4$ particles, to allow dye-penetrant analysis) cement. Radiolucent and hand-mixed cements have been shown to have inferior fatigue properties than radiopaque and vacuum mixed cements (Molino and Topoleski, 1996; Murphy and Prendergast, 2000). This may explain the increased levels of damage observed by Lennon et al. (2004).

There were a number of limitations with this study. The limitations with using the initial stress to simulate residual stress have been discussed previously (Chapter 4), as have limitations with the porosity simulation and the damage algorithm (Chapter 3). A limitation exclusive to this study is that the experimental testing took place in air, at room temperature. The characteristics of the cement (CMW-1), i.e. creep and fatigue, were

recorded in water at 37°C. Temperature and environment have been shown to influence both creep and fatigue (Lee et al., 2002; Roques, 2004), such that the simulated fatigue and creep behaviour may have been different to the experimental specimens. Another limitation is that the stress field in this study is simple compared to that *in vivo*. The stress distribution was essentially uniaxial, and the loading configuration simplified compared to *in vivo* conditions. A final limitation was that the experimental cement mantles were only assessed at the end of the fatigue loading. Complete cement mantle fractures were clearly visible, and damage elsewhere in the cement mantle was not visible, but may indeed have been present. The acoustic emission technique, discussed in Chapter 3, has been used to monitor polymerising cement in a simplified implanted femur construct (Roques et al. 2004), and could be developed to monitor cement damage in the current specimens.

Including pore/void distributions in each finite element models led to a degree of variability in the predicted damage levels (evident in Figure 6.6). However the time for distal cement fracture (10-1,000 load cycles) was lower than the experimental specimens (500-100,000 cycles). This may have been due to an over representation of pores in the finite element models. There is definitely a limitation in the method used to determine the number of pores in a given volume. A recent study, using microtomography, may provide a more robust means of determining the number of pores in a given volume (Sinnett-Jones *et al.*, 2004).

6.5 Conclusions

The *in silico* method, developed in Chapter 4 was successfully applied to an implanted femur model. The predicted fracture sites were in good agreement with experimental observations. Inducible displacement was also monitored throughout the tests, and correlation could be drawn between the computational and experimental data.

The *in silico* method was also able to model the cement mantle of a fully bonded cement/stem interface. This was notably different to the unbonded cases.

Including a unique pore distribution in each finite element model generated stochastic results, which allowed for a degree of data scatter in the computational results, although not to the extent of the experimental observations.

6.6 References

Harris, W.H., McCarthy, J.C. and O'Neill, D.A., 1982. Femoral component loosening using contemporary techniques of femoral cement fixation. Journal of Bone and Joint Surgery-American Volume, 64(7): 1063-1067.

Herberts, P., Malchau, H., Garellick, G., Soderman, P. and Eisler, T., 2002. Prognosis of total hip replacement, Goteborg University, http://www.jru.orthop.gu.se.

Jasty, M., Maloney, W.J., Bragdon, C.R., O'Connor, D.O., Haire, T. and Harris, W.H., 1991. The initiation of failure in cemented femoral components of hip arthroplasties. Journal of Bone and Joint Surgery-British Volume, 73(4): 551-558.

Lee, A.J.C., Ling, R.S.M., Gheduzzi, S., Simon, J.P. and Renfro, R.J., 2002. Factors affecting the mechanical and viscoelastic properties of acrylic bone cement. Journal of Materials Science-Materials in Medicine, 13(8): 723-733.

Lennon, A.B., McCormack, B.A.O. and Prendergast, P.J., 2003. The relationship between cement fatigue damage and implant surface finish in proximal femoral prostheses. Medical Engineering & Physics, 25: 833-841.

Lennon, A.B., McCormack, B.A.O. and Prendergast, P.J., 2004. Implications of acrylic bone cement porosity for computational modelling of variable failure of cemented joint reconstructions. In: Proceedings of the 14th annual meeting of the European Orthopaedic Research Society, Amsterdam, the Netherlands.

Maher, S.A. and Prendergast, P.J., 2002. Discriminating the loosening behaviour of cemented hip prostheses using measurements of migration and inducible displacement. Journal of Biomechanics, 35: 257-265.

McCormack, B.A.O. and Prendergast, P.J., 1999. Microdamage accumulation in the cement layer of hip replacements under flexural loading. Journal of Biomechanics, 32(5): 467-475.

McCormack, B.A.O., Prendergast, P.J. and O'Dwyer, B., 1999. Fatigue of cemented hip replacements under torsional loads. Fatigue & Fracture of Engineering Materials & Structures, 22(1): 33-40.

Molino, L.N. and Topoleski, L.D.T., 1996. Effect of $BaSO_4$ on the fatigue crack propogation rate of PMMA bone cement. Journal of Biomedical Material Research, 31(1): 131-137.

Murphy, B.P. and Prendergast, P.J., 2000. On the magnitude and variability of the fatigue strength of acrylic bone cement. International Journal of Fatigue, 22: 855-864.

Murphy, B.P. and Prendergast, P.J., 2003. Multi-axial fatigue failure of orthopaedic bone cement - experiments with tubular specimens. Journal of Materials Science-Materials in Medicine, 14(10): 857-861.

Roques, A., 2004. Novel approaches to the structural integrity assessment of acrylic bone cement as part of the bone/cement/stem construct. PhD Thesis, University of Southampton, United Kingdom.

Roques, A., Browne, M., Taylor, A., New, A. and Baker, D., 2004. Quantitative measurement of the stresses induced during polymerization of bone cement. Biomaterials, 25(18): 4415-4424.

Sinnett-Jones, P.E., Browne, M., Ludwig, W., Buffiere, J.Y. and Sinclair, I., 2004. Microtomography assessment of failure in acrylic bone cement. In proceedings of the 14th annual meeting of the European Orthopaedic Research Society, Amsterdam, the Netherlands.

Stauffer, R.N., 1982. Ten-year follow up study of total hip replacement. Journal of Bone and Joint Surgery-American Volume, 64(7): 983-990.

Stolk, J., Maher, S.A., Verdonschot, N., Prendergast, P.J. and Huiskes, R., 2003. Can finite element models detect clinically inferior cemented hip implants? Clinical Orthopaedics and Related Research, 409: 138-150.

Verdonschot, N. and Huiskes, R., 1997. The effects of cement-stem debonding in THA on the long-term failure probability of cement. Journal of Biomechanics, 30(8): 795-802.

Topoleski, L.D.T., Ducheyne, P. and Cuckler, J.M., 1990. A fractographic analysis of *in vivo* poly(methylmethacrylate) bone-cement failure mechanisms. Journal of Biomedical Materials Research, 24(2): 135-154.

CHAPTER 7

PARAMETERS INFLUENCING THE FATIGUE FAILURE OF THE CEMENT MANTLE[1]

The aim of this study was to isolate selected parameters active during normal loading of the implanted femur, and investigate the influence of each on fatigue. The *in silico* method described in previous chapters has the ability to switch on or off each of the simulated characteristics, i.e. porosity, initial stress and creep. The results of this study were that porosity and initial stress served to accelerate the damage process, but creep prolonged the life of the cement mantle. This does not provide any new insight to the fatigue process, as *in vitro* studies have previously investigated these factors. However, in the context of this thesis, this has two implications. Firstly, the computational method was not modified to generate these results – the only input was the constitutive laws to describe fatigue and creep. That the results were as expected and in agreement with existing *in vitro* studies was therefore a positive sign for the analysis. Secondly, the ability to modify each parameter independently may be a useful tool to the bone cement chemist.

Two further investigations were performed in this study – inducible displacements were used to predict the likelihood of early prosthesis loosening (DePuy C-stem), and the eventual mode of cement failure was investigated. The computational method predicted the prosthesis was not susceptible to short-term loosening and that eventual failure would occur by longitudinal splitting of the cement mantle. Both these findings were in agreement with clinical observations.

[1]Presented at the 19th European Conference on Biomaterials, Sorrento, Italy, 11th – 15th September 2005.

7.1 Introduction

A total hip replacement has a demanding life, being required to withstand loads that regularly exceed bodyweight over tens of years. Loads of up to five times bodyweight are commonly experienced in the hip joint for routine activities such as walking and jogging (Bergmann et al., 1993). These loads are capable of causing fracture of the cement used to fix the prosthesis in the bone. Fracture of the cement mantle is strongly associated with prosthesis loosening, which can lead to revision surgery (Harris et al., 1982). Inspection of *ex vivo* cement fracture surfaces has revealed evidence of fatigue crack growth (Jasty et al., 1991; Topoleski et al., 1990). This has led to the damage accumulation failure scenario being proposed, where microcracks grow under a fatigue load and eventually coalesce to form cement mantle fractures (Huiskes, 1993).

There are many factors involved in the fatigue failure of the cement mantle, particularly cement porosity, creep and residual stress. However, the relative contribution of each of these parameters is uncertain.

Pores in the cement mantle, created during the mixing and polymerisation processes, have been observed on *ex vivo* cement fracture surfaces and thought to be a cause of microcracking (Jasty et al., 1991). *In vitro* models of the implanted femur have also found porosity to have a negative effect on the fatigue resistance of the cement mantle, by acting as microcrack initiators (Britton et al., 2003; Lennon et al., 2003; McCormack et al., 1999). A reduced level of porosity has been shown to increase the fatigue resistance of the material (Davies et al., 1987; Murphy and Prendergast, 2000); indeed cement is now mixed under a vacuum to minimise the likelihood of pores in the material. Although vacuum mixing can reduce the level of porosity, it does not eliminate it entirely. Depending on the mixing device, the volume of porosity may still be between 1.4% and 10.3% (Dunne and Orr, 2001).

Regarding creep deformation, bone cement has a glass transition temperature of about 100°C and a number of experimental studies have found that creep occurs at body temperature under static and cyclic loads, in tension and compression (Chwirut, 1984; Verdonschot and Huiskes, 1994). As well as inducing strain, creep is capable of relaxing stress in the material over a period of time (Lee et al., 2002; Yetkinler and Litsky, 1998).

Computational simulations of bone cement creep have predicted that creep could relax peak stresses in the cement mantle, but not cause significant stem subsidence (Lu and McKellop, 1997; Verdonschot and Huiskes, 1997). By relaxing peak cement stresses, creep may act in a positive way to prevent fatigue cracking of the cement mantle.

Residual stress in the cement is induced during the exothermic polymerisation process due to the thermal contraction of the material and the density change as the liquid monomer polymerises to form a solid polymer. When the cement is constrained by a metallic stem, this stress is capable of initiating cracks in the cement mantle prior to loading (Lennon and Prendergast, 2002; Orr et al., 2003; Roques et al. 2004). The residual stress field itself, along with any pre-load cracks, may serve to accelerate the fatigue failure process (Lennon and Prendergast, 2002; McCormack and Prendergast, 1999).

In the current study, the fatigue of bone cement in the cement mantle of an implanted femur was simulated using a continuum damage mechanics approach. The prosthesis was the triple-taper polished C-stem (DePuy, UK). Creep and fatigue were simulated using constitutive laws based on uniaxial data. Initial stress was simulated by means of thermal contraction in the cement. Pores were simulated using the theoretical elastic solution for a spherical cavity subject to a remote stress, and the distribution of pores was modelled with Monte Carlo methods. These parameters were then switched on or off, allowing the influence of each on the fatigue process to be ascertained. Inducible displacements and cement damage patterns were recorded throughout testing to see what (if any) correlations could be drawn with clinical observations.

7.2 Materials and Methods

7.2.1 Finite element model generation

The finite element model of the femur was based on a CAD model of the third generation composite femur biomechanical model (Sawbones Europe AB, Sweden) available from the International Society of Biomechanics Finite Element Mesh Repository on the World Wide Web (Greer and Wang, 1999). A solid model of the prosthesis (C-stem, DePuy, UK) was supplied by DePuy (Figure 7.1), and virtually implanted into the femur. A 2mm cement mantle was generated around the prosthesis. The C-stem is a force-closed design, relying on subsidence within the cement mantle to achieve stability. No distal cement is desired for this to occur, so no cement distal to the tip of the prosthesis was modelled. This cement mantle represents the ideal clinical scenario (Wroblewski et al., 2001). Once the cement mantle was defined, the gap between the cement and the cortex was filled to model the cancellous bone.

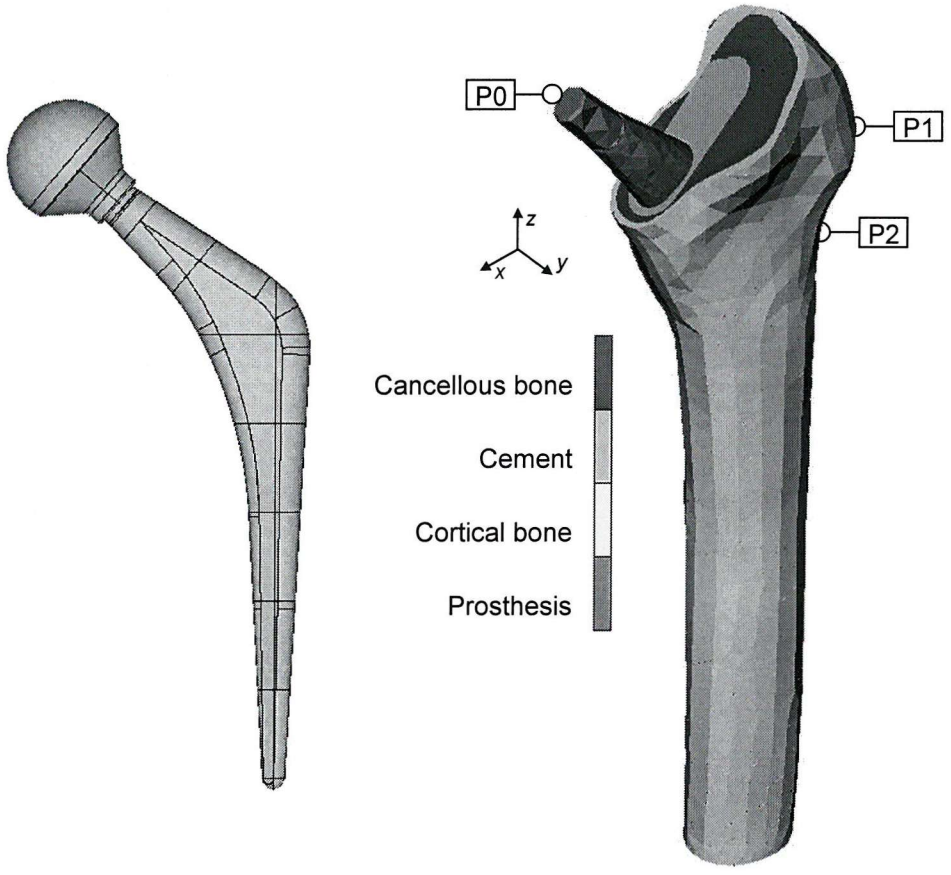

Figure 7.1: Solid model of the C-Stem prosthesis and finite element model of the implanted femur. P0 was at the centre of the femoral head and rigidly linked to the proximal prosthesis tip.

The solid model of the implanted C-stem was subsequently meshed with first order (linear) elements. Hexahedral elements were used in the cement mantle (these have been shown to perform superior to tetrahedral elements in the convergence study in Section 5.2.1, page 174) and tetrahedral elements used elsewhere, with pyramid transitional elements generated automatically to ensure a conforming mesh. Four hexahedral elements were used through the thickness of the cement mantle, which met the requirements of the convergence study (Section 5.2.1, page 174). There were 32,500 elements in the cement mantle, with an average volume of $0.6mm^3$. The prosthesis, cancellous and cortical bone were meshed with tetrahedral elements with characteristic edge length of 4mm. In total the model consisted of 92,800 elements (Figure 7.1).

All materials were assumed to be isotropic and linearly elastic, with Young's modulus and Poisson's ratio as follows: prosthesis, 220GPa and 0.3; cement, 2.8GPa and 0.3; proximal cancellous bone, 750MPa and 0.28; cortical bone 15.5GPa and 0.28. Boundary conditions were applied to simulate the peak loads experienced by a subject weighing 750N during level gait, as described by Bergmann (2001) and summarised in Table 7.1. Hip contact force was applied to a node at the centre of the femoral head, which was rigidly linked to the proximal tip of the stem. The stem/cement interface was modelled as unbonded and with a coefficient of friction of 0.25. The nodes at the distal end of the femur were clamped to restrain against rigid body motion.

Force [%BW]	x	y	z	acts at point
Hip contact	-54.0	-32.8	-229.2	P0
Abductor	58.0	4.3	86.5	P1
Tensor fascia lata, proximal part	7.2	11.6	13.2	P1
Tensor fascia lata, distal part	-0.5	-0.7	-19.0	P1
Vastus lateralis	-0.9	18.5	-92.9	P2

Table 7.1: Boundary conditions applied to finite element models (Bergmann, 2001). See Figure 7.1 for points of action.

7.2.2 Computational analysis

Prior to simulating the fatigue loading, an initial stress field was generated in the cement mantle in the same manner as described in Section 5.2.2 (page 176). This initial stress was to represent the residual stress field; the limitations associated with this simplification have been discussed in Section 5.4 (page 184). Pores were also simulated in the cement using a Monte Carlo simulation and the theoretical elastic solution for a spherical cavity in an infinite medium subject to a remote load (as described in Section 4.2.4, page 151). The loads described above were then applied to the model in a cyclic fashion to represent normal gait. Damage and creep in the cement mantle were simulated as described in Section 4.2.5 (page 157). For this analysis, approximately 150 iterations were required to simulate $2x10^6$ load cycles, with a wall clock time of approximately 200 hours.

Four finite element analyses were performed as described above, each with a unique pore distribution. Three further analyses were performed, one with porosity switched off, one with porosity and initial stress switched off and one with porosity, initial stress and creep switched off (Table 7.2). The following results were recorded as a function of time during the analysis: damage patterns in the cement mantle, peak and average stress and inducible displacement.

	Fatigue	Porosity	Initial stress	Creep
Model 1	●	●	●	●
Model 2	●	●	●	●
Model 3	●	●	●	●
Model 4	●	●	●	●
Model 5	●	○	●	●
Model 6	●	○	○	●
Model 7	●	○	○	○

Table 7.2: Parameters simulated in each of the finite element models (● included, ○ not included). Models 1-4 had unique pore distributions.

7.3 Results

Peak and average stresses in the cement mantle were recorded during the analysis (Figure 7.2). When an element or group of elements failed, the stresses on the neighbouring elements may have risen sharply, causing the spikes in the peak stress lines. These elevated stresses were highly localised and did not affect the average stress in the cement – this is evident from Figure 7.2 as the average stress lines are without spikes. The peak stresses were highest when all parameters were switched on; a peak magnitude of 80MPa was calculated in one of the models. Such a high value was caused by the stress concentration of a pore and caused immediate failure of that element. In all cases, high stresses were apparent within the first 0.1 – 0.2 million load cycles, but subsequently the peak stress remained relatively low. The peak stresses were dissipated by elemental failure but, because the peak stress only applied to one individual element, did not necessarily mean large numbers of elements failed.

The average stress in the cement mantle reduced as a function of time, due to cement creep being included in the analysis. When creep was switched off, the average stress in the cement remained relatively constant for the 2 million load cycles (Figure 7.2d).

The volume of failed elements was also recorded during the analysis (Figure 7.3). As expected, the analyses that included porosity predicted the greatest levels of damage in the cement mantle. Variation in levels of damage was observed in these four models, due to the unique pore distributions. Switching off porosity slowed the rate of damage accumulation significantly – for the analyses *with* porosity 4% damage was reached after between 0.4 and 1.2 million load cycles, but switching off porosity increased this value to just over 5 million load cycles. When the initial stress was also switched off, the 4% damage value was reached after about 7 million load cycles. Switching creep off (in addition to the other parameters) had a negative effect on the fatigue of the cement mantle; 4% damage was reached after 3.5 million load cycles (Figure 7.3).

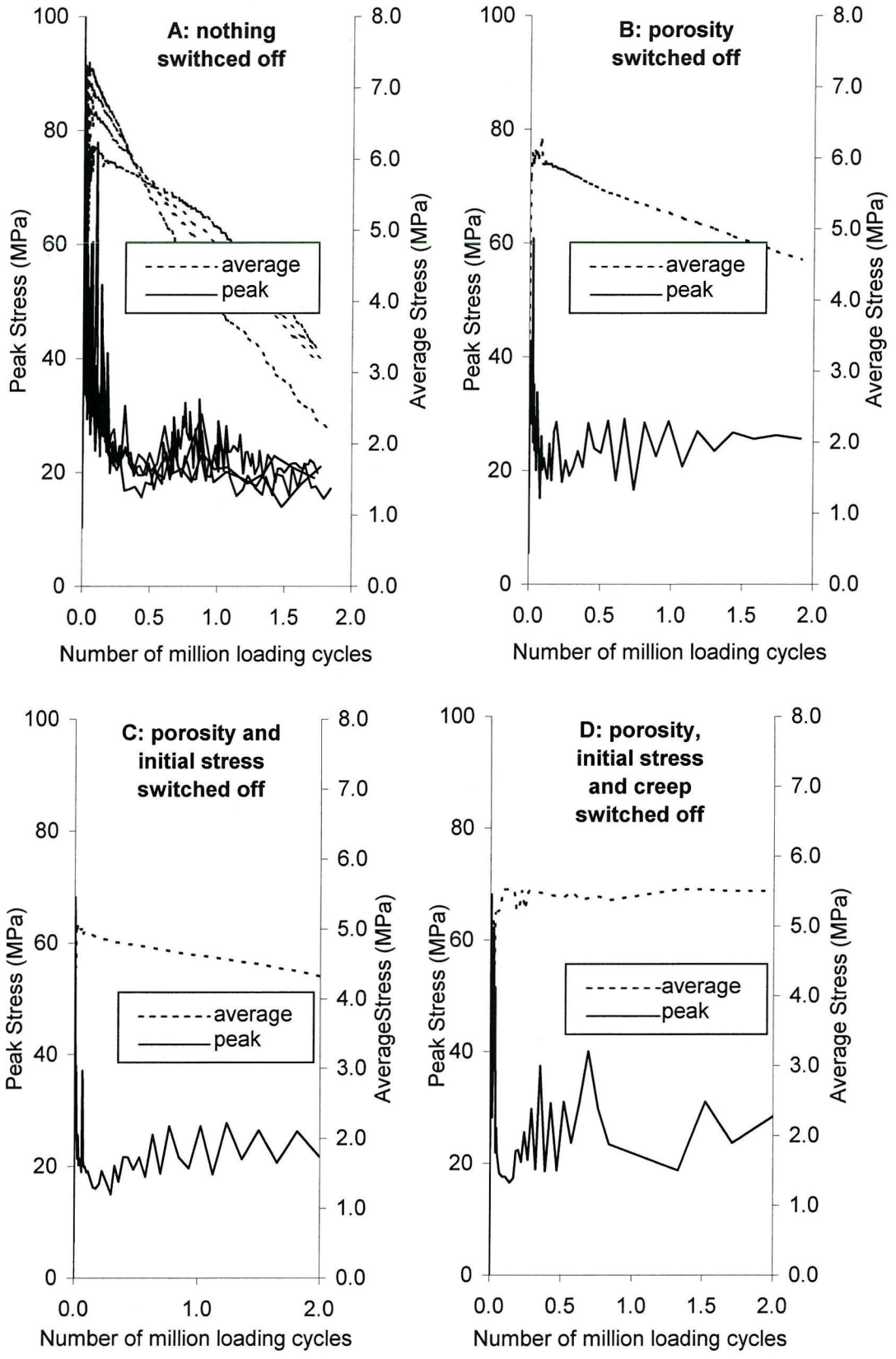

Figure 7.2: Peak (solid line) and average (dashed line) stress in the cement mantles of the different analyses as a function of load cycles.

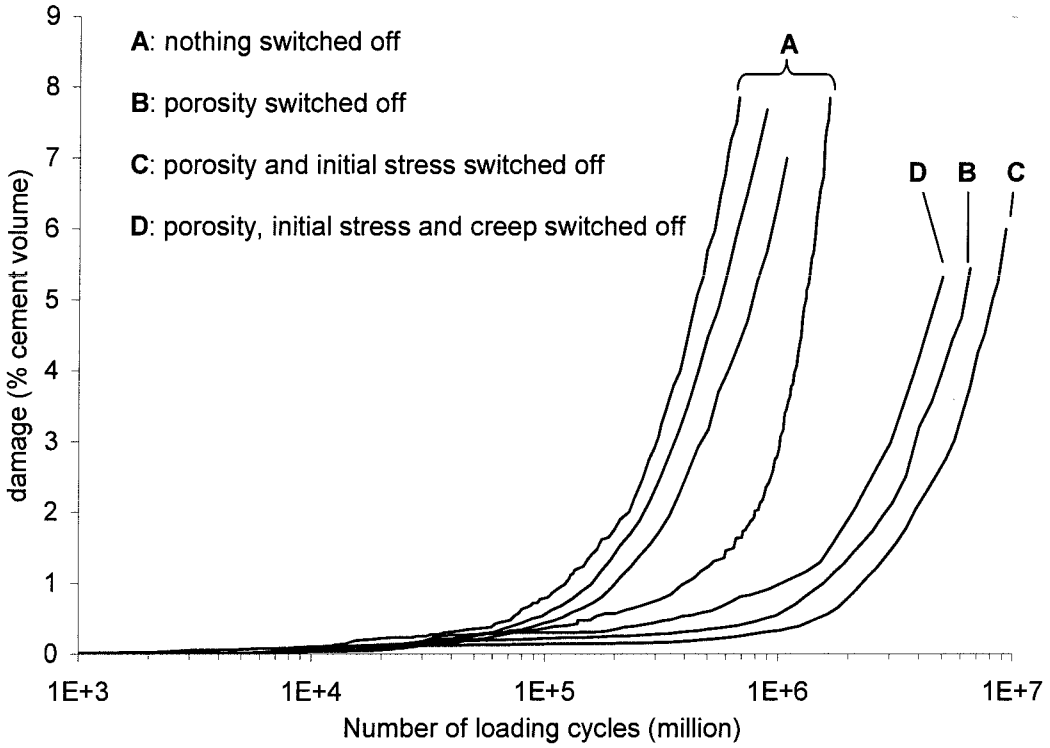

Figure 7.3: Damage in the cement mantle as a function of loading cycles for the different scenarios.

Inducible displacements were recorded throughout the test (Figure 7.4). The changes in inducible displacement were small, about 35 microns. However, there was a trend for reducing displacement as a function of loading cycles. The models with porosity exhibited greatest reduction in displacement, followed by the analysis with creep and initial stress and then the analysis with creep only. The smallest change in inducible displacement was when all parameters were switched off (Figure 7.4).

Figure 7.5 shows the damage pattern in the posterior cement mantle for one of the analyses with porosity, initial stress and creep simulated. After 1 million load cycles, non critical cement damage can be seen at a number of locations in the cement, but there are signs of a crack forming at the superolateral and distal areas of the cement (white arrows). Over the subsequent 0.75 million load cycles, these two cracks linked up to form a longitudinal split of the cement mantle. By this time there was another longitudinal split in the medial midsection of the cement. All the finite element models experienced a longitudinal split of the cement mantle. For models with increased porosity, the longitudinal split occurred in a similar timeframe to Figure 7.5, but with increased levels

of damage elsewhere in the cement. For the analyses without porosity, longitudinal splitting occurred in a longer timescale, between 7 million and 15 million simulated load cycles.

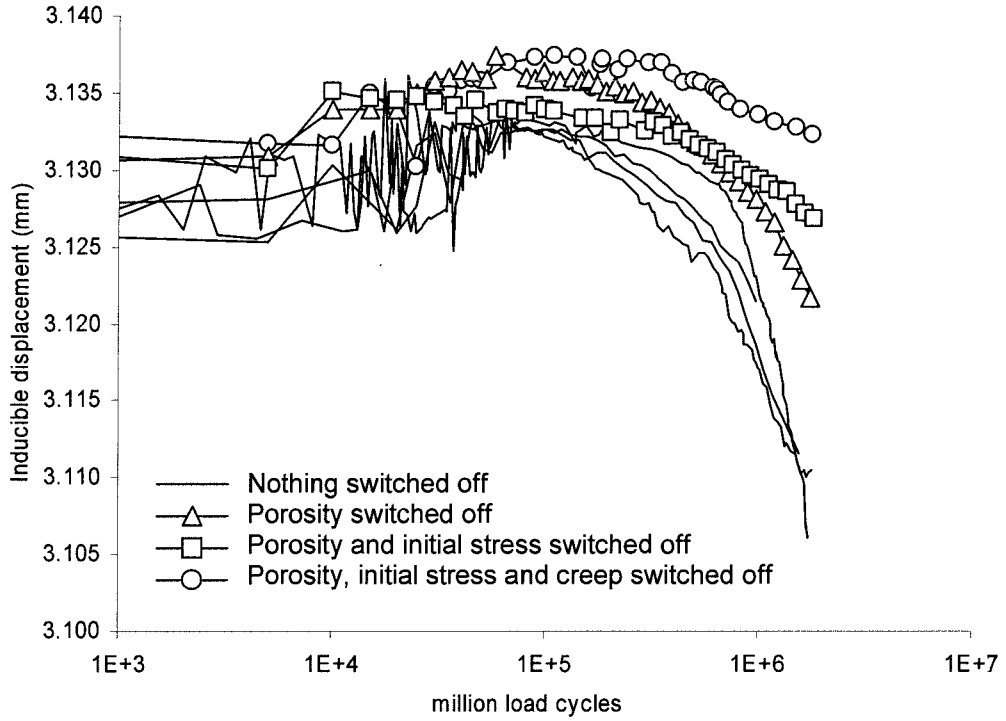

Figure 7.4: Inducible displacement as a function of load cycles.

7.4 Discussion

Fatigue failure of the cement mantle is a multi-factorial process. During *in vitro* tests it is difficult, if not impossible, to identify which mechanical parameters drive the failure process. In silico modelling has the capability of switching on/off mechanical parameters, allowing their significance in the fatigue process to be investigated. This was the motivation behind the present study.

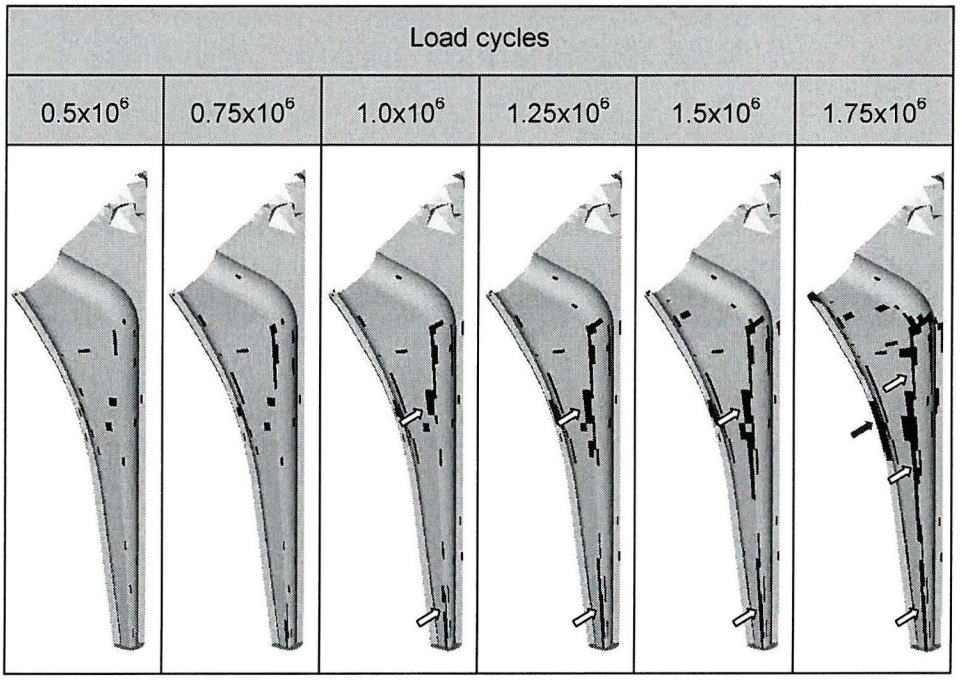

Figure 7.5: Damage in the cement mantle at seven stages through the loading history for a simulation with nothing switched off (i.e. simulating porosity, initial stress and creep). Dark regions represent damage. White arrows identify the crack that eventually causes splitting of the cement mantle. Black arrow identifies a through cement mantle fracture.

Of the parameters included in this study, porosity had the greatest influence on the damage accumulation process. Porosity led to damage occurring in many locations in the cement before any critical cracks developed, as shown in Figure 7.5 after 0.5 million load cycles. While this damage alone was not critical, it did facilitate the growth of the cement mantle splitting crack, identified in Figure 7.5 by white arrows. That porosity accelerates fatigue failure is not a new revelation, many *in vitro* studies have previously come to this conclusion (Britton et al., 2003; McCormack and Prendergast, 1999). The peak stresses

in the first 0.2 million cycles were noticeably higher for the analyses with porosity, but subsequently were quite similar to the other analyses, around the 20MPa mark (Figure 7.2). That the mean stress in the cement mantle was comparable to the other analyses indicates that these initial peak stresses were highly localised (at pores, as they were lower when porosity was switched off) and led to only localised cement damage. However, this localised damage eventually led to accelerated failure of the cement mantle.

Including porosity also served to generate stochastic results in the analysis. This was illustrated in Figure 7.3 where there were 4 distinct damage accumulation curves. Cement mantle splitting occurred between 0.6 million and 1.6 million load cycles when porosity was included – differing by a factor of 2.7. In this case, there was a relationship between time to failure and the number of pores in the cement, i.e. the model with the highest number of pores had the shortest time to failure. This may only have been the case because there were no instances of localised high pore density (as was found in one finite element model in Chapter 6, Figure 6.7a, page 201). As was discussed in Section 6.4 (page 201), the pore distribution is equally important, but no examples of this were observed in the present study.

The other parameters simulated in the finite element models had contrasting effects on the fatigue performance of the cement mantle. The initial stress field served to accelerate the fatigue process, but not to the extent of porosity. With initial stress switched off, cement mantle splitting occurred at 15 million load cycles; when switched on, cement mantle splitting occurred at 7 million load cycles, thus halving the fatigue timescale (a factor of 2). As with the porosity analysis, the greatest difference in peak stress was for the first 0.2 million load cycles, and while this may not have caused a great deal of damage itself, the initiation of damage at this time accelerated eventual failure (cement mantle splitting).

Regarding cement creep, damage in the cement was slowed by its inclusion. The finite element model that simulated creep only (with porosity and initial stress switched off) had the longest fatigue life, requiring 15 million cycles for cement mantle splitting to occur. Switching off creep shortened this value to 6 million load cycles (factor of 2.5). Creep also had the effect of reducing the stress in the cement during the tests. This was not apparent in the peak stress lines (as these were governed by element failure), rather

the average stress lines (Figure 7.2). For the analysis with creep switched off, the average stress remained relatively constant throughout the analysis. For all other analyses, i.e. those including creep, the average stress clearly reduced as a function of time, thus elongating the failure timescale.

A further point of interest regarding cement creep was exhibited in the inducible displacement results. The inducible displacement was not altered greatly when creep was switched off. This agrees with previous studies that suggest creep is responsible for minimal prosthesis subsidence (Lu and McKellop, 1997; Norman et al., 2001; Verdonschot and Huiskes, 1997). The inducible displacement results generally reduced in magnitude with respect to loading cycles. Maher and Prendergast (2002) used inducible displacement as a means to predict prosthesis performance *in vivo*, and suggested that reducing inducible displacement was a sign of a good prosthesis design, not susceptible to early loosening. The C-stem is a relatively new design of prosthesis; it was only introduced into clinical practice in November 1993. So far, follow up studies suggest the prosthesis is indeed not susceptible to early loosening – in a follow up study of 500 replacements, at up to 7 years, Wroblewski et al. (2001) reported no revisions for aseptic loosening, and no prostheses showing any risk of loosening. Ek and Choong (2005) performed a follow up study of C-stem and Exeter designs (up to 6 years post operatively) and found both designs comparable on radiological analysis and to perform equally well clinically. Interpreting the inducible displacement results in accordance with Maher and Prendergast (2002), the present study suggests that the C-stem is indeed not susceptible to early loosing, in accordance with these clinical studies. However, a limitation of this interpretation is that only one prosthesis design is considered. It may be that *all* prostheses analysed in this way exhibit reducing inducible displacement.

A second comparison to clinical observations was the damage pattern in the cement mantle. The results of the current study suggest the C-stem will eventually fail by longitudinal splitting of the cement mantle. At present, there does not appear to be any literature concerning failure modes of the C-stem, however correlations could be made with previous loosening studies. Stauffer (1982) performed a 10 year follow up study on the Charnley prosthesis, and reported the most common type of loosening as longitudinal splitting of the cement mantle. Stauffer (1982) went on to describe the cause of this splitting as a crack "starting proximally and propagating distally" through the cement

(Figure 7.6), and suggested it was caused by hoop stresses due to the axial loading of the tapered stem (Figure 7.6 is a generic sketch to show longitudinal cement mantle splitting. Stauffer did not exclusively notice splitting in the locations shown). He also predicted horizontal cracks towards the distal end of the prosthesis, where the stem punched through the distal cement. The damage patterns in Figure 7.5 appear to agree with the observations of Stauffer, but without the horizontal cracking in the distal cement. This can be explained by considering that the cement mantles of Stauffer had a distal cement pedestal, whereas the current cement mantles did not.

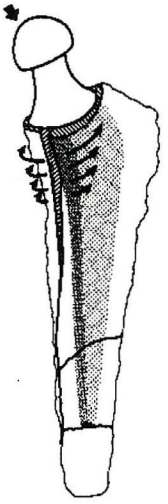

Figure 7.6: Schematic of cement mantle cracking that facilitates prosthesis loosening (Stauffer, 1982).

A number of limitations exist with the current study, most of which have been discussed before in Chapters 4,5&6. One of note here is that the number of pores may be over represented in the finite element models. Digressing slightly to consider the initial stress: the limitations of using an initial stress distribution to represent residual stress has been discussed in Chapter 5, but the present study suggests that it has a relatively small contribution to fatigue life when compared to the porosity, and could perhaps be neglected. A more detrimental effect of residual stress may be not the stress field itself, rather the pre-load damage associated with it. Considering again that the number of pores in the cement may be over represented, one could argue that this very limitation may serve to represent pre-load damage in the cement.

A second limitation concerns the stress field involved in the cement mantle of the structure. Until now (apart from Chapter 5), the stresses considered have been essentially of a uniaxial nature. The computational results of Chapter 4 and 6 compared well to experimental data, but no such comparison was possible here. It would seem likely that the *in silico* cement mantle fractures occurred in a conservative timescale – Heller *et al.* (2001) consider $1.1x10^6$ gait cycles to represent a year of loading. Interpreting our results with this in mind suggests the C-stem will split the cement mantle (when simulating all the parameters) after about 1 year of loading. However, our gait loading was simulated continuously, and didn't consider periods of rest that would occur *in vivo*. Even so, the failure timescale appears to be conservative – one factor in this may be limitations in applying uniaxial based constitutive laws to a multi-axial stress field. A second may be over representation of pores (or initial damage) in the cement as discussed previously.

7.5 Conclusions

Damage in the cement mantle of the implanted femur simulated by the computational method was influenced by creep, initial stress and porosity. Porosity and initial stress served to shorten the fatigue life of the cement mantle, but cement creep elongated the life of the cement.

The *in silico* inducible displacements suggested the C-stem prosthesis is not susceptible to early loosening, which agrees with clinical follow up studies. However, when failure does eventually occur, the current results predict longitudinal splitting of the cement mantle. This has been observed as a common loosening mechanism for the Charnley prosthesis.

7.6 References

Bergmann, G., Graichen, F. and Rohlmann, A., 1993. Hip joint loading during walking and running measured in two patients. Journal of Biomechanics, 28(8): 969-990.

Bergmann, G.E., 2001. Hip98, loading of the hip joint. Published as a CD-ROM attachment to the Journal of Biomechanics: ISBN 3-9807848-0-0.

Britton, J.R., Walsh, L.A. and Prendergast, P.J., 2003. Mechanical simulation of muscle loading on the proximal femur: Analysis of cemented femoral component migration with and without muscle loading. Clinical Biomechanics, 18: 637-646.

Chwirut, J., 1984. Long term compressive creep deformation and damage in acrylic bone cements. Journal of Biomedical Material Research, 18: 25-37.

Davies, J.P., Burke, D.W., O'Connor, D.O. and Harris, W.H., 1987. Comparison of the fatigue characteristics of centrifuged and uncentrifuged simplex p-bone cement. Journal of Orthopaedic Research, 5(3): 366-371.

Dunne, N.J. and Orr, J.F., 2001. Influence of mixing techniques on the physical properties of acrylic bone cement. Biomaterials, 22(13): 1819-1826.

Ek, E.T. and Choong, P.F.M., 2005. Comparison between triple-tapered and double-tapered cemented femoral stems in total hip arthroplasty. Journal of arthroplasty, 20(1): 94-100.

Greer, B. and Wang, E.L., 1999. 3rd generation composite femur model. Available for download from: The ISB Finite Element Repository, Istituti Rizzoli, Bologna, Italy , http://www.cineca.it/hosted/LTM-IOR/back2net/index.html.

Harris, W.H., McCarthy, J.C. and O'Neill, D.A., 1982. Femoral component loosening using contemporary techniques of femoral cement fixation. Journal of Bone and Joint Surgery-American Volume, 64(7): 1063-1067.

Heller, M.O., Bergmann, G., Deuretzbacher, G., Durselen, L., Pohl, M., Claes, L., Haas, N.P. and Duda, G.N., 2001. Musculo-skeletal loading conditions at the hip during walking and stair climbing. Journal of Biomechanics, 34(7): 883-893.

Huiskes, R., 1993. Failed innovation in total hip-replacement - diagnosis and proposals for a cure. Acta Orthopaedica Scandinavica, 64(6): 699-716.

Jasty, M., Maloney, W.J., Bragdon, C.R., O'Connor, D.O., Haire, T. and Harris, W.H., 1991. The initiation of failure in cemented femoral components of hip arthroplasties. Journal of Bone and Joint Surgery-British Volume, 73(4): 551-558.

Lee, A.J.C., Ling, R.S.M., Gheduzzi, S., Simon, J.P. and Renfro, R.J., 2002. Factors affecting the mechanical and viscoelastic properties of acrylic bone cement. Journal of Materials Science-Materials in Medicine, 13(8): 723-733.

Lennon, A.B. and Prendergast, P.J., 2002. Residual stress due to curing can initiate damage in porous bone cement: Experimental and theoretical evidence. Journal of Biomechanics, 35(3): 311-321.

Lennon, A.B., McCormack, B.A.O. and Prendergast, P.J., 2003. The relationship between cement fatigue damage and implant surface finish in proximal femoral prostheses. Medical Engineering & Physics, 25: 833-841.

Lu, Z. and McKellop, H., 1997. Effects of cement creep on stem subsidence and stresses in the cement mantle of a total hip replacement. Journal of Biomaterials Research, 34(2): 221-226.

Maher, S.A and Prendergast, P.J., 2002. Discriminating the loosening behaviour of cemented hip prostheses using measurements of migration and inducible displacement. Journal of Biomechanics, 35: 257-265.

McCormack, B.A.O. and Prendergast, P.J., 1999. Microdamage accumulation in the cement layer of hip replacements under flexural loading. Journal of Biomechanics, 32(5): 467-475.

McCormack, B.A.O., Prendergast, P.J. and O'Dwyer, B., 1999. Fatigue of cemented hip replacements under torsional loads. Fatigue & Fracture of Engineering Materials & Structures, 22(1): 33-40.

Murphy, B.P. and Prendergast, P.J., 2000. On the magnitude and variability of the fatigue strength of acrylic bone cement. International Journal of Fatigue, 22: 855-864.

Norman, T.L., Thyagarajan, G., Saligrama, V.C., Gruen, T.A. and Blaha, J.D., 2001. Stem surface roughness alters creep induced subsidence and 'taper-lock' in a cemented femoral hip prosthesis. Journal of Biomechanics, 34(10): 1325-1333.

Orr, J.F., Dunne, N.J. and Quinn, J.C., 2003. Shrinkage stresses in bone cement. Biomaterials, 24: 2933-2940.

Roques, A., Browne, M., Taylor, A., New, A. and Baker, D., 2004. Quantitative measurement of the stresses induced during polymerization of bone cement. Biomaterials, 25(18): 4415-4424.

Stauffer, R.N., 1982. Ten-year follow up study of total hip replacement. Journal of Bone and Joint Surgery-American Volume, 64(7): 983-990.

Topoleski, L.D.T., Ducheyne, P. and Cuckler, J.M., 1990. A fractographic analysis of *in vivo* poly(methylmethacrylate) bone-cement failure mechanisms. Journal of Biomedical Materials Research, 24(2): 135-154.

Verdonschot, N. and Huiskes, R., 1994. Creep-behavior of hand-mixed simplex-p bone-cement under cyclic tensile loading. Journal of Applied Biomaterials, 5(3): 235-243.

Verdonschot, N. and Huiskes, R., 1997. Acrylic cement creeps but does not allow much subsidence of femoral stems. Journal of Bone and Joint Surgery-British Volume, 79(4): 665-9.

Wroblewski, B.M., Siney, P.D. and Fleming, P.A., 2001. Triple taper polished cemented stem in total hip arthroplasty - rationale for the design, surgical technique, and 7 years of clinical experience. Journal of Arthroplasty, 16(8): 37-41 Supplement 1.

Yetkinler, D. and Litsky, A., 1998. Viscoelastic behaviour of acrylic bone cements. Biomaterials, 19: 1551-1559.

CHAPTER 8

GENERAL DISCUSSION

The penultimate chapter of the thesis takes a step back from the project to view the overall impact of the work contained within and is discussed in three ways: motivation, innovation and application.

8.1 Motivation

In the early 1990's, there were two notorious cases of failed innovation in relation to total hip replacement. The first was the titanium 3M Capital hip prosthesis, introduced to the market in 1991. This had a similar design to the Charnley, but was made from titanium and had a modular head (either cobalt chrome or titanium-nitride coated titanium). High failure rates were reported (26% at 26 months (Massoud et al., 1997)), leading to a hazard warning being issued by the UK Medical Devices Agency in January 1998 (Medical Devices Agency Hazard Notice HN9801). The second case of failed innovation was Boneloc bone cement, introduced in 1990. Boneloc was devised as a low temperature curing cement, which aimed to minimise temperature at the bone/cement interface and prevent cell necrosis. Short-term failure rates were high for prostheses implanted with Boneloc (21% failure at 48 months, but 45% showing radiographic signs of failure (Walczak et al., 2000)) and it was withdrawn from clinical use in 1995.

Preclinical testing can assist in the design and development of orthopaedic devices, and help prevent inferior medical devices such as the Capital hip and Boneloc cement reaching clinical trials and eventually the greater population. The current survival rate of hip arthroplasty is good, the figures speak for themselves – 88% survival at 30 years (Callaghan et al., 2004; Wroblewski et al., 2001a); 100% survival at 8-12 years (Williams et al., 2002); 100% survival at 7 years (Wroblewski et al., 2001b). However, these figures do not consider what happens to patients for whom failure occurs. There are approximately 1 million hip replacement procedures performed annually worldwide such that even 1% failure leaves 10,000 patients requiring revision surgery. The statistics on revision survival are not that great – a follow up study of revision procedures cites only 72% of patients free from pain six years post operatively (Raut et al., 1995). The associated cost of revision is also significant. The example used above (10,000 revision procedures) would cost approximately £56 million (€80 million, (O'Shea et al., 2002)). Considering *these* figures, it becomes clear that the development of preclinical testing methods is essential to improve the performance of the total hip replacement. Another argument for the development of preclinical testing methods is that the market has been flooded with new prosthesis designs, not necessarily better than the existing ones (the 3M hip is an example of a particularly bad case). Manufacturers are under pressure to release new prostheses designs to maintain their market share. Improved preclinical testing

methods should at least ensure ant prosthesis released to clinical trial is not *worse* than the existing benchmark (in this case the Charnley/Exeter designs).

One means of preclinical testing is in a laboratory, where hydraulic testing machines can apply various loads to structures and simulate many years of loading in an accelerated timescale. For such *in vitro* tests, physical models of the prostheses are required, making alterations to the design, based on the results of the tests, a complicated and expensive procedure. Finite element modelling overcomes this limitation, as virtual solid models can be easily modified to improve the results of the computational analyses. However, loosening of the cement fixed implanted femur is rarely a short-term event, rather a long-term process. For computational modelling to represent the long-term failure processes, it is not sufficient to assess merely the initial stress in the construct. This leads to a difficulty with *in silico* compared to *in vitro* methods. Applying a fatigue load to an implanted femur construct is relatively simple with a reliable hydraulic testing machine. The results gained by this method automatically consider all the mechanical properties of the materials involved. For example, there is no need to 'include' cement creep in the analysis – it happens in the test regardless. Finite element studies are a different matter – nothing happens unless the biomechanist *tells* it to happen. This point is nicely illustrated in the literature review where there are many studies that consider the *in vitro* fatigue loading of an implanted femur construct, but only a couple that have attempted to simulate this process computationally. (The inverse is also the case – there are few *in vitro* studies, but many finite element studies, that consider only the initial stress in the construct.)

Verdonschot (1995) was the first to simulate the long-term fatigue of bone cement, work which was continued by Stolk (2003). These authors pioneered the use of computational methods to simulate cement fatigue, and their seminal work on the topic demonstrated the ability of the method to differentiate between prosthesis designs in accordance with data from the Swedish hip register (Herberts and Malchau, 2000; Stolk, 2003). This was a very positive outcome, but the effects of residual stress and porosity were not included in the analyses. As has been discussed through the thesis, these factors are highly significant in relation to bone cement fatigue. The motivation behind the current project was to develop the methods introduced by Verdonschot (1995) to include the effects of porosity and residual stress. The method was first to be applied to simple structures –

tensile and 4-point bend fatigue, before being applied to an *in vitro* model. Comparison with experimental tests was planned for these stages. Finally, it was hoped that applying the analysis to an implanted femur construct would convince medical device manufactures of its merit as a viable preclinical test

8.2 Innovation

Before discussing the innovation in relation to the computational method, it is worthwhile discussing the series of fatigue tests performed in Chapter 3, and specifically the acoustic emission analysis. The acoustic emission technique had the advantage that information was gained from the volume of the specimen (not just the external surfaces), in real time. This data was capable of predicting the final fracture location, as well as detecting damage in other areas of the specimen. In addition to locating damage within the specimen, the acoustic emission data could be used to predict when failure of the specimen was imminent. This was particularly useful at low stress levels, where the number of cycles to failure was high, allowing the test to be stopped at 3 million cycles if failure was not imminent. This work sits well alongside that by Roques (2004), who used acoustic emissions to monitor fatigue in 4-point bend specimens under a fatigue load and polymerising cement in a bone/cement/stem construct. In the current work (Chapter 3), along with the acoustic emission sensors, fatigue specimens were equipped with a waterproof extensometer. This allowed S-N and creep data to be gathered simultaneously during the tests. This was necessary for the computational method as previous studies had used creep and S-N data from different cement brands (and mixing methods).

One of the differences between the current computational fatigue simulation and those which preceded it was the equation used to calculate the fatigue life of each element. Bone cement is a material that inevitably contains pores and weak regions, such that larger volumes of cement have a statistically greater chance of having more weak regions. As fatigue failure usually initiates at such weak areas, this indicates larger volumes of cement are statistically more likely to have inferior fatigue lives. This in turn suggests that uniaxial S-N data is not suitable for simulating fatigue of individual elements (or parts thereof), as the volume difference between the fatigue specimen and individual finite element is so great. This issue was addressed in Chapter 4, where a modified S-N

relationship was derived for elements of the size used in this project. The equation used to calculate cement fatigue required further modification when initial stress (residual stress) was simulated in the cement, as the R-ratio was then different to the experimental tests from which the S-N data was generated. This was achieved by using a modified Goodman rule, which assumes the fatigue life to be zero at a mean stress equal to the tensile strength of the material (Chapter 5).

Porosity was simulated in the finite element models by combining the theory of elasticity and Monte Carlo simulations. Simulating porosity has been achieved before, but the porosity *distribution* was new to the field of biomechanics (although at a recent conference, a paper was presented that described the simulation of a porosity distribution with Monte Carlo simulations (Lennon et al., 2004)). This pore distribution generated a degree of data scatter in the computational results, thus providing a superior representation of experimental testing than deterministic (i.e. without randomness) studies. When simulating the fatigue of the simplified implanted femur construct (Chapter 6), the pore distribution was shown to have equal importance to the number of pores in the cement. The finite element model with the least pores in the cement exhibited more cement mantle fractures than the other models, due solely to a high number of pores in a small volume of cement (this is discussed fully in Section 6.4, page 200). Monte Carlo simulations are reasonably new to biomechanics – a number of papers have been presented at recent conferences that use Monte Carlo and other probabilistic simulation techniques in finite element modelling (Bah and Browne, 2004; Mehrez et al., 2004; Pérez et al., 2003).

8.3 Application

There are a number of applications of the methods involved in this project, of which the acoustic emission technique is a good example. Ultimately, this technique could be used to monitor cement damage in implanted composite or cadaveric femora. However caution must be exercised with a structure as acoustically complex as the implanted femur. In relation to bone cement, current acoustic emission knowledge is limited to test specimens, but the implanted femur has complications of attenuation at interfaces, noise due to rubbing at the interfaces and point of load application. Perhaps the best way to

achieve successful acoustic emission analysis of the implanted femur is to gradually increase the complexity of test specimens, thus creating a methodical validation of the method before the implanted femur construct is considered.

Another application of the acoustic emission technique is to combine it with other novel assessment methods, for example microtomography and ultrasound. This former has been used to generate 3-D images of a volume of cement, enabling comprehensive investigation of the material, not possible by surface analysis or specimen sectioning. This method has the capability of generating 3-D images during fatigue testing in real time, allowing microcrack initiation and propagation to be investigated (Sinnett-Jones et al., 2004). A disadvantage of this method is that only small specimens can be tested, such that random selection of *ex vivo* cement is not desirable, as the volume selected may not contain any microdamage. Acoustic emission could be used to locate the microdamage in specimens without causing failure, and enable a more logical selection of cement for microtomographic assessment.

The computational analysis has a number of possible applications. The first of these is assessment of surgical variables. Patients for hip replacement come in a variety of shapes and sizes, and the surgical parameters that are best for one may not be best for another. Variables that can be analysed include prosthesis design and alignment and cement mantle thickness. Cement mantle thickness can be related to the withdrawal of the 3M Capital hip from the market in 1998 – one of the possible causes of failure was that the rasps designed for the prosthesis allowed for too thin a cement mantle (Massoud et al., 1997). Investigating the variables may also identify good combinations of prosthesis design and cement brand. For example, Boneloc cement, withdrawn from clinical use in 1995, had reasonable performance with the Exeter type prosthesis, 97% survival at 6 years (Furnes et al., 1997). The lower survival values quoted in the opening paragraph considered all prosthesis types.

Two further applications of the computational method involve the design and development of new bone cements and femoral prostheses (or indeed any medical device for which cement fatigue cracking is a mode of loosening). Considering the former, it was demonstrated in Chapter 7 that various mechanical parameters active in the cement during the fatigue process could be switched on or off. The work described in Chapter 7

could be expanded to simulate the fatigue of hypothetical bone cements, for which the fatigue, creep, porosity and residual stress characteristics may be different to conventional cements. An example of failed innovation regarding bone cement formulations was that of Boneloc, mentioned previously, but it may be that the increased creep and reduced residual stress (and therefore pre-load damage) characteristics of Boneloc can be incorporated in cement with reasonable fatigue properties. The computational analysis described was this thesis could provide information on the performance of any cement in development, and, incidentally, would have identified Boneloc as an inferior cement (see Appendix 1, abstract 4).

Considering the design and development of new prostheses, cement mantle fracture is one of the more common prosthesis loosening mechanisms. By designing prostheses against this loosening mechanism, its incidence can be reduced which would certainly be a positive outcome. However, designing prostheses against a specific loosening mechanism may induce other failure processes, yet to be widely recognised. For example, a recent study cautions against the use of cemented titanium components of any design, proposing that stem/cement micromotion abrades the oxide layer of the prosthesis and facilitates crevice corrosion, visible on the prosthesis at revision (Thomas et al., 2004). This would not be predicted by the methods developed in this thesis, and the results *must* therefore be interpreted with respect to other loosening mechanisms. This is currently practised by DePuy International (Leeds, UK) who have adopted the analysis developed in this thesis as part of their preclinical testing program.

The ultimate goal of *in silico* methods is to simulate as close as possible the *in vivo/in vitro* situation. The work presented in this thesis describes simulation of more mechanical properties of bone cement in a single study than has been attempted before. Although a lot has been done, there remains a lot that can still be done to provide a more realistic representation of *in vivo/in vitro* conditions. Limitations with the study have been discussed as they arose in each chapter, however, important understanding of trends and influences may still be discerned. Currently, preclinical testing cannot establish, in a definitive manner, the true performance of novel medical devices – clinical trials are required for this. However, as long as novel medical devices are being manufactured, preclinical testing is still essential to prevent any design susceptible to known failure scenarios reaching the clinical trial stage.

8.4 References

Bah, M.T. and Browne, M., 2004. Failure of the cement mantle in hip implants: A probabilistic approach. In: Transactions of the 50th annual meeting of the Orthopaedic Research Society, San Francisco, CA.

Callaghan, J.J., Templeton, J.E., Liu, S.S., Pedersen, D.R., Goetz, D.D., Sullivan, P.M. and Johnson, R.C., 2004. Results of Charnley total hip arthroplasty at a minimum of thirty years. Journal of Bone and Joint Surgery-American Volume, 86(4): 690-695.

Furnes, O., Lie, S.A., Havelin, L.I., Vollset, S.E. and Engesaeter, L.B., 1997. Exeter and Charnley arthroplasties with Boneloc or high viscosity cement - comparison of 1,127 arthroplasties followed for 5 years in the Norwegian arthroplasty register. Acta Orthopaedica Scandinavica, 68(6): 515-520.

Herberts, P. and Malchau, H., 2000. Prognosis of total hip replacement, Goteburg University, Sweden, http://www.jru.orthop.gu.se.

Lennon, A.B., McCormack, B.A.O. and Prendergast, P.J., 2004. Implications of acrylic bone cement porosity for computational modelling of variable failure of cemented joint reconstructions. In: Proceedings of the 14th annual meeting of the European Orthopaedic Research Society, Amsterdam, the Netherlands.

Massoud, S.N., Hunter, J.B., Holdsworth, B.J., Wallace, W.A. and Juliusson, R., 1997. Early femoral loosening in one design of cemented hip replacement. Journal of Bone and Joint Surgery-British Volume, 79(4): 603-608.

Mehrez, L., Bah, M.T. and Browne, M., 2004. Reliability and sensitivity analysis of two simplified THR models. In: Proceedings of the 14th annual meeting of the European Orthopaedic Research Society, Amsterdam, the Netherlands.

O'Shea, K., Bale, E. and Murray, P., 2002. Cost analysis of primary total hip replacement. The Irish Medical Journal, 95(6): 177-180.

Pérez, M.A., Grasa, J., Ferrer, R., Bea, J.A., García, J.M. and Doblaré, M., 2003. Probabilistic damage model for life prediction of cemented total hip arthroplasty. In: Proceedings of the 1st International congress on computational bioengineering, Zaragoza, Spain.

Raut, V.V., Siney, P.D. and Wroblewski, B.M., 1995. Revision for aseptic stem loosening using the cemented Charnley prosthesis - a review of 351 hips. Journal of Bone and Joint Surgery-British Volume, 77(1): 23-27.

Roques, A., 2004. Novel approaches to the structural integrity assessment of acrylic bone cement as part of the bone/cement/stem construct. PhD Thesis: University of Southampton, United Kingdom.

Sinnett-Jones, P.E., Browne, M., Ludwig, W., Buffiere, J.Y. and Sinclair, I., 2004. Microtomography assessment of failure in acrylic bone cement. In: Proceedings of the 14th annual meeting of the European Orthopaedic Research Society, Amsterdam, the Netherlands.

Stolk, J., 2003. A computerized pre-clinical test for cemented hip prostheses based on finite element techniques. PhD thesis: University of Nijmegen, the Netherlands.

Stolk, J., Maher, S.A., Verdonschot, N., Prendergast, P.J. and Huiskes, R., 2003. Can finite element models detect clinically inferior cemented hip implants? Clinical Orthopaedics and Related Research, 409: 138-150.

Thomas, S.R., Shukla, D. and Latham, P.D., 2004. Corrosion of cemented titanium femoral stems. Journal of Bone and Joint Surgery-British Volume, 86(7): 974-978.

Verdonschot, N., 1995. Biomechanical failure scenarios for cemented total hip replacement. PhD Thesis: University of Nijmegen, the Netherlands.

Walczak, J.P., D'Arcy, J.C., Ross, K.R., James, S.E., Bonnici, A.V., Koka, S.R. and Morris, R.W., 2000. Low-friction arthroplasty with Boneloc bone-cement - outcome at 2 to 4 years. Journal of Arthroplasty, 15(2): 205-209.

Williams, H.D.W., Browne, G., Gie, G.A., Ling, R.S.M., Timperley, A.J. and Wendover, N.A., 2002. The Exeter universal cemented femoral component at 8 to 12 years. Journal of Bone and Joint Surgery-British Volume, 84(3): 324-334.

Wroblewski, B.M., Siney, P.D. and Fleming, P.A., 2001a. Charnley low-frictional torque arthroplasty in patients under the age of 51 years. Journal of Bone and Joint Surgery-British Volume, 84(4): 540-543.

Wroblewski, B.M., Siney, P.D. and Fleming, P.A., 2001b. Triple taper polished cemented stem in total hip arthroplasty - rationale for the design, surgical technique, and 7 years of clinical experience. Journal of Arthroplasty, 16(8): 37-41 Supplement 1.

CHAPTER 9

RECOMMENDATIONS FOR FURTHER WORK

Chapter 8 included a section on possible applications of the computational method, but did not include further work that could improve the method. A number of limitations have been discussed throughout the thesis, and this chapter considers these specifically.

The computational method deactivates (modulus set to zero) elements in order to simulate damage in the cement. This does not consider the effects of crack closure or allow transferral of stresses in the plane of the crack. All the structures in the current study were based on constant amplitude loading conditions, and experimental validation was achieved for each. However, for variable amplitude loading conditions, the inability to simulate crack closure and stress transfer in the plane of the crack may become an issue. Stolk et al. (2004) presented a method that allowed stress transfer in the plane of the crack on an elemental scale, but neglected the crack closure issue. A recent publication by Lennon and Prendergast (2004) described a method to simulate both stress transfer in the plane of the crack and restoration of stiffness normal to the crack plane. The incorporation of a method such as this may be necessary for variable amplitude loading conditions to be considered.

Another possible area of development regarding the damage algorithm is to change the linear Palmgren-Miner cumulative damage rule to a non-linear approach. Chapter 3 describes the non-linear accumulation of damage in tensile fatigue specimens (as was also observed by Murphy and Prendergast (2001)). Simulating damage in this manner would not alter the number of cycles to failure for an element at a given stress level, but for variable amplitude loading conditions, the non-linear and linear damage approaches would give conflicting results. Lennon and Prendergast (2004) describe the implementation of this method in relation to bone cement fatigue.

The constitutive laws used to describe fatigue and creep were based on uniaxial data. Applying these to multi-axial stress models, for example the implanted femur, may have limitations, as was mentioned in Chapter 7. Studies of commercial PMMA have been able to use uniaxial constitutive laws to model creep under multi-axial stress states, but using an Eyring law to relate stress and strain rate in the deformed volume (Berthoud *et al.*, 1999). In the current work, the creep law was applied directly from uniaxial tests to the models considered. Further work could check the validity of this approach by modelling (relatively) simple multi-axial stressed experimental tests. The same argument applies to the fatigue law – cement fatigue under uniaxial and multi-axial conditions has been shown to be different (Murphy and Prendergast, 2003). A multi-axial damage accumulation law might provide a better simulation of *in vivo* cement fatigue.

The methods of porosity and residual stress simulation could also be improved. The mean and standard deviation of the porosity distribution was taken from Murphy and Prendergast (2001), but, as mentioned as a limitation in Chapter 4, these data only considered surface porosity, and may have been an overestimation of the pores in the cement. A number of studies have presented data on the volume of pores in a given specimen, but there is little information regarding the nature of the pore distribution within specimens. Recent work involving microtomography has been able to generate 3-D images of bone cement specimens, allowing the distribution of pores with respect to their size to be determined (Sinnett-Jones et al., 2004). Data such as this could be used to generate several pore distributions (of varying sizes) in each finite element model, and improve their representation of experimental specimens. Regarding the residual stress simulation, a couple of studies have presented more sophisticated methods of simulating residual stress than presented in this thesis (Lennon and Prendergast, 2002; Li et al., 2003). Although these are not without limitations, they represent an improvement on the thermal contraction from a uniform peak temperature used in Chapter 5. Incorporating them in the present work would represent an improved representation of in vitro/vivo conditions.

A final area of further work involves using the acoustic emission technique to locate and monitor damage accumulation in the in vitro implanted femur specimens. Application of the acoustic emission technique to the structure described in Chapter 6, verified with another non destructive evaluative technique, for example ultrasound or dye penetrant,

would provide useful information on the nature of acoustic activity generated in the structure, and allow differentiation between cement damage and noise due to stem/cement interface rubbing. This could in turn facilitate the use of acoustic emission for implanted composite femur models and ultimately may lead to cement damage analysis in vivo.

9.1 References

Berthoud, P., G'Sell, C. and Hiver, J.M., 1999. Elastic-plastic indentation creep of glassy poly(methyl methacrylate) and polystyrene: characterisation using uniaxial compression and indentation tests. Journal of Physics D: Applied Physics, 32: 2923-2932.

Lennon, A.B. and Prendergast, P.J., 2002. Residual stress due to curing can initiate damage in porous bone cement: experimental and theoretical evidence. Journal of Biomechanics, 35(3): 311-321.

Lennon, A.B. and Prendergast, P.J., 2004. Modelling damage growth and failure in elastic materials with random defect distributions. Mathematical proceedings of the Royal Irish Academy, 104A(2): 155-171.

Li, C., Wang, Y. and Mason, J., 2003. The effects of curing history on residual stress in bone cement during hip arthroplasty. Journal of Biomedical Material Research Part B: Applied Biomaterials, 70(1): 30-36.

Murphy, B.P. and Prendergast, P.J., 2001. The relationship between stress, porosity and nonlinear damage accumulation in acrylic bone cement. Journal of Biomedical Materials Research, 59: 646-654.

Murphy, B.P. and Prendergast, P.J., 2003. Multi-axial fatigue failure of orthopaedic bone cement - experiments with tubular specimens. Journal of Materials Science-Materials in Medicine, 14(10): 857-861.

Sinnett-Jones, P.E., Browne, M., Ludwig, W., Buffiere, J.Y. and Sinclair, I., 2004. Microtomography assessment of failure in acrylic bone cement. In proceedings of the 14th annual meeting of the European Orthopaedic Research Society, Amsterdam, the Netherlands.

Stolk, J., Verdonschot, N., Murphy, B.P., Prendergast, P.J. and Huiskes, R., 2004. Finite element simulation of anisotropic damage accumulation and creep in acrylic bone cement. Engineering Fracture Mechanics, 71(4-6): 513-528.

APPENDIX 1

CONFERENCE ABSTRACTS

MESH CONSIDERATIONS FOR ADAPTIVE FINITE ELEMENT ANALYSES OF CEMENT FAILURE IN TOTAL HIP REPLACEMENT

Jonathan R T Jeffers and Mark Taylor

Bioengineering Science Research Group
University of Southampton
SO17 1BJ
United Kingdom

INTRODUCTION

Failure of the cement mantle has been identified as a possible mode of failure of the implanted femur in total hip replacement (THR) [1]. Finite element (FE) analyses have been used to investigate the stresses experienced in the cement mantle [2] and to predict the life of the cement mantle when taking different factors into account [3]. The number of elements used, or mesh density, is an important consideration when creating a FE model. A model with an insufficient mesh density will not be able to fully capture the stress state in the area of interest, but increasing the mesh density dramatically increases the computational cost of the analysis.

The aim of this study is to determine the mesh density necessary to model creep and damage accumulation in the cement mantle of a cemented implanted femur. We compare the initial stress state and damage accumulation rate for different mesh densities and different element types.

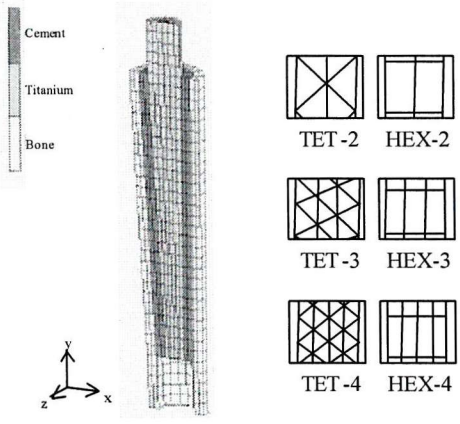

Figure 1. Finite element model (HEX-2) and different meshes used for the cement mantle

METHODS

The simplified implanted femur was generated and meshed in I-DEAS™ (figure 1). All the nodes at the distal end of the cortical bone were constrained in every direction. The nodes in the x – y plane were constrained in the z – direction, allowing displacements only in the x and y directions. All material interfaces were assumed perfectly bonded. The stem, bone cement and cortical bone were assigned Young's moduli of 110GPa, 2.8GPa and 15.5GPa respectively. The stem and cement were assigned a Poisson's ratio of 0.30 and the cortical bone was assigned a Poisson's ratio of 0.28. A load of 2100N at an angle of 16° to the y-axis in the x – y plane was applied to the proximal tip of the femoral stem [4]. Using the same geometry, material properties and loading conditions, six models in total were generated, as described in table 1.

Analysis Name	Element type (figure 1)	Number of elements through thickness of cement mantle (figure 1)
HEX-2	Hexahedral	2
HEX-3	Hexahedral	3
HEX-4	Hexahedral	4
TET-2	Tetrahedral	2
TET-3	Tetrahedral	3
TET-4	Tetrahedral	4

Table 1. Different FE analyses performed

Using the FE solver MARC™, the initial stress state within the cement on the lateral side was compared for each model. After comparing the initial stresses, the load described above was applied cyclically, simulating normal gait. Calculation of creep and damage at every loading cycle would have been both inefficient and unnecessary, so an iteration procedure was developed, based on a similar technique created by Verdonschot [3].

The iteration procedure consists of a number of iterations, each being capable of simulating a number of loading cycles. At the beginning of each iteration, the FE model is loaded, and the stresses

2003 Summer Bioengineering Conference, June 25-29, Sonesta Beach Resort in Key Biscayne, Florida

calculated. The number of cycles to failure (N_f) for the highest stressed element is calculated using data from S-N curves. The number of cycles to be simulated in the iteration is essentially a predefined percentage of N_f. Once the number of cycles to be simulated within the iteration is determined, creep and damage for all elements can be calculated. If damage reaches a predetermined value the element is deactivated and the load transferred to the surrounding elements. As the creep data and S-N curves come from uniaxial tests; the equivalent Von Mises stress must be used to calculate creep and N_f.

The damage (**D**) of an element is calculated using the following linear Palmgren-Miner law:

$$D = \frac{n}{N_f} \quad (1)$$

where n is the number of cycles completed. When **D** is gt. 1 for any element, the element has failed and is deactivated. **D** is a tensorial value, meaning that a deactivated element cannot transfer load in any direction, even though failure only occurs in one direction. The iteration process is repeated until bulk failure of the cement mantle.

RESULTS

The initial stress state through the length of the cement mantle on the lateral side is shown in figure 2. The values plotted here are nodal values, which are extrapolated from the integration point values where MARC™ calculates the stress. Therefore there may be a slight inaccuracy where the node is a distance from the integration point. This is found to occur commonly at outer surfaces, i.e. at either end of the cement layer. Figure 2 illustrates the rapid convergence of results for the static stress state.

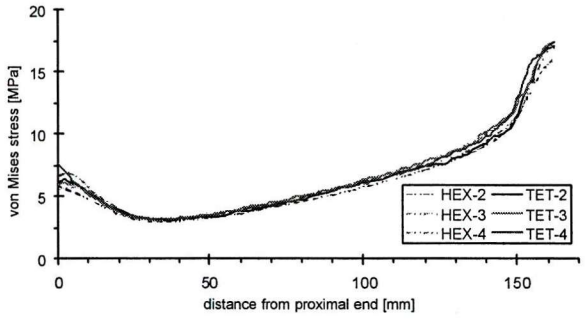

Figure 2. Initial stress state in lateral cement mantle

To monitor the damage accumulation in the cement mantle, the percentage of failure of the cement mantle is plotted against the number of cycles (figure 3).

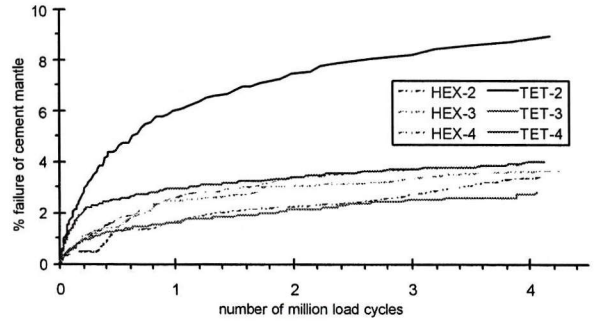

Figure 3. Element failure in cement mantle

The failure of elements can be seen over 4 million cycles. The TET-2 analysis gives a particularly high failure of elements, 9% after 4 million cycles. All other analyses report a failure of between around 3 and 4% for the same number of cycles.

DISCUSSION

The initial stress state is comparable for all analyses. Taking only the initial stress state into account, one could argue that all the analyses performed produce similar results and that the mesh that is least computationally expensive is adequate for an adaptive analysis that simulates creep and damage. This does not seem to be the case, as is demonstrated in figure 2. Even though the TET-2 analysis has a similar initial stress state to the others, the rate of damage accumulation is notably higher.

The HEX-4 and TET-4 analyses produce an almost identical damage accumulation rate from 2 million cycles; we can assume this is a reliable result. The HEX-2, HEX-3 and TET-3 damage accumulation rates all fall within a close range, but follow the same trend as HEX-4 or TET-4 and are certainly superior to the results from the TET-2 analysis. Even though the results for HEX-2, HEX-3 and TET-3 differ only by little more than 1% it must be noted that this is 1% in 3%, i.e. they differ by 30% at 4 million cycles.

The simplified implanted femur geometry used here is a gross simplification to the geometry of a real implanted femur, and given that for complex geometries a tetrahedral mesh is far easier to create than a hexahedral mesh, a tetrahedral mesh is preferred. This point becomes more relevant when it is considered that multiple implant geometries would ideally be meshed and compared. From this point of view the TET-4 mesh is the most advantageous, but when the computational cost of the analysis is taken into account, the TET-3 mesh must be considered. It follows the same trend as the TET-4 mesh and as long as it is used as a comparative tool the fact that it underestimates damage shouldn't pose a problem.

CONCLUSION

The initial stress is not a definitive guide to the performance of an FE mesh and must therefore be used with caution. Although the hexahedral mesh seems to perform better than the tetrahedral one, it is more difficult to use with anatomical models. A thickness of 4 elements through the cement mantle provides the most reliable results, but a tetrahedral mesh with three elements through the cement mantle offers the best compromise when computational cost is taken into account.

REFERENCES

1. Jasty, M., Maloney W. J., *et al.*, 1991, "The Initiation of Failure in Cemented Femoral Components of Hip Arthroplasties," Journal of Bone and Joint Surgery-British Volume, Vol. 73(4), pp. 551-558.
2. Lennon, A. B. and Prendergast P. J., 2001, "Evaluation of Cement Stresses in Finite Element Analyses of Cemented Orthopaedic Implants," Journal of Biomechanical Engineering, Vol 123, pp. 623-628.
3. Verdonschot, N., 1995, "Biomechanical failure scenarios for cemented total hip replacement," Ph.D. thesis, University of Nijmegen, The Netherlands.
4. Lu, Z. and McKellop H., 1997, "Effects of cement creep on stem subsidence and stresses in the cement mantle of a total hip replacement," Journal of Biomaterials Research, Vol. 34, pp. 221-226.

ACKNOWLEDGEMENTS

The authors would like to thank the Arthritis Research Campaign who provide funding for this work.

THE EFFECT OF CREEP AND LOAD LEVEL ON THE DAMAGE ACCUMULATION WITHIN THE CEMENT MANTLE OF THE CEMENTED IMPLANTED FEMUR

Jonathan R T Jeffers and Mark Taylor

Bioengineering Science Research Group
University of Southampton
SO17 1BJ
United Kingdom

INTRODUCTION

Failure, or loosening, of the femoral component in cemented total hip replacement (THR) is usually caused by fatigue failure of the cement mantle under cyclic loading. It has been shown that the likely mode of fatigue failure is damage accumulation, where small internal flaws and microcracks propagate under dynamic loading conditions to eventually form critical defects [1].

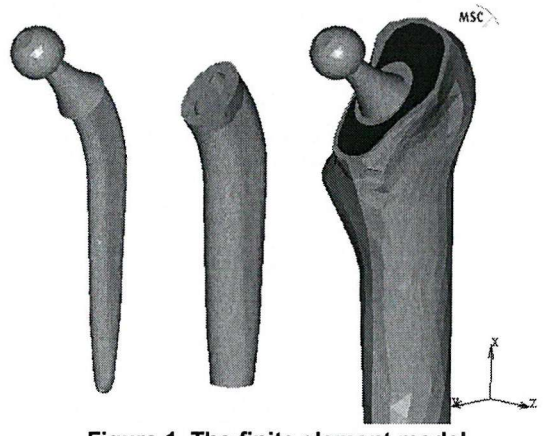

Figure 1. The finite element model

The finite element (FE) technique is a suitable tool to examine the cement mantle, being able to compute stresses and strains at every (finite) point within a complicated three-dimensional geometry. The addition of adaptive simulation algorithms makes it possible to study the cement mantle over time, simulating time dependant properties like creep and damage accumulation.

The aim of this study is to investigate the damage accumulation in the cement mantle for different load levels and to establish the effect creep has on the damage accumulation in a fatigue analysis. Although creep and damage accumulation have been simulated in separate FE studies before [2,3], this study models both time dependant properties simultaneously and aims to provide a direct relationship between creep and damage accumulation.

METHODS

The implanted femur was generated and meshed using I-DEAS™ (figure 1). The femur was based upon a composite Sawbones femur model. The stem used was a Charnley type with collar, based on the DePuy version. A 4mm cement mantle was used to fix the implant in the femur. The mesh used was a tetrahedral mesh, with three elements through the thickness of the cement mantle as this was the area of interest. The implant was assigned a Young's modulus of 200GPa, the cement 2.8GPa, the proximal and distal cancellous bone 0.75 and 5GPa respectively and the cortical bone 17GPa. The Poisson's ratio for the implant and cement was 0.3; the cancellous and cortical bone was given a Poisson's ratio of 0.28. A joint reaction force of 2450N acting on the prosthetic head was applied, with angles of 23° in the frontal plane and 6°in the sagittal plane. The muscle forces included were the abductor muscles, assumed acting on the greater trochanter with a total force of 1650N, with angles of 24° in the frontal plane and 15° in the sagittal plane [2]. This loadcase is hereafter referred to as the standard loadcase, being based upon a patient weighing 100kg (220lb). We introduce two more loadcases, for a lighter patient and an obese patient and scale the forces accordingly [4]. These loadcases are summarised in table 1.

Analysis Name	Patient weight (kg) - [lbs]	Time dependant properties simulated
Standard	100 - [220]	Creep & Damage
Light	70 - [154]	Creep & Damage
Heavy	150 - [330]	Creep & Damage

Table 1. Summary of analyses performed

One further analysis was performed to investigate the effect of creep on damage accumulation. This involved the standard loadcase analysis, but simulated damage accumulation without creep.

The loads described above were applied cyclically to simulate normal gait. Calculation of the time dependant properties of the cement at every loading cycle would be computationally expensive

and unnecessary, so to make the analysis more efficient an iteration procedure was developed, based on a similar technique created by Verdonschot [2]. The iteration procedure consists of a number of iterations, each being capable of simulating a number of loading cycles. At the beginning of each iteration, the FE model is loaded, and the stresses calculated. The number of cycles to failure ($\mathbf{N_f}$) for the highest stressed element is calculated using data from S–N curves. The number of cycles to be simulated in the iteration is essentially a set percentage of $\mathbf{N_f}$. Once the number of cycles to be simulated within the iteration is determined, creep and damage for all elements can be calculated. If damage reaches a predetermined value the element is deactivated and the load transferred to the surrounding elements. The equivalent Von Mises stress must be used to calculate creep and $\mathbf{N_f}$ as the creep data and S–N curves come from uniaxial tests.

The damage (**D**) of an element is calculated using the following linear Palmgren-Miner law:

$$D = \frac{n}{N_f} \tag{1}$$

where n is the number of cycles completed.

When **D** gt. 1 for any element, the element is deactivated. Damage is calculated as a scalar quantity, meaning that a failed element cannot transfer load in any direction, even though failure only occurs in one direction. The iteration process is repeated until bulk failure of the cement mantle takes place.

RESULTS

Figures 2 & 3 illustrate the effect creep has on the damage accumulation in the cement mantle for the standard loadcase. The dark elements in figure 3 represent the failed elements. The inclusion of creep within the analysis significantly reduced the damage within the cement mantle.

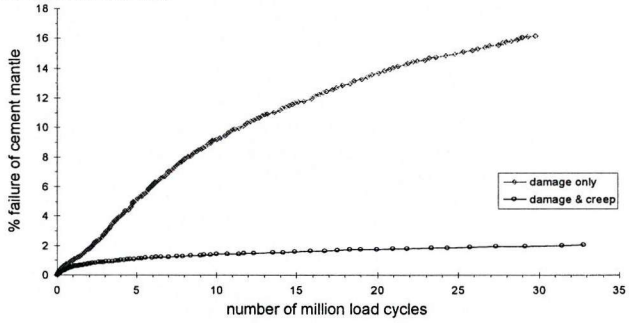

Figure 2. Element failure in cement, standard loadcase

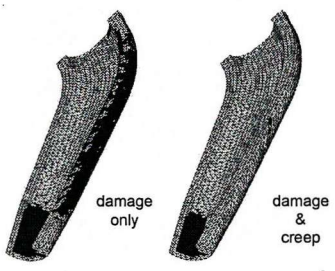

Figure 3. Element failure after 30 x 10^6 cycles

The effect different load levels have on the damage accumulation in the cement is shown in figure 4. The same percentage of damage at 30 million cycles in the light loadcase occurs at about 11 million cycles and 3 million cycles for the standard and heavy loadcases respectively.

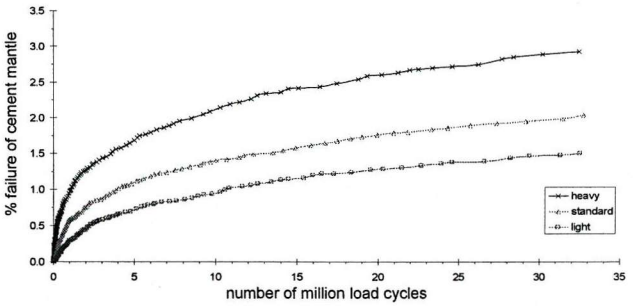

Figure 4. Element failure for different applied loads

DISCUSSION

This is a comparative study and does not claim to predict the life of a cemented hip replacement. The inclusion of creep was shown to significantly reduce the damage accumulation in the cement mantle. The reason for the reduced failure is that creep reduces the average stress within the cement mantle [3].

Considering figure 4, the level of damage reached by the light loadcase was reached by the heavy loadcase in about a tenth of the time. Cemented THRs enjoy a low failure rate at 10 years post operatively and are implanted into a wide spectrum of patients. It is likely that heavier patients account for a larger percentage of failed THRs. Further work should account for this elevated load level as well as the standard loadcase. Another variable that may affect the life of the cement mantle is the orientation of the implant. Not every implanted femur is orientated perfectly and a further study could assess how a misaligned implant affects the damage accumulation in the cement mantle.

The results presented here account for creep and damage accumulation only. Other time dependant properties such as stem-cement interface debonding and bone remodelling have not yet been included in the analysis.

CONCLUSION

Creep notably reduces the rate of damage accumulation in the cement mantle and should therefore be included in further FE analyses.

In order to adequately assess the performance of an implant design or type of bone cement, their sensitivities to variants in loading magnitude (body mass) should be assessed. Only by performing studies of this type will it be possible to identify potentially weak designs.

REFERENCES

1. McCormack, B.A.O. and Prendergast P.J., 1996, "An analysis of crack propagation paths at implant/bone-cement interfaces," Journal of Biomechanical Engineering, Vol. 118, pp. 579-585.
2. Verdonschot, N. and Huiskes, R., 1997, "The effects of cement-stem debonding in THA on the long-term failure probability of cement," Journal of Biomechanics, Vol. 30(8), pp. 795-802.
3. Verdonschot, N. and Huiskes R., 1997, "Acrylic cement creeps but does not allow much subsidence of femoral stems," Journal of Bone and Joint Surgery-British Volume, Vol. 79(4), pp. 665-669.
4. Bergmann, G. *et al.*, 2001, "Hip contact forces & gait patterns from routine activities," Journal of Biomechanics, Vol. 34(7), pp. 859-871.

ACKNOWLEDGEMENTS

The authors would like to thank the Arthritis Research Campaign for funding this work. Also thanks to DePuy International for providing the implant geometry.

RESIDUAL STRESS DECREASES THE LIFE OF THE CEMENT MANTLE IN TOTAL HIP REPLACEMENT

Jonathan R T Jeffers[1], Mark Taylor[1]

[1]*Bioengineering Science Research Group, University of Southampton, SO17 1BJ, United Kingdom*

1. INTRODUCTION

It is universally accepted that residual stresses are generated in the cement mantle of total hip replacement (THR) as the cement shrinks during polymerisation. What effect this stress has on the damage accumulation during the life of the THR is yet to be investigated. Although combined finite element/continuum damage mechanics (FE/CDM) analyses have been successful in differentiating between a clinically superior and an inferior implant, they have overestimated the life of the THR by an order of magnitude [1]. The inclusion of residual stress into analyses such as these may result in a more accurate timescale for damage accumulation.

2. METHODS

The FE model was created and meshed in I-DEAS™, based upon the Sawbones composite femur model and the Charnley prosthesis. Residual stress was created in the cement mantle by assigning a thermal expansion coefficient of 80e-6 to the cement and reducing the temperature by 10deg, using the FE solver MSC.Marc™. This created a peak residual stress in the distal cement mantle of similar magnitude (9.6MPa) to that found experimentally [2]. Once the residual stress was created it was possible to begin the damage accumulation simulation. An iteration method was employed, allowing the deactivation of elements and the simulation of creep in the bone cement. This method is based on a similar technique used by Verdonschot [3] & Stolk [1]. The stem was perfectly bonded to the cement during the analysis.

3. RESULTS

The percentage of the total volume of the cement mantle that has been deactivated is used to represent damage accumulation. Figure 1 shows the elevated damage levels due to the inclusion of residual stress in the analysis. Figure 2 represents the same model, but without loading after the creation of residual stress, and shows that the residual stress is never completely dissipated, even after a year.

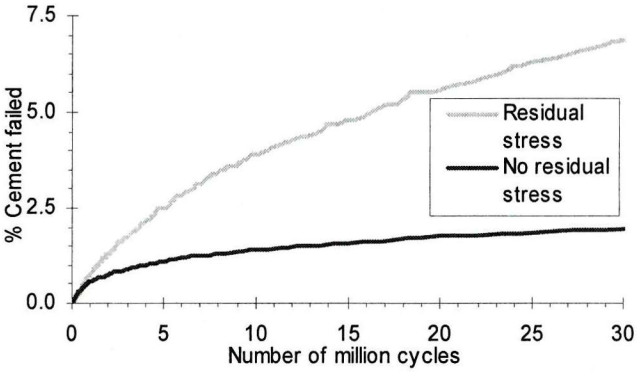

Figure 1. Damage in the cement mantle

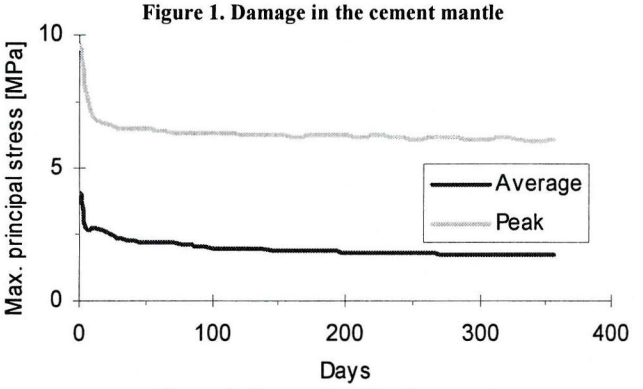

Figure 2. Stress relaxation in cement

4. DISCUSSION & CONCLUSION

The residual stress in the cement is only a fraction of the static strength, but it still affects the fatigue life. The residual stresses generated are a conservative value, the highest that could be expected [2]. Simulating the stem as being debonded would increase the failure rate of the cement [1,3]. The viscoelastic nature of cement allows stress relaxation, but the residual stress is never entirely dissipated, even when the THR is under no load for about 1 year. The increased damage rate caused by residual stress goes some way to explain the overestimation of life found in similar studies.

5. REFERENCES

[1] Stolk J, PhD Thesis, U. of Nijmegen, 2003.
[2] Roques A. et al, IV WCB, 2002.
[3] Verdonschot N, PhD Thesis, U. of Nijmegen, 1995.

CAN INITIAL CONDITIONS PREDICT THE LONG-TERM SURVIVAL OF THE CEMENT MANTLE IN TOTAL HIP ARTHROPLASTY?

+*Jeffers, J R T; *New, A M R; *Taylor, M
+*University of Southampton, SO17 1BJ, United Kingdom. Tel: +44 (0)23 8059 7665, e-mail: j.jeffers@soton.ac.uk

Introduction: Cemented total hip arthroplasty (THA) has become an extremely successful procedure, but the introduction of new implant designs and bone cement formulations have sometimes led to increased failure rates [1,2]. Questions must be asked of the preclinical testing procedures that allow the commercial release of such devices. The finite element (FE) method has the capability of calculating the stress level throughout the THA reconstruction and is widely used in preclinical testing. However, conventional FE studies only consider the initial stress distribution and neglect the time dependant properties of the reconstruction. Several FE studies have predicted the long-term survival of THA from the initial stress distribution [3], but the relationship between initial stress and long-term survival has not been convincingly proven.

Retrieval studies have identified damage accumulation in the cement mantle as a predominant THA failure mechanism [4]. Stolk and co-workers have developed a computational simulation of the cement damage accumulation process, and have been able to differentiate between stems according to clinical survival rates [5]. Using a similar method, the work presented here simulated cement mantle damage accumulation for two implant designs and four bone cement brands. The results of the damage accumulation analysis (long-term survival) were compared to the initial stress levels in the THA (initial conditions), to see if a relationship could be drawn between the two.

Methods: The finite element models generated were based on the Sawbones composite femur and (1) the C-stem and (2) the Charnley stem (both DePuy International). The properties of the following cements were used: Simplex P, Palacos R, Boneloc and CMW-1 [6]. The different bone cements were only applied to the Charnley FE model. A separate study demonstrated the significance of including residual stress on the life of the cement mantle [7]. Residual stress was generated in this analysis through thermal shrinkage of the cement from a uniform temperature. The load case (stance phase of gait [8]) was applied and the initial stress distribution in the cement mantle was recorded. The loadcase was then applied cyclically, to simulate normal gait. Damage accumulation was simulated in the cement mantle using a continuum damage mechanics approach. This approach simulated damage as a function of the stress level and number of loading cycles for every element in the cement mantle. Fatigue properties for the different brands of cement were generated from data in [6]. Cement creep was allowed to occur according to [9], and it was assumed all brands of cement had similar creep rates except Boneloc, which was allowed to creep 4 times more than the other cements.

Results: Figure 1 shows the initial stress distribution in the cement mantle for the different implant designs, with the same bone cement. The C-stem had a more favorable initial stress distribution, with a mean value of 2.9MPa as compared to 3.5MPa for the Charnley. The peak stress level in the cement was 8MPa and 16MPa for the C-stem and Charnley respectively, but only occurred in a tiny percentage of the cement volume (<0.001%). In general, 95% of the cement volume experienced stresses less than 5.5MPa and 7.3MPa for the C-stem and the Charnley respectively.

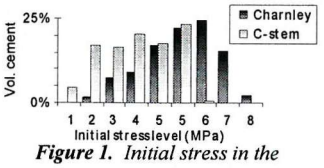

Figure 1. *Initial stress in the cement for Charnley and C-stem*

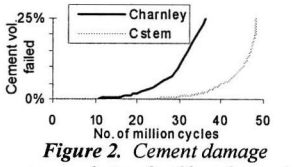

Figure 2. *Cement damage accumulation for Charnley and C-stem*

The C-stem performed better than the Charnley in the damage accumulation analysis. Figure 2 represents damage as the percentage volume of the cement mantle failed. The cement mantle of the C-stem was 25% damaged after 47 million load cycles. The Charnley reached the same level of damage at 37 million cycles.

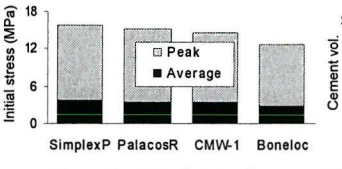

Figure 3. *Initial stress for different cements*

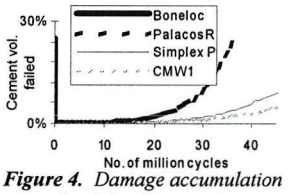

Figure 4. *Damage accumulation for different cements*

Only the Charnley stem was used to compare the different bone cements. The initial stress distribution was slightly different for each cement due to differences in their stiffness values (figure 3). Simplex P, Palacos R and CMW-1 all experienced initial peak stress levels of between 14.7MPa and 15.9MPa, with Simplex exhibiting the highest initial peak stress. The average initial stress levels for these three cements were between 3.3MPa and 3.7MPa, with Simplex again having the highest value. Boneloc exhibited the lowest initial peak and average stress levels – 12.7MPa and 2.6MPa respectively. These lower initial stresses were due to the lower stiffness of the Boneloc cement.

Figure 4 represents damage as the percentage of the cement mantle failed. The poor performance of Boneloc is highlighted – 25% of the Boneloc cement volume was damaged after only 60,000 load cycles. This was despite the lower initial stress levels for Boneloc cement. Simplex P and CMW-1 performed similarly in the damage accumulation analysis (figure 4), but the performance of Palacos R was significantly worse despite having similar initial stress levels to Simplex P and CMW-1 (figure 3).

Discussion: The long-term structural integrity of the C-stem cement mantle was superior to that of the Charnley, and the initial stress distribution was also more favorable. In this instance, the initial stress distribution could have been used to predict the superior long-term survival of the C-stem.

If the initial stress distribution was to be used predict the long-term survival of the different cements, Boneloc would appear superior to the others, as it had a lower initial stress distribution. Clinical studies have shown that Boneloc is not superior to the other cements [2], and only when the damage analysis is considered did the poor performance of Boneloc become apparent (figure 4). In this instance, the initial stress distribution was therefore misleading as it predicted superior performance from Boneloc cement. Simplex P and CMW-1 performed notably superior to Palacos R in the damage analysis, despite similar initial stress levels, and even though Simplex had the highest initial peak stress. This is further evidence that the initial stress cannot be used to predict the long-term behavior of the THA reconstruction.

Although the initial stress distribution calculated by the FE method was able to correctly predict the performance of the C-stem and the Charnley in the damage accumulation analysis, it may not have done so for all implant designs – further testing will determine this. Certainly for different bone cements predictions based on the initial stress field failed comprehensively to predict the long-term behavior of the THA, and therefore should be used only with caution as a preclinical testing method. The benefits of the FE method can still be taken advantage of in preclinical testing, but the time dependant properties of the THA must be considered. The damage simulation described here takes these into account and provides a more reliable preclinical test method.

Acknowledgements: The authors wish to thank the Arthritis Research Campaign who provide funding for this project and DePuy International.

References: [1] Sylvain *et al*, J Arthrop, 16: 141, 2001. [2] Havelin *et al*, JBJS, 77A: 1543, 1995. [3] Mann *et al*, J Orthop Res, 15: 700, 1997. [4] Jasty *et al*, JBJS, 73B: 551, 1991. [5] Stolk, PhD thesis, Nijmegen, 2003. [6] Harper *et al*, J Bio Mats Res, 53: 605, 2000. [7] Jeffers *et al*, ICCB, Zaragoza, 2003. [8] Bergmann, Hip98, Berlin, 2001. [9] Verdonschot, PhD Thesis, Nijmegen, 1995.

DAMAGE ACCUMULATION IN THE CEMENT MANTLE SURROUNDING THREE HIP PROSTHESES

+*New, AMR; *Jeffers, JRT; *Taylor, M
+*University of Southampton, SO17 1BJ, United Kingdom. Tel +44 (0)2380 592899, E-mail a.m.new@soton.ac.uk

INTRODUCTION: Cemented total hip arthroplasty remains the gold standard for the treatment of disabling hip disorders in many patients. When all patient groups are considered together, the cumulative frequency of revision of cemented hip prostheses is now less than 3% at 10 years [1]. However, the problem of aseptic loosening of prostheses remains, particularly in young and active patients, presumably because the mechanical demands they place on their reconstructed joints are greater. The design of the prosthesis is also known to be an important factor [1] and, while the precise aetiology of aseptic loosening remains unclear, several authors have proposed that progressive failure of the cement mantle plays a significant role [2].

Several authors have presented computational methods for modeling the failure processes in the cement mantle, with the continuum damage mechanics approach coupled with finite element stress analysis emerging as the most popular [3, 4]. The aim of this study was to use a similar technique to predict the performance of three hip prosthesis femoral components, the Charnley Roundback and C-Stem prostheses (DePuy International Ltd) and the Exeter prosthesis (Stryker Howmedica Osteonics).

METHODS: Three dimensional finite element models of the three prostheses implanted in the Sawbones third generation composite femur were generated using the ANSYS finite element package. Linear hexahedral elements were used in the cement mantle and linear tetrahedral elements in the implant and bone. The hexahedral-to-tetrahedral mesh transitioning feature of the ANSYS package ensured conforming meshes. A minimum of four elements were defined through the thickness of the cement mantle to give sufficient accuracy [5]. The resulting meshes are shown in Figure 1. The meshes were then exported to the MARC finite element package for stress analysis and damage accumulation simulation using methods based on previously published work [3, 4, 5].

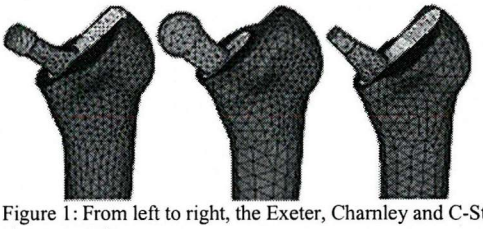

Figure 1: From left to right, the Exeter, Charnley and C-Stem finite element meshes.

Materials properties of the composite femur and the prostheses were assigned using the respective manufacturers data. Fatigue properties of the bone cement (CMW1) were taken from [6] and creep properties from [3]. All interfaces were considered to be perfectly bonded. Loads representing the stance phase of gait [7] were applied cyclically to simulate normal gait.

RESULTS: Figure 2 shows damage accumulation in the cement mantle for the three prostheses as a function of the number of loading cycles.

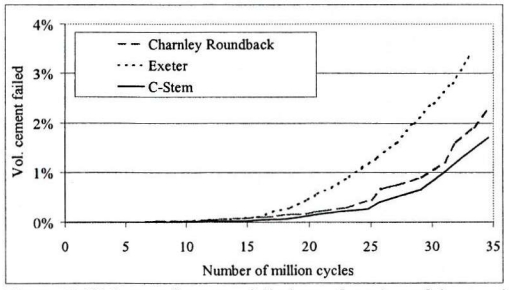

Figure 2: Volume of cement failed as a function of the number of loading cycles.

The amount of damage in the cement mantle was lowest for the C-Stem prosthesis throughout the loading history. Initially, the accumulated damage was greatest for the Charnley prosthesis, with the Exeter prosthesis falling between the Charnley and C-Stem. However, after approximately 16 million cycles, the accumulated damage for the Exeter overtook the Charnley and remained higher for the duration of the analysis. This was despite lower average stresses for the Exeter prosthesis for the great majority of the loading history (Figure 3).

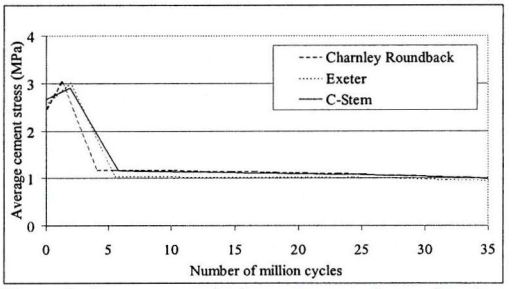

Figure 3: Average stress in the cement mantle as a function of the number of loading cycles.

DISCUSSION: This study predicts that the C-Stem prosthesis will outperform the Charnley and Exeter prostheses if damage accumulation in the cement mantle is an adequate predictor of clinical survival. However, there are several limitations to this study that should be born in mind when interpreting the results. The first is that the cement-prosthesis interfaces were considered to be bonded to reduce computation time. While it is known that debonding at this interface can greatly increase cement mantle stresses in standard linear static finite element models of the implanted femur [8], it also appears that FE models with bonded prosthesis-cement interface conditions produce results that more closely match experimental measurements of cement stresses in laboratory implanted prostheses [9]. The role of interface debonding in the predictions of non-linear models of the type presented here is uncertain and indeed two of the prostheses studied (Exeter and C-Stem) are specifically designed not to form a bond with the cement in order that, in principle, creep or localized damage in the cement mantle can be accommodated by controlled prosthesis migration and associated load redistribution. It may be that neither completely bonded nor completely debonded prosthesis-cement interface conditions are good approximations over the whole lifetime of the cement mantle and that explicit modeling of the debonding process is required to accurately model those interface conditions and their effects on cement damage accumulation. Neither did these models include the effects of the residual stresses developed in the cement mantle during cement cure. These residual stresses are now suspected of being important in both the development of pre-load damage in the cement mantle and the propagation of damage under service loads. Previous work suggests that including residual stresses decreases the life of the cement mantle and the current models thus appear likely to have overestimated its life. The investigation of both of these effects is the subject of ongoing work.

ACKNOWLEDGEMENTS: The authors would like to thank the UK Arthritis Research Campaign and DePuy International for funding this project.

REFERENCES: [1] Malchau *et al.*, American Academy of Orthopaedic Surgeons, Dallas, 2002 [2] Jasty *et al.*, J Bone Joint Surg, 73B: 551-558, 1991 [3] Verdonschot, PhD Thesis, Nijmegen, 1995 [4] Stolk, PhD Thesis, Nijmegen, 2003 [5] Jeffers *et al.*, ASME Summer Bioengineering Conference, Key Biscayne, 2003 [6] Harper *et al.*, J Biomed Mats Res, 53: 605-616, 2000 [7] Bergmann, Hip 98, Berlin, 2001 [8] Huiskes, Clin Orthop, 261: 27-38, 1990 [9] Stolk, J Biomech 35: 499-510, 2002

DAMAGE ACCUMULATION IN BONE CEMENT MEASURED BY ACOUSTIC EMISSIONS

Jonathan R T Jeffers (1), Anne Roques (1), Martin Browne (1) and Mark Taylor (1)

1. Bioengineering Sciences Research Group, University of Southampton, UK

INTRODUCTION

The bone cement used in the fixation of medical devices is susceptible to damage accumulation when subject to a dynamic load. This has been identified as a dominant failure mechanism for the cement fixed femoral component in total hip replacement (McCormack and Prendergast 1999). The ability of bone cement to resist damage accumulation is therefore advantageous.

Several authors have measured damage in bone cement by using a dye penetrant method (McCormack and Prendergast 1999; Murphy and Prendergast 2001; Lennon and Prendergast 2002). Dye was applied to the surface of the cement and penetrated into the microcracks, allowing them to be visualised under transmitted light. This method led to a conservative estimate of the level of damage, as cracks that were entirely within the cement could not be stained.

An alternate method for measuring damage is the acoustic emissions (AE) technique. When a microcrack initiates or propagates, it releases acoustic energy that propagates through the material in the form of an acoustic wave, which can be captured by a piezoelectric transducer, or AE sensor, attached to the surface of the test specimen. The AE method can be used for geometries that do not facilitate viewing of the cement, and allows the test to run uninterrupted, enabling creep properties to be assessed.

This study describes a series of uniaxial fatigue tests to generate a S-N curve for CMW-1 (DePuy-CMW) bone cement. Damage was monitored by the AE method. The damage accumulation by AE was then compared to that measured by the dye penetrant method (Murphy and Prendergast 2001).

METHODS

CMW-1 (DePuy CMW) cement was vacuum mixed at room temperature and injected into a polyethylene mould and clamped for 2 hrs. Specimens were removed and stored in Ringers solution until testing. The ageing period of the specimens was between 18 and 30 days. Testing took place in a purpose built environment chamber, filled with distilled water at 37deg and electrically insulated from the testing machine to prevent interference with the apparatus. The test specimen had an AE sensor attached at either end of the gauge length to collect the acoustic emissions released as damage occurred. The specimen was gripped with stainless steel grips and attached to the testing machine. A sinusoidal cyclic pure tensile load was applied at a freq. of 5Hz and a loading ratio of 0.1.

RESULTS

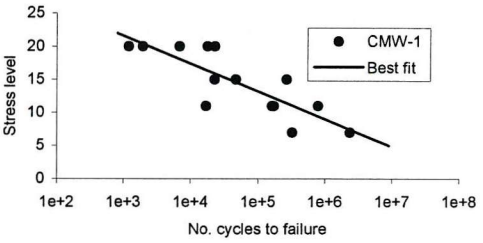

Figure 1: S-N curve for CMW-1 (pure tensile load).

The solid line in figure 1 is the 'best fit' for all the data points, and can be represented by equation 1.

$$\log N_f = (34.27 - \sigma)/4.21 \qquad (1)$$

The energy of the acoustic emissions was chosen as the damage parameter and cumulated over the number of cycles. The non-linear accumulation of damage is evident in figure 2, to a higher degree at greater stress levels.

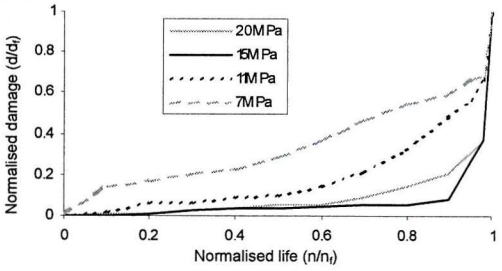

Figure 2: Non-linear damage at different stress levels. Degree of nonlinearity depends on stress level.

DISCUSSION & CONCLUSION

Non-linear damage accumulation was observed, and the degree of nonlinearity depended on the stress level. This is in good agreement with the results of the dye penetrant method (Murphy and Prendergast 2001). Therefore the AE technique is suitable for monitoring damage accumulation in bone cement, providing a quicker means of damage analysis, without interruption to the test. Given the viscoelastic nature of bone cement, this is surely advantageous.

ACKNOWLEDGEMENTS

The Arthritis Research Campaign and DePuy CMW.

REFERENCES

Lennon & Prendergast, J Biomech, 35:311-321, 2001. McCormack & Prendergast, J Biomech, 32:467-475, 1999. Murphy & Prendergast, J Biomed Mats Res 59: 646-654, 2001.

INFLUENCE OF CROSS-SHEAR ON THE WEAR OF POLYETHYLENE: A FINITE ELEMENT STUDY

*Knight, L A, **Galvin, A, *Jeffers, J R T, *Hopkins, A, **Fisher, J, +*Taylor, M
+*Bioengineering Sciences Research Group, University of Southampton, Southampton, SO17 1BJ, UK
M.Taylor@soton.ac.uk

Introduction: Total Knee Arthroplasties (TKAs) are increasingly implanted into younger and more active patients, placing high kinematic demands on devices that are now expected to last up to and beyond 20 years. It is currently considered that surface wear of the polyethylene-bearing component is a major limiting factor to the longevity of TKAs. Not only can the implant wear out, but polyethylene wear particles can invoke an osteolytic reaction, which may lead to aseptic loosening and premature revision surgery [1].

The volume of wear generated between two articulating surfaces is proportional to the applied load and the sliding distance. The relative kinematics of the articulating surfaces has also been shown to have a marked effect on the wear volume [2]. Knee simulator studies have shown that increasing the anterior/posterior (AP) displacement and internal/external (IE) rotation increases the wear volume [3]. One method of quantifying the relative kinematics is by calculating the cross-shear energy (see eqn.2). Cross-shear is a ratio of the displacement perpendicular to the principal direction of motion to that in the principal direction of motion. In the knee simulator study, increasing the kinematics caused greater cross-shear on the polymer surface, thereby accelerating polyethylene wear.

This study demonstrates the importance of including cross-shear in computational studies by simulating multidirectional pin on plate tests and comparing the results to experimental data.

Method: A polyethylene pin on metallic plate experiment was performed, with input kinematics of 60 mm stroke length and +/- 60° rotation (60-60). These parameters were applied to the pin along with a compressive load of 160 N, which was equivalent to a contact pressure of 3.18 MPa. A computational simulation of the experiment was performed as follows:

The computer simulation was run for 1 cycle and then simple wear theory was applied. The wear calculation is taken from work by Maxian et al. [4] and is shown in eqn. 1.

$$H = \sum_{t=0}^{t=n} K_w S p \qquad \textbf{Eqn. 1}$$

where H = wear depth, K_w = wear factor (dependent on material properties and kinematic conditions), S = sliding distance and p = contact pressure. This calculation is made for every node on the surface of the pin. An adaptive remeshing procedure was applied, which multiplied the wear data for one cycle by a specified number of cycles, removed material from the surface, and then re-ran the simulation. This method was based on a constant value of the wear factor, determined from experiment to be 1×10^{-8} mm^3/Nm, and uniform wear was expected.

A measure of the relative kinematics occurring between the articulating surfaces is the cross shear energy. This can be calculated by the eqn. 2 [5]:

$$CS = \left(\sum_{t=0}^{t=n} ML \Big/ \sum_{t=0}^{t=n} AP\right) \qquad \textbf{Eqn. 2}$$

where CS = cross-shear, ML = medial-lateral displacement and AP = anterior-posterior displacement. The cross-shear can be incorporated in the wear factor. This allows the effect of relative kinematics over the surface of the pin to be investigated. Including cross-shear will generate a different wear factor for each point on the pin surface, because each point has different kinematics, and therefore the wear on the surface will not be uniform. The wear factor for cross-shear motion is a function of the calculated cross-shear, and was assumed to be of the form $A(CS)^6$.

This study will present a comparison between the wear volumes from experimental results and computational simulation with and without the inclusion of cross-shear. It will also show the effect of the inclusion of cross shear on the wear distribution over the surface of the pin from computational simulation.

Results: Fig. 1 shows that the computational simulation including cross-shear correlates well with the experimental data. Not only does the final wear volume agree with the empirical data, but the wear volume per cycle is seen to progress in a similar manner. Neglecting cross-shear significantly under-predicts the wear volume observed in experiment.

Fig. 2 shows the wear depth distribution over the surface of the pin, with and without the inclusion of cross shear. The distribution of wear depth is very different. The pin without a measure of cross shear wears fairly uniformly across its surface. There is a slight difference between the 'medial and lateral' sides as the pin had a greater sliding distance medially. The pin from the simulation that included cross shear wore mainly on the 'anterior and posterior' and very little in the centre. This has the effect of increasing the contact pressure in the centre of the pin and decreasing it in the worn areas. This increased wear corresponds with the areas of greatest cross shear.

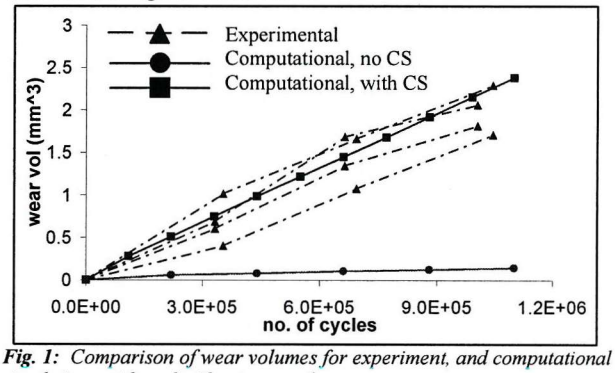

Fig. 1: *Comparison of wear volumes for experiment, and computational simulations with and without cross-shear.*

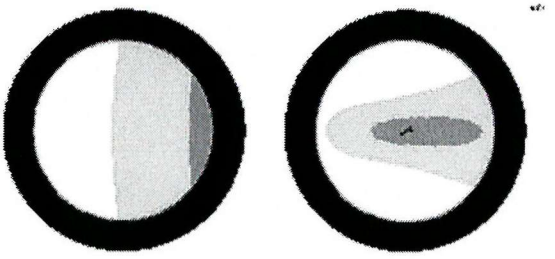

Fig. 2: *Distribution of wear over the surface of the polyethylene pins for computational simulation with (right) and without (left) the inclusion of cross shear. Maximum wear depth with and without cross-shear of 4.646×10^{-2} mm and 2.098×10^{-3} mm respectively (lighter areas indicate greater wear depth)*

Discussion: The results have shown that the influence of cross-shear on wear can be simulated using finite element analysis. This study has also outlined the importance of including some factor of cross-shear in computational simulations of wear. If the wear factor is assumed to be constant (i.e. without cross-shear), not only is the total wear volume under-predicted, but the distribution of the wear on the surface is miscalculated. The computational simulation including cross shear was observed to wear similarly to the experimental polyethylene pins, but this has only been evaluated qualitatively. This study suggests that simple wear theory will not be sufficient to predict the wear in TKA, and that the cross-shear should be included in simulations for them to be a useful pre-clinical tool.

References: [1].Ingham, E., Proc. IMechE, 214: 21-37; [2].Fisher, J., Proc. IMechE, 205: 73-79; [3].Barnett, P. I.; J. Mat. Sci, 12(10-12): 1039-1042; [4].Maxian, T. A., J. Orthop. Res., 14(4): 668-675; [5].McEwen, H. M. J., In BORS, 2003.

Acknowledgements: Funding provided by the Arthritis Research Campaign.

**Institute of Medical and Biological Engineering, University of Leeds, Leeds, LS2 9JT, UK

THE SIMULATION OF BONE CEMENT FATIGUE WITH EXPERIMENTAL VALIDATION

*Jeffers, J R T; *Browne, M; *Roques A; +*Taylor, M
+*Bioengineering Sciences Research Group, University of Southampton, SO17 1BJ, United Kingdom
m.taylor@soton.ac.uk

Introduction: Orthopaedic devices, such as hip, knee and shoulder replacement components are often fixed in the host bone with bone cement. There are great demands placed on these devices, as they should ideally remain functional for the lifetime of the patient. A possible failure mechanism of the implanted component is loosening caused by cracks forming in the bone cement mantle. This process is called damage accumulation and can be simulated computationally for use as a tool in preclinical testing. Studies have simulated this failure scenario for the femoral component of total hip arthroplasty [1], but little experimental validation of the method has taken place. In this study, we propose that experimental validation is only possible when the porous nature of bone cement is simulated in the finite element models. The computational method uses fatigue data from uniaxial tests, thus validation against uniaxial fatigue tests is inappropriate. Experimental validation is instead attempted with 4-point bend fatigue tests.

Methods: Experimental tests were conducted to generate an S-N curve for bone cement (DePuy CMW-1) under pure uniaxial tension. Dog-bone shaped specimens were tested at 37°C under load control with a sinusoidal applied load, an R-ratio of 0.1 and a frequency of 5Hz. The resulting S-N curve was represented by equation 1.

$$\log N_f = (46.25-\sigma)/6.3 \qquad \textbf{Equation 1.}$$

Finite element models of the tensile fatigue test specimen (as used in the experimental fatigue tests) were generated. Each element was assigned a damage parameter, d. Boundary conditions to simulate fatigue loading were applied. The stress (σ) and corresponding number of cycles to failure (N_f) were calculated for each element, using equation 1. A number of cycles were simulated (n), based on a predefined percentage of the element with the lowest calculated N_f. Damage was incremented accordingly ($d=n/N_f$) and creep was simulated according to [2]. When $d=1.0$ for an element, it was deactivated and the stresses transferred to the surrounding elements. The fatigue lives of the finite element models were exactly in agreement with equation 1, but this did not represent experimental validation, as equation 1 was used in the computational method. The method described above used S-N data directly from the experimental tests to calculate the fatigue life of individual elements in the finite element models, but this was invalid for the following reason. Bone cement contains pores and voids, and a larger volume of cement is statistically more likely to contain a greater number of defects. Ergo, larger volumes of cement are likely to have shorter fatigue lives. There is a great difference between the volume of an individual finite element and the gauge length of a fatigue test specimen (approx 1000x), so the fatigue life of a finite element should be much greater than a fatigue test specimen. The following method describes the derivation of an S-N curve for theoretical cement, free from pores. As no pores will be present, this theoretical S-N curve is volume independent. Twenty (20) finite element models of the tensile test specimen were generated and a number of pores for each specimen determined with a Monte Carlo simulation, taking the mean number of pores and standard deviation from an experimental study [3]. These pores were randomly assigned to elements in each finite element model. The fatigue simulation was performed as described above, but fatigue lives for elements with a pore were calculated using the elevated stress level caused by a spherical pore subject to a remote load [4]. The random number and distribution of pores introduced some scatter in the results, so fatigue was simulated in five models at each stress level. The inclusion of pores shortened the fatigue life considerably, such that the S-N curve used in the computational method (equation 1) required modification to bring the simulated fatigue lives back in agreement with the experimental data:

$$\log N_f = (78.39-\sigma)/11.22 \qquad \textbf{Equation 2.}$$

This modified S-N curve represented the fatigue of bone cement free from pores (as pores were simulated in the finite element models). Experimental validation could then be attempted with 4-point bend tests. 4-point bend specimens were fatigued at 37°C under load control with a sinusoidal applied load, an R-ratio of 0.1 and a frequency of 2Hz. Finite element models of the 4-point bend specimens were generated, and porosity simulated as before. The fatigue simulation was performed as described above, using the theoretical S-N curve for cement free from pores (under uniaxial tension) in the computational method. Results were compared to the experimental data.

Results: The computational fatigue predictions were in close agreement with the experimental data for 4-point bending (fig 2). A degree of scatter was introduced into the computational fatigue simulation, but not to the extent as observed in the experimental tests. Data scatter was due to the random number and distribution of pores in the finite element models (this also caused the data scatter in the experimental specimens).

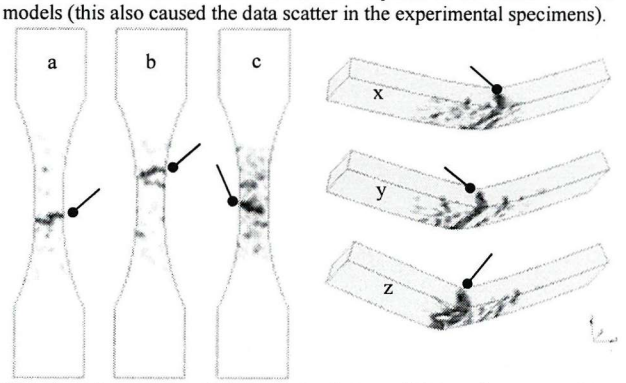

Fig. 1: *Computational fatigue simulation of finite element models: (a,b,c) tensile fatigue at 20MPa. N_f =(a) 3,564, (b) 12,669, (c) 20,341. (x,y,z) 4-point bend fatigue at 35MPa. N_f =(x) 66,696, (y) 80,496, (z) 79,185. Fracture site is indicated, but note damage at less critical sites.*

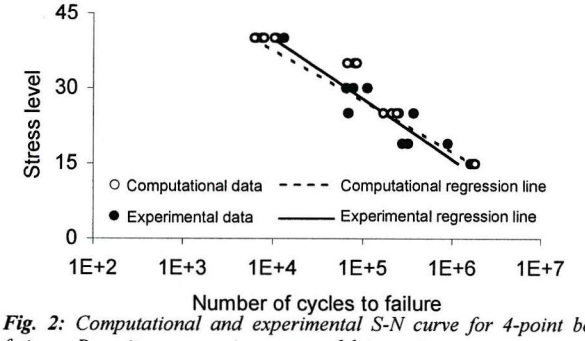

Fig. 2: *Computational and experimental S-N curve for 4-point bend fatigue. Porosity was a major source of data scatter.*

Discussion: This study demonstrates that an S-N curve from uniaxial fatigue tests could be used to simulate the fatigue of non-uniaxial loading (4-point bend). However, pores needed to be simulated in the finite element models, and element fatigue calculated according to equation 2. Neglecting pores and using equation 1 to calculate element fatigue led to a significant under-prediction of 4-point bend fatigue life. Using equation 2 calculated the fatigue of elements assuming no porosity. Stress concentrations in elements with a pore then shortened the fatigue of those individual elements. While shortening the fatigue life of an individual element will have a marginal effect on the fatigue life of the specimen, a critical region can be formed where two or three pores are in close proximity. Only a small volume of cement in the 4-point bend was subjected to the maximum tensile stress, therefore the probability of a critical region (two or three pores in close proximity) being present was relatively low. In the absence of a critical region, the fatigue life of elements under maximum stress was therefore increased by including porosity, as the fatigue life was calculated from equation 2. Successful validation for 4-point bending allows greater confidence to be placed in the method when applied to more complex geometries such as the implanted femur. This stochastic approach, which includes the random nature of porosity, enhances existing deterministic studies of bone cement failure, and is more representative of the clinical situation.

References: [1] Stolk, PhD Thesis, U. Nijmegen; [2] Verdonschot, J. of Appl. Biomats., 5(3), 235-43; [3] Murphy, J. of Biomed. Mats. Res., 59, 646-54; [4] Timoshenko, Theory of Elasticity, 3rd Edition, 396-8.

Acknowledgements: Funding provided by the Arthritis Research Campaign. Bone cement provided by DePuy CMW, Blackpool, UK.

CEMENT MANTLE FATIGUE FAILURE: IN SILICO SIMULATION WITH EXPERIMENTAL VALIDATION

Jonathan R T Jeffers, Martin Browne and Mark Taylor

University of Southampton, United Kingdom

1. INTRODUCTION

The total hip replacement should ideally remain functional for the lifetime of the patient, but unfortunately this is not always the case. A hip replacement is considered to have failed when it causes the patient pain, and requires a revision operation to relieve that pain. According to national hip register studies the most common cause of failure is aseptic loosening of the components [1]. There are a number of scenarios that can lead to component loosening; one of these is cracking of the cement mantle. Radiographic follow-up studies consider a cement mantle fracture a sign of definite component loosening [2]. Inspection of ex vivo fracture surfaces has led to fatigue failure being proposed as a possible failure mechanism [3-5].

These clinical observations have led to finite element based tests being developed to simulate bone cement fatigue in the implanted femur construct. Verdonschot and Huiskes [6] developed such a test to ascertain the influence a bonded or unbonded prosthesis/cement interface had on the fatigue failure of the cement mantle. More recently, Stolk et al. [7] demonstrated the potential of this computational method by predicting superior performance of the Lubinus II prosthesis over the Muller curved prosthesis – in agreement with findings from the Swedish hip register [1]. Although qualitative assessment of these prostheses was possible, an experimental validation study was unsuccessful. Experimental specimens of the implanted femur construct were subjected to 2e6 load cycles, but the computational models required 20e6 simulated load cycles to generate similar levels of cement mantle damage [7]. However, experimental validation of the computational method *was* achieved in a different study by Stolk et al. [8], but only for uniaxial tensile tests. It was not checked that the computational method could simulate another loading configuration.

The current study aims to develop the computational simulation of bone cement fatigue such that experimental validation is possible for the implanted femur construct. The method used to simulate bone cement fatigue is based on that described by Verdonschot and Huiskes [6] and includes cement creep as described by Stolk et al. [8], but also includes an initial stress field to simulate residual stress and porosity distributions in the cement. Inclusion of these parameters has led to excellent correlation between computationally predicted and experimental fatigue life for uniaxial and 4-point bend in a previous study [9]. The current study increases the complexity of the experimental validation to a simplified model of the implanted femur. By performing experimental validation at each stage of increasing complexity (tensile fatigue, 4-point bend fatigue and now a simplified model of the implanted femur), greater confidence can be placed in the results of the analysis.

2. MATERIALS AND METHODS

2.1 Experimental testing

The experimental specimens were based on the simplified implanted femur model as described by Lennon et al. [10] (Figure 1, with front cover removed). The cement used was vacuum mixed CMW-1 (DePuy CMW). Four specimens were made, three with an unbonded interface and one with a bonded interface. For the unbonded interface, the surface of the stem was polished. This was removed from and replaced into the cement prior to testing. The bonded interface used a grit blasted stem that was not removed from the cement prior to testing. Specimens were clamped at 12° to the vertical in an Instron servohydraulic testing machine. A load horse was attached to the greater trochanter and the head of the stem, which allowed a joint reaction force of 3kN at 20° to the vertical and an abductor force of 1.6kN at 15° to the vertical. This load was applied sinusoidally for 2e6 cycles at an r-ratio of 0.1 and a frequency of 5Hz.

2.2 Computational modelling

Four finite element models were generated to the same dimensions and interface conditions as the experimental specimens. Three models had an unbonded stem/cement interface (friction coefficient 0.25) and one a bonded interface. Boundary conditions were applied to simulate the experimental loading and a unique porosity distribution applied to

each model using Monte Carlo methods and the theoretical elastic solution for a spherical cavity in a volume of material subject to a remote load. This generated a unique pore distribution in each finite element model to represent the pores present in the experimental specimens. Initial stress (to simulate residual stress) was induced in the cement by means of thermal contraction. The magnitude of induced stress was similar to residual stress measured experimentally. Cement fatigue and creep were simulated in the models using a continuum damage mechanics approach. Details of the porosity, fatigue and creep simulations are described in full by Jeffers et al. [9].

3. RESULTS

Complete cement mantle fractures occurred in all three unbonded experimental specimens at the distal end of the stem (Figure 1). The computational analysis also predicted fractures in this location, (Figure 2). Distal fractures occurred before 3e5 load cycles for both the computational models and experimental specimens, but fractures generally occurred sooner in the computational models. The computational method also predicted damage elsewhere in the cement, but only in one case did this cause a cement mantle fracture in a location other than at the distal tip of the stem (Figure 2a).

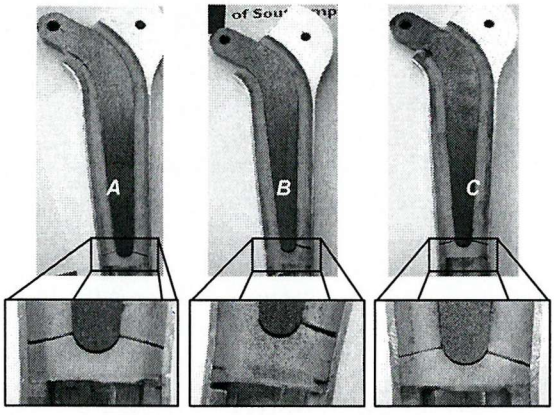

Figure 1: Cement mantle fractures in three different specimens after 2e6 load cycles (unbonded interface and front aluminum cover removed).

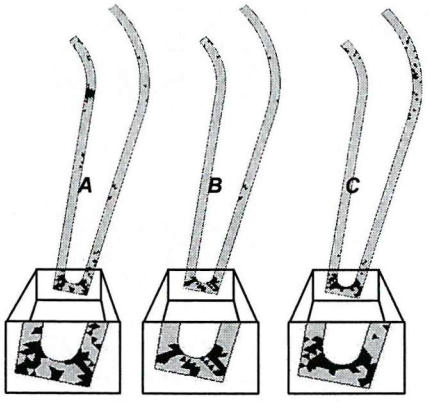

Figure 2: Cement mantle damage after 2e6 cycles predicted by the computational method.

For the bonded analysis, computational results were also in good agreement with the experimental, with no cement mantle fractures predicted after 2e6 load cycles (Figure 3).

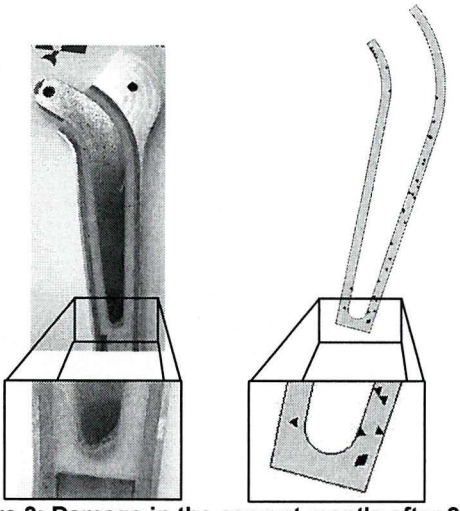

Figure 3: Damage in the cement mantle after 2e6 load cycles for the bonded interface.

4. DISCUSSION & CONCLUSIONS

Experimental validation of the computational method was successful as, for the unbonded stem/cement interface models, the fracture locations were predicted in similar locations and in a similar timeframe to the experimental specimens. The computational method also predicted no cement mantle fractures for the bonded case (Figure 3), which again was in agreement with experimental findings. Including a bonded interface in the study was not an attempt to ascertain the merits of a smooth or polished stem; it was performed purely for validation purposes. Including a unique porosity distribution in each finite element model allowed the generation of stochastic results. Figure 2 shows different damage patterns for each finite element model; models were identical save for the pore distributions. One finite element model, Figure 2a, predicted a cement mantle fracture in the medial proximal area of the cement mantle that did not occur in the experimental specimens. Further inspection of this area revealed a high localized concentration of pores. Lennon et al. [10] performed a stress analysis of a similar experimental model, and found a stress concentration in this location. Therefore, were a similar localized concentration of pores present in one of the experimental specimens, fracture may also have occurred.

ACKNOWLEDGEMENTS

This study was funded by the Arthritis Research Campaign (UK), grant ref. T0525 (www.arc.org.uk). Bone cement was kindly supplied by DePuy CMW, Blackpool, UK.

REFERENCES

1. Herberts P et al, 2002. http://www.jru.orthop.gu.se.
2. Harris WH et al, 1982. JBJS 64A, 1063-67.
3. Topoleski LDT et al, 1990. J Biomed Mater Res 24, 135-54.
4. Stauffer RN, 1982. JBJS 64A, 983-90.
5. Jasty M et al, 1991. JBJS 73B, 551-558.
6. Verdonschot N and Huiskes R, 1997. J Biomech 30, 795-802.
7. Stolk J et al, 2003. Clin Orth Rel Res 409, 138-50.
8. Stolk J et al, 2004. Eng Fract Mech 71, 513-28.
9. Jeffers JRT et al, 2005. Trans 51st ORS meeting, Washington DC.
10. Lennon AB et al, 2003. Med Eng Phys 25, 833-41.

Parameters Influencing the Fatigue Failure of the Implanted Femur Cement Mantle

JRT Jeffers, M Browne and M Taylor
Bioengineering Sciences Research Group, University of Southampton, UK

Introduction: Fatigue failure of the cement mantle has been identified as one of the more common reasons for prosthesis loosening. There are several factors involved in the fatigue failure of the cement mantle, particularly cement porosity, creep and residual stress. However, the relative contribution of each of these parameters is uncertain. In the current study, the fatigue of bone cement in the cement mantle of an implanted femur was simulated using a continuum damage mechanics approach. The prosthesis was the triple-taper polished C-stem (DePuy, UK, Figure 1). Cement creep, porosity and an initial stress field (to simulate residual stress) were included in the modelling. An advantage computational modelling has over experimental tests is that different mechanical parameters can be switched on or off, allowing the influence of each to be determined. In this way, the influence of creep, porosity and residual stress on the fatigue life of the cement mantle were investigated. The failed cement mantle was then compared to clinical observations to see what (if any) correlations could be drawn.

Materials and Methods: The finite element model is shown in Figure 1; boundary conditions were applied to simulate level gait loading. Porosity was simulated in the cement with a Monte Carlo simulation and using the theoretical elastic solution for a pore subject to a remote load. An initial stress field was simulated in the cement to represent residual stress as measured by Roques et al [1]. Cement fatigue was simulated with a continuum damage mechanics approach, with damage simulated by element modulus reduction. Creep was also simulated in the analysis, with creep data taken from experimental tests [2].

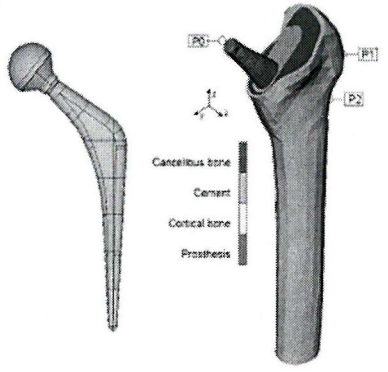

Figure 1. DePuy C-Stem and finite element model.

Four models were simulated each with a different porosity distribution; these generated a degree of variability in the results. Fatigue loading to represent level gait was applied until the cement mantle was no longer able to support the prosthesis. The analysis was then repeated, but with the different cement parameters either switched on or off. In this way, the influence of each on the fatigue life could be determined.

Results and Discussion: Figure 2 shows the posterior half of the cement mantle from 1 million to 2 million simulated gait loading cycles, after which, in this example, the cement mantle fractured. Fracture occurred by longitudinal splitting of the cement, in a similar manner as has been observed clinically [3]. The influence of switching parameters off is summarised in Figure 2. Switching porosity off led to an increased fatigue life of the cement mantle. Switching off residual stress had a similar effect, although to a lesser extent. Switching off cement creep shortened the fatigue life of the cement mantle, suggesting creep acted in a positive way to resist damage accumulation. The combined effect of all parameters also gave similar fatigue lives to those observed clinically, in contrast to previous cement fatigue simulations that only considered the effects of creep [4]. The methods developed in this study may be useful to bone cement chemists in developing new cements that provide increased fatigue resistance.

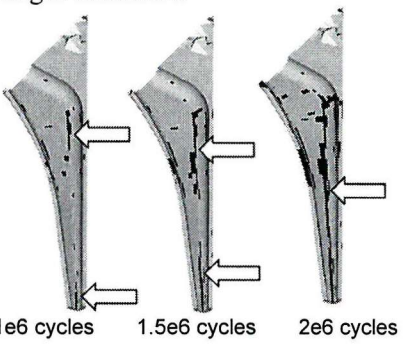

Figure 2. Progression of crack leading to cement mantle failure at 2 million simulated load cycles.

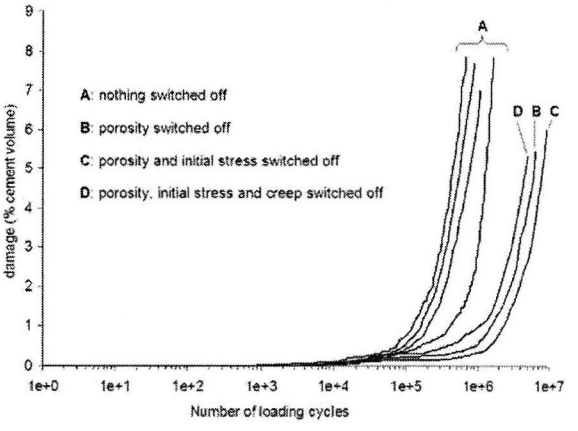

Figure 3. Damage versus loading cycles for analyses with different parameters switched off.

Acknowledgements: Project funded by the Arthritis Research Campaign (UK) www.arc.org.uk. Prosthesis solid model provided by DePuy (UK).

References: [1] Roques et al, 2004: Biomaterials 25:4415-24. [2] Jeffers et al, 2004: Proc 14th ESB, the Netherlands. [3] Stauffer, JBJS 64A:983-90. [4] Stolk et al 2003, CORR 409:138-50.

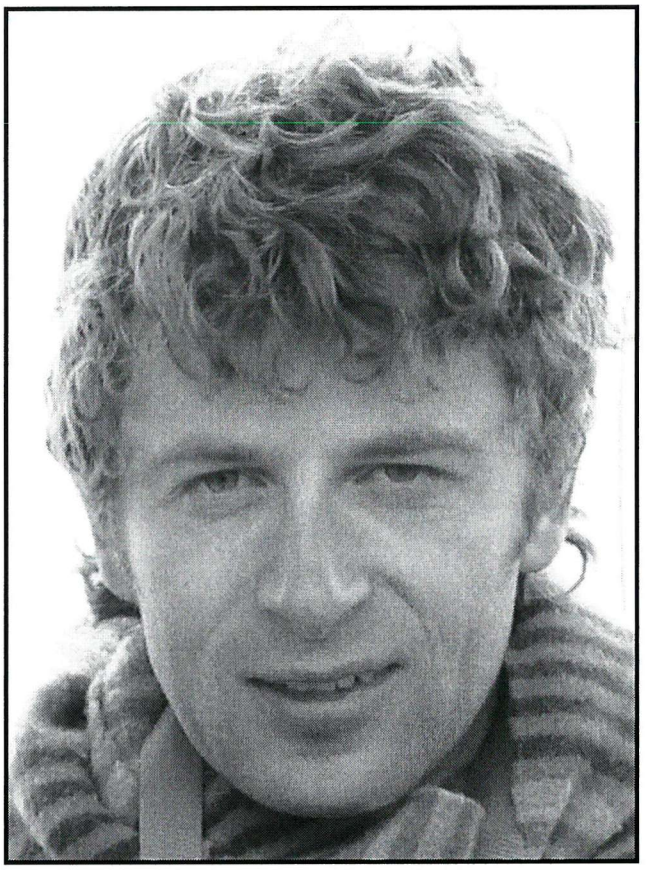

Thanks

Jonathan